The highly dynamic heterochromatin protein Swi6 mediates degradation of heterochromatic transcripts

Inauguraldissertation

zur
Erlangung der Würde eines Doktors der Philosophie
vorgelegt der
Philosophisch-Naturwissenschaftlichen Fakultät
der Universität Basel

von

Rieka Stunnenberg

aus den Niederlanden

Basel, 2015

Originaldokument gespeichert auf dem Dokumentenserver der
Universität Basel
edoc.unibas.ch

Genehmigt von der Philosophisch-Naturwissenschaftlichen Fakultät auf Antrag von Prof. Dr. Susan M. Gasser, Prof. Dr. Geneviève Almouzni und Dr. Marc Bühler.

Basel, den 11. November 2014

Prof. Dr. Jörg Schibler
Dekan

Table of Contents

SUMMARY **3**

INTRODUCTION **6**

1. **'Silent' chromatin in eukaryotes** **7**
    - Perspective on genomic features; from junk to regulation 7
    - Transcription factors 8
    - Sir proteins 8
    - Histones: more than just package material 9
    - The concept of epigenetics & stability 9
    - Position effect variegation 10
    - Histone modifications 10
    - X-chromosome inactivation 10
    - DNA methylation 11
2. **Chromatin dynamics** **12**
    - Chromatin organization in the nucleus 12
    - Chromatin interactions 12
    - The role of nuclear scaffold 12
    - Histone dynamics 13
    - Histone variants 13
    - Heterochromatin protein HP1 dynamics 14
3. **RNA interference and silencing** **16**
    - Post-transcriptional gene silencing 16
    - The piRNA pathway 17
    - Transcriptional gene silencing in plants 18
    - RNA-directed DNA methylation 18
    - Paramutation 19
4. **Co-transcriptional gene silencing in *S. pombe*** **20**
    - Constitutive heterochromatin 20
    - Mechanism of CTGS 21
    - Heterochromatin establishment; what comes first? 23
    - Temporal regulation of CTGS during the cell cycle 23
    - Facultative heterochromatin 23
    - Euchromatic RNAi targets 24

AIM OF THE THESIS **25**

RESULTS **27**

1. **RNAi represses stress response genes (Woolcock et al. 2012)** **28**
    - Summary 28
    - My contribution 29

2. **Elimination of heterochromatic RNA via HP1^{Swi6} (Keller et al. 2012) 30**
    - Summary 30
    - My contribution 30
3. **Dcr1 and Hsp104 regulate epigenetic robustness (Oberti et al. 2015) 32**
    - Summary 32
    - My contribution 32
4. **Swi6-mediated heterochromatin dynamics (Stunnenberg et al.) 34**
    - Summary 34
    - My contribution 35

DISCUSSION 36

1. **Heterochromatin propagation 37**
    - Swi6 and heterochromatin spreading 37
    - Chp2-mediated spreading 37
    - RNAi-mediated spreading 38
2. **Swi6-mediated heterochromatin boundary formation 39**
    - Swi6 inhibitory conformation 39
    - RNA-mediated Swi6 eviction 39
    - Epe1 recruitment 40
3. **Heterogeneity in heterochromatin regulation 41**
    - Diversity of DNA sequence elements at the boundaries 41
    - Pathway redundancy 41
4. **Balance between factors in border control 43**
    - Retaining balance to control heterochromatin integrity 43
    - Swi6 abundance dominates border dynamics 43

CONCLUSION 44

- Swi6 mediates heterochromatic RNA destruction 45
- Conservation 45

REFERENCES 46

ACKNOWLEDGEMENTS 59

APPENDIX 62

1. RNAi keeps Atf1-bound stress response genes in check at nuclear pores
   Woolcock et al., 2012, *Genes and Development*
2. HP1^{Swi6} mediates the recognition and destruction of heterochromatic RNA transcripts
   Keller et al., 2012, *Molecular Cell*
3. Dicer and Hsp104 function in a negative feedback loop to confer robustness to environmental stress
   Oberti et al., 2015, *Cell Reports*
4. H3K9 methylation extends across natural boundaries of heterochromatin in the absence of an HP1 protein
   Stunnenberg et al., 2015 *EMBO Journal*

SUMMARY

The genetic information that makes up an eukaryotic organism is encoded within DNA and wrapped around histone proteins, referred to as chromatin, and stored into the nucleus. In 1928, when light-microscopy pictures of the eukaryotic nucleus emerged, chromatin was divided into euchromatin and heterochromatin based respectively on light or dark stained areas. Euchromatin represented the open, dynamic structure, which was accessible for transcription and rich of protein-coding genes. Heterochromatin on the other hand was perceived as highly compact, static, transcriptional inert and gene-poor. However, this view was challenged by multiple lines of evidence, which show that heterochromatin is actually not such a rigid and silent structure. Transcripts emerged from so-called silent regions, RNA Polymerase occupancy was identified and even histone proteins showed to be mobile. All these finding let to a new concept of silent chromatin, which in fact can be dynamic, accessible and transcriptionally active, while concurrently remain repressed by different kinds of mechanisms.

One of these mechanisms is co-transcriptional gene silencing (CTGS) in fission yeast, which represents the main focus of our lab and comprises the work that I have done during my PhD. CTGS is an important mechanism that combines the actions of the RNA interference (RNAi) machinery together with chromatin modifying factors to ensure heterochromatin formation and silencing. The process embodies a paradox, as it requires transcription to keep the locus silent. Heterochromatic transcripts are processed by the RNAi machinery into small interfering RNAs (siRNAs) that guide RNA-induced transcriptional silencing (RITS) complexes back to the locus where they induce additional production of siRNAs and recruitment of histone modifying factors to repress the locus. It is a self-reinforcing feedback loop that ensures transmission of a heterochromatic state to subsequent generations.

During my PhD I focused on fission yeast heterochromatin protein Swi6, which is involved in CTGS and known to play an important role in silencing. Swi6 specifically binds to heterochromatic regions as it recognizes the repressive histone mark H3K9me and is thought to mediate heterochromatin spreading by forming an oligomer network. Such a model implies a structural role for Swi6 in heterochromatin formation of static nature. However, Swi6 and mammalian HP1 proteins have been shown to be highly dynamic, yet the reason and physiological relevance for this remained unclear. Moreover, such dynamics questioned a structural role for Swi6 in heterochromatin formation and spreading.

Driven by these finding, I set out to investigate the mechanism by which Swi6 mediates heterochromatin repression and focused on the *in vivo* dynamics as a functional read-out. Interestingly, *in vitro* data from our lab demonstrated that Swi6 exerts not only binding to H3K9me but also RNA, which resulted in its eviction off heterochromatin. Yet, RNA-binding was found to be required for silencing. These results led to a new working model in which Swi6 functions as a co-transcriptional checkpoint to mark and prime heterochromatic transcripts for RNA degradation. In addition, the model provided a possible explanation for the observed dynamics and was a good starting point for me to investigate the mechanism *in vivo*.

During my PhD I established a microscopy-based method, fluorescence recovery after photobleaching (FRAP), to measure *in vivo* dynamics of Swi6. Applying FRAP on endogenous EGFP-tagged Swi6, I confirmed rapid *in vivo* dynamics throughout the whole nucleus, with slower dynamics at heterochromatic loci compared to euchromatic areas. Fitting of the dynamic data to mathematical models revealed that only few Swi6 molecules, if any, are statically bound to heterochromatin, contrary to what was published before. Furthermore, FRAP on Swi6-EGFP in different mutant backgrounds demonstrated that RNA binding significantly decelerated Swi6 dynamics. Taking advantage of this feature, I used the dynamics as an indirect read-out for RNA production at the locus. Thereby, I was able to demonstrate that centromeres are permissive to transcription throughout the cell cycle; a question that has remained unanswered in the field. Importantly, the absence of a static population on heterochromatin challenged the existing models that infer a role for Swi6 in H3K9me spreading through formation of a rigid oligomeric network. In fact, H3K9me ChIP-seq experiments revealed that Swi6 was not required for H3K9me maintenance and even turned out to be dispensable for H3K9me spreading in certain regions. Yet, RNA expression data confirmed a role for Swi6 in repression. These results revealed unanticipated activities for Swi6 and supported a function in border control and heterochromatic RNA degradation, rather than a role in heterochromatin maintenance and spreading.

INTRODUCTION

1. 'Silent' chromatin in eukaryotes

Perspective on genomic features; from junk to regulation

The eukaryotic nucleus contains the genetic material necessary for the organism to develop, live and reproduce. The information is encoded within DNA, which is wrapped around histone proteins and packed into the cell nucleus. The genome was commonly divided into euchromatin and heterochromatin based on the compaction level seen respectively as light and dark stained areas (Heitz, 1928) (**Figure I**). Euchromatin was characterized as an open, dynamic, gene-rich and transcriptional active structure. In contrast, heterochromatin was generally seen as inaccessible, static, gene-poor and transcriptionally silent. Heterochromatin is a conserved feature of eukaryotes that is important for genome integrity and stability. It ensures proper chromosome segregation, nuclear organization, telomere stability, long-range chromatin interactions and regulation of gene expression (Grewal and Jia, 2007). Since the discovery of the first intron in 1977, everything but the gene-coding sequences (intergenic regions) in DNA was categorized as unimportant and received the term 'junk' DNA (Berk and Sharp, 1977). The only relevance that was given to intronic sequences was the potential to create different coding transcripts by alternative splicing events, while the remainder would be cut out and trashed. A big surprise came in 2001 when the human genome was sequenced and a surprisingly small percentage (±1%) of the genome revealed to consists of protein coding genes (Lander et al., 2001; Venter et al., 2001). Triggered by the question 'were does our complexity come from?' scientists revisited the view on junk DNA and the quest for relevance of intergenic regions took off. With the development of new techniques that allowed genome-wide analysis, a whole new spectrum of regulation was ready to be uncovered. From genome-wide RNA expression analysis it has become clear that the majority of DNA is being transcribed (Birney et al., 2007; Djebali et al., 2012; The ENCODE Project Consortium, 2004). Transcripts even emerged from so-called 'silent' heterochromatic regions (Azzalin et al., 2007; Li et al., 2008; Rouleux-Bonnin et al., 1996; Volpe et al., 2002). Moreover, intergenic regions did not only hold repeats and transposable elements (TE), but also non-coding RNAs and many other important regulatory elements that coordinate gene expression.

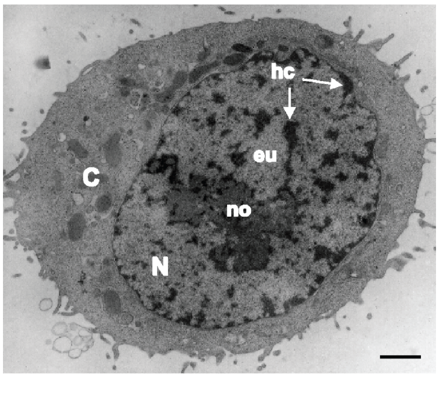

Figure I EM of a HeLa cell.
C: cytoplasm
N: nucleus
no: nucleolus
eu: euchromatin
hc: heterochromatin
(Cook, 2001)

Transcription factors

One of the important components that regulate gene expression are transcription factors (TFs). It all started in 1960, when Francois Jacob and Jacques Monod discovered the mechanism that controls the *lac* operon expression in *E. coli*. They found that the presence or absence of a molecule determined the transcriptional activity, which also seemed to be dependent on the DNA sequence surrounding the genes (JACOB and MONOD, 1961; Jacob et al., 1960). Later in 1981, the first eukaryotic transcription factor T-antigen of the SV40 virus was discovered (Tjian, 1981) and triggered the search for many more DNA binding factors. Before the discovery of chromatin modifications, TFs were thought to be the main actors of gene regulation. TFs are proteins that bind specifically to DNA sequences, called cis-acting elements, including gene promoters and more distal elements like enhancers to control gene expression. They function alone or in protein complexes by promoting or blocking recruitment of RNA polymerases to the locus to respectively activate or repress transcription. A recent study proposed that transcription factors and their sequence specificity are the foundation for determining transcriptional activity and create the boundaries between heterochromatin and euchromatin (Bulut-Karslioglu et al., 2012). Deletion of these TFs (Pax3 and Pax9) affected heterochromatin integrity and lead to an increase of major satellite repeats. However, the presence of a consensus DNA sequence is not enough for TF binding. Different studies have shown that accessibility and marks of active chromatin are necessary and precede TF binding (Guertin and Lis, 2013). There are also cases in which TFs are constitutively bound to their targets and get activated upon modification, like phosphorylation. In fission yeast, Atf1 is such a factor that targets stress response genes and plays an important role in silencing of the mating type locus (Jia et al., 2004; Kon et al., 1997).

Sir proteins

A great amount of knowledge on regulation of silent chromatin has come from studies in budding yeast. Budding yeast heterochromatin is found at mating type loci and telomeres. Here, DNA binding factors nucleate heterochromatin formation by binding to specific DNA sequences called silencer elements and recruit silent information regulatory (Sir) proteins to spread heterochromatin and ensure repression (Grunstein and Gasser, 2013). Sir proteins were identified in a screen for haploid sterility in which mutations impaired silencing of the mating type locus. In fact, mutations in *sir2*, *sir3* and *sir4* completely abrogate the ability to mate and demonstrated the necessity of these proteins for this region (Rine and Herskowitz, 1987). Heterochromatin formation is initiated by sequence specific binding of a TF that recruits Sir4. Through successive interactions between the different Sir proteins, the complex spreads in a sequence-independent manner throughout the locus (Grunstein and Gasser, 2013). The Sir-complex consists of nucleosome binding and modifying proteins that create a feedback loop that fuels heterochromatin propagation. A crucial part of the mechanism relies on the deacetylation of histone proteins by Sir2 that creates new binding sites for the Sir-complex to spread and ultimately lead to compaction of the locus (Imai et al., 2000).

Histones: more than just package material

Although histones have been discovered in 1884 by Albrecht Kossel, the significance of these proteins that were only seen as package material was revealed much later starting from the 1980s. Michael Grunstein was the first to demonstrate that histones have an important role in chromosomal segregation, replication and transcription *in vivo* (Han et al., 1987). The smallest unit of chromatin is the nucleosome consisting of 146bp DNA wrapped around a core of 8 histone proteins consisting of H2A, H2B, H3 and H4. It became clear that the degree of compaction influenced accessibility to factors needed for transcription (Knezetic and Luse, 1986; Lorch et al., 1987; Workman and Kingston, 1998). Anti-correlations were found between transcriptional activity and nucleosome occupancy within gene bodies and promoter regions (Bernstein et al., 2004; Lee et al., 2004; Sekinger et al., 2005). The importance of histone proteins became even more evident when the field became aware of the code within the package material of DNA. Histone tails perturbing from nucleosomes as well as the globular domains can be differentially modified and provide an additional layer of regulation for gene expression referred to as the epigenetic code.

The concept of epigenetics & stability

In Greek the term ‘epigenetics’ implies a code ‘over’ (epi) the genetic code that drives gene regulation. So, when people talk about epigenetics, they often refer to histone and DNA modifications. According to Ptashne this is a general misconception as it neglects the aspect of memory. Most of these modifications rely on constant signals and feedback to be maintained and inherited (Ptashne, 2013). The more complete description of epigenetics is “a change in the state of expression of a gene that does not involve a mutation, but that is nevertheless inherited in the absence of the signal or event that initiated the change”. Like the sequence information encoded within DNA, epigenetic marks can be passed on to the next generation, however, they also show plasticity as they can change during lifetime by environmental cues. Development itself can be seen as a form of epigenetics, since the observed changes in gene expression in different tissues occur without changes in the DNA sequence (Reik, 2007). But is this really epigenetic? It is true that during development some genes become transcriptionally activated and remain active even if the initial trigger is gone. Mostly, these kind of permanent states can be explained by constant maintenance due to the presence of positive feedback loops. In this case, only by studying the effects of removing recruiters can one tell whether histone modifications or other marks are self-perpetuating, or whether their continuing presence requires maintenance (Ptashne, 2013).

A well-studied phenomenon of an epigenetic stable inheritable change is vernalization. In short, vernalization is a cold induced epigenetic process that is necessary for the plants to flower after winter. It has been shown that longer periods of cold induce PRC2-mediated H3K27me, a repressive histone mark, on the floral repressor FLC gene. This mark gradually increases depending on the length of the cold period and ensures stable repression of the gene even after the cold is gone (Angel et al., 2011; Eichten et al., 2013).

Position effect variegation

Another well-known example of heritable gene regulation is position effect variegation (PEV). PEV was first discovered in *Drosophila* in 1930 in which the *white*-gene, required for red-pigmentation in the eye, showed a variegating red/white pattern when placed adjacent to centromeric heterochromatin (Muller, 1930). Comparably, placement of the *ade6+* gene into the central domain of centromeres in fission yeast resulted in red-white sectored colonies (Allshire et al., 1994). The color variegation observed in flies and fission yeast implied that some cells inherited the off-state while others switched back to the on-state. In contrast, insertion of marker genes in the outer repeats of the centromeric region established robust silencing over several generations (Allshire et al., 1995). Later it became clear that the observed instability of gene expression was induced by the neighboring conformational state of chromatin. Interestingly, the mechanism that ensures inheritance of the silent state in fission yeast is based on a positive feedback loop between transcription, RNA degradation and histone modifications as discussed in chapter 4.

Histone modifications

Histone modifications, unlike the DNA sequence, are subjected to changes and confer flexibility. Modifications include acetylation, methylation, phosphorylation, ubiquitination and sumoylation. Each of these marks create binding sites for a variety of chromatin binding factors and play a role in regulation of many different processes (Bannister and Kouzarides, 2011). Acetylation is generally associated with an active mark, as methylation mostly correlates with gene repression depending on the residue. From a chemical point of view, acetylated histones create a more open conformation with DNA due to repelling charges and have shown to facilitate histone displacement (Reinke and Hörz, 2003). Hypoacetylation and methylation on the other hand are important for higher order chromatin compaction.

A hallmark of heterochromatin is di- and tri-methylated histone H3 lysine 9 (H3K9me) and lysine 27 (H3K27me). The histone methyltransferase (HMTase) Suv39 methylates H3K9 and creates binding sites for chromodomain containing proteins like heterochromatin protein HP1 (Bannister et al., 2001; Carroll et al., 2000; Lachner et al., 2001). HP1 proteins are highly conserved and play an important role in silencing. Similar to Sir proteins, HP1 are thought to spread sequence-independently throughout the locus by dimerization and chromatin interactions as further discussed in chapter 2. H3K27 trimethylation is a mark set by the HMTase EZH2, which is part of the polycomb repressor complex 2 (PRC2) (Cao and Zhang, 2004). A classic and striking example in which histone modifications lead to stable repression and compaction is X-chromosome inactivation.

X-chromosome inactivation

X-chromosome inactivation (XCI) takes place in female cells to compensate for the dosage difference in males where only one X chromosome is present. XCI is regulated by a single cis-acting region called the X-inactivation center (XIC) (Brown et al., 1991). Yet, the mechanism, as far as understood, is remote from simple as multiple different pathways come together to regulate this process. The XIC harbors non-coding RNAs Xist and its antisense partner Tsix that induce or inhibit XCI respectively (Brockdorff et al., 1992; Brown et al., 1992; Lee and Lu, 1999; Lee et al., 1999). Interestingly, Xist decorates the inactive X-chromosome and functions as a recruitment platform for PRC2 to deposit the repressive H3K27me3 mark (Zhao et al., 2008). Furthermore, actual nucleation of the X-inactivation involves a transcription factor called YY1 (Jeon and Lee, 2011). On the other hand, Tsix recruits DNA methyltransferase activity to silence Xist on the active X chromosome (Sado et al., 2005; Sun et al., 2006). It's a complex interplay between non-coding RNAs, chromatin modifying factors as well as transcription factors to establish and maintain silencing (Lee and Bartolomei, 2013).

DNA methylation

Besides the action of transcription factors and histone modifications, gene expression is also regulated on the level of DNA methylation. In contrast to histone modifications, DNA methylation is seen as a rather long-term stable epigenetic mark. DNA methyltransferases (DNMTs) methylate cytosine bases typically in a CpG context. The mammalian genome is globally methylated in the majority of cell types with exceptions of CpG-rich regions (so-called CpG-islands (CGI)) at promoters, enhancers and TF binding sites (Baubec and Schübeler, 2014). Methylation of promoters is generally associated with gene repression. Interestingly, differentiation of a pluripotent stem cell into a lineage-committed cell is accompanied by changes in methylation patterns. Pluripotency-associated genes are methylated and stably silenced while developmental genes are activated by transcription factors (Feng et al., 2010). Once the mark is set by the *de novo* DNA methyltransferases DNMT3A/B, DNMT1 maintains the mark during cell division and ensures epigenetic memory. However, also DNA methylation can be erased by active enzymatic processes and passively by replication. In fact, during mammalian germ cell and early embryo development genome-wide epigenetic reprogramming takes place, which entails erasure of DNA methylation as well as histone modifications (Feng et al., 2010). Remarkably, some sequences in the genome are resistant to demethylation. These include members of the intracisternal A particle (IAP) retrotransposon family and adjacent CGI, as well as 250 CGIs in the genome, which are variably erased (Seisenberger et al., 2012). Also differentially methylated regions in imprinted loci show resistance against the wave of demethylation of the primordial germ cells and in the early embryo (Lee et al., 2014). In this way, epigenetic information can spill over to the next generation in a parent-specific way (Reik, 2007). However, since only few areas are resistant to the large-scale erasure most of the epigenetic marks that were acquired during life are not inherited, speaking against the original concept of epigenetics.

2. Chromatin Dynamics

Chromatin organization in the nucleus

Proper establishment of heterochromatic domains is important for regulation of gene expression, chromosome segregation and genome integrity. But, how is chromatin generally organized in the nucleus and what is the physiological relevance?
Unlike the simple thought that DNA is randomly distributed in the nucleus like a pool of spaghetti, or the opposing idea of rigid compartmentalization provoked by compaction due to limited space in the nucleus, the current knowledge implies rather a degree of chromatin organization that is in between these two extremes. Whereas large rings of chromatin diffuse freely through the nuclear volume, the nucleus can maintain functional subcompartments enriched for specific enzymes and chromatin states (Taddei and Gasser, 2012). Chromatin folding is determined by three factors: local compaction, long-range interactions and anchoring to nuclear scaffolds (van Steensel, 2011).

Chromatin interactions

Compaction is created by wrapping DNA around a series of nucleosomes coated by proteins that keep it dense. Several factors influence the compaction including chromatin remodeling and modifying proteins. A well-known compartment is the nucleolus, which is formed by ribosomal DNA and proteins involved in transcription and ribosomal particle formation (Scheer and Weisenberger, 1994). It is thought that compartmentalization and local high concentrations of factors promote the efficiency of occurring processes. Interactions between different chromatin regions have also been implicated in heterochromatin-euchromatin boundary formation. For instance, in fission yeast different boundary elements are bound by a common transcription factor TFIIIC which prevents H3K9me spreading, but also promotes clustering and ensures localization to the nuclear periphery (Noma et al., 2006). A recently developed technique, conformational chromatin capture (3C), revealed long-range interactions between regions within the same (intra) and different chromosomes (inter), of which the latter was less frequent (Lieberman-Aiden et al., 2009). Including previously observed interactions between telomeres and clustering of centromeres, 3C-based methods revealed interactions between regulatory elements like promoters and enhancers (Lieberman-Aiden et al., 2009; Thurman et al., 2012).

Role of the nuclear scaffold

Budding yeast centromeres also cluster, but in addition have a defined localization in the nucleus as they associate to the spindle pole body at the nuclear membrane (Guacci et al., 1997; Jin et al., 2000). Actually, a large part of chromatin organization is shaped by interactions with the nuclear membrane via nuclear lamins (NL) (however absent in yeast) and association to nuclear pores. Molecular mapping studies have shown that the genomes of *Drosophila*, mouse and humans interact extensively with the NL, via so-called lamina-associated domains (van Steensel, 2011). Whereas association to NL often correlates with gene repression, active genes tend to associate with nuclear pore complexes (Akhtar and Gasser, 2007). Nuclear membrane associations show dynamic properties as hundreds of genes were observed to move towards or from the NL during differentiation (Peric-Hupkes et al., 2010). Typically, heterochromatin is rather associated to the nuclear periphery, while euchromatin resides in the nucleoplasm (Kosak et al., 2007). Intriguingly, in rod photoreceptor cells of nocturnal animals this pattern is inverted as heterochromatin is found at the interior while euchromatin is at the rim of the nucleus. The inversion correlates with the absence of certain nuclear lamina proteins that have a role in anchoring heterochromatin (Solovei et al., 2009, 2013). Interestingly, nocturnal animals benefit from this nuclear architecture as it increases their visual power in the dark. Another example providing physiological relevance to chromatin organization and dynamics comes from studies in budding yeast where chromatin mobility is induced during double strand break repair. The increased mobility is suggested to benefit homologous recombination, as the chance to encounter its homologous target sequence is higher (Dion et al., 2012).

Histone dynamics

Even though chromatin is perceived as a rigid structure, histone-DNA interactions must be loosened to some extent to allow access to factors involved in replication, transcription and DNA repair. This can be achieved by replacement of nucleosomes by chromatin remodeling factors or active DNA unwinding (Bell et al., 2011). In addition, DNA seems to exert random movement that occasionally loosens the interactions to histones and locally denatures dsDNA referred to as DNA breathing (Choi et al., 2004). On top of nucleosome displacement, radiochemical labeling and *in vivo* photobleaching experiments revealed dynamic exchange of histone proteins (Kimura and Cook, 2001; Lever et al., 2000; Misteli et al., 2000). Even though 80% of the H3 and H4 population appeared to be immobile and tightly bound over a short period of time (seconds to minutes), FRAP over hours revealed slow exchange. In contrast, core histone H2B manifested in addition to slow exchange (40%), rapid exchange in the order of minutes (3%) (Kimura and Cook, 2001). This high mobility fraction is suggested to correlate to gene activity. In comparison to core histones, linker histone H1, which binds extranucleosomal DNA, exchanges continuously with a residence time of a few minutes even in heterochromatin or mitotic chromosomes (Kimura, 2005; Lever et al., 2000; Misteli et al., 2000). H1 is proposed to compete with chromatin binding factors underscoring the relevance for the observed mobility (Catez et al., 2002).

Histone variants

Another level of dynamic regulation comes from the incorporation of histone variants. Incorporation of canonical histones (H3, H4, H2B, H2A) is mostly restricted during S-phase, yet histone variants are independent of DNA replication and are expressed throughout the cell cycle. Histone variants are often connected to different kind of processes and mark specific regions. For instance, turnover of histone variant H3.3 highly correlates with active gene bodies, epigenetic regulatory elements and replication origins in *Drosophila* cells (Deal et al., 2010), while H3 variant CenH3 marks centromeric heterochromatin and creates a platform for kinetochore assembly (Dalal et al., 2007). Yet, another interesting example of histone replacement is observed in mammalian spermatogenesis. Here, sperm chromatin undergoes a series of remodeling events that are mediated by S-phase histones, histone variants, transition proteins and protamines. The result of these elaborate processes is transcriptionally inert mature sperm DNA, which holds the most highly condensed DNA structure known (Ooi and Henikoff, 2007). Upon fertilization, histones are reincorporated and DNA is decondensed and made compatible with somatic cellular processes.

Heterochromatin protein HP1 dynamics

Besides chromatin domain organization and histone exchange, yet another layer of dynamic regulation can be found in chromatin binding factors. A hallmark for heterochromatin is methylated H3K9 which is typically recognized by heterochromatin protein HP1 (Bannister et al., 2001; Lachner et al., 2001; Nakayama et al., 2001). HP1 was initially identified as a protein predominantly associated with heterochromatin in a study using immunofluorescence staining of the polytene chromosomes of *Drosophila* (James and Elgin, 1986). HP1s are highly conserved proteins from yeast to humans that play important roles in chromosome segregation, long-range chromatin interactions, genome stability, gene silencing, and heterochromatin formation (Grewal and Jia, 2007; Zofall et al., 2009). Although most of its functions are related to gene repression and formation of a compact chromatin structure, there are also reports of HP1 proteins having a role in gene activation (Lomberk et al., 2006a; Piacentini et al., 2003).

HP1 typically consist of a chromodomain (CD), a flexible hinge region and a chromoshadow domain (CSD). The CD recognizes methylated H3K9, while the CSD is thought to mediate dimerization and other protein interactions (Bannister et al., 2001; Brasher et al., 2000; Cowieson et al., 2000; Lachner et al., 2001; Smothers and Henikoff, 2000). Often HP1 has multiple homologs. Whereas *Drosophila* has 5 homologs, humans have 3 HP1 isoforms and fission yeast encodes two HP1s: Swi6 and Chp2 (Lomberk et al., 2006b). Budding yeast, however, lacks HP1 orthologs and does not utilize H3K9me to establish domain silencing, yet relies on the action of the Sir-complex. Here, establishment of silent domains is nucleated at specific elements but shows sequence-independent spreading mediated by oligomerization of Sir proteins and their interaction to chromatin. The work done in budding yeast provided a mechanistic basis for understanding the assembly of heterochromatin in other eukaryotes (chapter 1).

As such, a similar model inspired by the budding yeast system and based on fission yeast heterochromatin protein Swi6, was proposed to apply for HP1-mediated heterochromatin spreading. Through the combined action of H3K9me binding and the ability to form dimers, Swi6 is suggested to form higher-order oligomeric networks that promote H3K9me spreading (Canzio et al., 2011). Furthermore, *in vitro* data implicated the existence of a spreading-inhibiting Swi6 dimer conformation, which could potentially function in boundary control (Canzio et al., 2013). In this case, dimerization occurs between the two CSDs and the CDs, which restricts binding of the chromodomain to H3K9me (**Figure II**). However, this particular conformation requires a specific structure that is not conserved in the other HP1 (Canzio et al., 2013). Generally, iterative HP1 binding to methylated H3K9 and recruitment of histone methyltransferase (HMTase) activity is the prevalent model for heterochromatin spreading (Eissenberg and Elgin, 2014). Such a model implies the existence of an immobile fraction, yet the opposite has been reported.

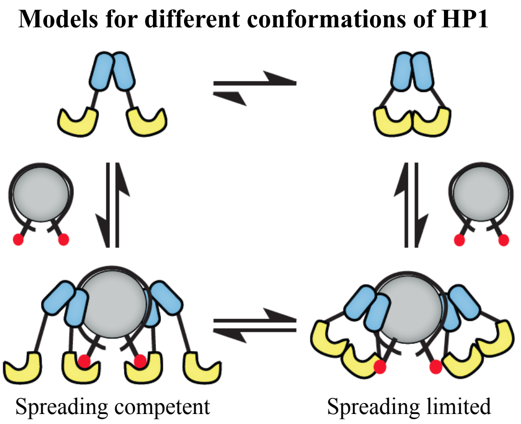

Figure II Association of different Swi6 conformations with nucleosomes. blue: Swi6 CSD, yellow: Swi6 CD, red: H3K9me, grey: nucleosome (Canzio et al., 2014)

While mammalian HP1s displayed exchange rates within minutes, dynamics in the range of seconds have been monitored in fission yeast (Cheutin et al., 2003, 2004; Festenstein et al., 2003). Generally, HP1s demonstrated to have shorter residence times in euchromatin than in heterochromatin. This was expected considering their binding affinity towards H3K9me. In addition to H3K9me binding, fission yeast HP1 Swi6 has recently been reported to bind RNA, which is required for heterochromatin silencing (Keller et al., 2012). In this model, Swi6 captures and primes heterochromatic transcripts for RNA decay by handing them over to the RNA degradation machinery. Interestingly, RNA binding results in the eviction of Swi6 off heterochromatin and provides a possible explanation for the observed dynamic nature (**Figure III**). Binding affinity towards RNA has also been proposed for human HP1alpha (Maison et al., 2011), yet also here, any influence on the dynamics remains to be determined. Noteworthy, while RNA binding was shown to evict Swi6 off heterochromatin, it is suggested to recruit HP1alpha to heterochromatin.

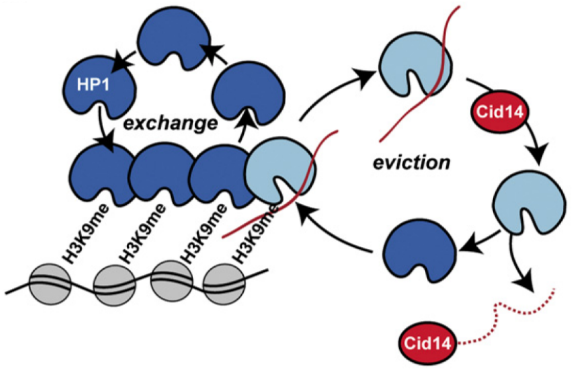

Figure III Model for $HP1^{Swi6}$-mediated degradation of heterochromatic RNA. $HP1^{Swi6}$ (dark blue) rapidly exchanges with H3K9me nucleosomes (grey). Transcribed RNAs (red) associate to $HP1^{Swi6}$ and cause a conformational change (light blue), which evicts $HP1^{Swi6}$ of heterochromatin due to competition between RNA and H3K9me. The RNA is passed on to Cid14 (red), which initiates RNA degradation. (Keller et al., 2012)

So far, I have shed light upon the different levels of regulation that come together to ensure repression of heterochromatic regions. I challenged the view of heterochromatin as a rigid, inaccessible and transcriptional inert structure and discussed different dynamic processes that occur within so-called silent chromatin. Not only do we find exchange of histones and mobility of chromatin binding factors, but also accessibility for the transcription machinery. Remarkably, in some cases transcriptional activity is even found to be required in order to sustain repression. In the next chapter I will discuss the role of RNA and the RNAi machinery in silencing and heterochromatin formation.

3. RNA interference and silencing

RNA interference (RNAi) was first discovered in *Caenorhabditis elegans* and plants as a gene-silencing pathway that is mediated by double-stranded RNA (dsRNA) (Fire et al., 1998; Hamilton, 1999). Originally, RNAi was defined as a post-transcriptional gene silencing (PTGS) process that relies on base paring between a short antisense RNA and its target sequence resulting in translational inhibition and/or cytoplasmic mRNA degradation. PTGS is important for gene regulation, virus defense and transposon silencing. Besides PTGS, RNAi is known to mediate silencing on a transcriptional level, by mechanisms called transcriptional gene silencing (TGS) and co-transcriptional gene silencing (CTGS). A common feature of the RNA-silencing pathway is the binding of small RNAs (sRNAs) to Argonaute (Ago) family effector proteins. RNA/Ago-complexes, generally known as RNA-induced silencing complexes (RISC), are guided to their complementary targets via sRNA base pairing and often lead to target cleavage or functional inhibition (Hammond et al., 2000; Zamore et al., 2000) (**Figure IV**). Below, I will introduce the different pathways and dedicate a separate chapter to CTGS in the fission yeast *S. pombe* since it comprises the work I have done during my PhD.

Post-transcriptional gene silencing

PTGS regulates gene expression by targeting transcripts in the cytoplasm using different classes of small RNAs. In this paragraph, I will focus on siRNAs and miRNAs, but will dedicate a separate section to piRNAs later on. Both siRNAs and miRNAs are generated from dsRNA precursors derived from non-coding transcripts that fold back into defined hairpin structures (miRNAs and siRNAs) or form long dsRNA duplexes (siRNAs) (**Figure IV**). Biogenesis of siRNAs is mediated by Dicer, a dsRNA-specific RNase III family ribonuclease, which processes long dsRNAs into small interfering RNAs (siRNAs) (Bernstein et al., 2001). siRNAs have a size of 20 to 25nt and show perfect sequence complementarity to its target. The Ago-complexes loaded with siRNAs guide target cleavage and degradation. Biogenesis of miRNAs typically follows a path that involves initial processing of hairpin precursor RNAs by the ribonuclease III Drosha into short hairpin RNAs (also referred as pre-miRNAs) followed by transport into the cytoplasm and sequentially processing by the RNAse III nuclease Dicer **(Figure IV)** (Ghildiyal and Zamore, 2009). miRNAs are ±22nt long and do not necessarily rely on full sequence complementarity of its target, but often require base pairing of only few nucleotides to exhibit translational repression and/or target instability (Brennecke et al., 2005). This results in a variety of different target mRNAs for only one miRNA and provides a wide spectrum of regulation, which, however, is challenging to predict. An important feature for target selection is the seed region at the 5-prime of the miRNA (Lewis et al., 2003, 2005). The sequence is about 7nt long and typically targets complementary sites on the 3-prime UTR of the mRNA. Binding of RISC to its mRNA target recruits destabilization factors, like deadenylation factors, and exerts translation repression (Krol et al., 2010).

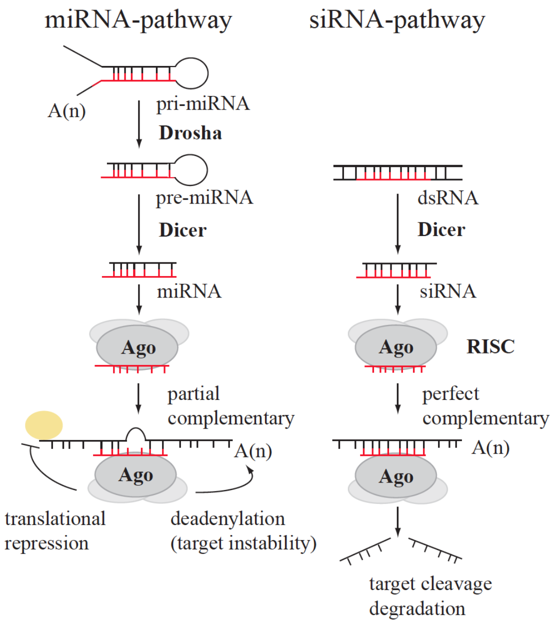
miRNA-pathway
siRNA-pathway
A(n)
pri-miRNA
Drosha
pre-miRNA
Dicer
miRNA
Ago
partial
complementary
A(n)
Ago
translational
repression
deadenylation
(target instability)
dsRNA
Dicer
siRNA
Ago
RISC
perfect
complementary
A(n)
Ago
target cleavage
degradation

Figure IV Basic components of the miRNA- and siRNA-pathway. The source of miRNAs and siRNAs are long hairpin RNAs (pri-miRNAs) or long dsRNAs respectively. pri-miRNAs are processed by Drosha into pre-miRNAs. Dicer processes both dsRNAs and pre-miRNAs into mature miRNAs or siRNAs, which are loaded into Ago-complexes (RISC). The RNA/Ago-complexes are guided to their targets by base pairing that results in translational repression and target instability or target degradation depending on the complementarity.

The piRNA pathway

The piRNA pathway was first discovered in the germ line of the fly *Drosophila melanogaster* where sRNAs of 25-30 nt were proposed to ensure germline stability by repressing transposable elements (TEs) (Lander et al., 2001). piRNAs are different from miRNAs and siRNAs as they bind to the Piwi clade of Argonaute proteins and are produced in a Dicer-independent manner. piRNAs map to genomic loci called piRNA clusters, which act as heritable repositories that store sequence information of TEs that are or have been active in a population (Brennecke et al., 2007). Transcription of the piRNA clusters gives rise to long, single stranded RNA precursors that are the source of piRNAs. The biogenesis of piRNAs is mediated by the so-called 'ping-pong cycle' (Aravin et al., 2007; Brennecke et al., 2007; Gunawardane et al., 2007). The ping-pong cycle is a feed-forward amplification mechanism based on consecutive interactions between different Piwi proteins, piRNAs and their transposon targets. In the cytoplasm, piRNA precursors are processed by unknown mechanisms into short 23-29 nt antisense piRNAs that have a strong 5'-uridine bias and bind to PIWI or Aubergine (AUB) (Castel and Martienssen, 2013). The Piwi-RNA complexes target and cleave complementary transposon mRNAs and create sense piRNAs, which in turn are bound by AGO3. The circle closes when RNA-loaded AGO3 directs cleavage of primary piRNA precursors thereby creating new antisense piRNAs for AUB/PIWI to target active transposons **(Figure V)**. Interestingly, also HP1 proteins, HMTs and H3K9me have been linked to the piRNA pathway and the repression of transposons (Klattenhoff et al., 2009; Rangan et al., 2011).

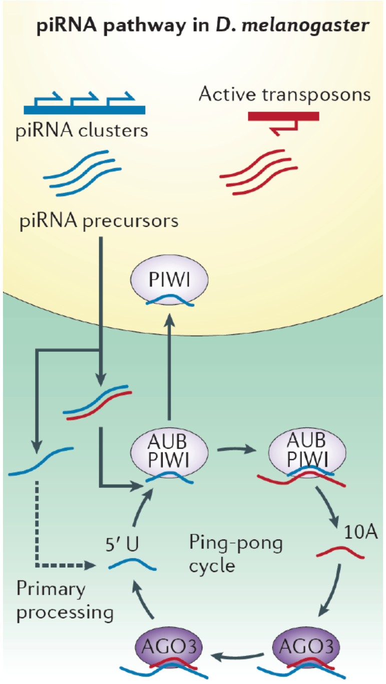

Figure V piRNA biogenesis pathway via the ping-pong cycle in the *D. melanogaster* female germ line. Primary precursor piRNA antisense to active transposons (blue) is transcribed from heterochromatic piRNA clusters and sense mRNA from active transposons (red). In the cytoplasm, primary processing generates antisense piRNAs (which have a 5′ uridine (5′ U)) from a primary precursor that is then loaded into AUB or PIWI and cleaves sense transposon mRNA to produce sense piRNAs, which have a strong adenine bias at position 10 (10A). Additional antisense piRNA is produced by AGO3-mediated cleavage of antisense primary piRNA transcripts, completing the cycle. Only loaded PIWI is imported into the nucleus. (Castel and Martienssen, 2013)

Transcriptional gene silencing in plants

In plants, as in other eukaryotes, transposable elements and repeated sequences are silenced in every generation by mechanisms that include DNA hypermethylation and/or histone modification that contribute to a chromatin state refractory to transcription (Blevins et al., 2014; Matzke et al., 2009). Interestingly, in 1994 it was first recognized that viral RNAs induce *de novo* methylation of genomic sequences (Wassenegger et al., 1994), however the connection to RNAi was unclear. Nowadays, the RNA-directed DNA methylation (RdDM) pathway in *Arabidopsis thaliana* represents a well-studied example of a direct link between the RNAi pathway and heterochromatin formation.

RNA-directed DNA methylation

The RdDM pathway involves two main phases: an upstream siRNA biogenesis phase and a downstream methylation targeting phase. RdDM is initiated by RNA polymerase IV (Pol IV) transcription of single stranded RNAs (ssRNAs) coming from repetitive genomic sequences including transposons and centromeric repeats (Herr et al., 2005; Kanno et al., 2005; Onodera et al., 2005). These ssRNAs are converted into dsRNAs by the action of RNA-dependent RNA Polymerase 2 (RDR2) and Dicer-like endonuclease 3 (DCL3) (Pontes et al., 2006; Xie et al., 2004). Although the actual repression takes place on chromatin in the nucleus, dsRNAs are initially transported to the cytoplasm and loaded into Argonaute 4 (AGO4) before transported back into the nucleus (Ye et al., 2012). This additional step is suggested to function as a quality-control mechanism for maturation of the complex in which the passenger strand is released and induces a conformational change in Ago4 that leads to its nuclear import **(Figure VI)**. In the nucleus, the mature siRNA/AGO4-complex is guided to nascent RNA Pol V transcripts via base pairing where it recruits of de novo DNA methyltransferase DRM2 and other chromatin-modifying factors, which deposit cytosine methylation and repressive histone modifications on the target locus (Cao and Jacobsen, 2002; Li et al., 2006; Qi et al., 2006; Wierzbicki et al., 2008). Both, the recruitment mechanisms of DNMTs as well as the connection between DNA methylation and methylation of histone tails were initially elusive. Though, recent publications by the Jacobsen lab shed light on this matter by demonstrating interactions between: Pol IV and a chromatin reader that recognizes both H3K9me and unmethylated H3K4 marks (Law et al., 2013, 2011), Pol V and a DNA-methyl binding protein (Johnson et al., 2014) and DRM2 and AGO4 (Zhong et al., 2014). These additional links further define the RdDM mechanism to entertain a self-reinforcing feedback loop that ensures heterochromatic silencing through the interplay of multiple pathways on different regulatory levels.

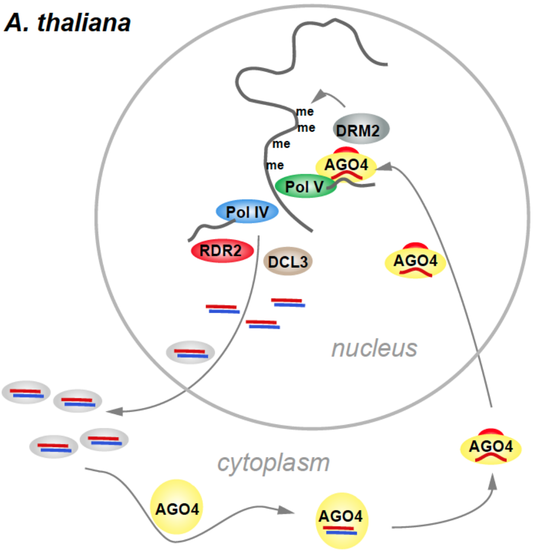

Figure VI Model of RdDM in *A. thaliana*. RNA polymerase IV (Pol IV) transcripts are processed by RDR2 and DCL3 into siRNAs that are transported to the cytoplasm. siRNAs are loaded into Ago4, which adopts a different conformation upon maturation of the siRNA/Ago4-complex resulting in nuclear import. Nuclear siRNA/Ago4-complexes are guided to RNA polymerase V (Pol V) nascent transcripts by complementary base pairing and direct interaction with Pol V and recruit DNA methyltransferase DMR2 to methylate the locus. Adapted from (Stunnenberg and Bühler, 2012).

Paramutation

Early on, in the 1950s, a phenomenon called paramutation was first described in maize showing non-Mendelian inheritance of modified gene expression that was not found in the primary context of the DNA (Brink, 1956). Paramutation occurs as a consequence of interallelic talk in which one allele (paramutagenic allele) induces a change in expression of the other allele (paramutable allele) that in turn becomes itself paramutagenic in the subsequent generation. Interestingly, mutational analyses in maize implied the requirement of components of the RNAi biogenesis pathway for paramutation and often showed dependence on the presence of tandem repeats, which at the same time fulfilled an enhancer role for gene expression (Alleman et al., 2006; Chandler, 2007; Kermicle et al., 1995; Sidorenko et al., 2000; Stam et al., 2002). Although these findings lead to the hypothesis that siRNAs themselves mediate paramutation interactions, an assessment of existing data supported the opinion that siRNAs alone are insufficient (Erhard and Hollick, 2011). For example, reports showed that the mere presence of tandem repeats and their corresponding siRNAs is not always enough to induce paramutation (Chan et al., 2006). Similar to the RdDM pathway, DNA methylation has been found at the sites of paramutation (Eichten et al., 2013; Regulski et al., 2013), however a clear link is yet missing.

4. Co-transcriptional gene silencing in *S. pombe*

Constitutive heterochromatin

Constitutive heterochromatin is defined as a chromosome region that is permanently condensed and silenced. In the fission yeast *S. pombe* constitutive heterochromatin is found at telomeres, centromeres and the mating type locus. Heterochromatin plays an important role for genome integrity and ensures proper chromosome segregation as well as mating type switching (Allshire et al., 1995; Grewal and Klar, 1997). Centromeres are made up of a large structure of repetitive sequences facing different orientations that surround the central core (Clarke and Baum, 1990; Fishel et al., 1988). The repetitive domains are assigned as the inner repeats (*imr*) and outer repeats (*otr*), in which the latter has two distinct repetitive elements called the *dg* and *dh* that are similar on all chromosomes, however vary in the number and orientation **(Figure VII)**. The mating type locus contains a region with high sequence-similarity to centromeric *dg/dh* repeats referred to as *cenH* (centromeric homology) (Grewal and Klar, 1997). Moreover, *tlh1* and *tlh2* genes located at the ends of chromosome 1 and 2 have high homology to the *cenH* sequence (Kanoh et al., 2005). These repeat elements are thought to nucleate heterochromatin formation through the action of the RNAi machinery (Hall et al., 2002). The RNAi pathway is important for heterochromatin establishment, however functions redundantly in maintenance of certain regions. Redundancy at the mating type locus comes from transcription factors Atf1/Pcr1 (Jia et al., 2004), while the telomere repeat-binding protein Taz1 acts redundant at telomeres (Kanoh et al., 2005). Also on the post-transcriptional level there are factors, other than the RNAi machinery, that process RNA transcripts to prevent translation. The TRAMP complex, including the noncanonical poly(A) polymerase Cid14, is necessary for robust heterochromatic gene silencing by polyadenylating and priming transcripts for degradation by the exosome (Bühler et al., 2007). Besides constitutive heterochromatin, other heterochromatic loci have been described to use alternative sets of RNAi components for heterochromatin formation. In the following paragraphs, I will discuss the co-transcriptional gene silencing (CTGS) mechanism of constitutive heterochromatin, then describe the role of RNAi components in a different type of heterochromatin, and last, but not least, end with a surprising role of RNAi-mediated repression of euchromatic genes.

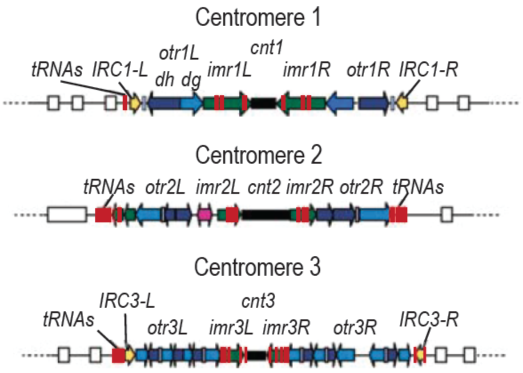

Figure VII Physical maps of *S. pombe* centromeres. otr: dh (dark blue), dg (light blue); imr (green); tRNAs (red); ORFs (open boxes); Inverted repeat elements flanking cen1 (IRC1-L/R) and cen3 (IRC3-L/R) (yellow arrows). Adapted from (Noma et al., 2006).

Mechanism of CTGS

Unlike other eukaryotes, fission yeast does not possess DNA methylation and relies on transcriptional gene silencing involving histone modifications and processing of noncoding transcripts to acquire heterochromatin silencing. This process is named co-transcriptional gene silencing (CTGS) and shows great importance for components of the RNAi machinery. In CTGS, nascent heterochromatic RNAs are transcribed by RNA Polymerase II (Pol II) and serve as a template for generation of dsRNAs by the RNA-dependent RNA polymerase complex (RDRC) containing the RNA-dependent RNA polymerase Rdp1 (Motamedi et al., 2004) (**Figure VIII**). The dsRNAs are processed by Dicer (Dcr1) into siRNAs and loaded into Argonaute (Ago1). Ago1 initially forms a complex with Arb1 and Arb2 (ARC complex) that is suggested to regulate the conversion of duplex siRNA to single-stranded siRNA by inhibiting the Ago1 intrinsic slicer activity (Buker et al., 2007; Irvine et al., 2006). siRNA-bound Ago1 is handed over to the RNA-induced transcriptional silencing (RITS) complex consisting of Tas3 and chromodomain protein Chp1 (Verdel et al., 2004). After release of the passenger strand, the mature RITS complex is guided back to the site of transcription via complementary base pairing with the nascent transcript and interaction of Chp1 with H3K9me (Bühler et al., 2006; Schalch et al., 2009). Furthermore, RITS was shown to interact with RDRC fueling the production of dsRNA (Colmenares et al., 2007; Motamedi et al., 2004). Importantly, concomitant recruitment of the CLRC complex, containing the sole histone lysine H3 methyltransferase Clr4, establishes H3K9 methylation of the locus and provides a direct link between the RNAi pathway and heterochromatin (Bayne et al., 2010; Zhang et al., 2008). H3K9me promotes binding of the HP1 proteins Swi6 and Chp2 to stabilize and spread the repressive mark. Both, Chp2 and Swi6 recruit the Snf2-histone deacetylase repressor complex (SHREC) holding the histone deacetylase Clr3, which deacetylates H3K14ac (Sadaie et al., 2008; Sugiyama et al., 2007; Yamada et al., 2005). Histone deacetylation limits the access of Pol II but promotes binding of chromodomain proteins like Clr4, Chp1, Chp2 and Swi6 to spread H3K9 methylation (Alper et al., 2013). In addition to Clr3, *S. pombe* contains histone deacetylases (HDACs) Clr6 and Sir2 that are required for heterochromatin silencing (Alper et al., 2013; Freeman-Cook et al., 2005; Shankaranarayana et al., 2003). CTGS represents a self-enforcing positive feedback loop that manages to keep the balance between transcriptional activity and RNAi- and chromatin-mediated repression (**Figure VIII**).

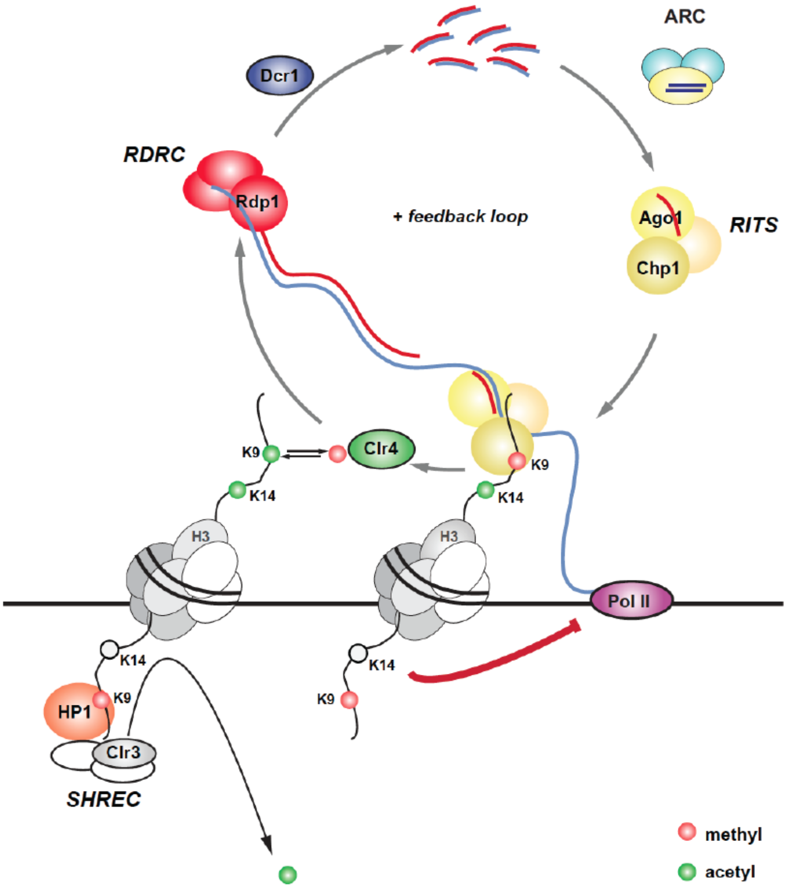
ARC
Dcr1
RDRC
Rdp1
+ feedback loop
Ago1
RITS
Chp1
Clr4
K9
K14
K9
K14
H3
H3
Pol II
K14
K9
HP1
Clr3
SHREC
K14
K9
● methyl
● acetyl

Figure VIII Model for co-transcriptional gene silencing in *S. pombe*. RITS (yellow) is guided by Dcr1-dependent siRNAs from the centromeric repeats to nascent Pol II transcripts via base pairing. RITS recruits Clr4 (green), which mediates H3K9 methylation (red balls). H3K9me stabilizes RITS association via Chp1 binding and creates binding sites for HP1 proteins (orange), Swi6 and Chp2. Chp2 recruits the SHREC complex containing the Clr3 histone deacetylase. Deacetylation of H3K14 reduces transcription. Furthermore, RITS helps to recruit RDRC resulting in more dsRNA substrates for Dcr1. dsRNAs are loaded initially into the ARC complex and then into RITS, which closes the feedback loop of CTGS. Adapted from (Woolcock, 2012)**.**

Heterochromatin establishment; what comes first?

Having a positive feedback loop raises the question about the origin of the process. It is debated if the initial trigger is preexisting H3K9me or RNA. Arguments that put methylation upstream of the RNAi pathway come from studies that show heterochromatin establishment while bypassing the RNAi machinery when tethering Clr4 to euchromatic loci (Kagansky et al., 2009). In addition, *clr4*Δ cells showed depletion of H3K9me accompanied by loss of silencing, while some methylation remained in *dcr1*Δ (Sadaie et al., 2004; Shanker et al., 2010). On the other hand, Clr4 deletion did not diminish siRNAs coming from centromeric *dg* repeats demonstrating H3K9me-independent production of heterochromatic RNAs (Bayne et al., 2010; Halic and Moazed, 2010), which could likewise represent the initial trigger for CTGS. These so-called primal RNAs are Dcr1-independent however depend on Argonaute. Supporting this hypothesis, tethering of RITS to native euchromatic *ura4+* transcript is sufficient, however inefficient, to induce silencing, recruit heterochromatin proteins, and generate siRNAs (Bühler et al., 2006). Suggested sources for dsRNAs include transcripts that form hairpin structures, Rdp1-mediated dsRNA synthesis and bidirectional transcription of repetitive elements, which nucleate heterochromatin formation (Djupedal et al., 2009; Halic and Moazed, 2010; Marasovic et al., 2013).

Temporal regulation of CTGS during the cell cycle

The positive feedback loop of CTGS raises an additional question as the mechanism represents a paradox: Why transcribe in order to silence?
A possible explanation came from the study by Kloc et al. in which they propose a temporal separation for transcription followed by RNAi-mediated degradation of heterochromatic transcripts and heterochromatin-mediated repression. In this model, H3S10 phosphorylation leads to dissociation of Swi6 from chromatin during M-phase (Chen et al., 2008), which opens up a window for transcription of centromeric RNAs. These transcripts are, however, immediately processed and degraded by the RNAi machinery in G1/S-phase. Subsequent recruitment of heterochromatic factors reestablishes a silent chromatin state and renders the RNAi machinery dispensable for the remaining G2-phase (Kloc et al., 2008).

Facultative heterochromatin

Besides euchromatin and constitutive heterochromatin, there are regions in the genome that occasionally adopt an open or closed chromatin structure referred to as facultative heterochromatin. These were initially described as developmentally regulated regions, holding genes that were shut down or activated upon differentiation. Genome-wide H3K9me chromatin immunoprecipitation (ChIP) in *S. pombe* showed the existence of heterochromatin islands that associated to meiotic genes (Cam et al., 2005; Zofall et al., 2012) and are silenced during vegetative growth. Heterochromatin formation at these genes was dynamically regulated in response to environmental signals and required the histone methyltransferase Clr4 and histone deacetylase Sir2, however was independent of SHREC and the RNAi factors Dcr1 and Ago1 (Zofall et al., 2012). Instead, meiotic mRNA transcripts were degraded by the exosome RNA degradation machinery. Deletion of Rrp6, an exosome-associated 3'-to-5' exonuclease, led to accumulation of these meiotic mRNA transcripts, but also revealed other genomic loci that were subjected to exosomal degradation. These loci, referred to as HOODs (heterochromatin domains), include retrotransposons, sexual differentiation genes and transmembrane domain proteins. Unlike meiotic genes, HOODs showed RNAi-dependent heterochromatin formation, however H3K9me and siRNAs coming from HOODs were only detected in an *rrp6*Δ background (Yamanaka et al., 2013).

Euchromatic RNAi-targets

In addition to the well-established role of the RNAi machinery in assembly of heterochromatin at centromeric repeats, the study by Woolcock et al. revealed an unexpected role for RNAi components in regulation of euchromatic protein-coding genes, in particular stress response genes referred to as BANCs (genes bound by Atf1 under normal conditions). Interestingly, the association of Dcr1 to BANCs was found to be independent of Clr4 and small RNAs and occurred at nuclear pores (Woolcock et al., 2012). BANCs are constitutively bound by transcription factor Atf1 and get activated upon heat stress (Lawrence et al., 2007). The model suggests RNAi-mediated repression by co-transcriptional RNA degradation to keep RNA levels in check under normal conditions and reduce the levels back to baseline after a transcriptional burst induced by transient heat stress. Whereas RNAi is involved in the regulation of heatshock gene expression, the RNAi pathway itself is regulated in a unique temperature-dependent manner. Elevated temperatures trigger a thermoswitch that deports Dcr1 to the cytoplasm abrogating RNAi-mediated degradation and thereby boosting mRNA levels of heat shock gene targets (Woolcock et al., 2012). This thermoswitch relies on the structural features of the dsRNA-binding domain (dsRBD) of Dicer, which adapts a specific fold through coordination of a Zn-ion that allows unfolding of the domain at elevated temperatures (Barraud et al., 2011). The dsRBD is known to be required for nuclear localization of Dcr1 and disruption of the Zn-coordination leads to unfolding, export into the cytoplasm and loss of silencing (Barraud et al., 2011; Emmerth et al., 2010). When the cells are switched back to normal temperatures, Dcr1 can refold and translocate back into the nucleus where it exerts its repression on BANCs and heterochromatic regions (**Figure IX**)(Woolcock et al., 2012).

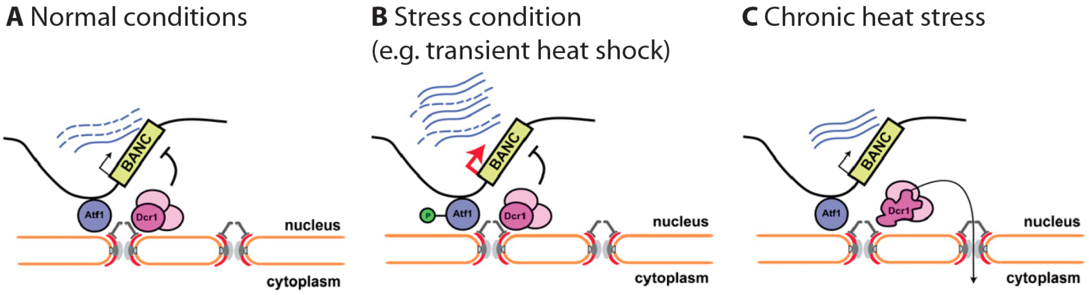

Figure IX Model of RNA-mediated CTGS of Atf1-bound genes (BANCS) at nuclear pores. **A** RNAi machinery colocalizes with BANCs at pores and contributes to their repression, presumably by degrading the nacent transcripts. **B** Upon stress, Atf1 phosphorylation leads to strong transcriptional activation of BANCs. After transient stress CTGS remains active and contributes to the transient nature of the stress response. **C** Chronic heat stress leads to relocalization of Dcr1 due unfolding of the dsRBD. Therefore, CTGS-mediated repression is abrogated and transcripts reaccumulate.

AIM OF THE THESIS

The aim of my thesis was to investigate the mechanism of heterochromatin repression mediated by heterochromatin protein Swi6 in *S. pombe*.

Research over the years challenged the view of heterochromatin as a static and transcriptionally inert structure. Especially in fission yeast it has become clear that heterochromatin silencing requires not only the action of chromatin modifying factors, but also transcriptional activity and RNA degradation processes. Moreover, heterochromatin protein Swi6 was shown to be highly dynamic, unlike what was expected for a protein that is perceived as a major structural component of heterochromatin. Yet, the prevailing model of heterochromatin establishment and spreading is thought to occur by iterative HP1 binding to methylated H3K9 and recruitment of histone methylation activity.

Driven by recent findings in our lab that described a new role for Swi6 in repression and provided a possible explanation for its dynamic behavior, I set out to investigate the mechanism *in vivo* by studying Swi6 dynamics. Therefore, a major focus of my PhD was to establish a suitable, robust microscopy-based method that allowed me to follow rapid dynamics and produce reliable data.

The questions that I set out to address:

- What are the *in vivo* dynamics of Swi6?
- How does Swi6 move in heterochromatic regions?
- Are there dynamic differences between the heterochromatic regions?
- What properties influence Swi6 dynamics?
- What is the relevance of Swi6 dynamics?
- Do the Swi6 dynamics coincide or contradict the prevalent spreading model?
- Can we find *in vivo* evidence for our *in vitro* model?
- What is the role of Swi6 in silencing?

RESULTS

1. RNAi represses stress response genes

(Woolcock et al., *Genes and Development* (2012))

Summary

In *S. pombe* the RNAi machinery plays an important role in the assembly of constitutive heterochromatin by a mechanism called CTGS. Whereas the mechanism at centromeric repeats is well-established, additional roles for the RNAi machinery and how it's initially targeted remained elusive. This paper revealed an unexpected role for RNAi components in regulation of stress response genes. Using DNA adenine methyltransferase identification (DamID) to capture protein interactions with the genome, Woolcock et al. showed association of the core RNAi machinery with many noncoding regions and certain protein-coding genes. DamID correlation plots between RNAi factors and nuclear pore components and microscopy-based methods demonstrated these interactions to occur at nuclear pores **(Figure X)**. Interestingly, targeting of Dcr1 and Rdp1 to centromeres and euchromatic regions was found to be independent of small RNAs and H3K9me. Amongst the euchromatic regions, strong enrichment was found for genes involved in stress response. These genes, referred to as bound by Atf1 under normal conditions (BANCs), get activated upon stress by phosphorylation of the transcription factor Atf1 (Lawrence et al., 2007). This study provided evidence for the RNAi machinery to contribute in repression of BANCs under normal conditions. Woolcock et al. proposed a model in which transcriptional degradation of the transcripts by CTGS keeps the RNA levels in check under normal conditions and helps to reduce the levels back to baseline after a transcriptional burst induced by transient stress. Furthermore, in chronic exposure to heat Dicer translocated to the cytoplasm, however relocalized to the nucleus when shifted back to physiological conditions. We speculated that the structure of Dicer harbors an internal thermoswitch that might play an important role in activating chronic heat-shock pathways. Together, this work demonstrated a critical function for a key stress response transcription factor, Atf1, and nuclear pores in coordinating the interplay between the RNAi machinery and the *S. pombe* genome (Woolcock et al., 2012).

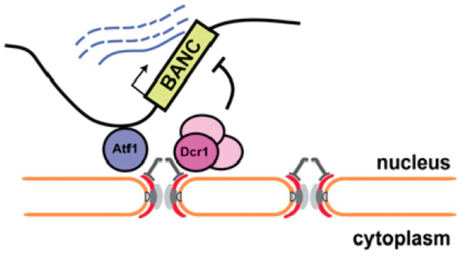

Figure X RNAi contributes to the repression of BANCs. Dcr1 colocalizes with Atf1-bound genes (BANCs) to nuclear pores and contributes in their repression by degrading the nascent transcripts. Adapted from (Woolcock et al., 2012).

My contribution

For this study I specifically looked at the localization of Dicer and several BANCs in normal and stress-induced conditions. To analyze the localization of the target genes in the nucleus I introduced the LacO/LacI-GFP system and followed individual heat-shock genes by live cell imaging (Taddei et al., 2004). The experiment provided *in vivo* evidence for the localization of BANCs at the nuclear periphery under normal and stress conditions, which was coherent with the biochemical data **(Figure XI)**. To provide further insight into the mechanism of gene repression under stress conditions, I used N-terminally tagged GFP-Dcr1 cells to perform live cell imaging in different conditions. The time course revealed translocation of Dcr1 from the nuclear periphery to the cytoplasm upon prolonged heat-stress **(Figure XII)**. These findings contributed to a model in which heat-induced translocation of Dicer impedes a functional RNAi pathway and releases gene repression of the heat shock genes for full activation.

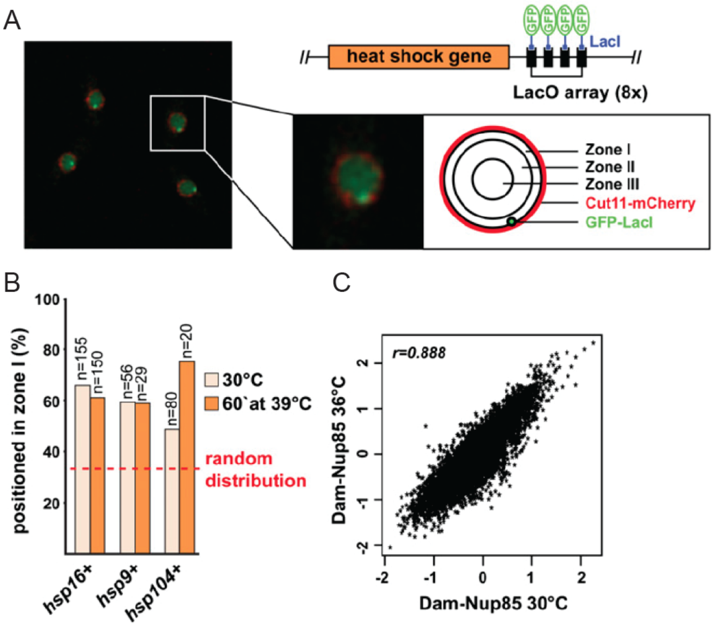

Figure XI BANCs are located at the nuclear periphery in normal and increased temperatures. **A** Summary of the LacO/LacI-GFP system used to analyze the location of individual heat-shock genes (Taddei et al., 2004). Confocal microscopy image at 30˚C of live cells with GFP-LacI-marked *lacO::hsp16+* locus and the nuclear membrane marker mCherry-Cut11.**B** Quantifications of assigned localization of three BANCs in zone I, which corresponds to the nuclear periphery at 30˚C and 39˚C. **C** Comparison of the genome-wide Nup85 enrichment (log2) at 30°C and 36°C.

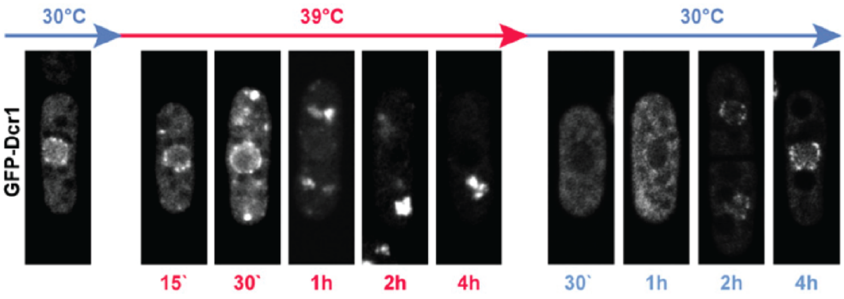

Figure XII Dicer looses nuclear retention at elevated temperatures. Fluorescence microscopy images of N'term tagged GFP-Dcr1 expressing cells followed over time (indicated below) upon exposure to heat (39˚C) and recovery after shifting back to a temperature of 30˚C. GFP1-Dcr1 nuclear peripheral localization is gradually lost over time and accumulates in cytoplasmic patches upon heat stress. Localization is restored after shifting back to a physiological temperature.

2. Elimination of heterochromatic RNA via HP1^{Swi6}

(Keller et al., *Molecular Cell* (2012))

Summary

S. pombe heterochromatin protein Swi6 is important for heterochromatic gene silencing, yet on a mechanistic level this was poorly understood. HP1 proteins are major component of heterochromatin, which is generally seen as an inaccessible, transcriptional silent and static structure. However, heterochromatic repeats are actively transcribed and HP1 proteins have shown to be dynamic (Cheutin et al., 2003, 2004; Festenstein et al., 2003). This study demonstrated Swi6 to function in linking transcription within heterochromatin to downstream RNA turnover and provided an explanation for the dynamic nature of Swi6. *In vitro* and *in vivo* data supported a model in which Swi6 functions as a heterochromatin-specific checkpoint, capturing transcripts via its hinge domain and handing them over to the RNA degradation machinery involving poly(A) polymerase Cid14. Interestingly, RNA binding was found to be in competition with H3K9me binding and therefore mediated Swi6-eviciton off heterochromatin. Only when the RNA was released from Swi6, it could turn back in a conformation favorable for H3K9me binding **(Figure III)**. Whereas recruitment of Swi6 to heterochromatin was independent of RNA-binding, it was required for full heterochromatic repression. In summary, the study provided new insights for the role of RNA in the regulation of higher order chromatin structures and demonstrated physiological relevance for the dynamic nature of Swi6.

My contribution

In order to address the functional relevance of RNA binding to Swi6, Claudia Keller designed a RNA-binding mutant of Swi6 in which all the lysines and arginines (K,R) of the hinge domain were mutated to alanines (KR25A). I contributed in characterizing the functionality of the RNA-binding mutant by studying its localization using a Dendra2 fluorescent tag. The *in vivo* localization data confirmed the importance of the hinge residues for its nuclear localization and provided evidence that the RNA binding property was not needed for association to heterochromatic domains **(Figure XIII)**. Furthermore, together with Laurent Gelman from the FMI-microscopy facility, I established fluorescence recovery after photobleaching (FRAP) to assess the highly dynamic nature of Swi6 **(Figure XIV)**.

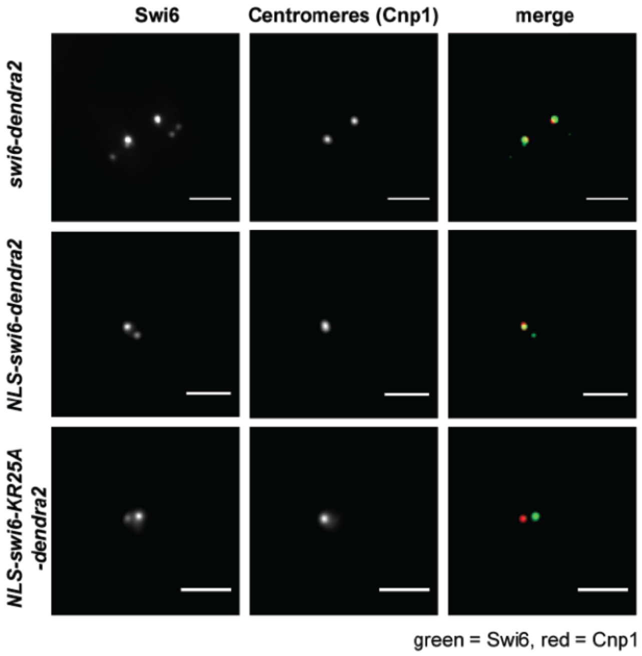
Swi6
Centromeres (Cnp1)
merge
swi6-dendra2
NLS-swi6-dendra2
NLS-swi6-KR25A -dendra2
green = Swi6, red = Cnp1

Figure XIII Co-localization of Swi6-Dendra2 variants with centromeric heterochromatin. Swi6, NLS-Swi6 and NLS-Swi6-KR25A tagged with C'terminal Dendra2, driven from the endogenous promoter co-localize with centromeric Cnp1-mcherry marker. 2μm scale bar

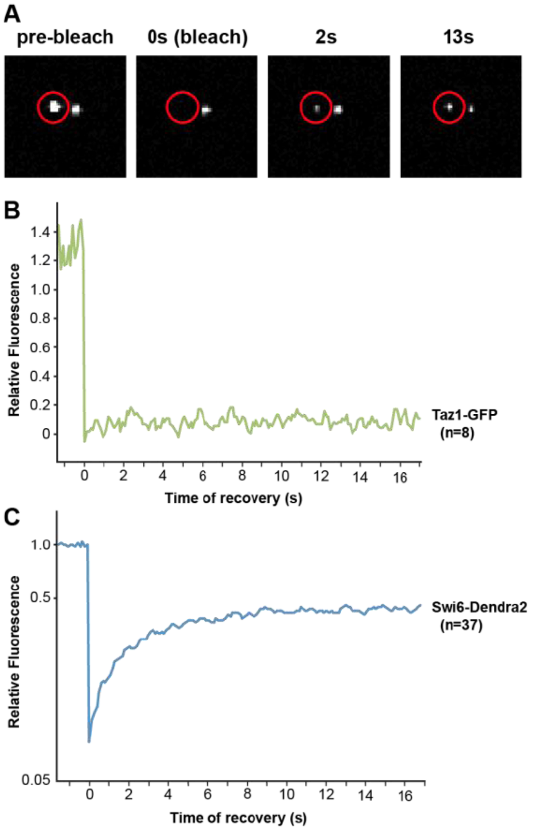

Figure XIV *In vivo* dynamics of Swi6-Dendra2. **A** Representative images of FRAP performed with cells expressing Swi6-Dendra2. Confocal pictures were taken before and after photobleaching with indicated times. Red circle: bleached loci. **B** FRAP analysis of cells expressing Taz1-GFP showing average fluorescence intensities of 8 bleached foci with a gliding time-average of 3 frames. **C** FRAP analysis of cells expressing Swi6-Dendra2. The fluorescence intensities were normalized to an unbleached focus in the same image. Average relative fluorescence intensities of 37 bleached foci (cells) with a gliding time-average of 3 frames are shown

3. Dcr1 and Hsp104 regulate epigenetic robustness

(Oberti et al., *Cell Reports* (2015))

Summary

In fission yeast the RNAi machinery is important for formation of constitutive heterochromatin and mediates genome stability and epigenetic robustness. Besides the repression of heterochromatic regions it is involved in regulation of stress response genes (Woolcock et al., 2012). These genes are referred to as BANCs; bound by Atf1 under normal conditions. At elevated temperature they become highly activated due to Atf1 phosphorylation and relieve of RNAi-mediated repression by the intrinsic thermoswitch in Dcr1 that leads to relocalization away from its target and disruption of a functional RNAi pathway (Woolcock et al., 2012). This, however, raised the question how integrity of centromeric heterochromatin is ensured at elevated temperatures and what would prevent Dcr1 from aggregating into cytoplasmic structures? The study demonstrated that resilencing of centromeric heterochromatin depends on heat shock protein and BANC, Hsp104 that dissolves Dcr1 aggregates at elevated temperatures. Live cell imaging experiments provided evidence for Hsp104 and Dcr1 to function in a negative feedback loop (**Figure XV**), dampening environmental-induced epigenetic variation. Furthermore, Hsp104 is known to play a crucial role in prion formation, propagation and elimination. In this light, Oberti et al. investigated and revealed an unanticipated role for Dcr1 in adverting toxic aggregation of a prionogenic protein. This is additionally exciting because it is the first paper that shows prion formation in *S. pombe*.

My contribution

To study the dynamic nature of the Dicer cytoplasmic aggregates, I applied FRAP on Dcr1-GFP tagged cells in different conditions. FRAP allows determination of the mobility of the fluorescent-tagged protein by irreversibly bleaching a fraction and monitoring its fluorescence recovery over time. FRAP on cytoplasmic Dcr1-GFP during continuous heat showed that the aggregates itself had no fluorescence exchange and are therefore immobile. In addition, it was important to know if the cytoplasmic aggregates can be resolved and provide functional Dicer in the nucleus. Therefore, I performed live cell imaging and monitored Dcr1-GFP cells over time that were recovering from heat conditions (holding cytoplasmic Dcr1-GFP patches) while being translationally inhibited. To confirm translational repression, I also monitored a bleached cell as a control. Indeed, nuclear Dicer reappeared while the cytoplasmic aggregates dissolved, indicating Dcr1 to be resolubilized and recycled. The same experiment was repeated in *hsp104*Δ cells confirming the role of Hsp104 as a disaggregase of Dicer (**Figure XVI**).

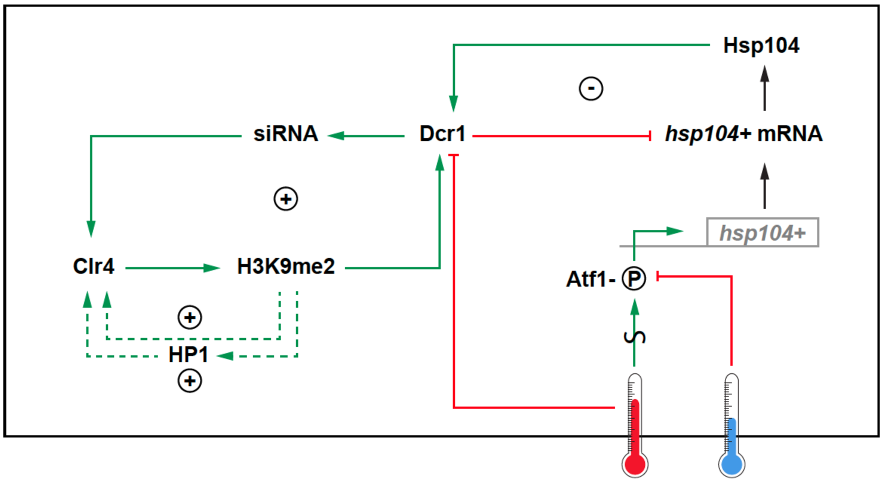
Hsp104
⊝
siRNA
Dcr1
hsp104+ mRNA
⊕
hsp104+
Clr4
H3K9me2
Atf1-Ⓟ
S
⊕
HP1
⊕

Figure XV Model for the formation of constitutive heterochromatin. The integration of multiple feedback loops confers robustness to the system and buffers environmental insults. Red: <34˚C, Blue: >34˚C. S depicts unknown oscillator, P indicates phosphorylation of Atf1.

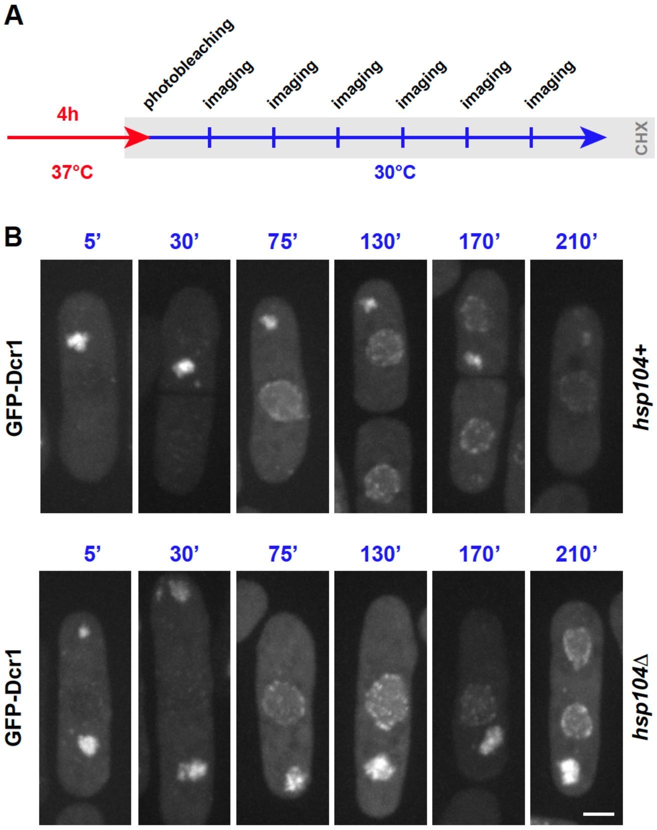
A
photobleaching
imaging
imaging
imaging
imaging
imaging
imaging
4h
37°C
30°C
CHX
B
5'
30'
75'
130'
170'
210'
GFP-Dcr1
hsp104+
5'
30'
75'
130'
170'
210'
GFP-Dcr1
hsp104Δ

Figure XVI Disaggregated Dcr1 reenters the nucleus.
A Schematic of the experiment.
B Live cell imaging of *hsp104+* and *hsp104Δ* cells expressing GFP-Dcr1 recovering from heat. Different cells are shown at different time points.
Scale bar: 2µm.

4. Swi6-mediated heterochromatin dynamics

(Stunnenberg et al., *EMBO Journal* (2015))

Summary

The *S. pombe* heterochromatin protein Swi6 is a well-known component of heterochromatin, a structure that is perceived as static, inaccessible and transcriptionally inactive. Prevailing models suggest Swi6 to serve in heterochromatin formation and spreading via H3K9me interaction and Swi6-oligomerization (Canzio et al., 2011, 2014). Such a model implies the existence of an immobile Swi6-population at heterochromatin. My study challenged this dogma and revealed unanticipated activities of Swi6. In contrast to a previous study that looked at exogenous expressed Swi6-GFP, I performed FRAP on endogenous tagged Swi6-EGFP and found that the majority of Swi6, if not all, is rapidly exchanging in heterochromatin under physiological expression conditions. In addition, RNA binding and H3K9me decelerated Swi6 dynamics. Taking advantage of this feature, we used Swi6 dynamics as an indirect measure to show that fission yeast is permissive to transcription throughout the cell cycle.
Continuous exchange of Swi6 in heterochromatin is consistent with the previously described role for Swi6 as a heterochromatic checkpoint, capturing transcripts and handing them over to the RNA degradation machinery (Keller et al., 2012). However, rapid dynamics challenged Swi6 to function as an inert, oligomeric network and lead us to investigate the role in spreading. ChIP-sequencing data of H3K9me unexpectedly revealed Swi6 to be dispensable for heterochromatin maintenance and, instead, put forward a role for Swi6 in demarcating heterochromatin from euchromatin. Together, the study demonstrated Swi6 to be highly dynamic, serving to repress, but not maintain, centromeric heterochromatin and anticipated a role in boundary formation (**Figure XVII**).

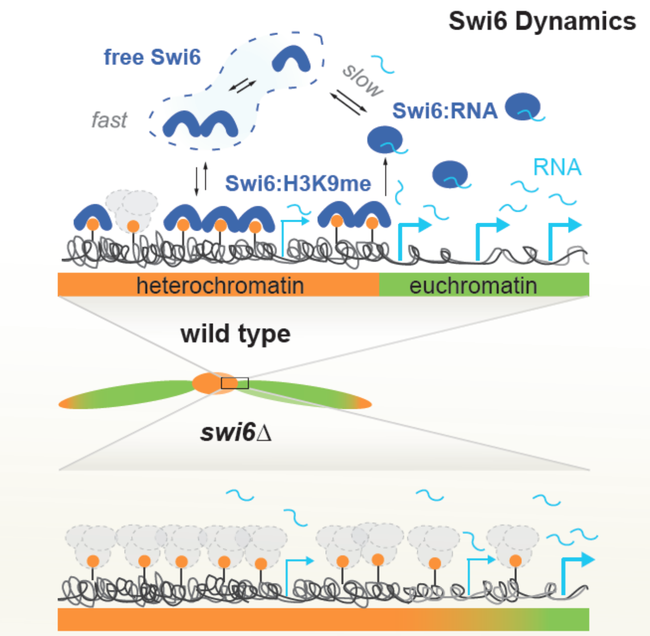

Figure XVII The regulation of Swi6 dynamics and the role of Swi6 in heterochromatin spreading, boundary formation, and repression. On top is the wild type situation in which Swi6 (blue) functions redundant with other factors (grey) to form and spread heterochromatin via dimerization and binding to H3K9me (orange balls). Spreading is prevented by binding of heterochromatic RNA to Swi6, which induces a conformational change (blue oval) eviction off heterochromatin. Swi6 has to release the RNA in order to come back to heterochromatin, which is the rate limiting process in the exchange dynamics. In the absence of Swi6 (*swi6Δ)*, heterochromatin spreads over its borders into euchromatin, which is mediated by redundant pathways as indicated below.

My contribution

In order to obtain high quality dynamic data on Swi6, I worked together with Laurent Gelman from the in house microscope facility to setup a suitable method to measure such rapid dynamics in vivo. We established FRAP on Swi6-EGFP tagged cells using two different microscopy systems that allowed us to measure several dynamic ranges. I performed FRAP on the spinning disk system to acquire FRAP curves of heterochromatic Swi6-EGFP and used the line-scan approach to achieve high-speed measurements for faster euchromatic Swi6-EGFP dynamics. To extract the fluorescence recovery and half recovery times from the data sets, Laurent Gelman and Moritz Kirschmann helped me to establish a semi-automatic program in Fiji (imaging software).

DISCUSSION

Swi6-mediated heterochromatin dynamics and silencing

Swi6 belongs to the highly conserved family of heterochromatin proteins HP1 that play an important role in heterochromatin silencing. It is generally thought that HP1s are crucial structural components that play a central role in the formation of a compact and transcriptional inert heterochromatic network. The current model implies repeated binding of HP1s to chromatin and recruitment of HMTase activities to establish and spread heterochromatin along the fiber (Eissenberg and Elgin, 2014). The work I have done during the last 2,5 years of my PhD challenge this view. My results highlight the dynamic nature of Swi6 and demonstrate the existence of a single and highly dynamic population in heterochromatin, thereby questioning the role in heterochromatin maintenance and spreading. Instead, the findings coincide with a role for Swi6 in heterochromatic-euchromatic boundary control and co-transcriptional gene silencing via RNA degradation.

1. Heterochromatin propagation

Swi6 and heterochromatin spreading

Iterative HP1 binding to methylated H3K9 and recruitment of HMTase activity is the prevalent model for heterochromatin spreading (Eissenberg and Elgin, 2014). Models of Swi6-mediated spreading are based on its biophysical properties to bind H3K9me, but also incorporate a suggested stepwise formation of higher-order oligomerization (Canzio et al., 2011, 2013, 2014). The role of Swi6 in spreading is reinforced by papers that use Swi6 overexpression to drive heterochromatin formation across its usual borders (Noma et al., 2006; Wang et al., 2013). Our study demonstrated that the vast majority of Swi6, if not all, is rapidly exchanging on heterochromatin *in vivo*. The absence of an immobile fraction questions the formation of an oligomeric network and therefore the role of Swi6 in heterochromatin spreading. In fact, H3K9me2 levels were maintained upon deletion of Swi6 and even showed spreading into different regions, rendering Swi6 dispensable for this process (Stunnenberg et al., 2014). Yet, increased transcript levels in *swi6*Δ indicated the importance of Swi6 for tight repression, consistent with previous reports (Motamedi et al., 2008). So if not (only) Swi6, what else could maintain and propagate heterochromatin?

Chp2-mediated spreading

A candidate to mediate heterochromatin propagation is the heterochromatin protein Chp2. Like Swi6, Chp2 possesses a chromodomain and chromoshadow domain required for recognition of H3K9me and potential self-propagation. Indeed, in vitro experiments indicated that Chp2 is able to adopt a dimer configuration that could mediate spreading (Sadaie et al., 2008) (**Figure XVIII**). Furthermore, the CD of Chp2 has a higher binding affinity to H3K9me than the CD of Swi6 (Sadaie et al., 2008). Chp2 interacts with SHREC, a histone deacetylation complex that removes H3K14ac, a mark associated with active transcription (Motamedi et al., 2008). Deacetylation promotes heterochromatin formation via association of Chp1, Swi6, and Clr4. Together, Chp2 seems to be a good candidate to mediate spreading, yet H3K9me levels largely remain in the absence of Chp2, implying redundancy or the involvement of other factors (Motamedi et al., 2008; Sadaie et al., 2004). It would be interesting to study heterochromatin distribution in chp2Δ and in a double deletion of Chp2 and Swi6. Would this completely diminish heterochromatin? Would H3K9me still spread? In addition, it would be worthwhile to investigate the dynamics of Chp2 to see if we find a static population that would fit with a role in formation of an oligomeric network.

RNAi-mediated spreading

Another possible mechanism could involve the RNAi machinery through the chromodomain-containing protein Chp1. Chp1 together with Tas3 and Ago1 form the RITS complex that is key for siRNA-mediated silencing at centromeres (Verdel et al., 2004). Furthermore, Chp1 and Tas3 have been reported as an independent subcomplex, involved in heterochromatin formation at telomeres and mating type locus (Debeauchamp et al., 2008; Petrie et al., 2005). Unlike Swi6 and Chp2, deletion of Chp1 significantly reduces H3K9me levels and leads to desilencing of the centromeric locus (Sadaie et al., 2004; Schalch et al., 2009). Chp1 has a high affinity for H3K9me, which is important for heterochromatin establishment (Schalch et al., 2009), however lacks a CSD for dimerization. Yet, formation of an oligomeric network has been proposed to occur via interactions between Tas3 with its TAM domain (Li et al., 2009) (**Figure XVIII**). In addition, RITS recruits the histone methyltransferase Clr4 via interaction with Stc1 (Bayne et al., 2010), fulfilling the criteria for a self-propagating loop needed for heterochromatin spreading. Also here, FRAP experiments on Chp1 and Tas3 could provide further insight into a potential mechanism. It would be interesting to compare the dynamics of a wild type background to *swi6*Δ.

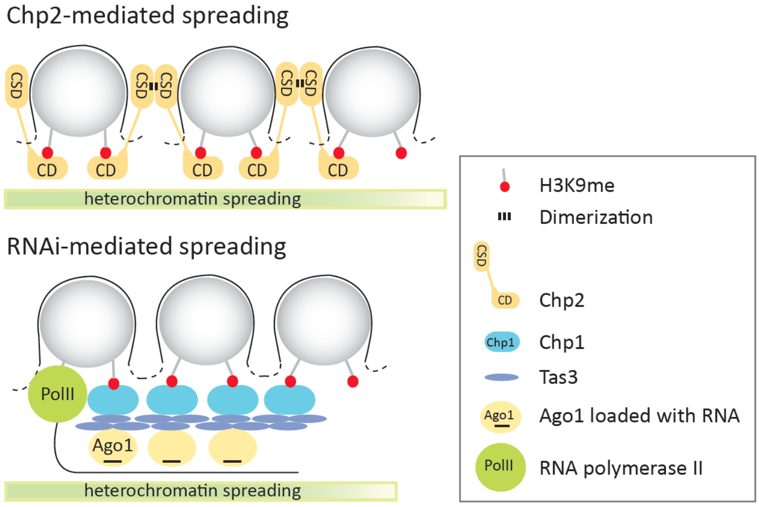

Figure XVIII Models of heterochromatin spreading by Chp2 and the RNAi machinery. HP1 protein Chp2 could mediate spreading via CSD-dimerization and CD-H3K9me interaction. RNAi-mediated spreading could function by Chp1-H3K9me interaction and oligomerization by Tas3. Additional interaction occurs via base pairing of the sRNA with the nascent Pol II transcript.

2. Swi6-mediated heterochromatin boundary formation

The fact that we observed heterochromatin spreading in the absence of Swi6 could be interpreted in different ways. As discussed before, it could mean that Swi6 is dispensable for spreading and other factors mediate this process or act redundantly. On the other hand, this could point towards a role for Swi6 in maintaining the boundary between heterochromatin and euchromatin (**Figure XIX**).

Swi6 inhibitory conformation

It has been proposed that Swi6 itself can form a barrier by adapting a spreading inhibitory conformation. Generally, Swi6 dimerizes through the CSD, while the CD recognizes methylated H3K9 (Bannister et al., 2001; Canzio et al., 2011; Cowieson et al., 2000). In vitro data, however, implicated the existence of a second dimer that in addition to the CSD also interacts through the CD. This interaction is mediated by an ARK-loop region in the CD that binds in the same binding pocket as H3K9me and renders these events mutual exclusive (Canzio et al., 2013). Such a conformation could potentially inhibit spreading and occur at heterochromatic borders (**Figure XIX**). Although deletion of the ARK-loop resulted in loss of silencing, it remains to be determined if this interaction truly occurs in vivo and what factors could specifically induce such an inhibitory conformation. It would be interesting to determine the localization and the dynamic changes of Swi6-loopΔ in addition to a global analysis of H3K9me distributions.

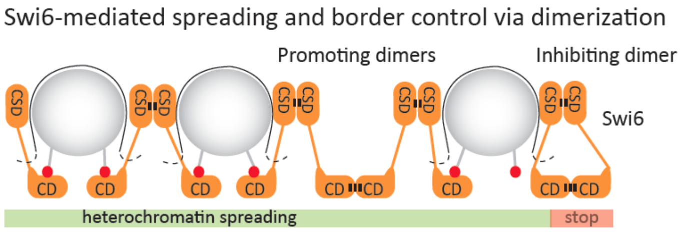
Swi6-mediated spreading and border control via dimerization
Promoting dimers
Inhibiting dimer
Swi6
CSD
CD
heterochromatin spreading
stop

Figure XIX Swi6-mediated heterochromatin border control by dimerization. Swi6 promotes H3K9me spreading by dimerization but can also form the inhibitory dimer conformation with simultaneous CD-CD and CSD-CSD interactions that can stop further oligomerization.

RNA-mediated Swi6 eviction

Swi6 contains an additional feature that affects its dynamics, is important for silencing and could play a part in boundary formation: RNA binding. As of recent, Swi6 was shown to bind heterochromatic RNA transcripts via its hinge domain (Keller et al., 2012). Interestingly, RNA binding induced a conformational change in the CD that obstructed the interaction to H3K9me and was suggested to result in eviction of Swi6 off heterochromatin. Consistent with this idea, partial heterochromatin spreading was observed in case of a Swi6 RNA binding mutant, which is still capable of interacting with H3K9me (Keller et al., 2012, 2013). RNA-mediated eviction could theoretically help to sustain the borders as high transcriptional activity in euchromatin could potentiate eviction. Together, most likely multiple mechanisms act together or in parallel to control the heterochromatin-euchromatin border and vary in strength and composition depending on the region. Proof of the latter is the observed heterogeneity of H3K9me spreading upon Swi6 deletion **(Figure XX)**. Below I will discuss the role of the DNA sequence as a possible explanation for these observed differences in heterochromatin regulation, but before that, I will discuss the connection of Swi6 to another factor that is involved in boundary formation.

Epe1 recruitment

Swi6 has been suggested to recruit the anti-silencing factor Epe1 (Zofall and Grewal, 2006). Epe1 is distributed across all major heterochromatic sides and is preferentially recruited to inverted repeats flanking the centromeres where it restrains the spread of heterochromatin. Epe1 contains a JmjC-domain that is required for its function, yet *in vitro* demethylase activity could not be detected so far (Ayoub et al., 2003; Tsukada et al., 2006; Zofall and Grewal, 2006). At specific boundary elements (IRCs), Epe1 has recently been demonstrated to recruit the double bromodomain protein Bdf2 that preferentially binds to acetylated histone tails and protects them from Sir2-mediated deacetylation of H4K16 (Wang et al., 2013). Deacetylation of H4K16 has been suggested to be required for heterochromatin to spread. Thus, Swi6 can not only mediate border control by itself but also recruit additional anti-silencing factors through Epe1.

3. Heterogeneity in heterochromatin regulation

Diversity of DNA sequence elements at the boundaries

As discussed in chapter 3 'Co-transcriptional gene silencing in *S. pombe*', constitutive heterochromatic domains have different DNA sequence elements that mark the borders to euchromatin. These elements recruit different sets of factors functioning in boundary formation and create a diverse degree of barrier control. This heterogeneity seems to be reflected by the observed change in H3K9me distribution between different regions upon deletion of Swi6 (Stunnenberg et al.,). While heterochromatin prominently spread into neighboring regions of centromere 1, H3K9me levels remained in check at centromere 2 (**Figure XX**). Centromere 2 is flanked by clusters of highly expressed tRNAs (Cam et al., 2005), whereas the mating type region and centromere 1 are flanked by different repeat sequences that help to restrain heterochromatin spread (**Figure VII**). tRNA genes have b-box sequences that are bound by the transcription factor TFIIIC complex and recruit RNA polymerase III (Pol III). TFIIIC is also recruited to inverted repeats (IR) at the mating type locus, however independently of Pol III (Noma K et al., 2001; Noma et al., 2006). Centromere 1 does not contain IR elements or tRNA clusters, but has IRCs that mark the borders. Here, neither TFIIIC nor Pol III is recruited, however Pol II-mediated transcription of the repeats has been detected in addition to recruitment of Bdf2 (Noma et al., 2006; Wang et al., 2013). Interestingly, centromere 1 shows the most prominent spreading of H3K9me in the absence of Swi6. Moreover, binding of Swi6 to a lncRNA called Borderline, which is expressed from the boundary region of centromere 1 between pericentromeric heterochromatin and euchromatin, prevents aberrant spreading of H3K9me (Keller et al., 2013). This could indicate that IRCs form weaker boundaries and/or that Swi6 has a more prominent role at centromere 1. This could be tested by genetically modifying the boundaries, replacing IRCs by tRNA clusters or IRs (or the reverse) and study H3K9me distribution in *swi6*Δ.

Pathway redundancy

As mentioned before, the observed heterogeneity in heterochromatin spreading provoked by Swi6 deletion can be a result of recruitment of different factors or pathway redundancy at the loci. Centromeric silencing for instance is highly dependent on the components of the RNAi pathway, while other factors are rendering the RNAi machinery dispensable for heterochromatin maintenance at the mating type locus and telomeres (Jia et al., 2004; Kanoh et al., 2005). Along with the differences in DNA sequence elements that make up the heterochromatin domains and the interplay of multiple pathways, it is not surprising to obtain such diverse H3K9me spreading patterns as we see in swi6Δ (**Figure XX**).

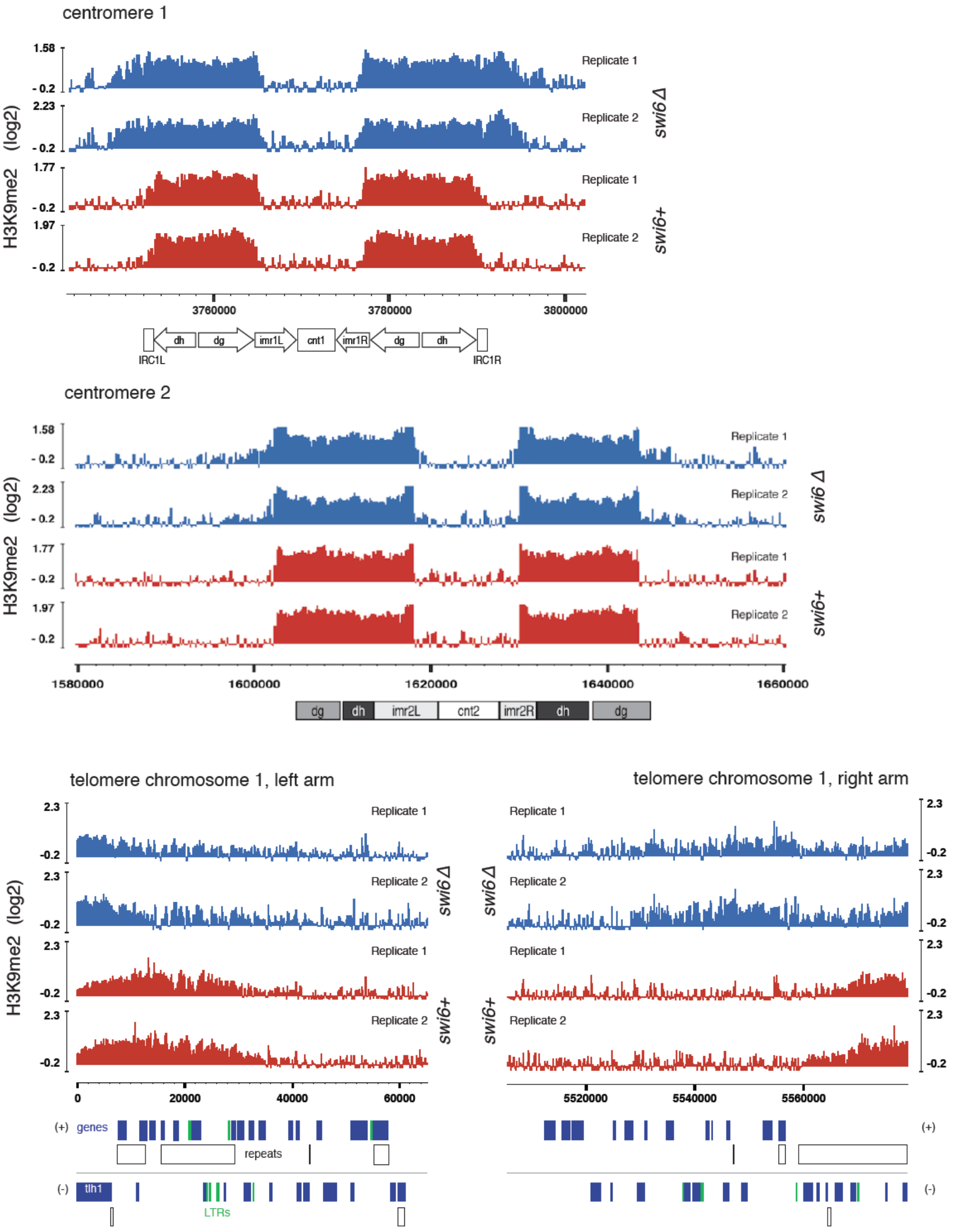

Figure XX H3K9me levels in constitutive heterochromatin regions in wild type and *swi6*Δ cells. H3K9me2 ChIP-seq enrichment profiles for *swi6+* (red) and *swi6Δ* (blue) cells at centromere1, centromere 2 and the telomeres of the left and right arm of chromosome 1. Centromeric repeat elements and other genomic elements are indicated below. IRC1 constitute heterochromatin boundaries in wild type cells, while centromere 2 is flanked by tRNA clusters (not shown). The *y* axes represent log2 ChIP-seq enrichments in 200-base-pair genomically tiled windows calculated over *clr4*Δ cells. Two independent biological replicates for each genotype were performed (replicate 1 or 2). Positions of genomic elements on the plus and minus strand are indicated. blue, protein-coding genes; white, repeats; green, long terminal repeat (LTR).

4. Balance between factors in border control

Retaining balance to control heterochromatin integrity

In order to keep heterochromatin in check, multiple factors interplay with each other maintaining the right balance between the different activities. Experiments that disturb such a balance, by either deleting or overexpressing involved factors, result in heterochromatin spreading or destabilization. Deletion of Epe1 leads to heterochromatin spreading while overexpression induces instability (Ayoub et al., 2003; Zofall and Grewal, 2006). Interestingly, Swi6 deletion and overexpression both seem to promote heterochromatin spreading (Noma et al., 2006; Wang et al., 2013). On the other hand, overexpression of the heterochromatin protein Chp2 replaced Swi6 and lead to loss of silencing, suggesting that Chp2 and Swi6 compete for the same binding sites (Sadaie et al., 2008).

Swi6 abundance dominates border dynamics

Compared to Chp1 and Chp2, Swi6 is more abundant and likely to occupy a higher fraction of heterochromatin due to competition for available binding sites (Sadaie et al., 2008). Although the residence time on heterochromatin for Chp1 and Chp2 is probably longer due to higher affinities to H3K9me (Sadaie et al., 2008; Schalch et al., 2009), the stoichiometric advantage of Swi6 might outcompete binding of the other factors to heterochromatin. Hypothetically, Swi6 could maintain heterochromatic borders by simply acting as a competitor for H3K9me binding, therefore preventing spreading mediated by potential candidates like Chp1 and Chp2. Would a certain degree of Swi6 downregulation in that case induce spreading?

CONCLUSION

Swi6 mediates heterochromatic RNA destruction

The work I have done during my PhD challenged the role of Swi6 in heterochromatin maintenance and spreading, but coincides with a clear involvement in sustaining tight repression. While H3K9me levels remained high in the absence of Swi6 and even spread into neighboring regions, heterochromatic transcript levels increased. These observations revealed unanticipated functions for Swi6 and made us reconsider the mechanism of Swi6-mediated silencing. As previously proposed, Swi6 could function as a co-transcriptional checkpoint that mediates RNA degradation (Keller et al., 2012). In this model RNA binds to Swi6 and gets primed for destruction as it is handed over to the RNA decay machinery, involving Cid14 and the exosome or the RNAi machinery. The target specificity depends on the epigenetic make-up of the locus, meaning the recognition of H3K9me by the CD of Swi6, while RNA binding occurs in a sequence independent manner (Keller et al., 2012). Therefore, additional processes that confer specificity, like siRNAs, are needed to ensure correct targeting of H3K9me marks to trigger Swi6-mediated turnover of unwanted RNA transcripts and not of any other random region in the genome.

Conservation

A similar mechanism as proposed for Swi6 in fission yeast might also occur in higher eukaryotes. HP1 was initially discovered as a protein that predominantly associates to heterochromatic regions in *Drosophila* (James and Elgin, 1986). Resembling the situation in fission yeast, more recent findings demonstrated that HP1s in worms and flies specifically associate to heterochromatic regions that are also found to be transcriptionally active and are required for silencing of repetitive elements (Ashe et al., 2012; Klattenhoff et al., 2009). The HP1 protein Rhino in *Drosophila* specifically binds to piRNA clusters and is needed for transposon silencing and the production of piRNAs (Klattenhoff et al., 2009; Mohn et al., 2014; Zhang et al., 2014). Recent publications shed light on this intriguing mechanism, as they show the requirement of the Rhino-Deadlock-Cutoff (RDC) complex for actual transcription of the piRNA source loci. Loss of any individual RDC factor resulted in loss of transcription at dual-strand piRNA source loci and in downstream distortions of piRNA populations and TE silencing (Mohn et al., 2014). Given the role of HP1 in transcriptional repression this was rather unexpected. Yet, it was suggested that RDC prevents transcriptional termination and transcript splicing, due to the action of Cutoff, allowing ‘read-through’ transcripts of otherwise non-transcribed regions (Mohn et al., 2014; Zhang et al., 2014). Intriguingly, Piwi has previously been found to guide H3K9me (Sienski et al., 2012; Le Thomas et al., 2013; Wang and Elgin, 2011), which is needed for the RDC complex to anchor. Consistently, depletion of Piwi resulted in loss of RDC and small RNAs at piRNA clusters. Similar to CTGS in fission yeast, this pathway confers a feedback loop between piRNA source loci and Piwi via recruitment of chromatin modifying and binding factors including the HP1-containing RDC complex. Although the actions of HP1 might differ between the two systems, in both fission yeast and flies HP1s mark the heterochromatic clusters that mediate silencing through RNA-dependent mechanisms and play a crucial role in its repression.

REFERENCES

Akhtar, A., and Gasser, S.M. (2007). The nuclear envelope and transcriptional control. Nat. Rev. Genet. *8*, 507–517.

Alleman, M., Sidorenko, L., McGinnis, K., Seshadri, V., Dorweiler, J.E., White, J., Sikkink, K., and Chandler, V.L. (2006). An RNA-dependent RNA polymerase is required for paramutation in maize. Nature *442*, 295–298.

Allshire, R.C., Javerzat, J.-P., Redhead, N.J., and Cranston, G. (1994). Position effect variegation at fission yeast centromeres. Cell *76*, 157–169.

Allshire, R.C., Nimmo, E.R., Ekwall, K., Javerzat, J.P., and Cranston, G. (1995). Mutations derepressing silent centromeric domains in fission yeast disrupt chromosome segregation. Genes Dev. *9*, 218–233.

Alper, B.J., Job, G., Yadav, R.K., Shanker, S., Lowe, B.R., and Partridge, J.F. (2013). Sir2 is required for Clr4 to initiate centromeric heterochromatin assembly in fission yeast. EMBO J. *32*, 2321–2335.

Angel, A., Song, J., Dean, C., and Howard, M. (2011). A Polycomb-based switch underlying quantitative epigenetic memory. Nature *476*, 105–108.

Aravin, A.A., Hannon, G.J., and Brennecke, J. (2007). The Piwi-piRNA pathway provides an adaptive defense in the transposon arms race. Science *318*, 761–764.

Ashe, A., Sapetschnig, A., Weick, E.-M., Mitchell, J., Bagijn, M.P., Cording, A.C., Doebley, A.-L., Goldstein, L.D., Lehrbach, N.J., Le Pen, J., et al. (2012). piRNAs can trigger a multigenerational epigenetic memory in the germline of C. elegans. Cell *150*, 88–99.

Ayoub, N., Noma, K., Isaac, S., Kahan, T., Grewal, S.I.S., and Cohen, A. (2003). A Novel jmjC Domain Protein Modulates Heterochromatization in Fission Yeast A Novel jmjC Domain Protein Modulates Heterochromatization in Fission Yeast. Mol. Cell. Biol. *23*.

Azzalin, C.M., Reichenbach, P., Khoriauli, L., Giulotto, E., and Lingner, J. (2007). Telomeric repeat containing RNA and RNA surveillance factors at mammalian chromosome ends. Science *318*, 798–801.

Bannister, A.J., and Kouzarides, T. (2011). Regulation of chromatin by histone modifications. Cell Res. *21*, 381–395.

Bannister, a J., Zegerman, P., Partridge, J.F., Miska, E. a, Thomas, J.O., Allshire, R.C., and Kouzarides, T. (2001). Selective recognition of methylated lysine 9 on histone H3 by the HP1 chromo domain. Nature *410*, 120–124.

Barraud, P., Emmerth, S., Shimada, Y., Hotz, H.-R., Allain, F.H.-T., and Bühler, M. (2011). An extended dsRBD with a novel zinc-binding motif mediates nuclear retention of fission yeast Dicer. EMBO J. *30*, 4223–4235.

Baubec, T., and Schübeler, D. (2014). Genomic patterns and context specific interpretation of DNA methylation. Curr. Opin. Genet. Dev. *25*, 85–92.

Bayne, E.H., White, S. a, Kagansky, A., Bijos, D. a, Sanchez-Pulido, L., Hoe, K.-L., Kim, D.-U., Park, H.-O., Ponting, C.P., Rappsilber, J., et al. (2010). Stc1: a critical link between RNAi and chromatin modification required for heterochromatin integrity. Cell *140*, 666–677.

Bell, O., Tiwari, V.K., Thomä, N.H., and Schübeler, D. (2011). Determinants and dynamics of genome accessibility. Nat. Rev. Genet. *12*, 554–564.

Berk, A.J., and Sharp, P.A. (1977). Sizing and mapping of early adenovirus mRNAs by gel electrophoresis of S1 endonuclease-digested hybrids. Cell *12*, 721–732.

Bernstein, B.E., Liu, C.L., Humphrey, E.L., Perlstein, E.O., and Schreiber, S.L. (2004). Global nucleosome occupancy in yeast. Genome Biol. *5*, R62.

Bernstein, E., Caudy, A.A., Hammond, S.M., and Hannon, G.J. (2001). Role for a bidentate ribonuclease in the initiation step of RNA interference. Nature *409*, 363–366.

Birney, E., Stamatoyannopoulos, J.A., Dutta, A., Guigó, R., Gingeras, T.R., Margulies, E.H., Weng, Z., Snyder, M., Dermitzakis, E.T., Thurman, R.E., et al. (2007). Identification and analysis of functional elements in 1% of the human genome by the ENCODE pilot project. Nature *447*, 799–816.

Blevins, T., Pontvianne, F., Cocklin, R., Podicheti, R., Chandrasekhara, C., Yerneni, S., Braun, C., Lee, B., Rusch, D., Mockaitis, K., et al. (2014). A Two-Step Process for Epigenetic Inheritance in Arabidopsis. Mol. Cell *54*, 30–42.

Brasher, S. V, Smith, B.O., Fogh, R.H., Nietlispach, D., Thiru, A., Nielsen, P.R., Broadhurst, R.W., Ball, L.J., Murzina, N. V, and Laue, E.D. (2000). The structure of mouse HP1 suggests a unique mode of single peptide recognition by the shadow chromo domain dimer. EMBO J. *19*, 1587–1597.

Brennecke, J., Stark, A., Russell, R.B., and Cohen, S.M. (2005). Principles of microRNA-target recognition. PLoS Biol. *3*, e85.

Brennecke, J., Aravin, A.A., Stark, A., Dus, M., Kellis, M., Sachidanandam, R., and Hannon, G.J. (2007). Discrete small RNA-generating loci as master regulators of transposon activity in Drosophila. Cell *128*, 1089–1103.

Brink, R.A. (1956). A Genetic Change Associated with the R Locus in Maize Which Is Directed and Potentially Reversible. Genetics *41*, 872–889.

Brockdorff, N., Ashworth, a, Kay, G.F., McCabe, V.M., Norris, D.P., Cooper, P.J., Swift, S., and Rastan, S. (1992). The product of the mouse Xist gene is a 15 kb inactive X-specific transcript containing no conserved ORF and located in the nucleus. Cell *71*, 515–526.

Brown, C.J., Lafreniere, R.G., Powers, V.E., Sebastio, G., Ballabio, A., Pettigrew, A.L., Ledbetter, D.H., Lvey, E., Craig, I.W., and Willard, H.F. (1991). Localization of the X inactivation centre on the human X chromosome in Xq13. Nature *349*.

Brown, C.J., Hendrich, B.D., Rupert, J.L., Lafrenière, R.G., Xing, Y., Lawrence, J., and Willard, H.F. (1992). The human XIST gene: analysis of a 17 kb inactive X-specific RNA that contains conserved repeats and is highly localized within the nucleus. Cell *71*, 527–542.

Bühler, M., Verdel, A., and Moazed, D. (2006). Tethering RITS to a Nascent Transcript Initiates RNAi- and Heterochromatin-Dependent Gene Silencing. Cell *125*, 873–886.

Bühler, M., Haas, W., Gygi, S.P., and Moazed, D. (2007). RNAi-Dependent and -Independent RNA Turnover Mechanisms Contribute to Heterochromatic Gene Silencing. Cell *129*, 707–721.

Buker, S.M., Iida, T., Bühler, M., Villén, J., Gygi, S.P., Nakayama, J.-I., and Moazed, D. (2007). Two different Argonaute complexes are required for siRNA generation and heterochromatin assembly in fission yeast. Nat. Struct. Mol. Biol. *14*, 200–207.

Bulut-Karslioglu, A., Perrera, V., Scaranaro, M., de la Rosa-Velazquez, I.A., van de Nobelen, S., Shukeir, N., Popow, J., Gerle, B., Opravil, S., Pagani, M., et al. (2012). A transcription factor–based mechanism for mouse heterochromatin formation. Nat. Struct. Mol. Biol. *19*, 1023–1030.

Cam, H.P., Sugiyama, T., Chen, E.S., Chen, X., FitzGerald, P.C., and Grewal, S.I.S. (2005). Comprehensive analysis of heterochromatin- and RNAi-mediated epigenetic control of the fission yeast genome. Nat. Genet. *37*, 809–819.

Canzio, D., Chang, E.Y., Shankar, S., Kuchenbecker, K.M., Simon, M.D., Madhani, H.D., Narlikar, G.J., and Sady, B. Al (2011). Chromodomain-mediated oligomerization of HP1 suggests a nucleosome bridging mechanism for heterochromatin assembly. Mol. Cell *41*, 67–81.

Canzio, D., Liao, M., Naber, N., Pate, E., Larson, A., Wu, S., Marina, D.B., Garcia, J.F., Madhani, H.D., Cooke, R., et al. (2013). A conformational switch in HP1 releases auto-inhibition to drive heterochromatin assembly. Nature *496*, 377–381.

Canzio, D., Larson, A., and Narlikar, G.J. (2014). Mechanisms of functional promiscuity by HP1 proteins. Trends Cell Biol. *24*, 377–386.

Cao, R., and Zhang, Y. (2004). The functions of E(Z)/EZH2-mediated methylation of lysine 27 in histone H3. Curr. Opin. Genet. Dev. *14*, 155–164.

Cao, X., and Jacobsen, S.E. (2002). Locus-specific control of asymmetric and CpNpG methylation by the DRM and CMT3 methyltransferase genes. Proc. Natl. Acad. Sci. U. S. A. *99 Suppl 4*, 16491–16498.

Carroll, Â.O., Strahl, B.D., Sun, Z., Schmid, M., Opravil, S., Mechtler, K., Rea, S., Eisenhaber, F., Ponting, C.P., Allis, C.D., et al. (2000). Regulation of chromatin structure by site-speci ® c histone H3 methyltransferases. 593–599.

Castel, S.E., and Martienssen, R. a (2013). RNA interference in the nucleus: roles for small RNAs in transcription, epigenetics and beyond. Nat. Rev. Genet. *14*, 100–112.

Catez, F., Brown, D.T., Misteli, T., and Bustin, M. (2002). Competition between histone H1 and HMGN proteins for chromatin binding sites. EMBO Rep. *3*, 760–766.

Chan, S.W.-L., Zhang, X., Bernatavichute, Y. V, and Jacobsen, S.E. (2006). Two-step recruitment of RNA-directed DNA methylation to tandem repeats. PLoS Biol. *4*, e363.

Chandler, V.L. (2007). Paramutation: from maize to mice. Cell *128*, 641–645.

Chen, E.S., Zhang, K., Nicolas, E., Cam, H.P., Zofall, M., and Grewal, S.I.S. (2008). Cell cycle control of centromeric repeat transcription and heterochromatin assembly. Nature *451*, 734–737.

Cheutin, T., McNairn, A.J., Jenuwein, T., Gilbert, D.M., Singh, P.B., and Misteli, T. (2003). Maintenance of stable heterochromatin domains by dynamic HP1 binding. Science *299*, 721–725.

Cheutin, T., Gorski, S.A., May, K.M., Prim, B., Misteli, T., and Singh, P.B. (2004). In Vivo Dynamics of Swi6 in Yeast : Evidence for a Stochastic Model of Heterochromatin. Mol. Cell. Biol. *24*, 3157–3167.

Choi, C.H., Kalosakas, G., Rasmussen, K., Hiromura, M., Bishop, A.R., and Usheva, A. (2004). DNA dynamically directs its own transcription initiation. Nucleic Acids Res. *32*, 1584–1590.

Clarke, L., and Baum, M.P. (1990). Functional analysis of a centromere from fission yeast: a role for centromere-specific repeated DNA sequences. Mol. Cell. Biol. *10*, 1863–1872.

Colmenares, S.U., Buker, S.M., Buhler, M., Dlakić, M., and Moazed, D. (2007). Coupling of Double-Stranded RNA Synthesis and siRNA Generation in Fission Yeast RNAi. Mol. Cell *27*, 449–461.

Cook, P.R. (2001). Principles of Nuclear Structure and Function (John Wiley & Sons).

Cowieson, N.P., Partridge, J.F., Allshire, R.C., and McLaughlin, P.J. (2000). Dimerisation of a chromo shadow domain and distinctions from the chromodomain as revealed by structural analysis. Curr. Biol. *10*, 517–525.

Dalal, Y., Furuyama, T., Vermaak, D., and Henikoff, S. (2007). Structure , dynamics , and evolution of centromeric nucleosomes. PNAS *104*.

Deal, R.B., Henikoff, J.G., and Henikoff, S. (2010). Genome-wide kinetics of nucleosome turnover determined by metabolic labeling of histones. Science *328*, 1161–1164.

Debeauchamp, J.L., Moses, A., Noffsinger, V.J.P., Ulrich, D.L., Job, G., Kosinski, A.M., and Partridge, J.F. (2008). Chp1-Tas3 interaction is required to recruit RITS to fission yeast centromeres and for maintenance of centromeric heterochromatin. Mol. Cell. Biol. *28*, 2154–2166.

Dion, V., Kalck, V., Horigome, C., Towbin, B.D., and Gasser, S.M. (2012). Increased mobility of double-strand breaks requires Mec1, Rad9 and the homologous recombination machinery. Nat. Cell Biol. *14*, 502–509.

Djebali, S., Davis, C.A., Merkel, A., Dobin, A., Lassmann, T., Mortazavi, A., Tanzer, A., Lagarde, J., Lin, W., Schlesinger, F., et al. (2012). Landscape of transcription in human cells. Nature *489*, 101–108.

Djupedal, I., Kos-Braun, I.C., Mosher, R.A., Söderholm, N., Simmer, F., Hardcastle, T.J., Fender, A., Heidrich, N., Kagansky, A., Bayne, E., et al. (2009). Analysis of small RNA in fission yeast; centromeric siRNAs are potentially generated through a structured RNA. EMBO J. *28*, 3832–3844.

Eichten, S.R., Briskine, R., Song, J., Li, Q., Swanson-Wagner, R., Hermanson, P.J., Waters, A.J., Starr, E., West, P.T., Tiffin, P., et al. (2013). Epigenetic and genetic influences on DNA methylation variation in maize populations. Plant Cell *25*, 2783–2797.

Eissenberg, J.C., and Elgin, S.C.R. (2014). HP1a: A structural chromosomal protein regulating transcription. Trends Genet. *30*, 103–110.

Emmerth, S., Schober, H., Gaidatzis, D., Roloff, T., Jacobeit, K., and Bühler, M. (2010). Nuclear retention of fission yeast dicer is a prerequisite for RNAi-mediated heterochromatin assembly. Dev. Cell *18*, 102–113.

Erhard, K.F., and Hollick, J.B. (2011). Paramutation: a process for acquiring trans-generational regulatory states. Curr. Opin. Plant Biol. *14*, 210–216.

Feng, S., Jacobsen, S.E., and Reik, W. (2010). Epigenetic reprogramming in plant and animal development. Science *330*, 622–627.

Festenstein, R., Pagakis, S.N., Hiragami, K., Lyon, D., Verreault, A., Sekkali, B., and Kioussis, D. (2003). Modulation of heterochromatin protein 1 dynamics in primary Mammalian cells. Science *299*, 719–721.

Fire, A., Xu, S., Montgomery, M.K., Kostas, S.A., Driver, S.E., and Mello, C.C. (1998). Potent and specific genetic interference by double-stranded RNA in Caenorhabditis elegans. Nature *391*, 806–811.

Fishel, B., Amstutz, H., Baum, M., Carbon, J., and Clarke, L. (1988). Structural organization and functional analysis of centromeric DNA in the fission yeast Schizosaccharomyces pombe. Mol. Cell. Biol. *8*, 754–763.

Freeman-Cook, L.L., Gómez, E.B., Spedale, E.J., Marlett, J., Forsburg, S.L., Pillus, L., and Laurenson, P. (2005). Conserved locus-specific silencing functions of Schizosaccharomyces pombe sir2+. Genetics *169*, 1243–1260.

Ghildiyal, M., and Zamore, P.D. (2009). Small silencing RNAs: an expanding universe. Nat. Rev. Genet. *10*, 94–108.

Grewal, S.I., and Klar, A.J. (1997). A recombinationally repressed region between mat2 and mat3 loci shares homology to centromeric repeats and regulates directionality of mating-type switching in fission yeast. Genetics *146*, 1221–1238.

Grewal, S.I.S., and Jia, S. (2007). Heterochromatin revisited. Nat. Rev. Genet. *8*, 35–46.

Grunstein, M., and Gasser, S.M. (2013). Epigenetics in Saccharomyces cerevisiae. Cold Spring Harb. Perspect. Biol. *5*.

Guacci, V., Hogan, E., and Koshland, D. (1997). Centromere position in budding yeast: evidence for anaphase A. Mol. Biol. Cell *8*, 957–972.

Guertin, M.J., and Lis, J.T. (2013). Mechanisms by which transcription factors gain access to target sequence elements in chromatin. Curr. Opin. Genet. Dev. *23*, 116–123.

Gunawardane, L.S., Saito, K., Nishida, K.M., Miyoshi, K., Kawamura, Y., Nagami, T., Siomi, H., and Siomi, M.C. (2007). A slicer-mediated mechanism for repeat-associated siRNA 5' end formation in Drosophila. Science *315*, 1587–1590.

Halic, M., and Moazed, D. (2010). Dicer-Independent Primal RNAs Trigger RNAi and Heterochromatin Formation. Cell *140*, 504–516.

Hall, I.M., Shankaranarayana, G.D., Noma, K.-I., Ayoub, N., Cohen, A., and Grewal, S.I.S. (2002). Establishment and maintenance of a heterochromatin domain. Science *297*, 2232–2237.

Hamilton, a. J. (1999). A Species of Small Antisense RNA in Posttranscriptional Gene Silencing in Plants. Science (80-.). *286*, 950–952.

Hammond, S.M., Bernstein, E., Beach, D., and Hannon, G.J. (2000). An RNA-directed nuclease mediates post-transcriptional gene silencing in Drosophila cells. Nature *404*, 293–296.

Han, M., Chang, M., Kim, U.J., and Grunstein, M. (1987). Histone H2B repression causes cell-cycle-specific arrest in yeast: effects on chromosomal segregation, replication, and transcription. Cell *48*, 589–597.

Heitz, E. (1928). Das Heterochromatin der Moose.

Herr, A.J., Jensen, M.B., Dalmay, T., and Baulcombe, D.C. (2005). RNA polymerase IV directs silencing of endogenous DNA. Science *308*, 118–120.

Imai, S., Armstrong, C.M., Kaeberlein, M., and Guarente, L. (2000). Transcriptional silencing and longevity protein Sir2 is an NAD-dependent histone deacetylase. Nature *403*, 795–800.

Irvine, D. V, Zaratiegui, M., Tolia, N.H., Goto, D.B., Chitwood, D.H., Vaughn, M.W., Joshua-Tor, L., and Martienssen, R.A. (2006). Argonaute slicing is required for heterochromatic silencing and spreading. Science *313*, 1134–1137.

JACOB, F., and MONOD, J. (1961). Genetic regulatory mechanisms in the synthesis of proteins. J. Mol. Biol. *3*, 318–356.

Jacob, F., Perrin, D., Sanchez, C., and Monod, J. (1960). The Operon: A group of genes whose expression is coordinated by an operator. Comptes Rendus Des Séances L'academie Des Sci. *250*, 1727–1729.

James, T.C., and Elgin, S.C. (1986). Identification of a nonhistone chromosomal protein associated with heterochromatin in Drosophila melanogaster and its gene. Mol. Cell. Biol. *6*, 3862–3872.

Jeon, Y., and Lee, J.T. (2011). YY1 Tethers Xist RNA to the inactive X nucleation center. Cell *146*, 119–133.

Jia, S., Noma, K., and Grewal, S.I.S. (2004). RNAi-independent heterochromatin nucleation by the stress-activated ATF/CREB family proteins. Science *304*, 1971–1976.

Jin, Q., Fuchs, J., and Loidl, J. (2000). Centromere clustering is a major determinant of yeast interphase nuclear organization. J. Cell Sci. *113*, 1903–1912.

Johnson, L.M., Du, J., Hale, C.J., Bischof, S., Feng, S., Chodavarapu, R.K., Zhong, X., Marson, G., Pellegrini, M., Segal, D.J., et al. (2014). SRA- and SET-domain-containing proteins link RNA polymerase V occupancy to DNA methylation. Nature *507*, 124–128.

Kagansky, A., Folco, H.D., Almeida, R., Pidoux, A.L., Boukaba, A., Simmer, F., Urano, T., Hamilton, G.L., and Allshire, R.C. (2009). Synthetic heterochromatin bypasses RNAi and centromeric repeats to establish functional centromeres. Science *324*, 1716–1719.

Kanno, T., Huettel, B., Mette, M.F., Aufsatz, W., Jaligot, E., Daxinger, L., Kreil, D.P., Matzke, M., and Matzke, A.J.M. (2005). Atypical RNA polymerase subunits required for RNA-directed DNA methylation. Nat. Genet. *37*, 761–765.

Kanoh, J., Sadaie, M., Urano, T., and Ishikawa, F. (2005). Telomere binding protein Taz1 establishes Swi6 heterochromatin independently of RNAi at telomeres. Curr. Biol. *15*, 1808–1819.

Keller, C., Adaixo, R., Stunnenberg, R., Woolcock, K.J., Hiller, S., and Bühler, M. (2012). HP1(Swi6) mediates the recognition and destruction of heterochromatic RNA transcripts. Mol. Cell *47*, 215–227.

Keller, C., Kulasegaran-Shylini, R., Shimada, Y., Hotz, H.-R., and Bühler, M. (2013). Noncoding RNAs prevent spreading of a repressive histone mark. Nat. Struct. Mol. Biol. *20*, 994–1000.

Kermicle, J.L., Eggleston, W.B., and Alleman, M. (1995). Organization of paramutagenicity in R-stippled maize. Genetics *141*, 361–372.

Kimura, H. (2005). Histone dynamics in living cells revealed by photobleaching. DNA Repair (Amst). *4*, 939–950.

Kimura, H., and Cook, P.R. (2001). Kinetics of core histones in living human cells: Little exchange of H3 and H4 and some rapid exchange of H2B. J. Cell Biol. *153*, 1341–1353.

Klattenhoff, C., Xi, H., Li, C., Lee, S., Xu, J., Khurana, J.S., Zhang, F., Schultz, N., Koppetsch, B.S., Nowosielska, A., et al. (2009). The Drosophila HP1 homolog Rhino is required for transposon silencing and piRNA production by dual-strand clusters. Cell *138*, 1137–1149.

Kloc, A., Zaratiegui, M., Nora, E., and Martienssen, R. (2008). RNA interference guides histone modification during the S phase of chromosomal replication. Curr. Biol. *18*, 490–495.

Knezetic, J.A., and Luse, D.S. (1986). The presence of nucleosomes on a DNA template prevents initiation by RNA polymerase II in vitro. Cell *45*, 95–104.

Kon, N., Krawchuk, M.D., Warren, B.G., Smith, G.R., and Wahls, W.P. (1997). Transcription factor Mts1/Mts2 (Atf1/Pcr1, Gad7/Pcr1) activates the M26 meiotic recombination hotspot in Schizosaccharomyces pombe. Proc. Natl. Acad. Sci. U. S. A. *94*, 13765–13770.

Kosak, S.T., Scalzo, D., Alworth, S. V, Li, F., Palmer, S., Enver, T., Lee, J.S.J., and Groudine, M. (2007). Coordinate gene regulation during hematopoiesis is related to genomic organization. PLoS Biol. *5*, e309.

Krol, J., Loedige, I., and Filipowicz, W. (2010). The widespread regulation of microRNA biogenesis, function and decay. Nat. Rev. Genet. *11*, 597–610.

Lachner, M., O'Carroll, D., Rea, S., Mchtler, K., and Jenuwein, T. (2001). Methylation of histone H3 lysine 9 creates a binding site for HP1 proteins. Nature *410*.

Lander, E.S., Linton, L.M., Birren, B., Nusbaum, C., Zody, M.C., Baldwin, J., Devon, K., Dewar, K., Doyle, M., FitzHugh, W., et al. (2001). Initial sequencing and analysis of the human genome. Nature *409*, 860–921.

Law, J. a, Du, J., Hale, C.J., Feng, S., Krajewski, K., Palanca, A.M.S., Strahl, B.D., Patel, D.J., and Jacobsen, S.E. (2013). Polymerase IV occupancy at RNA-directed DNA methylation sites requires SHH1. Nature *498*, 385–389.

Law, J.A., Vashisht, A.A., Wohlschlegel, J.A., and Jacobsen, S.E. (2011). SHH1, a homeodomain protein required for DNA methylation, as well as RDR2, RDM4, and chromatin remodeling factors, associate with RNA polymerase IV. PLoS Genet. *7*, e1002195.

Lawrence, C.L., Maekawa, H., Worthington, J.L., Reiter, W., Wilkinson, C.R.M., and Jones, N. (2007). Regulation of Schizosaccharomyces pombe Atf1 protein levels by Sty1-mediated phosphorylation and heterodimerization with Pcr1. J. Biol. Chem. *282*, 5160–5170.

Lee, J.T., and Bartolomei, M.S. (2013). X-inactivation, imprinting, and long noncoding RNAs in health and disease. Cell *152*, 1308–1323.

Lee, J.T., and Lu, N. (1999). Targeted mutagenesis of Tsix leads to nonrandom X inactivation. Cell *99*, 47–57.

Lee, C.-K., Shibata, Y., Rao, B., Strahl, B.D., and Lieb, J.D. (2004). Evidence for nucleosome depletion at active regulatory regions genome-wide. Nat. Genet. *36*, 900–905.

Lee, H.J., Hore, T. a, and Reik, W. (2014). Reprogramming the Methylome: Erasing Memory and Creating Diversity. Cell Stem Cell *14*, 710–719.

Lee, J.T., Davidow, L.S., and Warshawsky, D. (1999). Tsix, a gene antisense to Xist at the X-inactivation centre. Nat. Genet. *21*, 400–404.

Lever, M.A., Th, J.P.H., Sun, X., and Hendzel, M.J. (2000). Rapid exchange of histone H1 . 1 on chromatin in living human cells. *8916*, 873–876.

Lewis, B.P., Shih, I., Jones-Rhoades, M.W., Bartel, D.P., and Burge, C.B. (2003). Prediction of mammalian microRNA targets. Cell *115*, 787–798.

Lewis, B.P., Burge, C.B., and Bartel, D.P. (2005). Conserved seed pairing, often flanked by adenosines, indicates that thousands of human genes are microRNA targets. Cell *120*, 15–20.

Li, C.F., Pontes, O., El-Shami, M., Henderson, I.R., Bernatavichute, Y. V, Chan, S.W.-L., Lagrange, T., Pikaard, C.S., and Jacobsen, S.E. (2006). An ARGONAUTE4-containing nuclear processing center colocalized with Cajal bodies in Arabidopsis thaliana. Cell *126*, 93–106.

Li, F., Sonbuchner, L., Kyes, S. a., Epp, C., and Deitsch, K.W. (2008). Nuclear non-coding RNAs are transcribed from the centromeres of Plasmodium falciparum and are associated with centromeric chromatin. J. Biol. Chem. *283*, 5692–5698.

Li, H., Motamedi, M.R., Yip, C.K., Wang, Z., Walz, T., Patel, D.J., and Moazed, D. (2009). An alpha motif at Tas3 C terminus mediates RITS cis spreading and promotes heterochromatic gene silencing. Mol. Cell *34*, 155–167.

Lieberman-Aiden, E., van Berkum, N.L., Williams, L., Imakaev, M., Ragoczy, T., Telling, A., Amit, I., Lajoie, B.R., Sabo, P.J., Dorschner, M.O., et al. (2009). Comprehensive mapping of long-range interactions reveals folding principles of the human genome. Science *326*, 289–293.

Lomberk, G., Bensi, D., Fernandez-Zapico, M.E., and Urrutia, R. (2006a). Evidence for the existence of an HP1-mediated subcode within the histone code. Nat. Cell Biol. *8*, 407–415.

Lomberk, G., Wallrath, L., and Urrutia, R. (2006b). The Heterochromatin Protein 1 family. Genome Biol. *7*, 228.

Lorch, Y., LaPointe, J.W., and Kornberg, R.D. (1987). Nucleosomes inhibit the initiation of transcription but allow chain elongation with the displacement of histones. Cell *49*, 203–210.

Maison, C., Bailly, D., Roche, D., Montes de Oca, R., Probst, A. V, Vassias, I., Dingli, F., Lombard, B., Loew, D., Quivy, J.-P., et al. (2011). SUMOylation promotes de novo targeting of HP1α to pericentric heterochromatin. Nat. Genet. *43*, 220–227.

Marasovic, M., Zocco, M., and Halic, M. (2013). Argonaute and triman generate dicer-independent prirnas and mature siRNAs to initiate heterochromatin formation. Mol. Cell *52*, 173–183.

Matzke, M., Kanno, T., Daxinger, L., Huettel, B., and Matzke, A.J.M. (2009). RNA-mediated chromatin-based silencing in plants. Curr. Opin. Cell Biol. *21*, 367–376.

Misteli, T., Gunjan, A., Hock, R., Bustin, M., and Brown, D.T. (2000). Dynamic binding of histone H1 to chromatin in living cells. Nature *408*, 877–881.

Mohn, F., Sienski, G., Handler, D., and Brennecke, J. (2014). The rhino-deadlock-cutoff complex licenses noncanonical transcription of dual-strand piRNA clusters in Drosophila. Cell *157*, 1364–1379.

Motamedi, M.R., Verdel, A., Colmenares, S.U., Gerber, S. a., Gygi, S.P., and Moazed, D. (2004). Two RNAi complexes, RITS and RDRC, physically interact and localize to noncoding centromeric RNAs. Cell *119*, 789–802.

Motamedi, M.R., Hong, E.J.E., Li, X., Gerber, S., Denison, C., Gygi, S., and Moazed, D. (2008). HP1 Proteins Form Distinct Complexes and Mediate Heterochromatic Gene Silencing by Nonoverlapping Mechanisms. Mol. Cell *32*, 778–790.

Muller, H.J. (1930). Types of visible variations induced by X-rays inDrosophila. J. Genet. *22*, 299–334.

Nakayama, J., Rice, J.C., Strahl, B.D., Allis, C.D., and Grewal, S.I. (2001). Role of histone H3 lysine 9 methylation in epigenetic control of heterochromatin assembly. Science *292*, 110–113.

Noma, K., Cam, H.P., Maraia, R.J., and Grewal, S.I.S. (2006). A role for TFIIIC transcription factor complex in genome organization. Cell *125*, 859–872.

Noma K, Allis, C.D., and Grewal, S.I. (2001). Transitions in distinct histone H3 methylation patterns at the heterochromatin domain boundaries. Science *293*, 1150–1155.

Onodera, Y., Haag, J.R., Ream, T., Costa Nunes, P., Pontes, O., and Pikaard, C.S. (2005). Plant nuclear RNA polymerase IV mediates siRNA and DNA methylation-dependent heterochromatin formation. Cell *120*, 613–622.

Ooi, S.L., and Henikoff, S. (2007). Germline histone dynamics and epigenetics. Curr. Opin. Cell Biol. *19*, 257–265.

Peric-Hupkes, D., Meuleman, W., Pagie, L., Bruggeman, S.W.M., Solovei, I., Brugman, W., Gräf, S., Flicek, P., Kerkhoven, R.M., van Lohuizen, M., et al. (2010). Molecular maps of the reorganization of genome-nuclear lamina interactions during differentiation. Mol. Cell *38*, 603–613.

Petrie, V.J., Wuitschick, J.D., Givens, C.D., Kosinski, A.M., and Partridge, J.F. (2005). RNA interference (RNAi)-dependent and RNAi-independent association of the Chp1 chromodomain protein with distinct heterochromatic loci in fission yeast. Mol. Cell. Biol. *25*, 2331–2346.

Piacentini, L., Fanti, L., Berloco, M., Perrini, B., and Pimpinelli, S. (2003). Heterochromatin protein 1 (HP1) is associated with induced gene expression in Drosophila euchromatin. J. Cell Biol. *161*, 707–714.

Pontes, O., Li, C.F., Costa Nunes, P., Haag, J., Ream, T., Vitins, A., Jacobsen, S.E., and Pikaard, C.S. (2006). The Arabidopsis chromatin-modifying nuclear siRNA pathway involves a nucleolar RNA processing center. Cell *126*, 79–92.

Ptashne, M. (2013). Epigenetics: core misconcept. Proc. Natl. Acad. Sci. U. S. A. *110*, 7101–7103.

Qi, Y., He, X., Wang, X.-J., Kohany, O., Jurka, J., and Hannon, G.J. (2006). Distinct catalytic and non-catalytic roles of ARGONAUTE4 in RNA-directed DNA methylation. Nature *443*, 1008–1012.

Rangan, P., Malone, C.D., Navarro, C., Newbold, S.P., Hayes, P.S., Sachidanandam, R., Hannon, G.J., and Lehmann, R. (2011). piRNA production requires heterochromatin formation in Drosophila. Curr. Biol. *21*, 1373–1379.

Regulski, M., Lu, Z., Kendall, J., Donoghue, M.T.A., Reinders, J., Llaca, V., Deschamps, S., Smith, A., Levy, D., McCombie, W.R., et al. (2013). The maize methylome influences mRNA splice sites and reveals widespread paramutation-like switches guided by small RNA. Genome Res. *23*, 1651–1662.

Reik, W. (2007). Stability and flexibility of epigenetic gene regulation in mammalian development. Nature *447*, 425–432.

Reinke, H., and Hörz, W. (2003). Histones are first hyperacetylated and then lose contact with the activated PHO5 promoter. Mol. Cell *11*, 1599–1607.

Rine, J., and Herskowitz, I. (1987). Four genes responsible for a position effect on expression from HML and HMR in Saccharomyces cerevisiae. Genetics *116*, 9–22.

Rouleux-Bonnin, F., Renault, S., Bigot, Y., and Periquet, G. (1996). Transcription of four satellite DNA subfamilies in Diprion pini (Hymenoptera, Symphyta, Diprionidae). Eur. J. Biochem. *238*, 752–759.

Sadaie, M., Iida, T., Urano, T., and Nakayama, J.-I. (2004). A chromodomain protein, Chp1, is required for the establishment of heterochromatin in fission yeast. EMBO J. *23*, 3825–3835.

Sadaie, M., Kawaguchi, R., Ohtani, Y., Arisaka, F., Tanaka, K., Shirahige, K., and Nakayama, J.-I. (2008). Balance between distinct HP1 family proteins controls heterochromatin assembly in fission yeast. Mol. Cell. Biol. *28*, 6973–6988.

Sado, T., Hoki, Y., and Sasaki, H. (2005). Tsix silences Xist through modification of chromatin structure. Dev. Cell *9*, 159–165.

Schalch, T., Job, G., Noffsinger, V.J., Shanker, S., Kuscu, C., Joshua-Tor, L., and Partridge, J.F. (2009). High-Affinity Binding of Chp1 Chromodomain to K9 Methylated Histone H3 Is Required to Establish Centromeric Heterochromatin. Mol. Cell *34*, 36–46.

Scheer, U., and Weisenberger, D. (1994). The nucleolus. Curr. Opin. Cell Biol. *6*, 354–359.

Seisenberger, S., Andrews, S., Krueger, F., Arand, J., Walter, J., Santos, F., Popp, C., Thienpont, B., Dean, W., and Reik, W. (2012). The dynamics of genome-wide DNA methylation reprogramming in mouse primordial germ cells. Mol. Cell *48*, 849–862.

Sekinger, E. a., Moqtaderi, Z., and Struhl, K. (2005). Intrinsic histone-DNA interactions and low nucleosome density are important for preferential accessibility of promoter regions in yeast. Mol. Cell *18*, 735–748.

Shankaranarayana, G.D., Motamedi, M.R., Moazed, D., Grewal, S.I.S., Harbor, C.S., and York, N. (2003). Sir2 Regulates Histone H3 Lysine 9 Methylation and Heterochromatin Assembly in Fission Yeast. Curr. Biol. *13*, 1240–1246.

Shanker, S., Job, G., George, O.L., Creamer, K.M., Shaban, A., and Partridge, J.F. (2010). Continuous requirement for the Clr4 complex but not RNAi for centromeric heterochromatin assembly in fission yeast harboring a disrupted RITS complex. PLoS Genet. *6*, 1–16.

Sidorenko, L. V, Li, X., Cocciolone, S.M., Chopra, S., Tagliani, L., Bowen, B., Daniels, M., and Peterson, T. (2000). Complex structure of a maize Myb gene promoter: functional analysis in transgenic plants. Plant J. *22*, 471–482.

Sienski, G., Dönertas, D., and Brennecke, J. (2012). Transcriptional silencing of transposons by Piwi and maelstrom and its impact on chromatin state and gene expression. Cell *151*, 964–980.

Smothers, J.F., and Henikoff, S. (2000). The HP1 chromo shadow domain binds a consensus peptide pentamer. Curr. Biol. *10*, 27–30.

Solovei, I., Kreysing, M., Lanctôt, C., Kösem, S., Peichl, L., Cremer, T., Guck, J., and Joffe, B. (2009). Nuclear Architecture of Rod Photoreceptor Cells Adapts to Vision in Mammalian Evolution. Cell *137*, 356–368.

Solovei, I., Wang, A.S., Thanisch, K., Schmidt, C.S., Krebs, S., Zwerger, M., Cohen, T. V, Devys, D., Foisner, R., Peichl, L., et al. (2013). LBR and lamin A/C sequentially tether peripheral heterochromatin and inversely regulate differentiation. Cell *152*, 584–598.

Stam, M., Belele, C., Dorweiler, J.E., and Chandler, V.L. (2002). Differential chromatin structure within a tandem array 100 kb upstream of the maize b1 locus is associated with paramutation. Genes Dev. *16*, 1906–1918.

Van Steensel, B. (2011). Chromatin: constructing the big picture. EMBO J. *30*, 1885–1895.

Stunnenberg, R., and Bühler, M. (2012). A Detour to Mature. Mol. Cell *46*, 719–721.

Sugiyama, T., Cam, H.P., Sugiyama, R., Noma, K., Zofall, M., Kobayashi, R., and Grewal, S.I.S. (2007). SHREC, an effector complex for heterochromatic transcriptional silencing. Cell *128*, 491–504.

Sun, B.K., Deaton, A.M., and Lee, J.T. (2006). A transient heterochromatic state in Xist preempts X inactivation choice without RNA stabilization. Mol. Cell *21*, 617–628.

Taddei, A., and Gasser, S.M. (2012). Structure and function in the budding yeast nucleus. Genetics *192*, 107–129.

Taddei, A., Hediger, F., Neumann, F.R., Bauer, C., and Gasser, S.M. (2004). Separation of silencing from perinuclear anchoring functions in yeast Ku80, Sir4 and Esc1 proteins. EMBO J. *23*, 1301–1312.

The ENCODE Project Consortium (2004). The ENCODE (ENCyclopedia Of DNA Elements) Project. Science *306*, 636–640.

Le Thomas, A., Rogers, A.K., Webster, A., Marinov, G.K., Liao, S.E., Perkins, E.M., Hur, J.K., Aravin, A.A., and Tóth, K.F. (2013). Piwi induces piRNA-guided transcriptional silencing and establishment of a repressive chromatin state. Genes Dev. *27*, 390–399.

Thurman, R.E., Rynes, E., Humbert, R., Vierstra, J., Maurano, M.T., Haugen, E., Sheffield, N.C., Stergachis, A.B., Wang, H., Vernot, B., et al. (2012). The accessible chromatin landscape of the human genome. Nature *489*, 75–82.

Tjian, R. (1981). T antigen binding and the control of SV40 gene expression. Cell *26*, 1–2.

Tsukada, Y., Fang, J., Erdjument-Bromage, H., Warren, M.E., Borchers, C.H., Tempst, P., and Zhang, Y. (2006). Histone demethylation by a family of JmjC domain-containing proteins. Nature *439*, 811–816.

Venter, J.C., Adams, M.D., Myers, E.W., Li, P.W., Mural, R.J., Sutton, G.G., Smith, H.O., Yandell, M., Evans, C.A., Holt, R.A., et al. (2001). The sequence of the human genome. Science *291*, 1304–1351.

Verdel, A., Jia, S., Gerber, S., Sugiyama, T., Gygi, S., Grewal, S.I.S., and Moazed, D. (2004). RNAi-mediated targeting of heterochromatin by the RITS complex. Science *303*, 672–676.

Volpe, T. a, Kidner, C., Hall, I.M., Teng, G., Grewal, S.I.S., and Martienssen, R. a (2002). Regulation of heterochromatic silencing and histone H3 lysine-9 methylation by RNAi. Science *297*, 1833–1837.

Wang, S.H., and Elgin, S.C.R. (2011). Drosophila Piwi functions downstream of piRNA production mediating a chromatin-based transposon silencing mechanism in female germ line. Proc. Natl. Acad. Sci. U. S. A. *108*, 21164–21169.

Wang, J., Tadeo, X., Hou, H., Tu, P.G., Thompson, J., Yates, J.R., and Jia, S. (2013). Epe1 recruits BET family bromodomain protein Bdf2 to establish heterochromatin boundaries. Genes Dev. *27*, 1886–1902.

Wassenegger, M., Heimes, S., Riedel, L., and Sänger, H.L. (1994). RNA-directed de novo methylation of genomic sequences in plants. Cell *76*, 567–576.

Wierzbicki, A.T., Haag, J.R., and Pikaard, C.S. (2008). Noncoding transcription by RNA polymerase Pol IVb/Pol V mediates transcriptional silencing of overlapping and adjacent genes. Cell *135*, 635–648.

Woolcock, K.J. (2012). RNA interference-mediated co-transcriptional gene silencing in fission yeast. 1–171.

Woolcock, K.J., Stunnenberg, R., Gaidatzis, D., Hotz, H.R., Emmerth, S., Barraud, P., and Bühler, M. (2012). RNAi keeps Atf1-bound stress response genes in check at nuclear pores. Genes Dev. *26*, 683–692.

Workman, J.L., and Kingston, R.E. (1998). Alteration of nucleosome structure as a mechanism of transcriptional regulation. Annu. Rev. Biochem. *67*, 545–579.

Xie, Z., Johansen, L.K., Gustafson, A.M., Kasschau, K.D., Lellis, A.D., Zilberman, D., Jacobsen, S.E., and Carrington, J.C. (2004). Genetic and functional diversification of small RNA pathways in plants. PLoS Biol. *2*, E104.

Yamada, T., Fischle, W., Sugiyama, T., Allis, C.D., and Grewal, S.I.S. (2005). The nucleation and maintenance of heterochromatin by a histone deacetylase in fission yeast. Mol. Cell *20*, 173–185.

Yamanaka, S., Mehta, S., Reyes-Turcu, F.E., Zhuang, F., Fuchs, R.T., Rong, Y., Robb, G.B., and Grewal, S.I.S. (2013). RNAi triggered by specialized machinery silences developmental genes and retrotransposons. Nature *493*, 557–560.

Ye, R., Wang, W., Iki, T., Liu, C., Wu, Y., Ishikawa, M., Zhou, X., and Qi, Y. (2012). Cytoplasmic assembly and selective nuclear import of Arabidopsis Argonaute4/siRNA complexes. Mol. Cell *46*, 859–870.

Zamore, P.D., Tuschl, T., Sharp, P.A., and Bartel, D.P. (2000). RNAi: double-stranded RNA directs the ATP-dependent cleavage of mRNA at 21 to 23 nucleotide intervals. Cell *101*, 25–33.

Zhang, K., Mosch, K., Fischle, W., and Grewal, S.I.S. (2008). Roles of the Clr4 methyltransferase complex in nucleation, spreading and maintenance of heterochromatin. Nat. Struct. Mol. Biol. *15*, 381–388.

Zhang, Z., Wang, J., Schultz, N., Zhang, F., Parhad, S.S., Tu, S., Vreven, T., Zamore, P.D., Weng, Z., and Theurkauf, W.E. (2014). The HP1 homolog rhino anchors a nuclear complex that suppresses piRNA precursor splicing. Cell *157*, 1353–1363.

Zhao, J., Sun, B.K., Erwin, J. a, Song, J.-J., and Lee, J.T. (2008). Polycomb proteins targeted by a short repeat RNA to the mouse X chromosome. Science *322*, 750–756.

Zhong, X., Du, J., Hale, C.J., Gallego-Bartolome, J., Feng, S., Vashisht, A.A., Chory, J., Wohlschlegel, J.A., Patel, D.J., and Jacobsen, S.E. (2014). Molecular mechanism of action of plant DRM de novo DNA methyltransferases. Cell *157*, 1050–1060.

Zofall, M., and Grewal, S.I.S. (2006). Swi6/HP1 recruits a JmjC domain protein to facilitate transcription of heterochromatic repeats. Mol. Cell *22*, 681–692.

Zofall, M., Fischer, T., Zhang, K., Zhou, M., Cui, B., Veenstra, T.D., and Grewal, S.I.S. (2009). Histone H2A.Z cooperates with RNAi and heterochromatin factors to suppress antisense RNAs. Nature *461*, 419–422.

Zofall, M., Yamanaka, S., Reyes-Turcu, F.E., Zhang, K., Rubin, C., and Grewal, S.I.S. (2012). RNA elimination machinery targeting meiotic mRNAs promotes facultative heterochromatin formation. Science *335*, 96–100.

ACKNOWLEDGEMENTS

And now comes one of the most important parts of the thesis: the acknowledgements.

First of all I like to express my gratitude to Marc Bühler who gave me the opportunity to work in his lab and for being an outstanding mentor. His enthusiasm and optimism helped me through difficult times when my naïve world as a fresh PhD student was about to collapse due to the feeling of failure and frustration by the eternal struggle to make science work. I'm grateful for his patience, positive attitude and the ability to come up with new interesting projects at any time. Marc supported me and was always very understanding also when I faced difficult times outside of science. Next, I like to acknowledge my committee members Geneviève Almouzni, Susan Gasser and Jeffrey Chao for good and critical feedback and fruitful discussions that helped to shape my project.

A lot of work that I have done during my PhD is connected to the FMI facilities with a main focus on the imaging facility. Therefore, I like to thank the FAIM facility for all their help in establishing and optimizing different methods and the data analysis. With special thanks to Laurent Gelman and Moritz Kirschmann who contributed a lot to my work. It was important to have good colleagues that are always glad to help and provide input for further improvement. Besides, it was comforting to see that I wasn't the only one that got slightly insane from analyzing FRAP-data, and so I shared the pain with Moritz.

As I spend hours in the dark behind the microscope, hunting and shooting fluorescent dots, I like to thank my inline skates and Lange Erlen for a good break in nature and mediating my 'FRAP-frustration-outlet'. I think it is normal to have a lot of frustration moments during your PhD, but fortunately also a lot of great moments. Especially in the first two years I enjoyed the company of many awesome people including Katy, Claudia, Kasia, Elli, Enrico, Mariano, Paolo, Andi, Steffen, Rabih, Silvio and Rodrigo with whom I attended happy hours, had coffee breaks, spend time at Paddy's, played Rockband and of course discussed some occasional science. This reminds me to apologize and also thank the people on the first floor for bearing the intense moments in which Claudia, Katy and me listened to the 'Crappy-Happy-Hour'-songs in the lab. While it represented a good outlet of positive and negative feelings for us, the rest of the lab rather suffered.

The lab! I am really grateful to have spent my time as a PhD student in such a great lab. It was a good working environment in which we freely discussed science and helped each other whenever needed. I learned a lot from Heiko (previous PostDoc), Yukiko, Nathalie and Claudia who introduced me to different techniques and aspects of the fission yeast model system. Besides, the general atmosphere in the lab was great and I had a good connection to many people on a personal level. Special thanks go to Katy and Rodrigo for great times outside of the lab. Not only the 'old' people from my lab deserve my recognition, but also the newer recruits added a lot of scientific and personal value to my time at FMI. The recruitment of Vale and Adriano significantly increased the fun level in the lab, which also increased the hours of scientific productivity, since staying late was not such a sad thing anymore. I like to thank Daniele for challenging discussions, scientific input and for being there as a friend. Again, I want to thank the entire lab for all the nice outside activities we did together: Beach volley with Vale and Matyas, parties at Daniele's place, BBQ's at Philips place and chilling and swimming at/in the Rhine in the summer.

Furthermore, I am grateful for the support I received from my family. Especially my mom and dad are always there for me and gave me a lot of love and advice (sometimes even scientific). I am also indebted with my best friends Manuela and Magdalena who supported me at all times and really helped me to get through the tough times. Thanks a lot! Likewise, I want to thank Elli, a great friend at FMI with whom I shared a lot awesome moments. I think without her, I would have gone insane and quit my PhD long time ago. The same goes for Juliane and Angeline. The moments I needed it the most, they were there for me and cheered me up. Especially Angeline has become of great importance in the last year of my PhD. The last two years of my PhD have been a big crisis in my life, as I had to rethink my career and experienced a lot of personal problems. Angeline has become one of my best friends, who supported me through these tough times and together we managed to gain back energy and enthusiasm for work and enjoy life! Therefore, I also like to acknowledge Sonnendeck and Grenzwert for the tasty cocktails, relaxing atmosphere and the great people.

APPENDIX

Woolcock et al., 2012

Genes and Development

Downloaded from genesdev.cshlp.org on January 26, 2013 - Published by Cold Spring Harbor Laboratory Press

RNAi keeps Atf1-bound stress response genes in check at nuclear pores

Katrina J. Woolcock, Rieka Stunnenberg, Dimos Gaidatzis, et al.

Genes Dev. 2012 26: 683-692 originally published online March 19, 2012
Access the most recent version at doi:10.1101/gad.186866.112

Supplemental Material	**http://genesdev.cshlp.org/content/suppl/2012/03/12/gad.186866.112.DC1.html**
References	This article cites 35 articles, 9 of which can be accessed free at: **http://genesdev.cshlp.org/content/26/7/683.full.html#ref-list-1** Article cited in: **http://genesdev.cshlp.org/content/26/7/683.full.html#related-urls**
Related Content	**RNAi in fission yeast finds new targets and new ways of targeting at the nuclear periphery** Daniel Holoch and Danesh Moazed Genes Dev. April 15, 2012 26: 741-745
Email alerting service	Receive free email alerts when new articles cite this article - sign up in the box at the top right corner of the article or **click here**

TrueORF Gold cDNA Clones
Validated for Protein Expression!
LEARN MORE >
ORIGENE Your Gene Company

To subscribe to *Genes & Development* go to:
http://genesdev.cshlp.org/subscriptions

Copyright © 2012 by Cold Spring Harbor Laboratory Press

Downloaded from genesdev.cshlp.org on January 26, 2013 - Published by Cold Spring Harbor Laboratory Press

RNAi keeps Atf1-bound stress response genes in check at nuclear pores

Katrina J. Woolcock,[1,2] Rieka Stunnenberg,[1,2] Dimos Gaidatzis,[1,2,3] Hans-Rudolf Hotz,[1,2,3] Stephan Emmerth,[1,2] Pierre Barraud,[4] and Marc Bühler[1,2,5]

[1]Friedrich Miescher Institute for Biomedical Research, 4058 Basel, Switzerland; [2]University of Basel, 4003 Basel, Switzerland; [3]Swiss Institute of Bioinformatics, 4058 Basel, Switzerland; [4]Institute of Molecular Biology and Biophysics, ETH Zürich, CH-8093 Zürich, Switzerland

RNAi pathways are prevalent throughout the eukaryotic kingdom and are well known to regulate gene expression on a post-transcriptional level in the cytoplasm. Less is known about possible functions of RNAi in the nucleus. In the fission yeast *Schizosaccharomyces pombe*, RNAi is crucial to establish and maintain centromeric heterochromatin and functions to repress genome activity by a chromatin silencing mechanism referred to as cotranscriptional gene silencing (CTGS). Mechanistic details and the physiological relevance of CTGS are unknown. Here we show that RNAi components interact with chromatin at nuclear pores to keep stress response genes in check. We demonstrate that RNAi-mediated CTGS represses stress-inducible genes by degrading mRNAs under noninduced conditions. Under chronic heat stress conditions, a Dicer thermoswitch deports Dicer to the cytoplasm, thereby disrupting CTGS and enabling expression of genes implicated in the acquisition of thermotolerance. Taken together, our work highlights a role for nuclear pores and the stress response transcription factor Atf1 in coordinating the interplay between the RNAi machinery and the *S. pombe* genome and uncovers a novel mode of RNAi regulation in response to an environmental cue.

[*Keywords*: RNAi; CTGS; NPC; stress response; thermoswitch; Atf1 transcription factor]

Supplemental material is available for this article.

Received January 7, 2012; revised version accepted February 24, 2012.

The fission yeast *Schizosaccharomyces pombe* has been an invaluable model to study the assembly of centromeric heterochromatin, which depends on the processing of long noncoding repeat RNAs into double-stranded siRNAs by Dcr1 (Volpe et al. 2002; Moazed 2009). Double-stranded siRNAs are found in the ARC chaperone complex (consisting of Ago1, Arb1, and Arb2), which is involved in siRNA maturation (Buker et al. 2007). Mature, single-stranded siRNAs are found in the RNA-induced transcriptional silencing complex (RITS; consisting of Ago1, Chp1, and Tas3) (Verdel et al. 2004) and function to target RITS to nascent chromatin-bound transcripts. Subsequently, this recruits Clr4, the enzyme that methylates histone H3 at Lys 9 (H3K9). H3K9 methylation, a hallmark of heterochromatin, is crucial to stabilize the association of RITS with chromatin via Chp1, triggering a self-enforcing positive feedback mechanism in which RITS recruits the Rdp1-containing RNA-directed RNA polymerase complex (RDRC) (Motamedi et al. 2004). This activates siRNA amplification, which eventually leads to high levels of H3K9 methylation and functional heterochromatin at centromeric repeats. Although this pathway has been investigated in great detail, the mechanisms by which the RNAi machinery is initially targeted to centromeric repeats have remained elusive (Halic and Moazed 2010; Shanker et al. 2010).

Whereas the involvement of RNAi in the assembly of centromeric heterochromatin is well established, additional roles remain ill-defined. Recently, we obtained evidence that the RNAi pathway might also function to repress genomic elements other than the well-studied regions of constitutive heterochromatin. We proposed a cotranscriptional gene silencing (CTGS) model, in which RNAi functions in direct association with euchromatin to trigger RNA decay (Woolcock et al. 2011). The physiological relevance of this mode of genome regulation and, similar to centromeric heterochromatin, how specific targeting of RNAi components to particular regions in the genome is achieved are not known.

Results

Nuclear RNA turnover proteins physically associate with the S. pombe *genome*

An inherent difficulty in studying the cross-talk between the RNAi machinery and chromatin has been that some

---

[5]**Corresponding author.**
E-mail marc.buehler@fmi.ch.

Article published online ahead of print. Article and publication date are online at http://www.genesdev.org/cgi/doi/10.1101/gad.186866.112.

Downloaded from genesdev.cshlp.org on January 26, 2013 - Published by Cold Spring Harbor Laboratory Press

RNAi components hardly cross-link to chromatin. A solution to this problem is DNA adenine methyltransferase identification (DamID), a highly sensitive method that allowed us to map Dcr1 interactions with the genome (Woolcock et al. 2011). To profile other RNA turnover proteins implicated in chromatin silencing, we produced and compared genome-wide binding maps for Dcr1, Rdp1, Ago1, Arb1, Cid14, Rrp6, and the heterochromatin protein HP1^{Swi6} by DamID in combination with tiling arrays (Fig. 1A). Of the RNAi proteins, Ago1 and Rdp1 show a high enrichment at major heterochromatic regions, as observed for HP1^{Swi6}. Dcr1 is also enriched at centromeric heterochromatin but not at other heterochromatic loci. Surprisingly, Arb1 is not enriched at any region. Thus, whereas Dcr1, RITS, and RDRC operate in close proximity to heterochromatin, ARC is the only RNAi complex that seems to function further away (Fig. 1A).

The Cid14 nucleotidyltransferase and the RNA exosome have been recently suggested to be involved in siRNA 3′ end processing by untemplated nucleotide addition and trimming, respectively (Halic and Moazed 2010). Consistent with an involvement in siRNA maturation, Cid14 shows an enrichment similar to that observed for Dcr1 at centromeric heterochromatin (Fig. 1A). This indicates that siRNA maturation by the exosome and Cid14 is initiated in association with chromatin. Interestingly, the nucleus-specific 3′-to-5′ exoribonuclease Rrp6 is depleted at centromeres. Therefore, trimming of siRNAs is most likely mediated by another exonuclease, which is consistent with the observation that centromeric siRNA levels are drastically reduced in *cid14*Δ but not *rrp6*Δ cells (Buhler et al. 2007). In contrast to centromeric heterochromatin, Rrp6 is slightly enriched at the mating type locus and telomeres, which is in line with its role in RNAi-independent repression at these regions (Buhler et al. 2007).

Although not generally enriched in euchromatin, RNAi factors and Cid14 do associate with particular euchromatic loci. Except for Arb1, all RNAi proteins are enriched to similar levels at long terminal repeats (LTRs), consistent with an increase in RNA from LTRs in RNAi mutants (Fig. 1B; Woolcock et al. 2011). Similar profiles can be observed at regions coding for long intergenic noncoding RNAs (lincRNAs), snoRNAs, and snRNAs, as well as at replication origins. wtf and tf2 retrotransposons are exceptional, as they are specifically enriched by Dcr1 and Cid14 only (Fig. 1B).

Taken together, these DamID experiments provide a comprehensive data set for interactions of the *S. pombe* genome with nuclear RNA turnover proteins implicated in chromatin silencing. Importantly, we found that the core RNAi machinery associates with many noncoding regions of the genome and certain protein-coding genes.

Interactions between chromatin and the RNAi pathway occur at nuclear pores independently of Argonaute

A unifying feature of RNAi pathways is that Argonaute-containing complexes are guided to their respective targets by small RNAs. Coherent with this paradigm, a transcriptome surveillance mechanism in which Ago1 associates with random, Dcr1-independent RNA degradation products in *S. pombe* has been recently proposed (Halic and Moazed 2010). These small RNAs are referred to as primal RNAs (priRNAs) and may function to target Ago1 to chromatin independently of Dcr1 or the H3K9 methylation status. Subsequently, RDRC and Dcr1 would be recruited and the siRNA amplification loop started. Indeed, the high enrichment observed for Rdp1 at centromeres is strongly affected in ago*1*Δ, *dcr1*Δ, and *clr4*Δ cells (Fig. 2A), implicating H3K9 methylation and a functional RNAi pathway in the establishment of the positive feedback loop. However, although reduced, the association of Rdp1 with chromatin is not completely lost in ago*1*Δ, *dcr1*Δ, or *clr4*Δ cells (Fig. 2A). Similarly, the enrichment of Dcr1 with centromeres remains unaffected in ago*1*Δ, *rdp1*Δ, or *clr4*Δ cells (Fig. 2B). These results demonstrate that neither priRNAs nor H3K9 methylation is required for targeting Dcr1 and Rdp1 to centromeric chromatin initially. However, Clr4 stabilizes RITS and RDRC association with heterochromatin, and priRNAs might be required to prime the amplification of centromeric siRNAs.

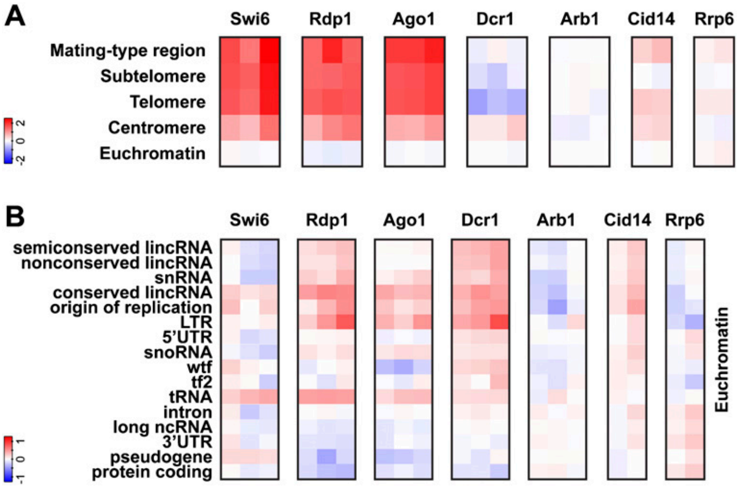

Figure 1. DamID for RNAi and nuclear surveillance components reveals association with genomic regions in both heterochromatin and euchromatin. (*A*) Enrichments ($\log_2$) at heterochromatic regions compared with euchromatin. (*B*) Enrichments ($\log_2$) at the indicated genomic features present in euchromatin. Individual columns represent biological replicates. (Tf2) Tf2 LTR retrotransposons; (wtf) with Tf2-type LTRs.

Downloaded from genesdev.cshlp.org on January 26, 2013 - Published by Cold Spring Harbor Laboratory Press

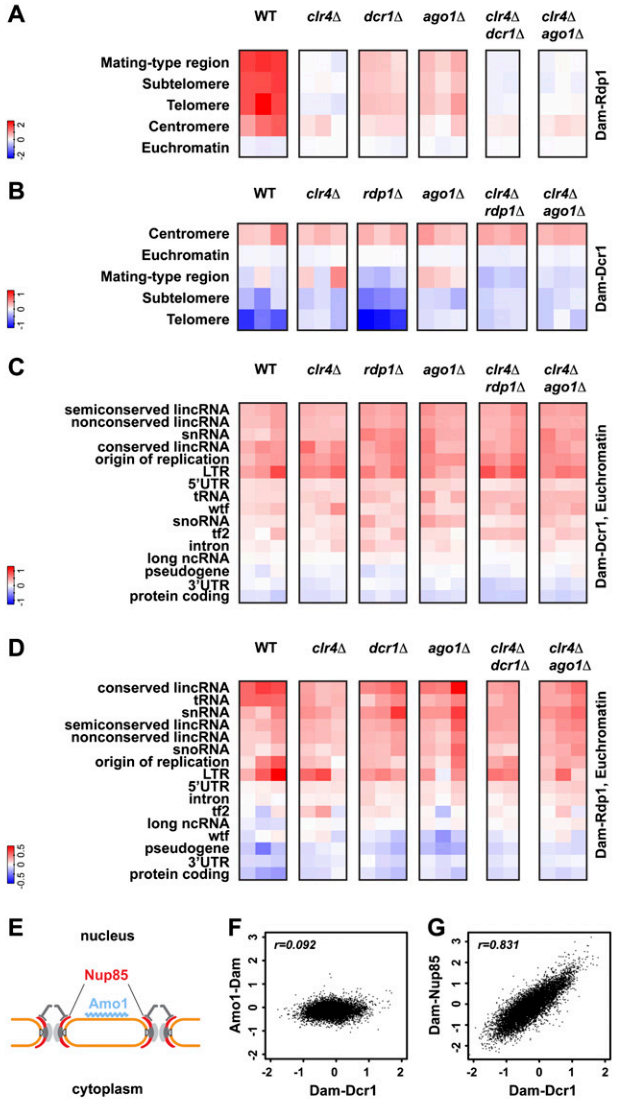

Figure 2. Interactions between chromatin and the RNAi pathway occur at NPCs, independently of small RNAs. (*A*–*D*) Rdp1 and Dcr1 enrichments ($\log_2$) in the mutant backgrounds indicated. Individual columns represent biological replicates. (*E*) Representation of Nup85 and Amo1 locations at the nuclear periphery. (*F*,*G*) Comparison of Dcr1 enrichments ($\log_2$) at individual features with Amo1 and Nup85 enrichments, respectively.

A requirement for priRNAs in actively targeting the RNAi machinery to euchromatic sites can also be ruled out because neither Dcr1 nor Rdp1 association with euchromatic loci was affected in *ago1*Δ cells (Fig. 2C,D). This raises the question of how RNAi components and specific regions of the genome are brought in close proximity, if not by small RNAs. Intriguingly, Dcr1 accumulates at the nuclear periphery in association with pores (Emmerth et al. 2010). Similarly, heterochromatin localizes at the nuclear periphery, prompting us to speculate that the interaction between RNAi components and the *S. pombe* genome might be orchestrated at the nuclear envelope. To test this hypothesis, we performed DamID for two nuclear peripheral proteins (Fig. 2E): Nup85, a scaffold nucleoporin and part of the Nup107–120 complex (Bai et al. 2004), and Amo1, which localizes to the nuclear rim in a punctate pattern that does not overlap with nuclear pore complex (NPC) components (Pardo and Nurse 2005). In contrast to Amo1, which does not strongly associate with specific regions of the genome, Nup85 is enriched at several genomic loci (Fig. 2F,G; Supplemental Fig. S1). Intriguingly, comparing the sites associated with Dcr1 or Nup85 revealed a strong correlation across the whole genome, demonstrating that NPCs preferentially associate with genomic loci that are also targets of Dcr1 (Fig. 2G). Furthermore, Ago1 seems to be largely dispensable for the association of Nup85 with the genome (Supplemental Fig. S1). These results strongly suggest that the interactions between chromatin and the RNAi pathway are coordinated by one or several components of the NPC and not by small RNAs. Because nuclear pore association of Dcr1 does not depend on a functional RNAi pathway or heterochromatin (Emmerth et al. 2010), Dcr1 is likely to interact with NPCs directly.

Dcr1 binds promoter regions and Atf1-bound genes at nuclear pores

Although genes as a class are not generally enriched in the DamID data (Fig. 1B), we noticed that certain genes are strongly enriched for RNAi components. We observed that Nup85, Dcr1, and Rdp1 are depleted from the intergenic region between convergent genes (Fig. 3A). In contrast, Dcr1 and Nup85 are enriched most highly at divergent intergenic regions and intermediately at tandem ones, suggesting that Dcr1 and Nup85 preferentially associate with promoter regions. This is confirmed by the profiles of the average DamID enrichment of Dcr1 and Nup85 1 kb on either side of the translation start site (Fig. 3B). Rdp1 shows a less-pronounced decrease in enrichment from the 5′ end to the 3′ end.

Intriguingly, we noticed that many of the genes with the highest enrichment for RNAi proteins are involved in responses to stressful conditions. RNAi components show a weak preference for induced core environmental stress response (CESR) genes (Chen et al. 2003) and a strong preference for genes that we refer to as bound by Atf1 under normal conditions (BANC; as judged by chromatin immunoprecipitation [ChIP]–chip data) (Fig. 3C–F; Eshaghi et al. 2010). Atf1 is a basic leucine zipper (bZIP) transcriptional activator and is constitutively bound to its targets (Kon et al. 1997). Upon stress, it becomes phosphorylated and causes an increase in transcription of most of its target genes (Lawrence et al. 2007). Importantly, HP1^{Swi6} has no preference for BANCs, demonstrating that they are euchromatic (Supplemental Fig. S2). Finally, Nup85 shows a strong preference for BANCs, independently of Ago1, whereas Amo1 is depleted (Fig. 3G,H; Supplemental Fig. S2E). These results demonstrate that the RNAi machinery associates with protein-coding genes that are implicated in responses to stressful conditions. These genes are bound by the Atf1 transcription factor and colocalize with the RNAi machinery at NPCs, independently of small RNAs/Argonaute.

Downloaded from genesdev.cshlp.org on January 26, 2013 - Published by Cold Spring Harbor Laboratory Press

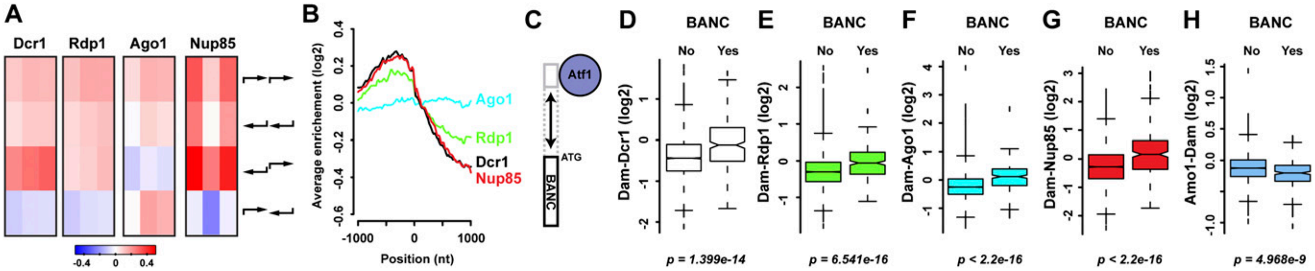

Figure 3. Promoter regions and genes associated with Atf1 colocalize with the RNAi machinery at NPCs. (*A*) Dcr1, Rdp1, Ago1, and Nup85 enrichments ($\log_2$) at tandem, divergent, and convergent intergenic regions. Individual columns represent biological replicates. (*B*) Average enrichments 1 kb on either side of the beginning of ORFs. One representative replicate is shown for each experiment. (*C*) BANCs are defined as having an Atf1 ChIP–chip peak under nonstressful conditions in their probable promoter regions (Eshaghi et al. 2010). (*D–H*) DamID enrichment ($\log_2$) at BANCs ("Yes"; 261 genes) compared with all other genes ("No"; 4715 genes).

RNAi contributes to repression of stress response genes

The physical association of the core RNAi machinery with stress response genes strongly suggests that RNAi is involved in cellular responses to environmental stress conditions. To test this hypothesis, we did expression profiling in strains lacking *dcr1*$^+$, *ago1*$^+$, or *rdp1*$^+$. Indeed, BANC genes are significantly up-regulated in all mutants (Fig. 4A–C). Importantly, they are not up-regulated in a *swi6Δ* mutant, confirming that the activation of BANC genes upon deletion of RNAi factors is not an indirect effect of losing heterochromatin, which can be considered a stressful condition (Fig. 4D). Ago1-bound small RNAs that are significantly enriched for BANCs compared with other genes further support the conclusion that the RNAi machinery is directly involved in repressing these loci (Fig. 4E). However, these small RNAs do not seem to be required for the organization of BANCs, Dcr1, and Rdp1 at NPCs, which is independent of Ago1, and their functional relevance is unclear. In summary, the RNAi machinery associates with BANC genes independently of small RNAs/Argonaute, although all three core components of the RNAi machinery are required for BANC repression.

To study the effect of stressful insults on expression of Atf1-bound genes in the absence or presence of RNAi, we chose heat shock as a paradigm and monitored expression of candidate heat-shock genes over time. Consistent with impaired repression of BANC genes in the absence of RNAi, heat-shock RNA levels in *dcr1*Δ cells, compared with wild type, are higher under noninduced conditions (Fig. 4F; data not shown). Interestingly, RNA polymerase 2 (RNAP2) occupancy changes at some but not all heat-shock genes in *dcr1*Δ cells (Fig. 4G; Supplemental Fig. S3). Thus, cotranscriptional degradation of RNA might feed back on RNAP2 at some genes. When grown at elevated temperatures, we observed that RNA levels of certain heat-shock genes decrease at a slower rate after their initial induction in *dcr1Δ* compared with wild-type cells (Fig. 4H,I; data not shown).

These results demonstrate that RNAi, when associated with BANCs, contributes to their repression under normal conditions. This regulation can occur on a truly cotranscriptional RNA decay level, although a regulatory effect on transcription at some genes cannot be ruled out at this point. We propose a model in which Atf1-bound stress response genes are recruited to NPCs and poised for rapid mRNA export, but kept in check by RNAi-mediated CTGS under normal conditions. Upon stress, strongly increased transcription rates simply overcome CTGS, with most transcripts escaping cotranscriptional degradation and accumulating to high levels. After a transient burst of transcription, CTGS contributes to the subsequent decrease in RNA levels.

This model predicts that the association of NPCs with Dcr1 and BANC genes is not disturbed under stressful conditions. Indeed, live-cell imaging of cells in which individual heat-shock genes have been tagged with the LacO/LacI-GFP system did not reveal significant delocalization of heat-shock genes (Fig. 5A,B). Similarly, the association of Dcr1 with NPCs was not affected under oxidative stress conditions or short exposure to elevated temperatures (Supplemental Fig. S4). By DamID, associations of Nup85 with the genome remained unchanged at elevated temperatures, as did Dcr1–genome associations under osmotic or oxidative stress conditions (Fig. 5C,D; Supplemental Fig. S5).

Dcr1 translocates to the cytoplasm under chronic heat stress conditions

In contrast to temporary heat-shock conditions, we observed a striking translocation of Dcr1 to the cytoplasm when cells were exposed to chronic heat stress (Fig. 6A). Consistent with this observation, DamID in the Dam–Dcr1 strain, but not the Dam-only strain, resulted in much lower DNA concentrations at the end of the protocol when performed at elevated temperatures (Fig. 6B), indicating that Dam–Dcr1 has left the nucleus and cannot further methylate DNA. Remarkably, Dcr1 protein levels are comparable at low and high temperatures (Supplemental Fig. S6), and perinuclear Dcr1 localization is restored within 1–2 h when cells are shifted back to 30°C after prolonged heat stress, hinting at a possible thermosensitive switch that regulates the nucleo–cytoplasmic distribution of Dcr1 (Fig. 6A).

We previously demonstrated a nucleo–cytoplasmic shuttling function for the dsRNA-binding domain (dsRBD)

Downloaded from genesdev.cshlp.org on January 26, 2013 - Published by Cold Spring Harbor Laboratory Press

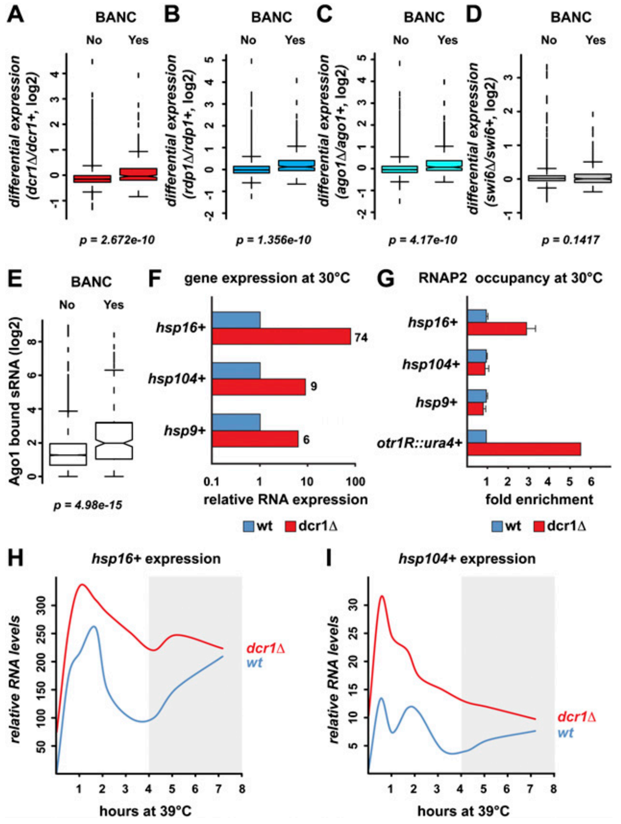

Figure 4. RNAi contributes to cotranscriptional degradation of BANCs. (*A–D*) Expression analysis by tiling arrays showing differential expression of BANCs ("Yes"; 261 genes) compared with all other genes ("No"; 4715 genes) in *dcr1Δ*, *rdp1Δ*, *ago1Δ*, and *swi6Δ*. (*E*) Small RNA deep-sequencing data (Halic and Moazed 2010) was reannotated to show the number of Ago1-bound sRNAs at BANCs compared with all other genes. (*F*) RNA levels of candidate heat-shock genes in *dcr1Δ* relative to wild-type cells at 30°C were determined by quantitative RT–PCR. Actin mRNA was used for normalization. (*G*) RNAP2 enrichment at candidate heat-shock genes in *dcr1Δ* relative to wild-type cells at 30°C. U6 snRNA was used for normalization. o*tr1R::ura4*$^+$ is located within centromeric heterochromatin and serves as a positive control. (*H*,*I*) RNA levels of candidate heat-shock genes were measured by quantitative RT–PCR in wild-type and *dcr1Δ* cells 0 min, 30 min, 1 h, 1 h 40 min, 2 h 10 min, 3 h 10 min, 4 h 10 min, 5 h 10 min, and 7 h 10 min after shifting to 39°C. RNA levels were normalized to actin and are represented as fold increase compared with wild-type at 30°C.

of Dcr1 (Emmerth et al. 2010). However, the physiological relevance of this property has remained mysterious. Intriguingly, the translocation phenotype as a response to chronic heat stress is reminiscent of Dcr1 alleles that harbor mutations in the dsRBD. These mutations either abolish the coordination of zinc, which aids proper folding of the dsRBD, or alter the protein–protein interaction surface required for nuclear retention (Fig. 6C; Barraud et al. 2011). Because the integrity of the dsRBD is crucial for nuclear retention of Dcr1, we monitored, by heteronuclear nuclear magnetic resonance (NMR), potential structural changes upon temperature increase. We noticed a global temperature instability of the domain, revealed by protein precipitation from ~35°C and progressive disappearance of NMR signals. Consistent with this observation, differential scanning fluorimetry (Niesen et al. 2007) revealed a melting temperature of 45°C for the domain (Fig. 6D). Interestingly, the initiation of the unfolding transition occurs around 34°C–38°C—the same temperature at which Dcr1 starts leaving the nucleus. Therefore, the Dcr1 translocation phenotype that we observed at temperatures >36°C can most likely be attributed to the temperature sensitivity of Dcr1's dsRBD.

We propose that the dsRBD of Dcr1 constitutes a thermoswitch that has nuclear retention and NPC interaction properties at temperatures up to 34°C (Emmerth et al. 2010; Barraud et al. 2011). At higher temperatures, the protein–protein interaction surface necessary for nuclear retention dissipates and the domain switches to a nuclear export promoter. As a result, RNAi no longer represses BANCs. Consistent with this, BANC genes are significantly up-regulated in Dcr1 mutants that cannot fold the dsRBD properly under normal conditions (Fig. 6E,F). We speculate that this thermoswitch might play an important role in activating chronic heat-shock pathways.

Discussion

This work points to a critical function for a key stress response transcription factor, Atf1, and nuclear pores in coordinating the interplay between the RNAi machinery and the *S. pombe* genome. That RNAi components colocalize with their targets independently of an Argonaute protein is unusual for RNAi–target interactions. For the establishment of RNAi-mediated CTGS, we foresee the requirement of a scaffold such as the NPC that brings the RNAi machinery and the target locus in close proximity. We propose a model in which transcription factors mediate the specific recruitment of genomic loci such as BANC genes to NPCs, where they meet the RNAi machinery (Fig. 7A). A scaffolding function similar to the one proposed here for NPCs might be attributed to endosomes, multivesicular bodies, or mitochondria in mammalian RNA silencing pathways (Gibbings et al. 2009; Huang et al. 2011; Watanabe et al. 2011).

Besides its crucial role in assembling noncoding repeats into heterochromatin, our work reveals that the *S. pombe* RNAi pathway also contributes to the regulation of protein-coding genes in response to environmental cues. Our results demonstrate that RNAi serves a general function to repress stress response genes. Although we cannot rule out a direct impact on transcription rates at some genes, we favor a CTGS model in which RNAi generally functions on a truly post- or cotranscriptional level by degrading newly synthesized RNA in association with its gene.

Whereas RNAi is involved in the regulation of heat-shock gene expression, the RNAi pathway itself is regulated in a unique temperature-dependent manner. Temperatures >34°C trigger a thermoswitch that deports Dcr1 to the cytoplasm. Importantly, although reversible, the kinetics of Dcr1 translocation to the cytoplasm is slow. Complete loss of perinuclear Dcr1 signal was only observed

Downloaded from genesdev.cshlp.org on January 26, 2013 - Published by Cold Spring Harbor Laboratory Press

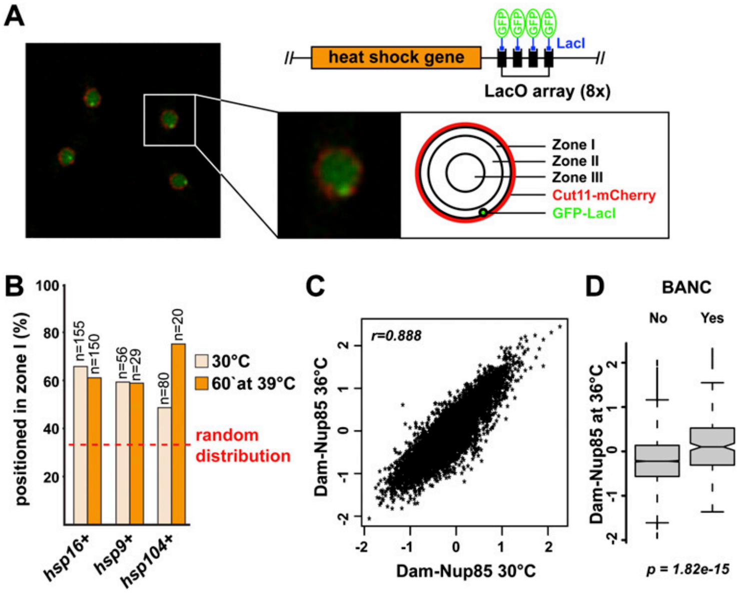

Figure 5. Genes associating with RNAi components do not change their nuclear localization upon temperature increase. (*A*) Summary of the LacO/LacI-GFP system used to analyze the location of individual heat-shock genes (Taddei et al. 2004). Live cells with GFP-LacI-marked *lacO::hsp16*$^+$ locus and the nuclear membrane marker mCherry-Cut11 were imaged at 30°C (single-plane confocal image). (*B*) Heat-shock gene localization was assigned to one of three concentric nuclear zones of equal area (shown in *A*). Percentage of cells with the GFP focus at the nuclear periphery (zone I) before and after a 1-h shift to 39°C is shown. (Dotted line) Random localization. (*C*) Comparison of the genome-wide Nup85 enrichment (log$_2$) at 30°C and 36°C. (*D*) BANCs remain highly enriched for Nup85 at 36°C.

after several hours. This indicates that RNAi-mediated CTGS occurring at nuclear pores is only disrupted completely under chronic heat-shock conditions. Consistent with this idea, two heat-shock genes, *hsp104*$^+$ and *hsp16*$^+$, show reaccumulation of mRNA when incubated for >4 h at 39°C (Fig. 4H,I). Intriguingly, these genes have been implicated in the acquisition of thermotolerance (Yoshida and Tani 2005; Senechal et al. 2009), which requires mild pretreatment of cells with sublethal heat stress (Ribeiro et al. 1997). We speculate that transcription of certain genes is activated by mild heat shock, but the response is kept transient by RNAi-mediated CTGS, which remains functional for several hours (Fig. 7B). Upon prolonged incubation at elevated temperatures or recurrent heat shock, the Dcr1 thermoswitch could contribute to reactivation of such genes to help the cells tolerate temperatures that would otherwise be deadly (Fig. 7C). Interestingly, loss of silencing at centromeres after chronic heat stress amounts to a maximum increase in RNA of approximately fivefold, much less than the ~100-fold increase observed in *dcr1Δ* cells under normal conditions (data not shown), suggesting the existence of compensatory mechanisms that keep some regions repressed under chronic heat stress despite loss of Dcr1 from the nucleus.

Finally, we note that RNAi components have recently been implicated in heat-shock gene regulation in *Drosophila melanogaster* and that human Dicer has been demonstrated to physically interact with a nuclear pore protein (Ando et al. 2011; Cernilogar et al. 2011). This suggests that mechanisms similar to the ones described here might also be operational in animals.

Material and methods

Strains and plasmids

Fission yeast strains (grown at 30°C in YES medium; MP Biomedicals no. 4101-532) and plasmids used in this study are described in Supplemental Tables S1 and S2. All strains were constructed using a standard PCR-based protocol (Bahler et al. 1998). LacO repeats were inserted into the genome as described previously (Rohner et al. 2008). Constructs on plasmids and in yeast strains were confirmed by sequencing.

DamID

DamID was done as previously described (Woolcock et al. 2011). For DamID under stress conditions, the cells were grown to OD$_{600}$ ~0.5, diluted again to OD$_{600}$ = 0.08, and grown again to OD$_{600}$ ~0.4. This should dilute out parental methylation so that the new methylation pattern reflects association of the fusion protein with the genome under the stress condition. Heat: 36°C; osmotic: cells grown in YES with 1 M sorbitol; oxidative: cells grown in YES with 0.5 mM H_2O_2.

S. pombe *genome annotation*

Two annotations sets ("chromosomal regions" and "genomic elements") were created and can be used in the form of GFF, BED, or Fasta files. The sequence of the genomic DNA is taken from the assembly "pombe_09052011.fasta" (downloaded from ftp://ftp.sanger.ac.uk/pub/yeast/pombe/GFF).

Chromosomal regions

The three chromosomes were split into centromere, euchromatin, subtelomere, telomere, and mating type regions using the coordinates described in Supplemental Table S4. The centromere ranges were taken from http://www.sanger.ac.uk/Projects/S_pombe/centromere.shtml. The mating type region and the chromosome ends were divided into regions of high H3K9me2 (telomeres and mating type region) and lower H3K9me2 (subtelomeres) enrichment based on published data (Cam et al. 2005).

For the Fasta files, the "mating_type_region" sequence fragment provided in the genomic DNA file was used instead of the region on chromosome 2. The euchromatin was extended to include the whole range from 1,644,747 to 4,497,199. The "Spmit" and the "telomeric_contig" sequences from the genomic DNA file were used as well.

Downloaded from genesdev.cshlp.org on January 26, 2013 - Published by Cold Spring Harbor Laboratory Press

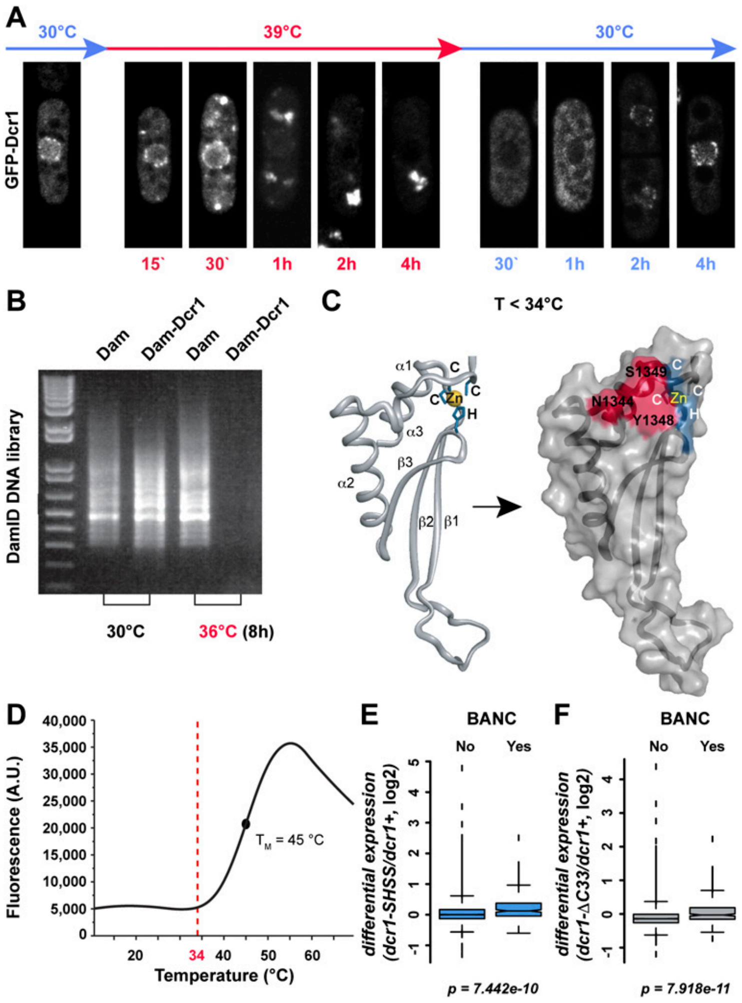

Figure 6. The dsRBD of Dcr1 loses nuclear retention properties at elevated temperatures. (*A*) Fluorescence microscopy of living cells expressing N-terminally tagged GFP-Dcr1. Cells were grown at 30°C, temperature was shifted to 39°C, and confocal images were taken at the indicated times (in red). The nuclear peripheral localization of Dcr1 is gradually lost and accumulates in bright foci in the cytoplasm, although some nuclear rim signal remains up to 4 h. Recovery of nuclear Dcr1 was monitored during 4 h after shifting the temperature from 39°C (cells having been at this temperature overnight) back to 30°C (in blue). (*B*) Much lower DamID library DNA concentrations are obtained for Dam–Dcr1 strains when performed at 36°C compared with 30°C (confirmed by at least four independent replicates). (*C*) Cartoon representation of the Dcr1 dsRBD is shown on the *left* (Barraud et al. 2011). Zinc-coordinating residues are indicated in blue, and the zinc ion is shown as a yellow sphere. Visualization of the dsRBD fold on the protein surface is shown on the *right*. The residues highlighted in red form a protein–protein interaction surface that is required to retain Dcr1 in the nucleus (Barraud et al. 2011). (*D*) Thermal unfolding of Dcr1's C-terminal domain shown in *C* monitored by differential scanning fluorimetry. (Dotted line) Temperature at which unfolding transition initiates. (*E*,*F*) Expression analysis by tiling array (Barraud et al. 2011) showing differential expression of BANCs compared with all other genes in a Dcr1 mutant in which the dsRBD can no longer coordinate a zinc ion and in a Dcr1 mutant lacking the C-terminal 33 amino acids, respectively. Both of these mutants are unable to fold the dsRBD properly and hence lose nuclear retention properties.

Genomic elements

Initial identification of elements is based on the features described in the GFF file "pombe_09052011.gff" (downloaded from ftp://ftp.sanger.ac.uk/pub/yeast/pombe/GFF).

The sequence ranges of the following features were taken directly from the GFF file. "rep_origin," "LTR," tRNA," "snRNA," and "snoRNA". "rRNA" was built from the rRNA features in the GFF file plus adding SPRRNA.25 (misc_feature). "pre_rRNA" was built from the "misc_feature" features in the GFF file, where the phrase "ribosomal RNA" was present in the attributes column. "pseudogene" was built from the mRNA and "misc_feature" features in the GFF file, where the word "pseudogene" was present in the attributes column, plus adding the mRNA features for SPAC23A1.20 and SPCC622.17. "repeats" was built from the "repeat_region" feature, where the words "wtf" and "tf2" were not present. Lists of "wtf" and "tf2" identifiers were built from the mRNA features in the GFF file, where the words "wtf" and "tf2," respectively, were present in the attributes column. Sequence regions derived from "pseudogenes," "wtf," and "tf2" elements were removed from the "unspliced_transcripts," "3UTR," and "5UTR" sets built from the mRNA, 3′ untranslated region (UTR), and 5′ UTR features, respectively. The same restrictions were applied to the "intron" set, in addition to the removal of "tRNA" intron sequences. "tf2" was built by adding the mRNA features from the "tf2" list to the "misc_feature" features in the GFF file, where the phrase "transpos" was present in the attributes column. The "misc_RNA" features were separated based on conservation between different fission yeasts (Rhind et al. 2011; Z Chen, N Rhind, pers. comm.). "conserved_lincR" were conserved in sequence and location. "semiconserved_lincR" were conserved in location with at least one other species. "nonconserved_lincR" were the remaining "intergenic ncRNA" from the work by Rhind et al. (2011). All remaining "misc_RNA" features (which included all "antisense ncRNA" from the work by Rhind et al. [2011]) were used for "longncRNA."

All resulting GFF files were used to create the BED and Fasta files. In addition, a Fasta file for "mRNA" (i.e., spliced transcripts) was built by combining the sequence for the 5′ UTR (if annotated), CDS (one or more per gene), and 3′ UTR (if annotated) features for each gene (after removing all features with identifiers present on the "pseudogene," "wtf," and "tf2" lists). The Fasta file for "wtf" was built from sequences of mRNA features from the "wtf" list, where no splicing (i.e., no intron was annotated) occurred. These sequence ranges were also used for the corresponding GFF and BED files. For the remaining identifiers, the sequence was built the same way as the "mRNA" file and was added to the Fasta file. Furthermore, all BED and Fasta files were split into four different files (e.g., "repeats.fa," "repeats_centromere.fa," "repeats_subtelomere.fa," and "repeats_telomere.fa") depending on whether the start of the original feature was within the "euchromatin," "centromere," "subtelomere," and

Downloaded from genesdev.cshlp.org on January 26, 2013 - Published by Cold Spring Harbor Laboratory Press

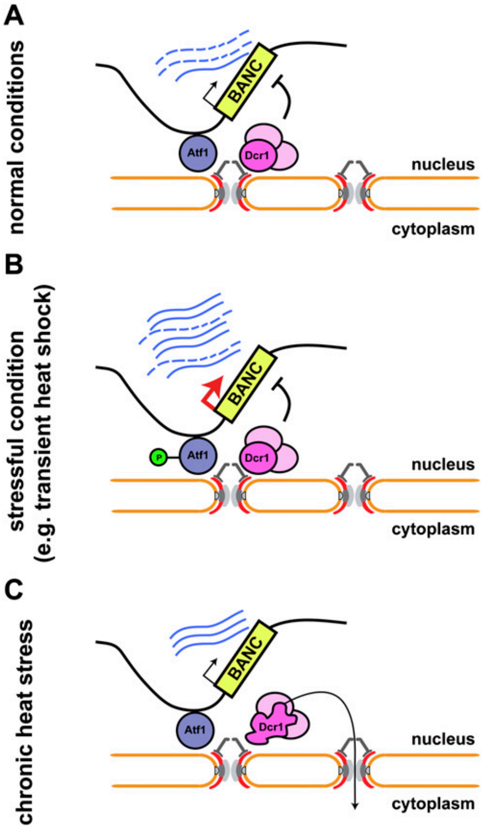

Figure 7. Proposed model for RNAi-mediated CTGS of Atf1-bound genes (BANCs) at nuclear pores. (*A*) The RNAi machinery colocalizes with BANCs at pores, contributing to their repression, presumably by degrading the nascent transcripts. (*B*) Upon stress, Atf1 becomes rapidly and transiently phosphorylated and causes strong transcriptional activation of BANCs. After a transient burst of transcription, CTGS remains active and contributes to the transient nature of the stress response. (*C*) After several hours at elevated temperatures, Dcr1 is lost from the nucleus, presumably due to unfolding of its dsRBD. This abrogates CTGS and causes the reaccumulation of some BANCs, which may be important for thermotolerance.

"telomere," respectively, region describe above. The features present on the "mating_type_region," "Spmit," and "telomeric_contig" sequences were ignored. The Fasta file for the mitochondrion (i.e., "Spmit") was added as one separate sequence.

DamID analysis

DamID analysis was done as previously described (Woolcock et al. 2011) but using the above annotation. Intergenic regions were generated as previously described (Woolcock et al. 2011), except that regions interrupted by an LTR were also excluded from the analysis to prevent the high enrichments found at LTRs from influencing the data. Profiles around translation start sites were as follows: For each transcript, we selected all of the uniquely mapping oligos that overlapped within a region of −1000 to 1000 from the start of the ORF. For each base, from the perspective of the translation start site, we calculated the mean enrichment and smoothed the resulting profiles with a lowess normalizer. Profiles from multiple samples were made comparable by subtracting their respective means.

Expression profiling

RNA isolation and processing were done as previously described (Emmerth et al. 2010). All tiling arrays were processed in R (Ihaka and Gentleman 1996) using bioconductor (Gentleman et al. 2004) and the packages tilingArray (Huber et al. 2006) and preprocessCore. The arrays were RMA background-corrected, quantile-normalized, and log2-transformed on the oligo level using the following command: expr < –log2{normalize.quantiles[rma.background.correct(exprs{readCel2eSet[filenames, rotated=TRUE]})]}. Oligo coordinates were intersected with the genome annotation and used to calculate average expression levels for individual genomic features (excluding those with <10 oligos) as well as broader annotation categories. In the latter case, multimapping oligos were counted only once per category (avoiding multiple counts from the same oligo).

Statistical analysis

Box plots and scatter plots were produced in R and show the average of at least two biological replicates for all experiments unless otherwise stated. All *P*-values were generated using the R command t.test.

RNA isolation, cDNA synthesis, and quantitative RT–PCR

RNA isolation, cDNA synthesis, and quantitative RT–PCR were done as previously described (Emmerth et al. 2010). Primer pairs used for PCR reactions can be found in Supplemental Table S3.

ChIP

PolII ChIP was performed as previously described (Buhler et al. 2006) using the 8GW16 antibody (Covance) and M-280 sheep anti-mouse IgG Dynabeads (Invitrogen). Primer pairs used for PCR reactions can be found in Supplemental Table S3.

Live fluorescence microscopy

Images were acquired with a LSM710 laser-scanning confocal microscope equipped with a multiline argon 458/488/514-nm (25-mW) laser and a Plan-Apochromat 63×/1,40 oil DIC M27 objective. Images were processed with ImageJ and Adobe Photoshop. In zoning assays, a second channel was added to visualize cut11-mCherry using the DPSS 561-nm (15-mW) laser. In addition, Z-stacks of 200-nm step size were taken and distance measurements of the foci were extracted using the plug-in "PointPicker" of ImageJ. Assignment of zones and statistical analysis was done as previously described (Taddei et al. 2004). The cells were imaged in a Ludin chamber coated with Lectin (BS-1, Sigma). For heat-shock conditions, the microscope was preheated to 39°C, cells were kept in a Ludin chamber, and pictures were acquired at different time points.

To monitor Dcr1 relocalization in response to temperature changes, cells expressing N-terminally GFP-tagged Dcr1 driven by the nmt1 (3×) promoter were grown in YES at 30°C or 39°C. After the respective temperature shift, aliquots from log phase cells were taken for each time point and spread onto agarose patches containing YES medium with 3% glucose. Images were acquired using 3.5% laser power (argon, 488 nm) with a gain of 700, a pinhole of 1.5 AU, and an averaging of 4. The microscope was preheated to 30°C for the recovery experiments and to 39°C in the case of heat induction.

NMR and differential scanning fluorimetry (DSF)

Protein samples for NMR and DSF were prepared as previously described (Barraud et al. 2011). NMR spectra were recorded with

Downloaded from genesdev.cshlp.org on January 26, 2013 - Published by Cold Spring Harbor Laboratory Press

a 0.2 mM ^{15}N-labeled sample at temperatures ranging from 298 K to 318 K in a buffer containing 25 mM NaPi (pH 7.0), 75 mM KCl, 2 mM DTT, and 10 mM $ZnCl_2$ on Bruker AVIII-500 MHz. Thermal unfolding was monitored in the same buffer conditions by DSF in the presence of SYPRO orange using a real-time PCR instrument (Bio-Rad CFX96). Excitation and emission wave lengths were 492 nm and 610 nm, respectively. Melting temperature value (T_M) was calculated using the first derivative of the unfolding transition.

Accession codes

All data sets were deposited under accession number GSE36214 (NCBI Gene Expression Omnibus).

Acknowledgments

We thank Yukiko Shimada and Nathalie Laschet for technical assistance, Laurent Gelman for assistance with light microscopy, Stéphane Thiry for hybridizing tiling arrays, Tim Roloff for help with quality control and archiving of the DamID data sets, Susan Gasser and Peter Meister for strains and plasmids, and Philip Knuckles for comments on the manuscript. Research in the laboratory of M.B. is supported by the Swiss National Science Foundation, the European Research Council, and the Gebert Rüf Stiftung. The Friedrich Miescher Institute for Biomedical Research is supported by the Novartis Research Foundation.

References

Ando Y, Tomaru Y, Morinaga A, Burroughs AM, Kawaji H, Kubosaki A, Kimura R, Tagata M, Ino Y, Hirano H, et al. 2011. Nuclear pore complex protein mediated nuclear localization of dicer protein in human cells. *PLoS ONE* **6:** e23385. doi: 10.1371/journal.pone.0023385.

Bahler J, Wu JQ, Longtine MS, Shah NG, McKenzie A 3rd, Steever AB, Wach A, Philippsen P, Pringle JR. 1998. Heterologous modules for efficient and versatile PCR-based gene targeting in *Schizosaccharomyces pombe*. *Yeast* **14:** 943–951.

Bai SW, Rouquette J, Umeda M, Faigle W, Loew D, Sazer S, Doye V. 2004. The fission yeast Nup107-120 complex functionally interacts with the small GTPase Ran/Spi1 and is required for mRNA export, nuclear pore distribution, and proper cell division. *Mol Cell Biol* **24:** 6379–6392.

Barraud P, Emmerth S, Shimada Y, Hotz HR, Allain FH, Buhler M. 2011. An extended dsRBD with a novel zinc-binding motif mediates nuclear retention of fission yeast Dicer. *EMBO J* **30:** 4223–4235.

Buhler M, Verdel A, Moazed D. 2006. Tethering RITS to a nascent transcript initiates RNAi- and heterochromatin-dependent gene silencing. *Cell* **125:** 873–886.

Buhler M, Haas W, Gygi SP, Moazed D. 2007. RNAi-dependent and -independent RNA turnover mechanisms contribute to heterochromatic gene silencing. *Cell* **129:** 707–721.

Buker SM, Iida T, Buhler M, Villen J, Gygi SP, Nakayama J, Moazed D. 2007. Two different Argonaute complexes are required for siRNA generation and heterochromatin assembly in fission yeast. *Nat Struct Mol Biol* **14:** 200–207.

Cam HP, Sugiyama T, Chen ES, Chen X, FitzGerald PC, Grewal SI. 2005. Comprehensive analysis of heterochromatin- and RNAi-mediated epigenetic control of the fission yeast genome. *Nat Genet* **37:** 809–819.

Cernilogar FM, Onorati MC, Kothe GO, Burroughs AM, Parsi KM, Breiling A, Sardo FL, Saxena A, Miyoshi K, Siomi H, et al. 2011. Chromatin-associated RNA interference components contribute to transcriptional regulation in *Drosophila*. *Nature* **480:** 391–395.

Chen D, Toone WM, Mata J, Lyne R, Burns G, Kivinen K, Brazma A, Jones N, Bahler J. 2003. Global transcriptional responses of fission yeast to environmental stress. *Mol Biol Cell* **14:** 214–229.

Emmerth S, Schober H, Gaidatzis D, Roloff T, Jacobeit K, Buhler M. 2010. Nuclear retention of fission yeast dicer is a prerequisite for RNAi-mediated heterochromatin assembly. *Dev Cell* **18:** 102–113.

Eshaghi M, Lee JH, Zhu L, Poon SY, Li J, Cho KH, Chu Z, Karuturi RK, Liu J. 2010. Genomic binding profiling of the fission yeast stress-activated MAPK Sty1 and the bZIP transcriptional activator Atf1 in response to H_2O_2. *PLoS ONE* **5:** e11620. doi: 10.1371/journal.pone.0011620.

Gentleman RC, Carey VJ, Bates DM, Bolstad B, Dettling M, Dudoit S, Ellis B, Gautier L, Ge Y, Gentry J, et al. 2004. Bioconductor: Open software development for computational biology and bioinformatics. *Genome Biol* **5:** R80. doi: 10.1186/gb-2004-5-10-r-80.

Gibbings DJ, Ciaudo C, Erhardt M, Voinnet O. 2009. Multivesicular bodies associate with components of miRNA effector complexes and modulate miRNA activity. *Nat Cell Biol* **11:** 1143–1149.

Halic M, Moazed D. 2010. Dicer-independent primal RNAs trigger RNAi and heterochromatin formation. *Cell* **140:** 504–516.

Huang H, Gao Q, Peng X, Choi SY, Sarma K, Ren H, Morris AJ, Frohman MA. 2011. piRNA-associated germline nuage formation and spermatogenesis require MitoPLD profusogenic mitochondrial-surface lipid signaling. *Dev Cell* **20:** 376–387.

Huber W, Toedling J, Steinmetz LM. 2006. Transcript mapping with high-density oligonucleotide tiling arrays. *Bioinformatics* **22:** 1963–1970.

Ihaka R, Gentleman R. 1996. R: A language for data analysis and graphics. *J Comput Graph Statist* **5:** 299–314.

Kon N, Krawchuk MD, Warren BG, Smith GR, Wahls WP. 1997. Transcription factor Mts1/Mts2 (Atf1/Pcr1, Gad7/Pcr1) activates the M26 meiotic recombination hotspot in *Schizosaccharomyces pombe*. *Proc Natl Acad Sci* **94:** 13765–13770.

Lawrence CL, Maekawa H, Worthington JL, Reiter W, Wilkinson CR, Jones N. 2007. Regulation of *Schizosaccharomyces pombe* Atf1 protein levels by Sty1-mediated phosphorylation and heterodimerization with Pcr1. *J Biol Chem* **282:** 5160–5170.

Moazed D. 2009. Small RNAs in transcriptional gene silencing and genome defence. *Nature* **457:** 413–420.

Motamedi MR, Verdel A, Colmenares SU, Gerber SA, Gygi SP, Moazed D. 2004. Two RNAi complexes, RITS and RDRC, physically interact and localize to noncoding centromeric RNAs. *Cell* **119:** 789–802.

Niesen FH, Berglund H, Vedadi M. 2007. The use of differential scanning fluorimetry to detect ligand interactions that promote protein stability. *Nat Protoc* **2:** 2212–2221.

Pardo M, Nurse P. 2005. The nuclear rim protein Amo1 is required for proper microtubule cytoskeleton organisation in fission yeast. *J Cell Sci* **118:** 1705–1714.

Rhind N, Chen Z, Yassour M, Thompson DA, Haas BJ, Habib N, Wapinski I, Roy S, Lin MF, Heiman DI, et al. 2011. Comparative functional genomics of the fission yeasts. *Science* **332:** 930–936.

Ribeiro MJ, Reinders A, Boller T, Wiemken A, De Virgilio C. 1997. Trehalose synthesis is important for the acquisition of thermotolerance in *Schizosaccharomyces pombe*. *Mol Microbiol* **25:** 571–581.

Downloaded from genesdev.cshlp.org on January 26, 2013 - Published by Cold Spring Harbor Laboratory Press

Rohner S, Gasser SM, Meister P. 2008. Modules for cloning-free chromatin tagging in *Saccharomyces cerevisae*. *Yeast* **25:** 235–239.

Senechal P, Arseneault G, Leroux A, Lindquist S, Rokeach LA. 2009. The *Schizosaccharomyces pombe* Hsp104 disaggregase is unable to propagate the [PSI] prion. *PLoS ONE* **4:** e6939. doi: 10.1371/journal.pone.0006939.

Shanker S, Job G, George OL, Creamer KM, Shaban A, Partridge JF. 2010. Continuous requirement for the Clr4 complex but not RNAi for centromeric heterochromatin assembly in fission yeast harboring a disrupted RITS complex. *PLoS Genet* **6:** e1001174. doi: 10.1371/journal.pgen.1001174.

Taddei A, Hediger F, Neumann FR, Bauer C, Gasser SM. 2004. Separation of silencing from perinuclear anchoring functions in yeast Ku80, Sir4 and Esc1 proteins. *EMBO J* **23:** 1301–1312.

Verdel A, Jia S, Gerber S, Sugiyama T, Gygi S, Grewal SI, Moazed D. 2004. RNAi-mediated targeting of heterochromatin by the RITS complex. *Science* **303:** 672–676.

Volpe TA, Kidner C, Hall IM, Teng G, Grewal SI, Martienssen RA. 2002. Regulation of heterochromatic silencing and histone H3 lysine-9 methylation by RNAi. *Science* **297:** 1833–1837.

Watanabe T, Chuma S, Yamamoto Y, Kuramochi-Miyagawa S, Totoki Y, Toyoda A, Hoki Y, Fujiyama A, Shibata T, Sado T, et al. 2011. MITOPLD is a mitochondrial protein essential for nuage formation and piRNA biogenesis in the mouse germline. *Dev Cell* **20:** 364–375.

Woolcock KJ, Gaidatzis D, Punga T, Buhler M. 2011. Dicer associates with chromatin to repress genome activity in *Schizosaccharomyces pombe*. *Nat Struct Mol Biol* **18:** 94–99.

Yoshida J, Tani T. 2005. Hsp16p is required for thermotolerance in nuclear mRNA export in fission yeast *Schizosaccharomyces pombe*. *Cell Struct Funct* **29:** 125–138.

SUPPLEMENTARY INFORMATION

RNA interference keeps Atf1-bound stress response genes in check at nuclear pores

Katrina J Woolcock, Rieka Stunnenberg, Dimos Gaidatzis, Hans-Rudolf Hotz, Stephan Emmerth, Pierre Barraud, and Marc Bühler

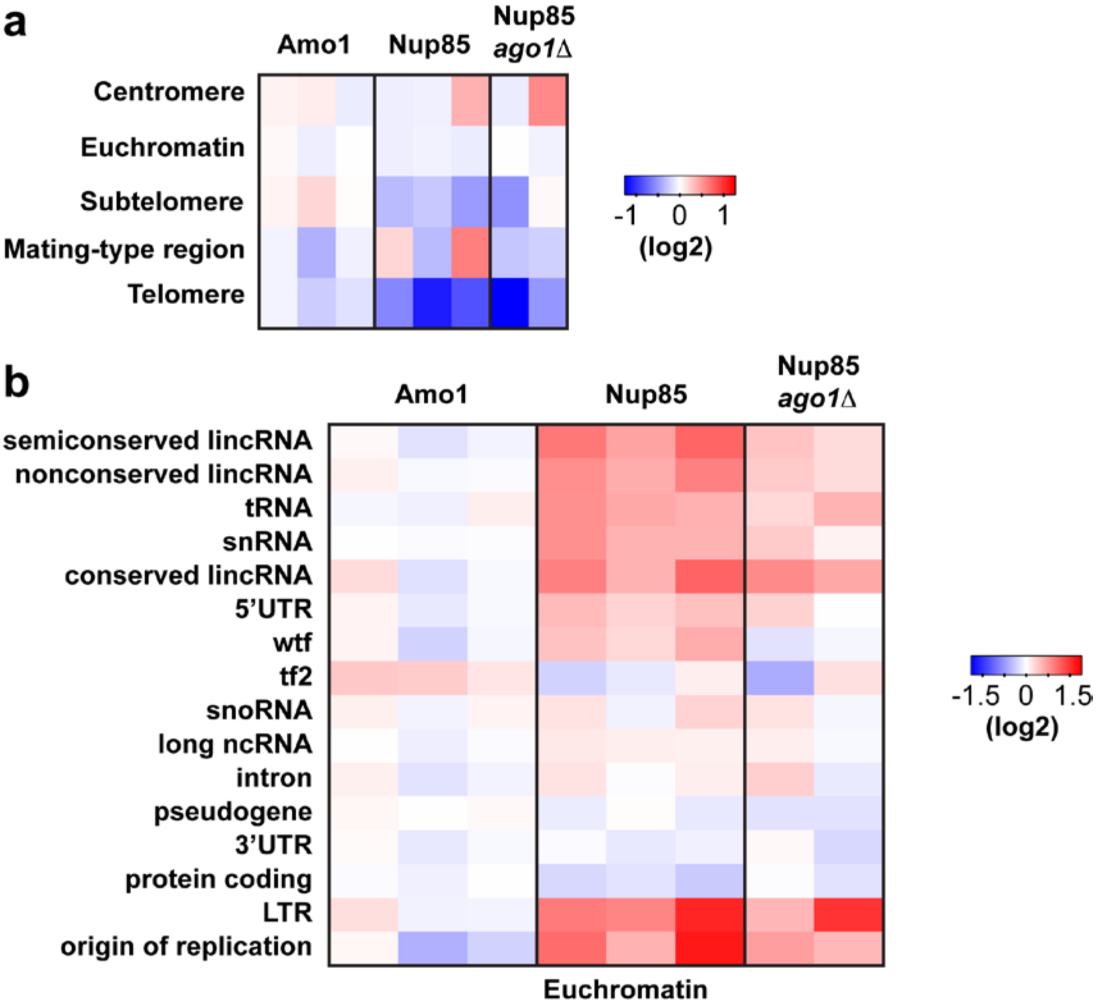

Figure S1. Nup85 interacts with several genomic regions, independently of Ago1, whereas Amo1 does not associate strongly with any class of features. (**a**) Enrichments ($\log_2$) at heterochromatic regions compared to euchromatin. (**b**) Enrichments ($\log_2$) at the indicated genomic features present in euchromatin. Individual columns represent biological replicates.

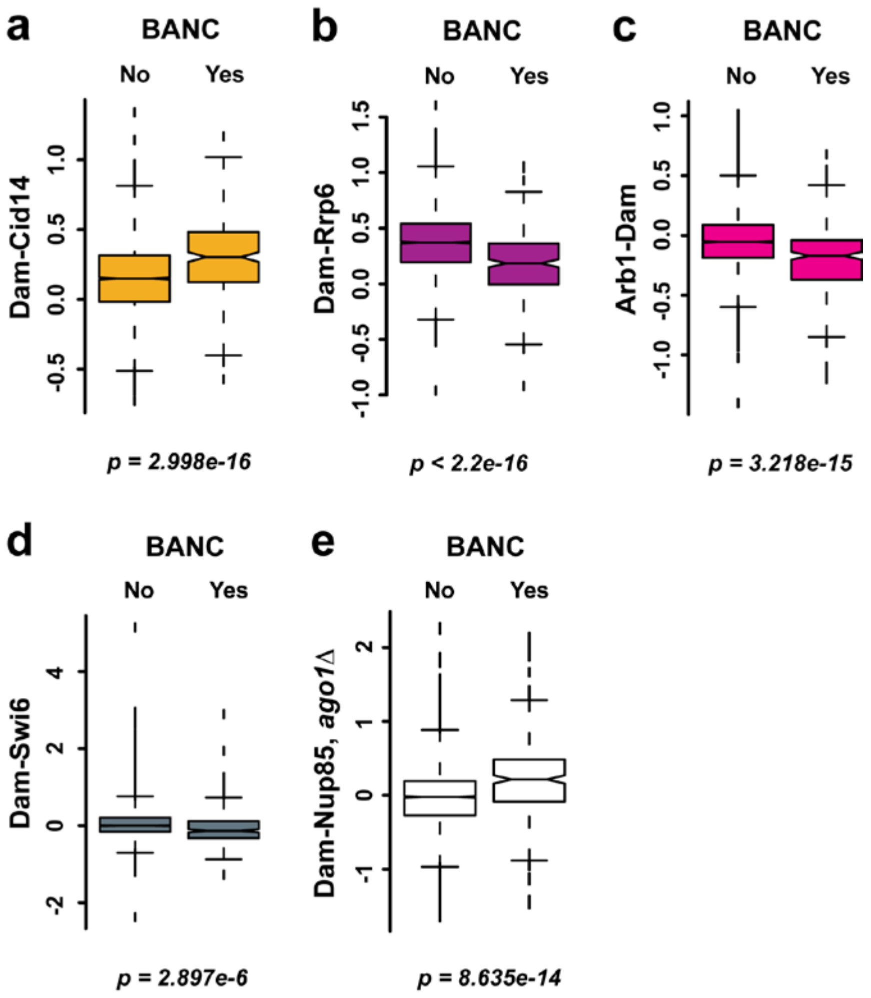

Figure S2. Cid14 is relatively enriched at BANCs, whereas Rrp6, Arb1 and Swi6 are relatively depleted. (**a**-**e**) DamID enrichment ($\log_2$) at BANCs compared to all other genes. (**e**) Preferential association of BANCs with Nup85 is preserved in the absence of Ago1 (compare to Fig. 3G).

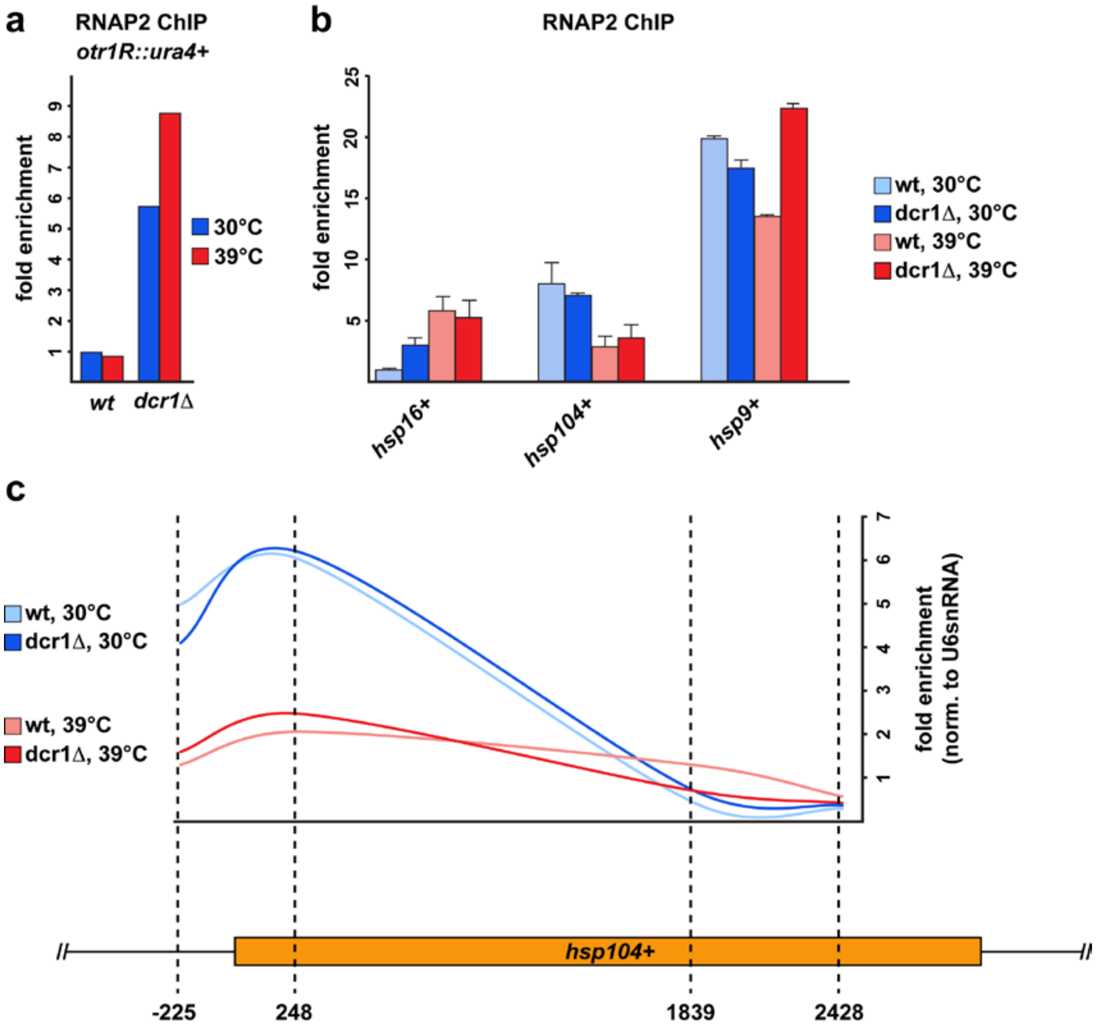

Figure S3. RNAi may influence RNAP2 occupancy on heat shock genes in some cases. (**a**) RNAP2 occupancy on the *ura4+* gene that has been inserted into centromeric heterochromatin (*otr1R::ura4+*). Because centromeric heterochromatin is disrupted in RNAi mutants, transcription of this gene becomes more active in the absence of Dcr1. (**b**) From the same samples as used in (a), the amount of RNAP2 at different heat shock genes was also determined. This result demonstrates that RNAi might be involved in transcriptional repression of *hsp16+* only (light and dark blue bars). Values are relative to the enrichment at *hsp16+* in wt at 30°C, which is set to 1. (**c**) *hsp104+* is shown as an example of heat shock gene regulation that might be mediated by promoter proximal pausing of RNAP2. Because wild-type and *dcr1Δ* cells are not different at normal or heat shock conditions, we conclude that RNAi does not contribute to RNAP2 pausing at this gene. Heat shock at 39°C was for 15 min.

Although transcription regulation at stress response genes in the presence or absence of RNAi will need to be studied in further detail and on a genome-wide scale, our data strongly support a model in which stress response genes are poised for rapid mRNA export at NPCs, but kept in check by RNAi-mediated co-transcriptional degradation (CTGS). Upon stress, strongly increased transcription rates simply overcome CTGS with most transcripts escaping co-transcriptional degradation and accumulating to high levels. After a transient burst of transcription, CTGS contributes to the subsequent decrease in RNA levels.

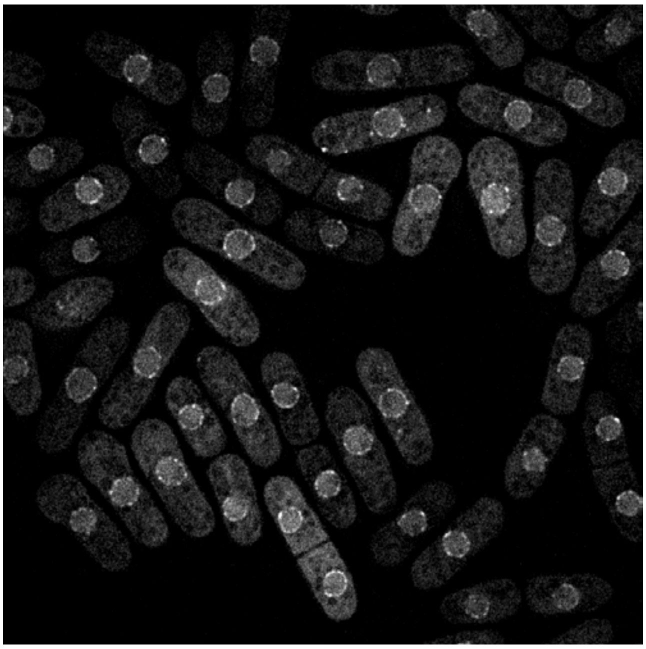

Figure S4. Dcr1 association with NPCs remains unaffected under oxidative stress conditions. Cells expressing N-terminally GFP tagged Dcr1 were grown to exponential phase and treated with 0.5 mM H_2O_2 for 15 min and then spread on agarose patches. Images were captured on a Delta Vision built of an Olympus IX70 widefield microscope equipped with a CoolSNAP HQ2/ICX285 camera. Image stacks were acquired with a Z-step size of 200 nm and deconvolved using the softworks (Delta Vision) software.

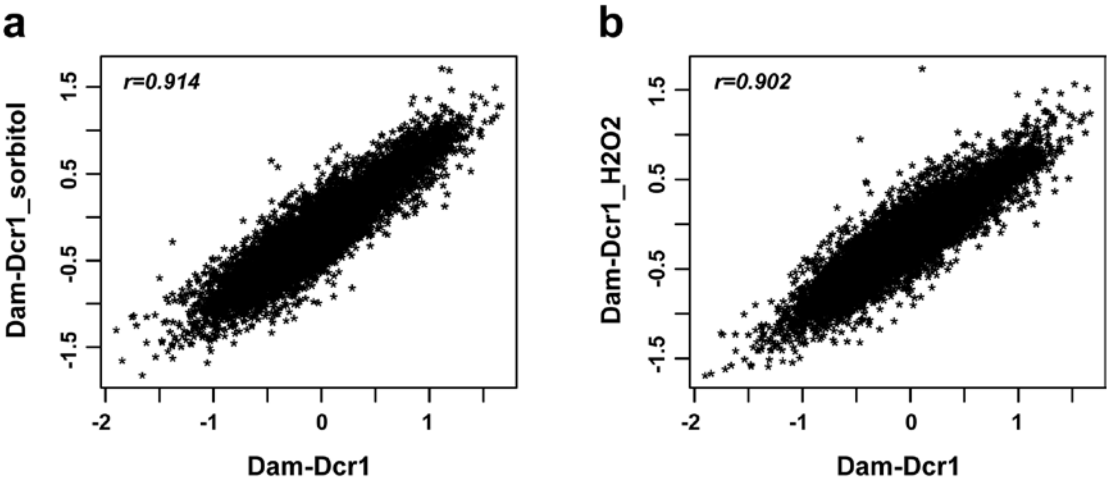

Figure S5. Dcr1 association with the genome does not change under conditions of osmotic or oxidative stress. (**a**-**b**) Dcr1 DamID for cells grown in normal YES compared to cells grown in YES with 1 M sorbitol or 0.5 mM H_2O_2, respectively. Only one replicate performed for each condition.

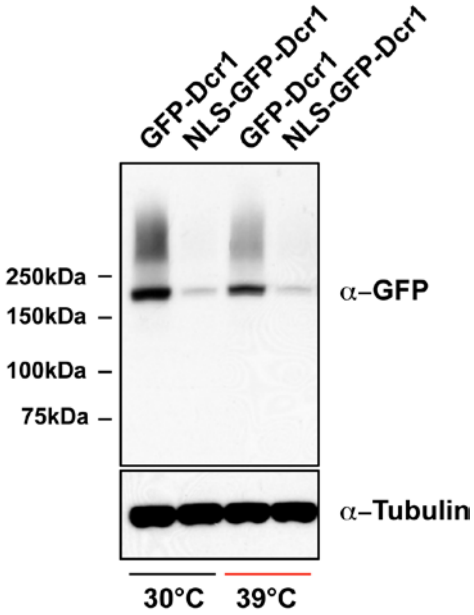

Figure S6. Dcr1 protein levels at normal and elevated temperatures. Western blot was performed with cells expressing GFP-tagged Dcr1 alleles. Cells were incubated at 30°C or 39°C for 8 hours, proteins extracted using TCA and separated on a NuPAGE® 4-12% Bis-Tris gel (Invitrogen). The following antibodies were used: GFP (Roche; 1:1000) and tubulin (Woods et al. 1989); 1:3000). This result demonstrates that total levels of Dcr1 are similar before and after translocation of Dcr1 to the cytoplasm (compare with Figure 6).

Supplementary Tables

Table S1. Strains used in this study

Strain	Genotype	Source
SPB492	*h+ otr1R(SphI)::ura4+ ura4-DS/E ade6-M210 leu1Δ::nmt1(81x)-dam-myc-kan*	1
SPB330	*h+ otr1R(SphI)::ura4+ ura4-DS/E ade6-M210 leu1Δ::nmt1(81x)-dam-myc-swi6-kan*	1
SPB381	*h+ otr1R(SphI)::ura4+ ura4-DS/E ade6-M210 leu1Δ::nmt1(81x)-dam-myc-dcr1-kan*	1
SPB494	*h+ otr1R(SphI)::ura4+ ura4-DS/E ade6-M210 leu1Δ::nmt1(81x)-dam-myc-rdp1-kan*	1
SPB926	*h+ otr1R(Sph1)::ura4+ ura4-DS/E ade6-M210 leu1Δ::nmt1(81x)-arb1-myc-dam-kan*	2
SPB927	*h+ otr1R(Sph1)::ura4+ ura4-DS/E ade6-M210 leu1Δ::nmt1(81x)-dam-myc-ago1-kan*	2
SPB1150	*h+ otr1R(SphI)::ura4+ ura4-DS/E ade6-M210 leu1Δ::nmt1(81x)-amo1-myc-dam-kan*	2
SPB1151	*h+ otr1R(SphI)::ura4+ ura4-DS/E ade6-M210 leu1Δ::nmt1(81x)-dam-myc-nup85-kan*	2
SPB435	*h+ leu1-32 ade6-M216 ura4Δ::nmt1(81x)-dam-myc-kan*	2
SPB436	*h+ leu1-32 ade6-M216 ura4Δ::nmt1(81x)-dam-myc-cid14-kan*	2
SPB437	*h+ leu1-32 ade6-M216 ura4Δ::nmt1(81x)-dam-myc-rrp6-kan*	2
SPB711	*h+ otr1R(SphI)::ura4+ ura4-DS/E ade6-M210 leu1Δ::nmt1(81x)-dam-myc-kan clr4Δ::nat*	1
SPB709	*h+ otr1R(SphI)::ura4+ ura4-DS/E ade6-M210 leu1Δ::nmt1(81x)-dam-myc-dcr1-kan clr4Δ::nat*	1
SPB851	*h+ otr1R(SphI)::ura4+ ura4-DS/E ade6-M210 leu1Δ::nmt1(81x)-dam-myc-dcr1-kan rdp1Δ::hph*	2
SPB852	*h+ otr1R(SphI)::ura4+ ura4-DS/E ade6-M210 leu1Δ::nmt1(81x)-dam-myc-dcr1-kan ago1Δ::hph*	2
SPB853	*h+ otr1R(SphI)::ura4+ ura4-DS/E ade6-M210 leu1Δ::nmt1(81x)-dam-myc-kan rdp1Δ::hph*	2
SPB854	*h+ otr1R(SphI)::ura4+ ura4-DS/E ade6-M210 leu1Δ::nmt1(81x)-dam-myc-kan ago1Δ::hph*	2
SPB855	*h+ otr1R(SphI)::ura4+ ura4-DS/E ade6-M210 leu1Δ::nmt1(81x)-dam-myc-kan clr4Δ::nat rdp1Δ::hph*	2
SPB856	*h+ otr1R(SphI)::ura4+ ura4-DS/E ade6-M210 leu1Δ::nmt1(81x)-dam-myc-kan clr4Δ::nat ago1Δ::hph*	2
SPB857	*h+ otr1R(SphI)::ura4+ ura4-DS/E ade6-M210 leu1Δ::nmt1(81x)-dam-myc-dcr1-kan clr4Δ::nat rdp1Δ::hph*	2
SPB858	*h+ otr1R(SphI)::ura4+ ura4-DS/E ade6-M210 leu1Δ::nmt1(81x)-dam-myc-dcr1-kan clr4Δ::nat ago1Δ::hph*	2
SPB712	*h+ otr1R(SphI)::ura4+ ura4-DS/E ade6-M210 leu1Δ::nmt1(81x)-dam-myc-rdp1-kan clr4Δ::nat*	1
SPB912	*h+ otr1R(SphI)::ura4+ ura4-DS/E ade6-M210 leu1Δ::nmt1(81x)-dam-myc-kan dcr1Δ::hph*	2
SPB913	*h+ otr1R(SphI)::ura4+ ura4-DS/E ade6-M210 leu1Δ::nmt1(81x)-dam-myc-rdp1-kan dcr1Δ::hph*	2
SPB914	*h+ otr1R(SphI)::ura4+ ura4-DS/E ade6-M210 leu1Δ::nmt1(81x)-dam-myc-rdp1-kan ago1Δ::hph*	2
SPB915	*h+ otr1R(SphI)::ura4+ ura4-DS/E ade6-M210 leu1Δ::nmt1(81x)-dam-myc-kan clr4Δ::nat dcr1Δ::hph*	2
SPB916	*h+ otr1R(SphI)::ura4+ ura4-DS/E ade6-M210 leu1Δ::nmt1(81x)-dam-myc-rdp1-kan clr4Δ::nat dcr1Δ::hph*	2
SPB917	*h+ otr1R(SphI)::ura4+ ura4-DS/E ade6-M210 leu1Δ::nmt1(81x)-dam-myc-rdp1-kan clr4Δ::nat ago1Δ::hph*	2
SPB1475	*h+ otr1R(SphI)::ura4+ ura4-DS/E ade6-M210*	2

	leu1Δ::nmt1(81x)-dam-myc-nup85-kan ago1Δ::hph	
SPB74	*h+ otr1R(SphI)::ura4+ ura4-DS/E leu1-32 ade6-M210*	3
SPB94	*h+ otr1R(SphI)::ura4+ ura4-DS/E leu1-32 ade6-M210 dcr1Δ::nat*	3
SPB96	*h+ otr1R(SphI)::ura4+ ura4-DS/E leu1-32 ade6-M210 swi6Δ::nat*	3
SPB763	*h+ otr1R(SphI)::ura4+ ura4-DS/E leu1-32 ade6-M210 rdp1Δ::kan*	2
SPB764	*h+ otr1R(SphI)::ura4+ ura4-DS/E leu1-32 ade6-M210 ago1Δ::kan*	2
SPB278	*h+ leu1-32 ura4-D18 ori1 ade6-216 imr1R(Nco1)::ura4+ Kan-nmt1(3x)-gfp::dcr1*	2
SPB1087	*h+ ura4- ade6- leu1-32 cut11::mCherry-Nat dis1-promoter-GFP-lacI::his7+ lacO(8x4)LexA(4x)::hsp16+*	2
SPB1199	*h+ ura4- leu1-32 dis1-promoter-GFP-lacI::his7+ lacO(8x4)LexA(4x)::hsp9+ cut11+::mCherry-natR*	2
SPB1200	*h+ ura4- leu1-32 dis1-promoter-GFP-lacI::his7+ lacO(8x4)LexA(4x)::hsp104+ cut11+::mCherry-natR*	2
SPB354	*h+ leu1-32 ura4-D18 ori1 ade6-216 imr1R(Nco1)::ura4+ Kan-nmt1(3x)-nls-gfp::dcr1*	

1 = (Woolcock et al.), 2 = This study, 3 = Danesh Moazed

Table S2. Plasmids used in this study

Name	**Common name**
pMB681	pFA6a - 81xL - arb1 - myc - dam - kanMX6
pMB682	pFA6a - 81xL - dam - myc - ago1 - kanMX6
pMB774	pFA6a - 81xL - amo1 - myc - dam - kanMX6
pMB798	pFA6a - 81xL - dam - myc - nup85 - kanMX6
pMB399	pFA6a - 81xL - dam - myc - kanMX6
pMB348	pFA6a - 81xL - dam - myc - cid14 - kanMX6
pMB349	pFA6a - 81xL - dam - myc - rrp6 - kanMX6
pMB308	placO(8x4)lexA(4x)-LEU2

Table S3. Primers used for quantitative RT-PCR

Name	**Sequence**
hsp16 for	AAAGCACCGAGGGTAACCAA
hsp16 rev	TGGTACGAGAGAATGAGCCAAA
hsp104 for	CGTGAATCTCAGCCCGAAGT
hsp104 rev	TCAACGCGGAGTTGTCGAA
hsp9 for	GAACAAGGCAAGGAGAAAATGACT
hsp9 rev	AATGGATTCCTTGGCCTTGTC
act1 for	TCCTCATGCTATCATGCGTCTT
act1 rev	CCACGCTCCATGAGAATCTTC
For ChIP:	
hsp16 for	GATTGATGCAGATCGCATTGAG
hsp16 rev	TTGGGCAAGGTGACAGTCAATA
hsp104 (-225) for	TCCTTTCCTTCCCATAGTAACATCAT
hsp104 (-225) rev	GTTGAGGATGCCGCAGGTA
hsp104 (248) for	CGCTTGCCTGCTCAGGAT
hsp104 (248) rev	TCGCACTTTCAGGTGACAGAGT
hsp104 (1839) for	CGTGCTGGTCTTTCTGATCCTA
hsp104 (1839) rev	CGGAAGGACCGCAAAACA
hsp104 (2428) for	GAGGTTCAGAAACGGCTTCAAT
hsp104 (2428) rev	GCTTCGTCGCTAACCTCGAT
hsp9 for	GAACAAGGCAAGGAGAAAATGACT
hsp9 rev	AATGGATTCCTTGGCCTTGTC
ura4 for	TACAAAATTGCTTCTTGGGCTCAT
ura4 rev	AGACCACGTCCCAAAGGTAAAC
U6 snRNA for	GATCTTCGGATCACTTTGGTCAA
U6 snRNA rev	TGTCGCAGTGTCATCCTTGTG

Table S4. Chromosomal regions

chromosome	start	end	region
1	1	19999	telomere
1	20000	35599	subtelomere
1	35600	3753686	euchromatin
1	3753687	3789420	centromere
1	3789421	5529999	euchromatin
1	5530000	5571499	subtelomere
1	5571500	5579133	telomere
2	1	15799	subtelomere
2	15800	1602263	euchromatin
2	1602264	1644746	centromere
2	1644747	2113999	euchromatin
2	2114000	2136999	mating type region
2	2137000	4497199	euchromatin
2	4497200	4516199	subtelomere
2	4516200	4539804	telomere
3	1	1070903	euchromatin
3	1070904	1137002	centromere
3	1137003	2452883	euchromatin

The coordinates are given in a 1-based notation.

References

Woods, A., Sherwin, T., Sasse, R., MacRae, T.H., Baines, A.J., and Gull, K. 1989. Definition of individual components within the cytoskeleton of Trypanosoma brucei by a library of monoclonal antibodies. *J Cell Sci* 93 (Pt 3): 491-500.

Woolcock, K.J., Gaidatzis, D., Punga, T., and Buhler, M. Dicer associates with chromatin to repress genome activity in Schizosaccharomyces pombe. *Nat Struct Mol Biol* 18(1): 94-99.

Keller et al., 2012

Molecular Cell

Molecular Cell
Article

HP1^{Swi6} Mediates the Recognition and Destruction of Heterochromatic RNA Transcripts

Claudia Keller,[1,2] Ricardo Adaixo,[3] Rieka Stunnenberg,[1,2] Katrina J. Woolcock,[1,2] Sebastian Hiller,[3,*] and Marc Bühler[1,2,*]
[1]Friedrich Miescher Institute for Biomedical Research, Maulbeerstrasse 66, 4058 Basel, Switzerland
[2]University of Basel, Petersplatz 10, 4003 Basel, Switzerland
[3]Biozentrum, University of Basel, Klingelbergstrasse 70, 4056 Basel, Switzerland
*Correspondence: sebastian.hiller@unibas.ch (S.H.), marc.buehler@fmi.ch (M.B.)
DOI 10.1016/j.molcel.2012.05.009

SUMMARY

HP1 proteins are major components of heterochromatin, which is generally perceived to be an inert and transcriptionally inactive chromatin structure. Yet, HP1 binding to chromatin is highly dynamic and robust silencing of heterochromatic genes can involve RNA processing. Here, we demonstrate by a combination of in vivo and in vitro experiments that the fission yeast HP1^{Swi6} protein guarantees tight repression of heterochromatic genes through RNA sequestration and degradation. Stimulated by positively charged residues in the hinge region, RNA competes with methylated histone H3K9 for binding to the chromodomain of HP1^{Swi6}. Hence, HP1^{Swi6} binding to RNA is incompatible with stable heterochromatin association. We propose a model in which an ensemble of HP1^{Swi6} proteins functions as a heterochromatin-specific checkpoint, capturing and priming heterochromatic RNAs for the RNA degradation machinery. Sustaining a functional checkpoint requires continuous exchange of HP1^{Swi6} within heterochromatin, which explains the dynamic localization of HP1 proteins on heterochromatin.

INTRODUCTION

Heterochromatin is a distinct chromatin structure that is late replicating, gene poor, and rich in transposons or other parasitic genomic elements. Heterochromatic structures are required for proper centromere function, repression of recombination, sister chromatid cohesion, and the maintenance of telomere stability, and they also play an essential role in heritable gene silencing in a variety of organisms from yeast to humans (Grewal and Jia, 2007). One hallmark of heterochromatin is its association with members of the highly conserved heterochromatin protein 1 (HP1) family of proteins (James and Elgin, 1986). HP1 proteins consist of an N-terminal chromodomain (CD) and a structurally related C-terminal chromo shadow domain (CSD), separated by a hinge region. The CSD can mediate homodimerization of HP1 and binding to other proteins through a degenerate pentapeptide motif, PxVxL (Cowieson et al., 2000; Smothers and Henikoff, 2000). The CD binds the N-terminal tail of histone H3 when it is di- or trimethylated with high specificity but low affinity (Bannister et al., 2001; Jacobs and Khorasanizadeh, 2002; Jacobs et al., 2001; Lachner et al., 2001; Nielsen et al., 2002) and the hinge region has been implicated in nucleic acid binding (Muchardt et al., 2002). The fission yeast *Schizosaccharomyces pombe* contains two HP1 homologs, HP1^{Chp2} and HP1^{Swi6}, which both bind to methylated lysine 9 of histone H3 (H3K9) and are involved in heterochromatin silencing (Grewal and Jia, 2007). In contrast to other eukaryotes, *S. pombe* contains only a single member of the SUV39 histone methyltransferase family of proteins, Clr4, which is responsible for the methylation of H3K9 (Nakayama et al., 2001).

Heterochromatin is generally perceived to be a structurally rigid and static chromatin compartment that is inaccessible to the transcription machinery, yet several findings challenge this view. For example, the H3K9 methyl-binding affinity of HP1 proteins can be rather low, and their association with heterochromatin is surprisingly dynamic (Cheutin et al., 2004, 2003; Festenstein et al., 2003; Schalch et al., 2009). Furthermore, recent work has revealed that both RNAi-dependent and -independent RNA turnover mechanisms are crucial for the quiescence of heterochromatic sequences in *S. pombe*, indicating that silencing of heterochromatin does not occur exclusively at the transcriptional level (Bühler et al., 2007). Repression of marker genes when inserted into heterochromatin depends on the noncanonical poly(A) polymerase Cid14, which is thought to target the heterochromatic RNA for degradation via the RNA exosome and/or the RNAi pathway. Similarly, silencing of subtelomeric genes marked by H3K9 methylation also depends on Cid14 (Keller et al., 2010; Wang et al., 2008). Importantly, heterochromatic gene silencing is impaired in Cid14 mutant strains, yet heterochromatin remains intact (Bühler et al., 2007). Thus, some level of transcription within heterochromatin is possible, and pathways to cope with the unwanted heterochromatic RNA do exist (Bühler, 2009). However, the mechanism of specific recognition of heterochromatic transcripts and thus their targeting for the Cid14-dependent degradation has remained elusive.

HP1^{Swi6}, one of the two *S. pombe* heterochromatin proteins, is best known for its critical role in proper centromere function. In *swi6* mutant cells, centromeres lag on the spindle during anaphase, and chromosomes are lost at a high rate (Ekwall et al., 1995). This is associated with a failure in the recruitment of cohesin to pericentromeric heterochromatin (Bernard et al., 2001; Nonaka et al., 2002). Thus, one function of HP1^{Swi6} is the attraction of a high concentration of cohesin to *S. pombe* centromeres, which guarantees proper chromosome segregation. HP1^{Swi6} has also been implicated in the recruitment of cohesin outside constitutive heterochromatin, thus regulating transcription termination between convergent gene pairs (Gullerova and Proudfoot, 2008). Besides cohesin subunits, HP1^{Swi6} also copurifies with a diverse set of other nuclear nonhistone proteins that are involved in a variety of nuclear functions such as chromatin remodelling and DNA replication (Fischer et al., 2009; Motamedi et al., 2008). Even though many of these interactions remain to be confirmed, HP1^{Swi6} may partner with many different factors and ensure genomic integrity. Apart from these functions, HP1^{Swi6} is also required for heterochromatic gene silencing, but on a mechanistic level this is poorly understood.

Here, we demonstrate that HP1^{Swi6} serves a general function linking transcription within heterochromatin to downstream RNA turnover. HP1^{Swi6} binds RNA via a molecular mechanism that involves the hinge region, the CD, and the N-terminal domain. Rather than tethering heterochromatic transcripts to chromatin, HP1^{Swi6} complexed with RNA dissociates from H3K9-methylated nucleosomes and escorts its associated RNAs to the RNA decay machinery. This detachment of HP1^{Swi6} from chromatin results from a competition mechanism that combines the interactions of RNA and methylated H3K9 to HP1^{Swi6} on the single-molecule level with dynamic exchange between the histone-bound and -unbound HP1^{Swi6} ensemble. Our results provide an explanation for the dynamic localization of HP1 proteins on heterochromatin and reveal insights into the role of RNA in the regulation of higher order chromatin structures.

RESULTS

Heterochromatic mRNA Transcripts Are Not Translated into Protein

Previous work revealed that the noncanonical polyA-polymerase Cid14 processes or eliminates a variety of RNA targets to control processes such as the maintenance of genomic integrity, meiotic differentiation, ribosomal RNA maturation, and heterochromatic gene silencing (Keller et al., 2010; Wang et al., 2008; Win et al., 2006). The effect of *cid14+* mutations on heterochromatin silencing has previously been studied using the *ura4+* reporter gene/5-FOA assay (Bühler et al., 2007). Because this assay does not allow a quantification of the resulting protein levels, and because it is also compromised by a general sensitivity of *cid14+* mutant cells to 5-FOA (Figure S1), we created reporter strains carrying a *gfp+* transgene inserted at the innermost centromeric repeat region (*imr1R::gfp+*) or at the *mat3M* locus (*mat3M::gfp+*) (Figure 1A). Consistent with previous results (Bühler et al., 2007), heterochromatic *gfp+* mRNA levels from centromeric locations increased significantly in *clr4Δ* and *dcr1Δ* cells, but only modestly in *cid14Δ* cells (Figure 1B), with no corresponding increase in GFP protein levels upon *cid14+* deletion (Figures 1C and S1A). Therefore, Cid14 plays a redundant role, if any at all, in the silencing of a reporter gene located in centromeric heterochromatin. In contrast, deleting the *cid14+* gene resulted in strongly elevated *gfp+* mRNA levels from the mating-type locus. Unexpectedly, however, this was not accompanied by a concomitant increase in GFP protein levels (Figures 1D and E).

To test whether mRNAs originating from heterochromatic genes engage in translation at all, we set out to profile their association with polyribosomes (Figure 1F). *S. pombe* cell lysates were separated on sucrose gradients and RNA was extracted from the individual fractions. The relative amount of a given mRNA in each fraction was then quantified by quantitative real-time RT-PCR (qRT-PCR). As expected, *act1+* mRNA was highly enriched, whereas the nuclear U6 snRNA was absent from the polysomal fractions (Figure 1F). When transcribed from its endogenous locus, mRNA encoded by the *ura4+* gene was also highly enriched in polysomes (data not shown). Similarly, *ura4+* mRNA originating from a *mat3M::ura4+* reporter was found in the polysomal fractions in the absence of the H3K9 methyltransferase Clr4. However, no considerable association with polysomes was observed for heterochromatic *ura4+* reporter mRNA in wild-type or *cid14Δ* cells (Figure 1F).

Thus, although heterochromatic mRNAs can be over 10-fold more abundant in *cid14Δ* cells than in wild-type cells, they are not translated into protein effectively.

HP1^{Swi6} Functions as an H3K9 Methylation-Specific Checkpoint to Assemble Translationally Incompetent Ribonucleoprotein Particles

Atypical processing of 5′ or 3′ ends of heterochromatic mRNAs could explain why heterochromatic mRNAs do not engage in translation. However, our analysis of mRNA termini revealed no major differences between heterochromatic and euchromatic transcripts (Figure S2 and data not shown), suggesting that heterochromatic mRNAs per se do not contain aberrant features that would signal their destruction or render them translationally inactive. Rather, transcripts emerging from heterochromatin are more likely to be channeled into the RNA decay pathway by the assembly of a heterochromatin-specific ribonucleoprotein particle (hsRNP). Therefore, we postulate the existence of an H3K9 methylation-specific checkpoint that would function on chromatin and assemble emerging transcripts into hsRNPs that are translationally incompetent and prone for degradation (Figure 2A).

Obvious candidates for proteins that could function as such a checkpoint are HP1 proteins, because they have been reported to have affinity for both H3K9-methylated histone H3 tails and RNA. Therefore, HP1 proteins might capture heterochromatic RNAs in an H3K9 methylation-specific manner. The *S. pombe* genome contains two HP1 homologs, HP1^{Chp2} and HP1^{Swi6}. Interestingly, even though HP1^{Swi6} is essential for the full repression of heterochromatin, its contribution to transcriptional gene silencing is minimal. Furthermore, heterochromatic RNAs have been observed to copurify with HP1^{Swi6} but not HP1^{Chp2} (Motamedi et al., 2008).

Therefore, we tested whether heterochromatic mRNAs would become translated in cells lacking HP1^{Swi6}. Consistent with the checkpoint model, GFP protein expression from the *mat3M::gfp+* allele was restored in *swi6Δ* and *swi6Δ cid14Δ* cells (Figure 2B). However, deletion of *swi6+* also resulted in a significant reduction in H3K9me2 at *mat3M::gfp+* (Figure 2C),

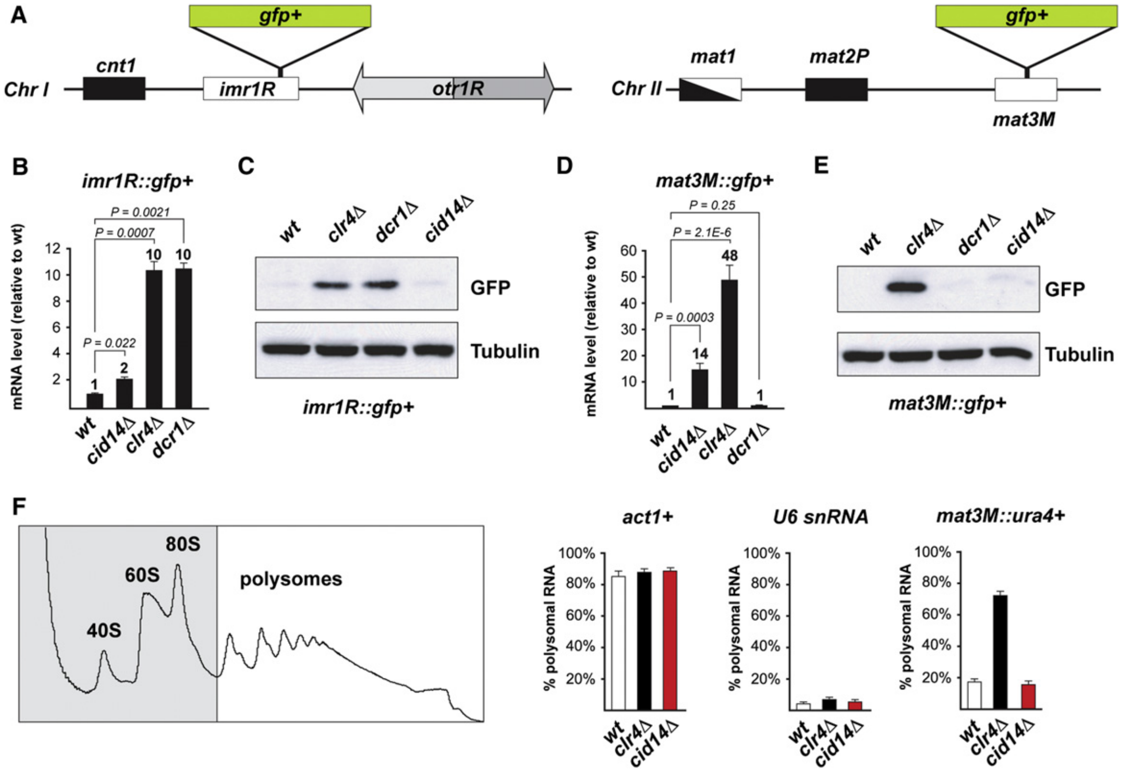

Figure 1. Heterochromatic mRNAs Are Not Translated into Protein

(A) Diagram representing DNA organization at the centromere of chromosome I and at the mating-type locus (chromosome II). cnt1, central core; imr1, innermost repeats; otr1, outermost repeat. *gfp+* reporter transgenes are driven by the *ura4+* promoter, whereas the ORF is followed by a natMX6 cassette (Tadh1 terminator).

(B) Quantitative real-time RT-PCR showing *gfp+* mRNA levels in *imr1R::gfp+* cells. Mean values normalized to *act1+* are shown (n = 3). Error bars represent SEM; p values were calculated using the Student's t test.

(C) Western blot showing GFP protein levels in *imr1R::gfp+* cells. Total protein from an equivalent number of cells was extracted by TCA. Tubulin served as a loading control.

(D) Quantitative real-time RT-PCR showing *gfp+* mRNA levels in *mat3M::gfp+* cells. Mean values normalized to *act1+* are shown (n = 14). Error bars represent SEM, p values were calculated using the Student's t test.

(E) Western blot showing GFP protein levels in *mat3M::gfp+* cells. Total protein from an equivalent number of cells was extracted by TCA. Tubulin served as a loading control.

(F) A representative polysome profile (OD 254 nm) with monosomal (fractions 1–5) and polysomal fractions (fractions 6–12 polysomal) is shown on the left. RNA levels were determined by quantitative real-time RT-PCR and the enrichment in the polysomal fraction was calculated as a percentage of the total. Error bars represent SEM. Act1+ RNA and U6 snRNA served as positive and negative controls, respectively.

not allowing us to definitely assign the checkpoint function to HP1^{Swi6}. In contrast, deletion of *swi6+* or *cid14+* or both did not significantly lower H3K9 methylation levels at the subtelomeric *tlh1/2+* genes, yet resulted in a strong upregulation of the respective mRNAs (Figures 2D and 2E). Importantly, association of *tlh1/2+* mRNA with polysomes was only observed in cells lacking *swi6+* but not *cid14+* (Figure 2F). These results place HP1^{Swi6} upstream of Cid14 and directly support a model in which HP1^{Swi6} acts on H3K9-methylated nucleosomes and promotes the assembly of translationally incompetent hsRNPs.

HP1^{Swi6} Binds RNA via the Hinge Region

The above results implicate HP1^{Swi6} in the checkpoint model as the H3K9 methylation "reader," yet it was not clear whether HP1^{Swi6} itself or any of its interacting proteins could capture heterochromatic RNAs. Whereas RNA-binding affinity has been demonstrated for mammalian HP1α (Muchardt et al., 2002), it was not known whether fission yeast HP1^{Swi6} can bind RNA directly. We purified recombinant HP1^{Swi6} and performed electrophoretic mobility shift assays (EMSA) using various RNA and DNA probes. In these assays, recombinant HP1^{Swi6} bound efficiently to the different RNAs but only weakly to DNA (Figure 3B). Furthermore, RNA binding could be competed with unlabeled RNA probes (Figure S3). HP1^{Swi6} consists of four domains: An N-terminal domain (NTD, residues 1–74), which is presumably flexibly disordered; a chromodomain (CD, residues 75–139), which binds K9-methylated histone tails (Bannister et al., 2001); a hinge region (H, residues 140–264); and a C-terminal chromo shadow domain (CSD, residues 265–328) (Cowieson et al., 2000). The hinge region of mammalian HP1α has been implicated in RNA binding (Muchardt et al., 2002). To test whether the hinge region also confers RNA binding

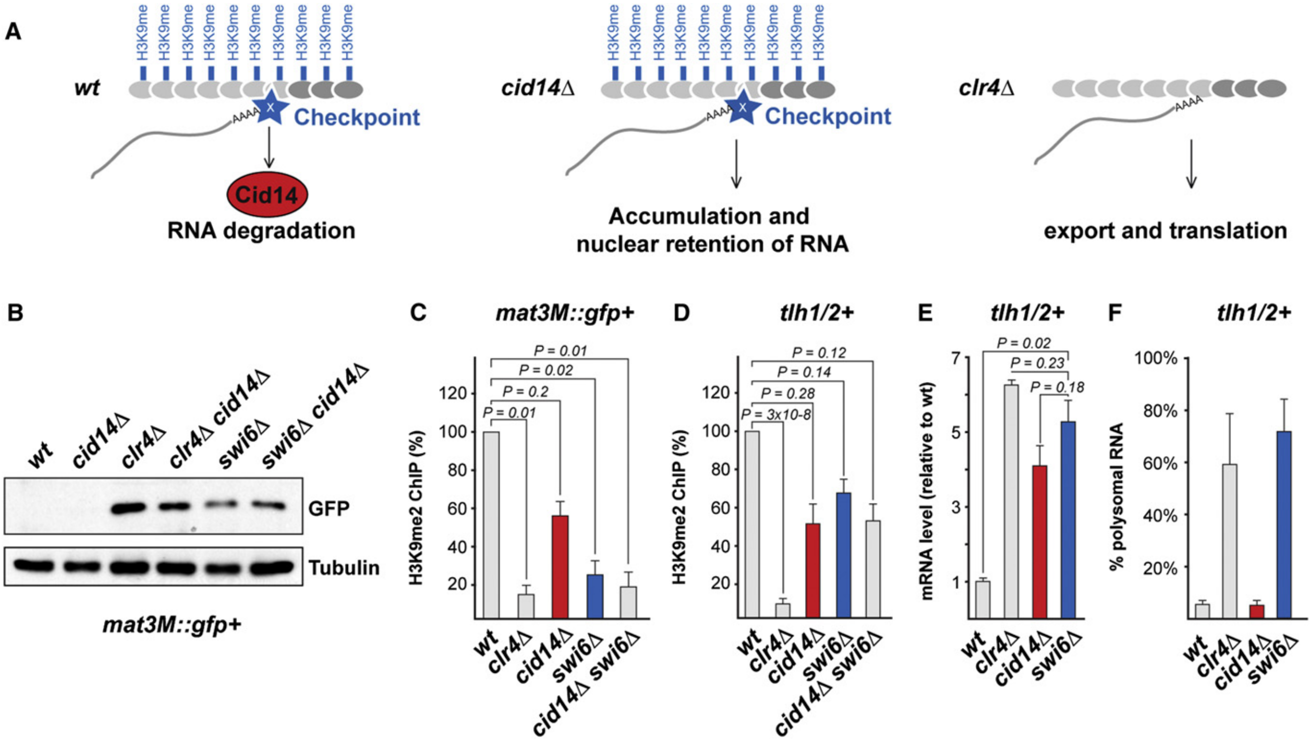

Figure 2. HP1^{Swi6} Prevents Translation of Heterochromatic RNAs

(A) Checkpoint model for the specific recognition of mRNA originating from heterochromatin. When H3K9 is unmethylated (*clr4Δ* or euchromatin), the checkpoint cannot assemble and mRNAs are exported and translated. In *WT* and *cid14Δ* cells, the checkpoint assembles on H3K9 methylated nucleosomes and captures heterochromatic mRNA transcripts. Eventually, these mRNAs are degraded in a Cid14-dependent manner. In the absence of Cid14 (*cid14Δ*), heterochromatic mRNAs accumulate but are not translated because they are retained by the checkpoint.

(B) Western blot showing GFP protein levels in *mat3M::gfp+* cells. Total protein from an equivalent number of cells was extracted by TCA. Tubulin served as a loading control.

(C and D) ChIP experiment showing that H3K9me2 levels at *mat3M::gfp+* are significantly reduced in *swi6Δ* and *cid14Δ swi6Δ* cells but not in *cid14Δ* cells. H3K9me2 levels at the telomeric *tlh1+* and *tlh2+* genes are not significantly reduced in *cid14Δ*, *swi6Δ*, and *cid14Δ swi6Δ* cells. Enrichment was determined by quantitative real-time PCR. Mean values normalized to *act1+* are shown (n = 4). Error bars represent SEM, p values were calculated using the Student's t test.

(E) *tlh1/2+* mRNA levels were determined by quantitative real-time RT-PCR. Mean values normalized to *act1+* are shown (n = 9). Error bars represent SEM, p values were calculated using the Student's t test.

(F) *tlh1/2+* mRNA associates with polysomes in *swi6Δ* but not in *cid14Δ* cells, although total mRNA levels are not significantly different in *swi6Δ* and *cid14Δ* cells (E). Enrichment of *tlh1/2+* mRNA in polysomal fractions of the indicated mutants was determined by polysome profiling as in Figure 1F. Error bars represent SEM.

properties to HP1^{Swi6}, we purified recombinant CD, hinge, and CSD. In contrast to the CD and the CSD, the isolated hinge region was sufficient for strong RNA binding (Figure 3B). By using NMR chemical shift titrations monitored on amide resonances in the flexible hinge region, we determined the binding constant of full-length HP1^{Swi6} to a 20-mer RNA as 38 ± 13 μM (Figure 3C). These results demonstrate that HP1^{Swi6} is able to bind RNA alone and that the hinge region is substantially involved in this binding interaction.

Design of an HP1^{Swi6} Mutant that Affects RNA but Not H3K9me Binding

Because heterochromatin at certain loci disintegrates upon removal of the *swi6+* gene (Figure 2C), we aimed to develop an HP1^{Swi6} mutant with compromised RNA- but normal H3K9me-binding affinity. Therefore, we mutated the positively charged residues of the hinge region, 20 lysines and 5 arginines, to alanines (Figure 4A). For the resulting mutant protein, HP1^{Swi6}-KR25A, RNA binding was indeed drastically reduced when compared to the wild-type protein (Figure 4B). For the subsequent use of the protein in vivo, we assessed the impact of these 25 mutations on protein architecture by solution NMR spectroscopy using recombinant HP1^{Swi6} and HP1^{Swi6}-KR25A protein. Based on the full-length proteins and subconstructs thereof, we established complete sequence-specific resonance assignments for the isolated CD (residues 75–139) (Figure S4A), as well as domain-specific resonance assignments for the NTD, the hinge region, and the CSD of wild-type HP1^{Swi6}. The chemical shift dispersion and intensities of the resonances in full-length HP1^{Swi6} indicated the CD and the CSD to be folded domains and the NTD and the hinge region to be flexibly unfolded polypeptide segments, as expected from predictions of the secondary structure. Analysis of the $^{13}C^{\alpha}$ and $^{13}C^{\beta}$ secondary chemical shifts of the isolated CD indicates three β-strands and one large α-helix at the C-terminal end of the domain (Figure S4E), which is well in agreement with the known

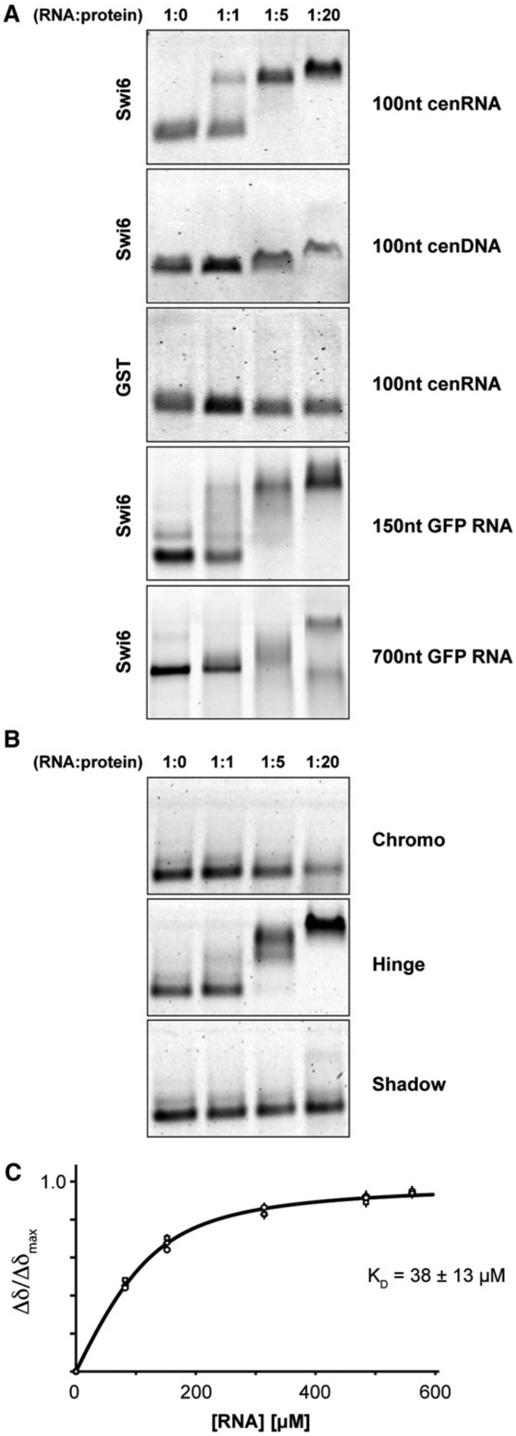

Figure 3. HP1^{Swi6} Is an RNA-Binding Protein

(A and B) Electrophoretic mobility shift assay (EMSA) using recombinant HP1^{Swi6}, HP1^{Swi6} subdomains or GST and different substrate nucleic acids (see Supplemental Information). RNA probes were labeled with fluorescein-UTP by in vitro transcription. DNA probes were produced by standard PCR. Protein-nucleic acid complexes were separated on 1.6%-TB agarose gels and the signal detected using a typhoon scanner.

(C) NMR chemical shift perturbation assay. The open circles are combined amide chemical shifts $\Delta\delta = \sqrt{0.04 \cdot \Delta\delta(^{15}N)^2 + \Delta\delta(^{1}H)^2}$ of three selected amide resonances plotted versus the RNA concentration. The line is the result of a nonlinear least-squares fit of a single binding curve to the data. The resulting dissociation constant K_D is indicated.

secondary structure elements in the homologous human chromobox homolog 3 (Kaustov et al., 2011). Importantly, 2D [^{15}N,^{1}H]-TROSY NMR spectra revealed the subspectra for the CD, the CSD, and the NTD, but not the hinge region of recombinant HP1^{Swi6}-KR25A, to be essentially identical to wild-type HP1^{Swi6} (Figures 4D and 4E). Thus, the 25 Lys and Arg to Ala mutations in the hinge region abolish RNA binding without affecting the global fold of the CD and CSD domains or having a structural effect on the unfolded NTD. Binding to methylated H3K9 is, therefore, expected to be maintained in the HP1^{Swi6}-KR25A mutant. This we could confirm by surface plasmon resonance (SPR) measurements (Figure 4C). The binding constants of wild-type and HP1^{Swi6}-KR25A to an immobilized peptide corresponding to residues 1–20 of a K9 trimethylated histone H3 tail (H3K9me3 peptide) (2.5 ± 0.5 μM and 7.8 ± 0.8 μM, respectively), were akin to and in correspondence with published values for the individual domains (Jacobs and Khorasanizadeh, 2002; Schalch et al., 2009).

Silencing but Not the Integrity of Heterochromatin Is Affected in the HP1^{Swi6} RNA-Binding Mutant

To study the functional relevance of RNA binding through the hinge region of HP1^{Swi6}, we replaced the endogenous *swi6+* open reading frame (ORF) with the HP1^{Swi6}-KR25A mutant ORF. Consistent with previous results that assigned a nuclear localization signal (NLS) function to the hinge region (Wang et al., 2000), we observed that the HP1^{Swi6}-KR25A protein localized mainly to the cytoplasm (Figure S5A and data not shown). Therefore, we added an N-terminal SV40 NLS to the wild-type and mutant HP1^{Swi6} alleles, which restored the characteristic heterochromatic foci in the nucleus and the specific association with RNA from heterochromatic regions (Figures 5A and S5B–S5F). Furthermore, in contrast to *swi6Δ* cells, neither NLS-HP1^{Swi6}- nor NLS-HP1^{Swi6}-KR25A-expressing cells were sensitive to thiabendazole (TBZ), showing that RNA binding to HP1^{Swi6} is not required for proper chromosome segregation (Figure 5B). Importantly, the H3K9 methylation defect observed at the *mat3M::gfp+* locus in *swi6Δ* cells (Figure 2C) was rescued by the *nls-swi6-KR25A* allele (Figure 5D). Similarly, H3K9 methylation within telomeric heterochromatin remained unaffected in *nls-swi6-KR25A* cells (Figures 5E and 5F).

These results demonstrate that neither H3K9 methylation nor recruitment of HP1^{Swi6} to heterochromatin depend on RNA binding through the hinge region of HP1^{Swi6}. However, silencing of heterochromatic genes was nonfunctional in *nls-swi6-KR25A* cells (Figures 5G–5J). Thus, RNA binding to HP1^{Swi6} is required for full repression of heterochromatic genes but dispensable for the integrity of heterochromatin. In summary, with *nls-swi6-KR25A* we created a separation-of-function allele of HP1^{Swi6} that fails to repress heterochromatic genes but still fulfills its architectural roles, with no impact on H3K9 methylation or chromosome segregation.

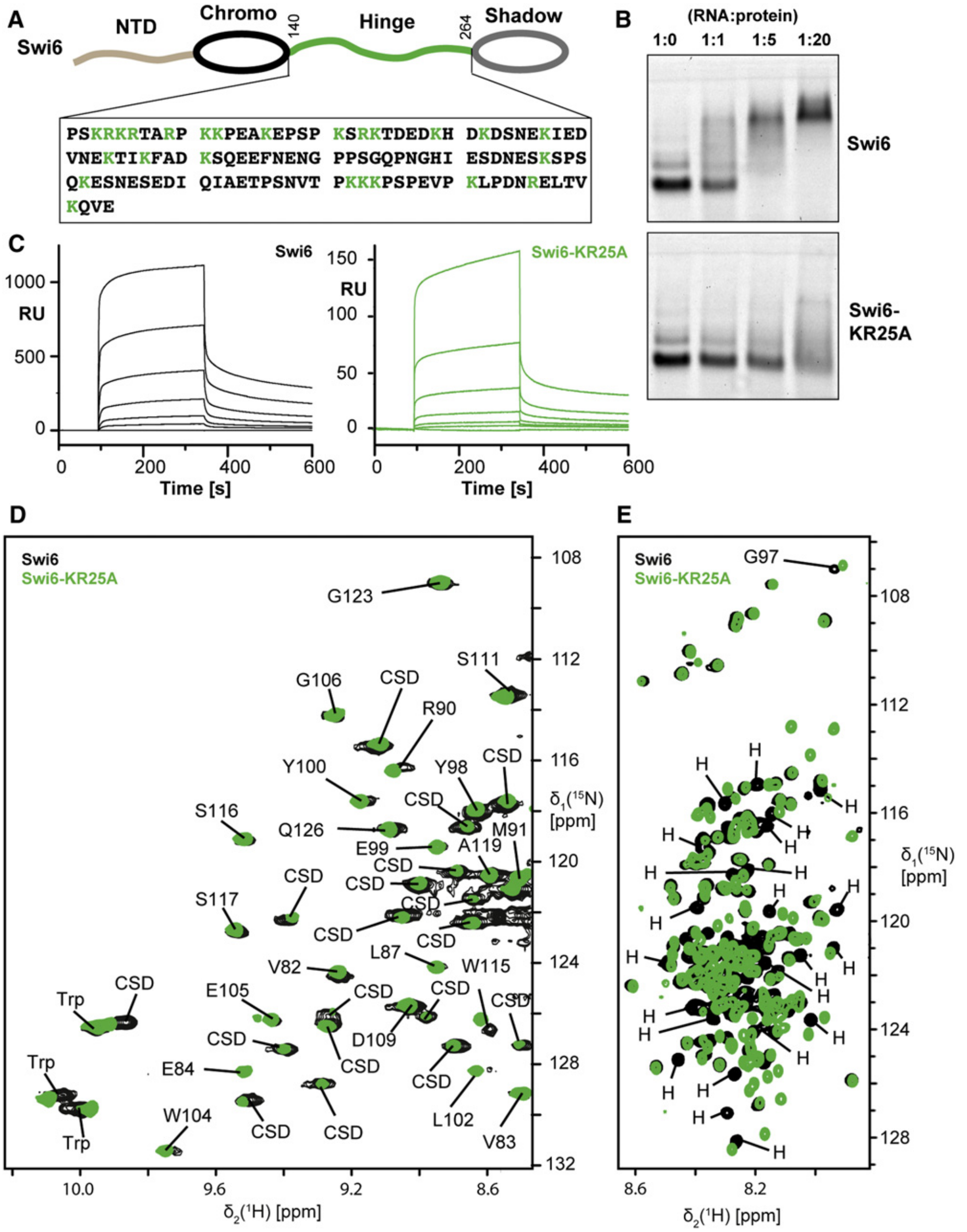

Figure 4. Characterization of HP1^{Swi6}-KR25A

(A) Domain architecture of HP1^{Swi6}. The two folded domains are indicated as ellipses, the two flexible domains as wavy lines. The amino acid sequence of the hinge region (residues 140–264) is given below. Lys and Arg residues that are mutated to Ala in the HP1^{Swi6}-KR25A protein are marked in green.

(B) EMSA showing that RNA binding of HP1^{Swi6}-KR25A is strongly impaired compared with the wild-type protein. A 100 nt centromeric RNA probe was used.

(C) SPR sensorgrams for binding of HP1^{Swi6} (black) and HP1^{Swi6}-KR25A (green) to an H3K9me3 surface. The protein concentrations are from bottom to top 0, 0.015, 0.047, 0.15, 0.43, 1.3, and 3.8 μM.

(D and E) Comparison of 2D [^{15}N,^{1}H]-TROSY correlation spectra of HP1^{Swi6} (black) and HP1^{Swi6}-KR25A (green). In (D), the downfield region of the spectrum is plotted at a low base level, showing mainly resonances from folded parts of the proteins. The sequence-specific resonance assignments for the CD and domain-specific assignments for the CSD (labeled "CSD") are indicated. In (E), the random-coil region of the same spectra are plotted at high base level, showing mainly resonances from the flexibly disordered NTD and hinge region. Domain-specific resonance assignments are shown for those resonances that are altered by the KR25A mutations. These are all located in the hinge region ("H"). The complete domain-specific resonance assignments are given in Figure S4.

HP1^{Swi6} Binding to K9 Methylated Histone H3 Is Highly Dynamic

Consistent with published results (Cheutin et al., 2004), fluorescence recovery after photobleaching (FRAP) experiments revealed that HP1^{Swi6} proteins are highly dynamic at the cellular ensemble level in vivo (Figure S5A). For proteins that are bound tightly to chromatin, recovery kinetics can be expected to be slow or not detectable, as observed for the telomere-binding

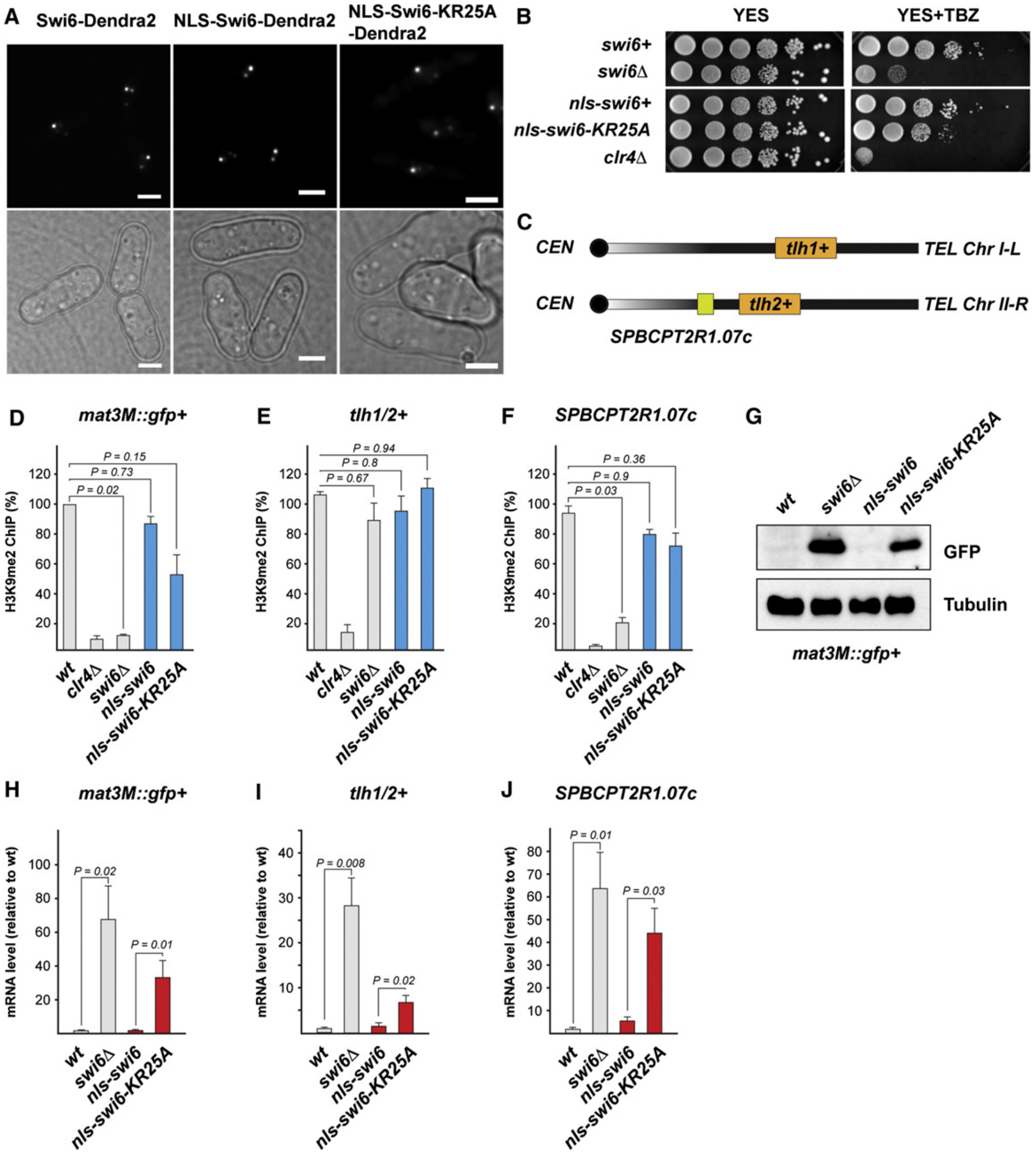

Figure 5. RNA Binding through the Hinge Region of HP1^{Swi6} Is Required for Silencing but Not Maintenance of Heterochromatin

(A) Microscopy of living *S. pombe* cells expressing C-terminally Dendra2-tagged HP1^{Swi6} variants driven from the endogenous promoter. Cells were grown in YES medium at 30°C. To restore nuclear localization of the HP1^{Swi6}-KR25A mutant (Figure S4), a SV40 NLS was added N-terminally. Scale bar = 2 μm.

(B) In contrast to *swi6Δ* cells, cells expressing the RNA-binding mutant NLS-HP1^{Swi6}-KR25A are not sensitive to thiabendazole (TBZ), indicating that chromosome segregation is normal. Cells were spotted on YES agar plates containing either 0 or 14 mg/l TBZ.

(C) Schematic diagram showing the location of three heterochromatic genes at the telomeres of chromosome I and II. *tlh1+* and *tlh2+* produce identical transcripts (Mandell et al., 2005). CEN, centromere; TEL, chromosome end.

(D–F) ChIP experiments demonstrating that H3K9me2 levels are not significantly reduced at *mat3M::gfp+* (D), *tlh1/2+* (E), and *SPBCPT2R1.07c* (F) in *nls-swi6+* and *nls-swi6-KR25A* cells compared with wild-type cells. Mean values normalized to *act1+* are shown (n = 4). Error bars represent SEM, p values were calculated using the Student's t test.

(G) Western blot showing GFP protein levels in *mat3M::gfp+* cells. Total protein from an equivalent number of cells was extracted by TCA. Tubulin serves as a loading control.

(H–J) Quantitative real-time RT-PCR showing *mat3M::gfp+* (I), *tlh1/2+* (K), or SPBCPT2R1.07c (L) transcript levels in the respective mutants. Mean values normalized to *act1+* are shown (n = 5). Error bars represent SEM, p values were generated using the Student's t test.

protein Taz1 (Figure S5B). This is not the case for HP1^{Swi6}, for which fluorescence recovered rapidly after photobleaching with an exponential lifetime of 1.8 ± 0.1 s (Figure S5C). This dynamic exchange of the HP1^{Swi6} ensemble from chromatin in vivo is qualitatively consistent with the rapid exchange dynamics we observed in NMR peptide titration experiments in vitro. We found that the resonances of the CD involved in H3K9me3 peptide binding underwent line broadening due to intermediate chemical exchange. This indicates kinetic on/off rates for the exchange between bound and unbound forms of individual HP1^{Swi6} molecules in the range of about 0.01–1.0 ms^{-1}, corresponding to lifetimes of 1–100 ms. These in vivo and in vitro data thus demonstrate the highly dynamic behavior of HP1^{Swi6} and rule out the possibility that individual HP1^{Swi6} molecules remain tightly bound to heterochromatin for minutes or longer. Therefore, HP1^{Swi6} alone cannot tether heterochromatic RNAs to chromatin.

Localization of the HP1^{Swi6} Interaction Sites with RNA and H3K9me

To obtain insight into the interactions of HP1^{Swi6} with RNA and methylated H3K9 at the atomic level, we used NMR chemical shift perturbation to identify residues structurally involved in these interactions. To this end, we monitored amide moiety chemical shifts, which are sensitive to structural changes of the polypeptide backbone. For the interaction of full-length HP1^{Swi6} with the H3K9me3 peptide, we observed chemical shift changes for 21 out of the 65 residues in the CD, as well as for one tryptophan side chain indole moiety (Figures 6A and 6B). The location of these residues in the amino acid sequence in HP1^{Swi6} corresponds to the location of the known binding pocket for the peptide in homologous domains (Jacobs and Khorasanizadeh, 2002; Kaustov et al., 2011; Nielsen et al., 2002). No significant chemical shift changes occurred for the backbone amide resonances of the CSD, but smaller chemical shift perturbations were observed for 8 residues of the N-terminal domain and 1 residue of the hinge region (Figure 6B). On the other hand, interaction with 20-mer-GFP RNA induced chemical shift changes for resonances of three different domains: 13 residues from the hinge region, 19 from the CD, and 10 from the N-terminal domain (Figures 6C and 6D). Furthermore, all resonances of the CD underwent line broadening at intermediate RNA concentrations due to intermediate exchange indicating kinetic on/off rate constants for RNA binding below about 1 ms^{-1}.

These data show that binding of RNA as well as binding of H3K9me3 peptide to HP1^{Swi6} occurs by a molecular mechanism that includes structural changes in three domains of HP1^{Swi6}. The observation that these interaction sites partially overlap thereby points toward the intriguing possibility that histone tail and RNA binding are not independent. Rather, these could be competitive processes, meaning that HP1^{Swi6} dissociates from H3K9-methylated nucleosomes when complexed with RNA. Consistent with this idea, steady-state competition assays using SPR showed competitive behavior (Figure 6E). At substoichiometric RNA:HP1^{Swi6} ratios, the initial SPR response increased. This can be rationalized by the dimeric nature of HP1^{Swi6} caused by its CSD, which leads to complexes with 2 RNA and 2 peptide-binding sites. At concentrations above stoichiometry, however, the SPR response decreased with increasing RNA concentration, indicating competition for the peptide surface. Importantly, the 20-mer GFP-RNA did not bind to the immobilized peptide surface in a control experiment under the same buffer conditions (Figure S6D). Furthermore, binding of the HP1^{Swi6} -KR25A mutant to H3K9me was insensitive and noncompetitive to the addition of RNA (Figures 6E and S6D).

In summary, our results implicate a mechanism by which RNA and methylated H3K9 compete for HP1^{Swi6} binding at the ensemble as well as the single-molecule level. Binding of RNA to HP1^{Swi6} structurally involves the hinge, the CD, and the NTD and impedes binding of HP1^{Swi6} to methylated H3K9. Thus, rather than tethering RNA to heterochromatin firmly, HP1^{Swi6} dynamically complexes with RNA and dissociates from H3K9-methylated nucleosomes.

Cid14 Functions in the Vicinity of Heterochromatin

The above results have established HP1^{Swi6} as a crucial constituent of hsRNPs, tagging RNAs as a result of their heterochromatic origin and priming them for degradation. Importantly, the dynamic properties of HP1^{Swi6} imply that the degradation of heterochromatic RNA originating from telomeres and the mating-type locus occurs off chromatin, but it is unclear whether Cid14 would join the hsRNP before or after dissociation from H3K9 methylated nucleosomes. If it would occur before dissociation from heterochromatin, it should be possible to crosslink Cid14 to telomeres or the mating-type locus. However, ChIP experiments did not show enrichment of Cid14 at these loci (data not shown), suggesting that Cid14 joins the HP1^{Swi6}/RNA complex only after dissociation from heterochromatin.

To test whether this still occurs in close proximity to heterochromatin, we employed the DNA adenine methyltransferase identification method (DamID, Figure 7A), a sensitive chromatin profiling technique that is suited to capture indirect or transient protein–chromatin interactions. We generated strains that express HP1^{Swi6} and Cid14 fused to the Dam DNA methyltransferase (Figure 7A; Woolcock et al., 2011) and assessed GATC methylation throughout the *S. pombe* genome using tiling arrays. As expected, HP1^{Swi6} was highly enriched at the mating-type locus, the centromeres, and the telomeric regions when compared to a Dam-only control (Figure 7B). Similarly, GATC methylation within the different heterochromatic regions was also observed for Dam-Cid14, demonstrating that Cid14 resides in close proximity to heterochromatin. Importantly, GATC methylation by Dam-Cid14 at the mating-type locus and telomeres is fully dependent on HP1^{Swi6} and not as strong as for Dam-HP1^{Swi6} (Figure 7C). This indicates that Cid14 joins hsRNPs after assembly and dissociation from heterochromatin at the mating-type region and the telomeres.

In conclusion, these results demonstrate that Cid14 resides in the vicinity of heterochromatin and that heterochromatic RNA originating from telomeres or the mating-type locus is delivered to Cid14 in a close spatial and temporal correlation to the dissociation of HP1^{Swi6} from H3K9-methylated nucleosomes. We speculate that the actual degradation of heterochromatic RNA might also occur near heterochromatin. The functional relevance of the HP1^{Swi6}-independent association of Cid14 with centromeric heterochromatin remains unknown.

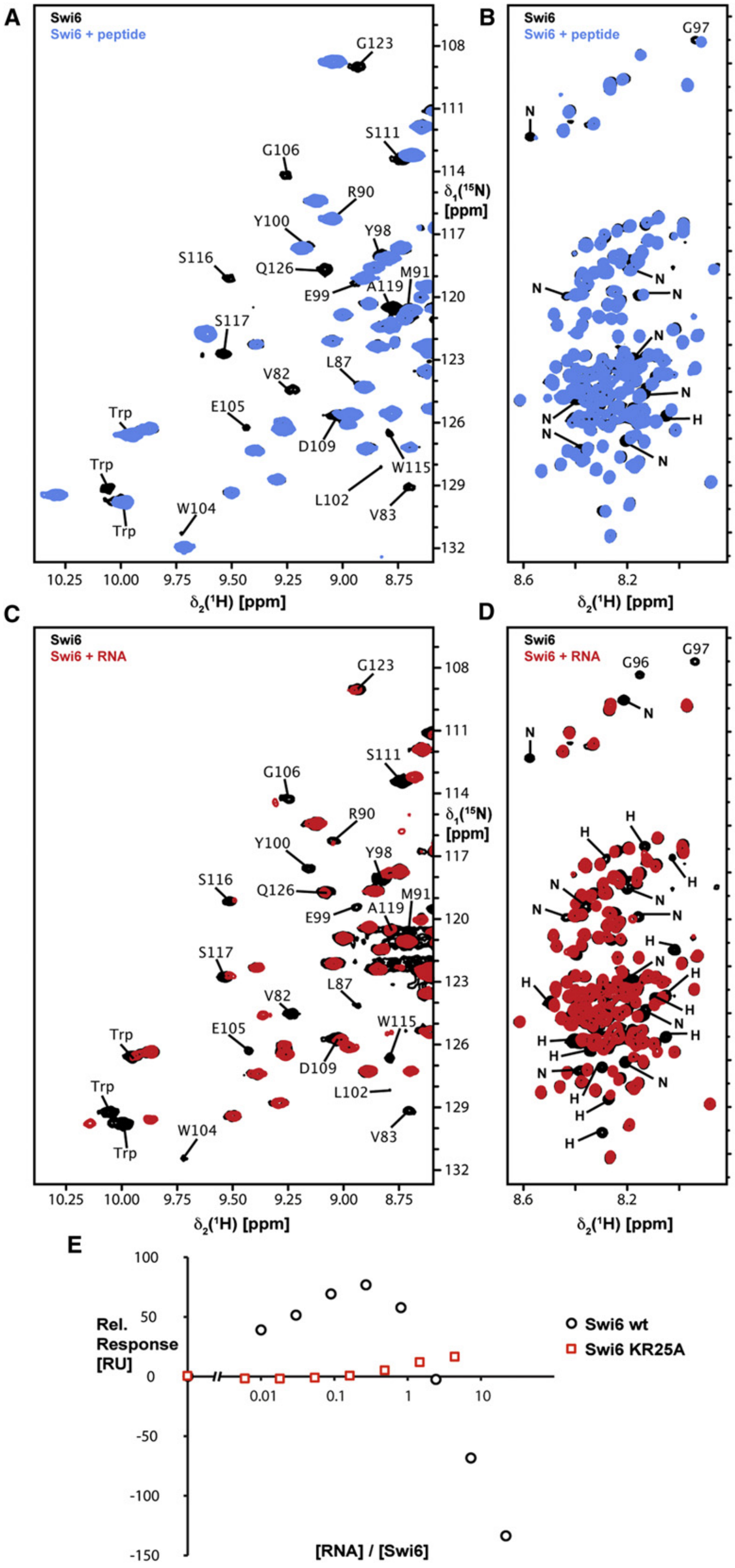

Figure 6. Localization and Competition of the HP1^{Swi6} Interactions

(A–D) Overlay of 2D [^{15}N,^{1}H]-TROSY correlation spectra of HP1^{Swi6}. The spectra are plotted in (A) and (C) at low base level, showing mainly resonance peaks from the two folded domains CD and CSD. The spectra are plotted in (B) and (D) at high base level, showing mainly resonances from the flexibly unfolded hinge and N-terminal domains. Residue type and number indicate sequence-specific resonance assignments for the CD. "H," "N," and "Trp" denote resonances from the hinge region, the NTD, and tryptophan side chains, respectively. (A and B) Black: HP1^{Swi6}; blue: 138 μM HP1^{Swi6} + 513 μM H3K9me3 peptide. (C and D) Black: HP1^{Swi6}; red: 95 μM HP1^{Swi6} + 560 μM RNA.

(E) SPR responses for competitive binding of H3K9me3 and RNA to HP1^{Swi6}. A constant concentration of 1 μM HP1^{Swi6} (black circles) or 5 μM HP1^{Swi6}-KR25A (red squares) with increasing concentrations of 20-mer GFP-RNA was injected to the H3K9me3 surface. The maximal SPR response after 200 s injection is plotted versus the RNA:protein concentration ratio. For each of the two proteins, the response in the absence of RNA was set to zero (raw data, see Figure S6D).

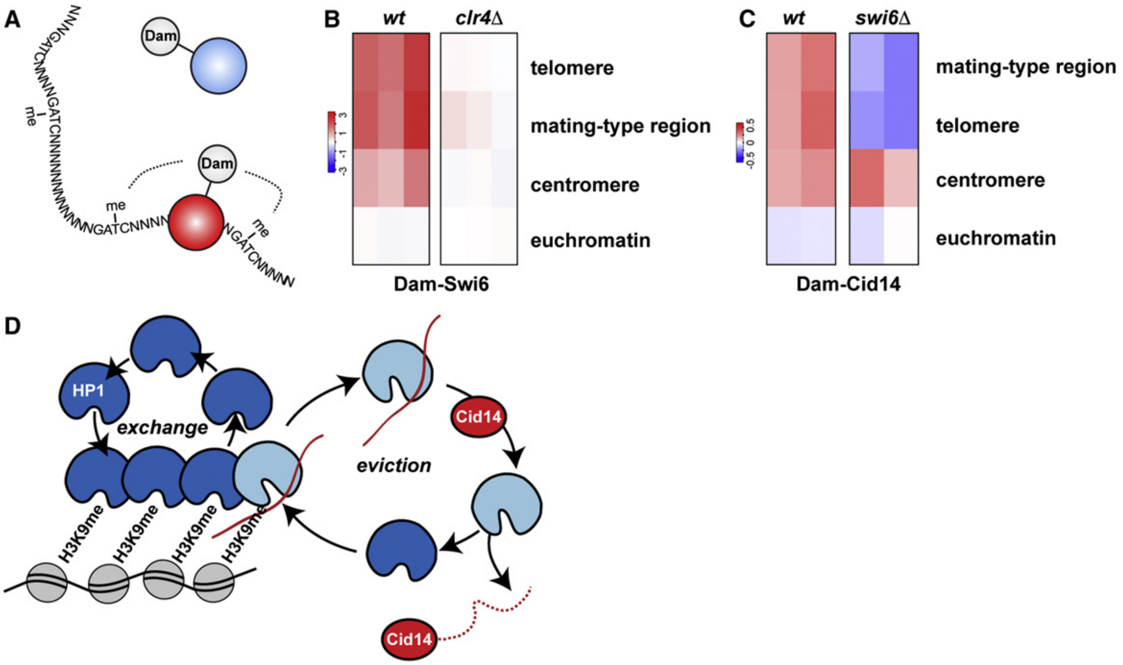

Figure 7. Cid14 Functions in the Vicinity of Heterochromatin

(A) In DamID, a Dam fusion protein is expressed at very low levels. On interaction of the fusion protein with chromatin (red), Dam methylates the adenine in the sequence context of GATC, which can be mapped by a methylation-specific PCR protocol.

(B and C) HP1^{Swi6} and Cid14 enrichments from DamID experiments (log$_2$) at chromosomal regions.

(D) Model for HP1^{Swi6}-mediated degradation of heterochromatic RNA. HP1^{Swi6} proteins associate with H3K9-methylated nucleosomes (gray) only transiently and readily exchange from heterochromatin (dark blue). This continuous exchange of HP1^{Swi6} prevents saturation of heterochromatin with RNA. In case transcription within heterochromatin occurs, HP1^{Swi6} binds the newly synthesized RNA (red) and dissociates from H3K9 methylated nucleosomes as a result of competition between RNA and the histone tail for HP1^{Swi6} binding (light blue). Subsequently, the RNA is passed on to Cid14 (red), which in turn initiates RNA degradation.

DISCUSSION

Association of HP1 Proteins with RNA

It was recognized earlier that proteins involved in chromatin regulation have the ability to bind RNA, although the functional relevance of this interaction has remained elusive. RNA binding was first demonstrated for the CDs of MOF and MSL-3, proteins involved in dosage compensation in *Drosophila* (Akhtar et al., 2000). For mammalian HP1α, the hinge region has been implicated in RNA binding (Muchardt et al., 2002). Here we demonstrate that HP1^{Swi6}, the fission yeast homolog of HP1α, can also bind RNA directly. Importantly, we have found that the interaction of HP1^{Swi6} with RNA mechanistically includes the hinge region, the CD, and the NTD, a property that could be easily overlooked when working with isolated domains. Therefore, it will be interesting to revisit the RNA-binding properties of other HP1 proteins, such as mammalian HP1α, β, or γ, by approaches similar to those in this study. It might be that different HP1 isoforms display important differences in their interaction with RNA, which could reveal novel insights into their functional diversification. It will also be very interesting to elucidate the structural basis of the RNA and peptide binding of HP1^{Swi6} at the atomic level, which should give additional insights into the biophysical nature of their competitive binding mechanism.

It has been speculated that the functional relevance of the RNA affinities of HP1α or the dosage compensation complex might be the targeting to chromatin by major satellite or roX noncoding RNAs, respectively (Akhtar et al., 2000; Maison et al., 2002, 2011). In such a model, RNA is proposed to be involved structurally in the assembly of a higher order chromatin structure by serving as a recruitment platform. This is unlikely to apply to *S. pombe* HP1^{Swi6}, as neither H3K9 methylation nor recruitment of HP1^{Swi6} to heterochromatin depends on RNA binding. In contrast, RNA bound to HP1^{Swi6} dissociates from chromatin as a result of exchange with the cellular HP1^{Swi6} ensemble and a decrease in affinity for methylated H3K9.

Stable Repression of Heterochromatin through RNA Sequestration and Degradation

The results of our work reinforce previous findings that heterochromatin is not always refractory to transcription, yet is tightly repressed. We demonstrate here that HP1^{Swi6} assures coupling between heterochromatin transcription and RNA turnover by serving as an H3K9 methylation-specific checkpoint. Based on the data presented, we propose a model for the action of the HP1^{Swi6} ensemble, which dynamically exchanges with the bulk in a maintenance cycle. Free RNA is captured in the eviction cycle and passed on to the degradation machinery. Constant flux of RNA-unbound HP1^{Swi6} from the bulk ensemble prevents saturation of heterochromatin with RNA. Competition between RNA and methylated H3K9 for HP1^{Swi6} binding at the ensemble level guarantees that RNA-free HP1^{Swi6} is preferably recruited to heterochromatin, thereby sustaining a functional checkpoint on the H3K9-methylated nucleosome and ensuring constant turnover of heterochromatic RNAs (Figure 7C).

In our model, HP1^{Swi6} functions on chromatin to bind to and assemble emerging heterochromatic transcripts into special RNPs, which we refer to as hsRNPs. Thereby, HP1^{Swi6} guarantees specific and tight repression of heterochromatic genes on at least two levels. First, HP1^{Swi6} prevents protein synthesis by sequestration of mRNAs from ribosomes, most likely through nuclear retention. Thus, a heterochromatic mRNA remains repressed even in the absence of RNA degradation. This explains why classical PEV screens failed to recover RNA decay factors such as Cid14. Notably, Cid14 itself is involved in the processing of ribosomal RNA and also associates with 60S ribosomal proteins (Keller et al., 2010; Win et al., 2006), raising the possibility that loss of Cid14 might result in a general defect in translation. However, association of euchromatic mRNAs with polyribosomes, as well as protein expression levels, remain unaffected in *cid14Δ* cells (Figure 1 and data not shown), strongly arguing against such an indirect effect. Second, the HP1^{Swi6} ensemble ensures elimination of heterochromatic mRNAs by capturing the RNA at the site of transcription and escorting it to the degradation machinery. Rather than the classical features of an aberrant RNA, such as a truncated open reading frame or defective 5′ or 3′ ends, our data suggests that it is the physical association of a heterochromatic mRNA with HP1^{Swi6} that primes it for destruction. We note that artificial tethering of HP1^{Swi6} to a euchromatic mRNA does not result in RNA degradation (data not shown), suggesting that canonical mRNPs are immune to HP1^{Swi6}-mediated RNA turnover. Furthermore, since the kinetics of RNA binding to HP1^{Swi6} are fast, the hsRNPs may be stabilized by additional factors. However, at this point we can only speculate on such contributions by additional proteins or other molecules.

Concluding Remarks

In this study, we have discovered a function for one of the fission yeast HP1 proteins that provides the missing link between transcriptional origin and Cid14-dependent degradation of heterochromatic mRNAs. Our results highlight the role of RNA as a negative regulator of HP1^{Swi6} binding to chromatin and provide insights into the repression of heterochromatic domains at a posttranscriptional level. The high degree of conservation of HP1 proteins and heterochromatin-mediated gene silencing phenomena suggest that our findings may also apply to other eukaryotes.

Our work has revealed that HP1^{Swi6}, in addition to its role in proper centromere function, also guarantees tight repression of heterochromatic genes through RNA sequestration and degradation. Interestingly, the *Drosophila* HP1 protein Rhino has been linked recently to the piRNA pathway (Klattenhoff et al., 2009). In analogy to our checkpoint model, Rhino may bind the initial sense transcript at the heterochromatic transposon locus and subsequently escort it to the perinuclear "nuage" structure, where it can enter the ping-pong amplification cycle. Thus, rather than forming repressive chromatin, Rhino might specify the recognition and ensure efficient elimination of transposon RNA.

Finally, our results add another layer of complexity to the crosstalk between RNA and chromatin. In contrast to the emerging theme that RNA can serve as a scaffold to assemble, recruit, or guide chromatin-modifying complexes to their respective targets (Wang and Chang, 2011), we demonstrate that they may also function as "repellents." RNA-mediated eviction might be a possible mechanism that counteracts HP1 spreading along the chromatin fiber or the formation of ectopic heterochromatin. Importantly, neither coding potential nor stability is important for an RNA to function as a repellent, offering a possible molecular function for the many short-lived, low-abundant noncoding RNAs that are present in the eukaryotic cell.

EXPERIMENTAL PROCEDURES

Strains and Plasmids

Fission yeast strains and plasmids used in this study are described in Supplemental Information.

Western Blot and Polysome Profiling

Total proteins from exponentially growing cells were extracted using TCA and separated by SDS-PAGE. Antibodies for western blotting were used at the following concentrations: GFP (Roche; 1:3000), tubulin (Woods et al., 1989; 1:5000), Swi6 (Bioacademia; 1:10,000). Polysome profiling is described in Supplemental Information.

Chromatin Immunoprecipitation and Gene Expression Analysis

RNA isolation, cDNA synthesis, and quantitative RT-PCR was performed as described in Emmerth et al. (2010). Chromatin immunoprecipitation (ChIP) was performed as described in Bühler et al. (2006), using 2.5 μg of an antibody against dimethylated H3K9 (Kimura et al., 2008).

Electrophoretic Mobility Shift Assay (EMSA)

The desired amount of protein was diluted into 9 μl of 1 × electrophoretic mobility shift assay (EMSA) buffer (20 mM HEPES-KOH [pH 7.5], 100 mM KCl, 0.05% NP-40) and incubated for 10 min at RT. The substrate was added, incubated at 30°C for 30 min, and followed by gel electrophoresis (1.6% TB-agarose). Fluorescently labeled RNA was detected using a TyphoonTM 9400 Gel Scanner. RNA labeling is described in Supplemental Information.

Recombinant Protein Expression and Purification for NMR

Expression and purification was performed as described in Supplemental Information with the following modifications. Bacteria were grown in 6 l of M9 minimal medium containing ^{15}N-NH$_4$Cl as a nitrogen source. Induction was carried out using 0.5 mM IPTG. The lysate was incubated with 10 ml of glutathione-sepharose FF (GE). The protein was released from the glutathione-resin by TEV-cleavage o/n at 4°C using acTEV (Invitrogen). This was followed by Source15Q ion exchange chromatography (GE Healthcare). The purification was completed by size exclusion chromatography (Superdex 200; GE Healthcare) in 50 mM MES pH 6.5, 100 mM KCl, 5 mM DTT. The purified complex was concentrated to 100 μM by centrifugal filtration.

Solution NMR Spectroscopy and SPR

NMR experiments were performed on Bruker 800 MHz and 600 MHz spectrometers. The sequence-specific resonance assignments for the isolated HP1^{Swi6} CD (residues 75–139) were obtained from the two APSY-type experiments 4D APSY-HNCACB (15 projections) and 5D APSY-HNCOCACB (16 projections) (Gossert et al., 2011; Hiller et al., 2005, 2007) and subsequent automated backbone assignment by the algorithm MATCH (Volk et al., 2008). For SPR, samples were analyzed using a Biacore T-100 instrument (GE Healthcare). Further details are given in Supplemental Information.

DamID

DamID was carried out as previously published (Woolcock et al., 2011). Coordinates of heterochromatic regions are given in Supplemental Information.

ACCESSION NUMBERS

DamID data sets were deposited under accession number GSE36956 (NCBI Gene Expression Omnibus).

SUPPLEMENTAL INFORMATION

Supplemental Information includes six figures, Supplemental Experimental Procedures, Supplemental References, and five tables and can be found with this article online at doi:10.1016/j.molcel.2012.05.009.

ACKNOWLEDGMENTS

We are grateful to Yukiko Shimada, Nathalie Laschet, Sébastien Morin, Larisa Kapinos, and Alvar Gossert for technical assistance and discussions; Ben Hurschler and Helge Grosshans for help with polysome profiling; Tessi Iida for sharing protocols; Antoine Peters for peptides; the Nicolas Thomä lab, i.e., Andrea Scrima, Eric Fischer, and Mahamadou Faty, for technical advice and sharing awesome equipment; Laurent Gelman for assistance with FRAP analysis; and Heinz Gut and Hans-Rudolf Hotz for help with domain mappings and bioinformatics. Research in the lab of M.B. is supported by the Swiss National Science Foundation, the European Research Council, and the Gebert Rüf Stiftung. The Friedrich Miescher Institute for Biomedical Research is supported by the Novartis Research Foundation. Research in the lab of S.H. is supported by the Swiss National Science Foundation. R.A. acknowledges the Werner-Siemens Foundation.

Received: December 23, 2011
Revised: March 21, 2012
Accepted: May 3, 2012
Published online: June 7, 2012

REFERENCES

Akhtar, A., Zink, D., and Becker, P.B. (2000). Chromodomains are protein-RNA interaction modules. Nature *407*, 405–409.

Bannister, A.J., Zegerman, P., Partridge, J.F., Miska, E.A., Thomas, J.O., Allshire, R.C., and Kouzarides, T. (2001). Selective recognition of methylated lysine 9 on histone H3 by the HP1 chromo domain. Nature *410*, 120–124.

Bernard, P., Maure, J.F., Partridge, J.F., Genier, S., Javerzat, J.P., and Allshire, R.C. (2001). Requirement of heterochromatin for cohesion at centromeres. Science *294*, 2539–2542.

Bühler, M. (2009). RNA turnover and chromatin-dependent gene silencing. Chromosoma *118*, 141–151.

Bühler, M., Verdel, A., and Moazed, D. (2006). Tethering RITS to a nascent transcript initiates RNAi- and heterochromatin-dependent gene silencing. Cell *125*, 873–886.

Bühler, M., Haas, W., Gygi, S.P., and Moazed, D. (2007). RNAi-dependent and -independent RNA turnover mechanisms contribute to heterochromatic gene silencing. Cell *129*, 707–721.

Cheutin, T., McNairn, A.J., Jenuwein, T., Gilbert, D.M., Singh, P.B., and Misteli, T. (2003). Maintenance of stable heterochromatin domains by dynamic HP1 binding. Science *299*, 721–725.

Cheutin, T., Gorski, S.A., May, K.M., Singh, P.B., and Misteli, T. (2004). In vivo dynamics of Swi6 in yeast: evidence for a stochastic model of heterochromatin. Mol. Cell. Biol. *24*, 3157–3167.

Cowieson, N.P., Partridge, J.F., Allshire, R.C., and McLaughlin, P.J. (2000). Dimerisation of a chromo shadow domain and distinctions from the chromodomain as revealed by structural analysis. Curr. Biol. *10*, 517–525.

Ekwall, K., Javerzat, J.P., Lorentz, A., Schmidt, H., Cranston, G., and Allshire, R. (1995). The chromodomain protein Swi6: a key component at fission yeast centromeres. Science *269*, 1429–1431.

Emmerth, S., Schober, H., Gaidatzis, D., Roloff, T., Jacobeit, K., and Bühler, M. (2010). Nuclear retention of fission yeast dicer is a prerequisite for RNAi-mediated heterochromatin assembly. Dev. Cell *18*, 102–113.

Festenstein, R., Pagakis, S.N., Hiragami, K., Lyon, D., Verreault, A., Sekkali, B., and Kioussis, D. (2003). Modulation of heterochromatin protein 1 dynamics in primary Mammalian cells. Science *299*, 719–721.

Fischer, T., Cui, B., Dhakshnamoorthy, J., Zhou, M., Rubin, C., Zofall, M., Veenstra, T.D., and Grewal, S.I. (2009). Diverse roles of HP1 proteins in heterochromatin assembly and functions in fission yeast. Proc. Natl. Acad. Sci. USA *106*, 8998–9003.

Gossert, A.D., Hiller, S., and Fernández, C. (2011). Automated NMR resonance assignment of large proteins for protein-ligand interaction studies. J. Am. Chem. Soc. *133*, 210–213.

Grewal, S.I., and Jia, S. (2007). Heterochromatin revisited. Nat. Rev. Genet. *8*, 35–46.

Gullerova, M., and Proudfoot, N.J. (2008). Cohesin complex promotes transcriptional termination between convergent genes in S. pombe. Cell *132*, 983–995.

Hiller, S., Fiorito, F., Wüthrich, K., and Wider, G. (2005). Automated projection spectroscopy (APSY). Proc. Natl. Acad. Sci. USA *102*, 10876–10881.

Hiller, S., Wasmer, C., Wider, G., and Wüthrich, K. (2007). Sequence-specific resonance assignment of soluble nonglobular proteins by 7D APSY-NMR spectroscopy. J. Am. Chem. Soc. *129*, 10823–10828.

Jacobs, S.A., and Khorasanizadeh, S. (2002). Structure of HP1 chromodomain bound to a lysine 9-methylated histone H3 tail. Science *295*, 2080–2083.

Jacobs, S.A., Taverna, S.D., Zhang, Y., Briggs, S.D., Li, J., Eissenberg, J.C., Allis, C.D., and Khorasanizadeh, S. (2001). Specificity of the HP1 chromo domain for the methylated N-terminus of histone H3. EMBO J. *20*, 5232–5241.

James, T.C., and Elgin, S.C. (1986). Identification of a nonhistone chromosomal protein associated with heterochromatin in Drosophila melanogaster and its gene. Mol. Cell. Biol. *6*, 3862–3872.

Kaustov, L., Ouyang, H., Amaya, M., Lemak, A., Nady, N., Duan, S., Wasney, G.A., Li, Z., Vedadi, M., Schapira, M., et al. (2011). Recognition and specificity determinants of the human cbx chromodomains. J. Biol. Chem. *286*, 521–529.

Keller, C., Woolcock, K., Hess, D., and Bühler, M. (2010). Proteomic and functional analysis of the noncanonical poly(A) polymerase Cid14. RNA *16*, 1124–1129.

Kimura, H., Hayashi-Takanaka, Y., Goto, Y., Takizawa, N., and Nozaki, N. (2008). The organization of histone H3 modifications as revealed by a panel of specific monoclonal antibodies. Cell Struct. Funct. *33*, 61–73.

Klattenhoff, C., Xi, H., Li, C., Lee, S., Xu, J., Khurana, J.S., Zhang, F., Schultz, N., Koppetsch, B.S., Nowosielska, A., et al. (2009). The Drosophila HP1 homolog Rhino is required for transposon silencing and piRNA production by dual-strand clusters. Cell *138*, 1137–1149.

Lachner, M., O'Carroll, D., Rea, S., Mechtler, K., and Jenuwein, T. (2001). Methylation of histone H3 lysine 9 creates a binding site for HP1 proteins. Nature *410*, 116–120.

Maison, C., Bailly, D., Peters, A.H., Quivy, J.P., Roche, D., Taddei, A., Lachner, M., Jenuwein, T., and Almouzni, G. (2002). Higher-order structure in pericentric heterochromatin involves a distinct pattern of histone modification and an RNA component. Nat. Genet. *30*, 329–334.

Maison, C., Bailly, D., Roche, D., Montes de Oca, R., Probst, A.V., Vassias, I., Dingli, F., Lombard, B., Loew, D., Quivy, J.P., and Almouzni, G. (2011). SUMOylation promotes de novo targeting of HP1α to pericentric heterochromatin. Nat. Genet. *43*, 220–227.

Mandell, J.G., Bähler, J., Volpe, T.A., Martienssen, R.A., and Cech, T.R. (2005). Global expression changes resulting from loss of telomeric DNA in fission yeast. Genome Biol. *6*, R1.

Motamedi, M.R., Hong, E.J., Li, X., Gerber, S., Denison, C., Gygi, S., and Moazed, D. (2008). HP1 proteins form distinct complexes and mediate heterochromatic gene silencing by nonoverlapping mechanisms. Mol. Cell *32*, 778–790.

Muchardt, C., Guilleme, M., Seeler, J.S., Trouche, D., Dejean, A., and Yaniv, M. (2002). Coordinated methyl and RNA binding is required for heterochromatin localization of mammalian HP1alpha. EMBO Rep. *3*, 975–981.

Nakayama, J., Rice, J.C., Strahl, B.D., Allis, C.D., and Grewal, S.I. (2001). Role of histone H3 lysine 9 methylation in epigenetic control of heterochromatin assembly. Science *292*, 110–113.

Nielsen, P.R., Nietlispach, D., Mott, H.R., Callaghan, J., Bannister, A., Kouzarides, T., Murzin, A.G., Murzina, N.V., and Laue, E.D. (2002). Structure of the HP1 chromodomain bound to histone H3 methylated at lysine 9. Nature *416*, 103–107.

Nonaka, N., Kitajima, T., Yokobayashi, S., Xiao, G., Yamamoto, M., Grewal, S.I., and Watanabe, Y. (2002). Recruitment of cohesin to heterochromatic regions by Swi6/HP1 in fission yeast. Nat. Cell Biol. *4*, 89–93.

Schalch, T., Job, G., Noffsinger, V.J., Shanker, S., Kuscu, C., Joshua-Tor, L., and Partridge, J.F. (2009). High-affinity binding of Chp1 chromodomain to K9 methylated histone H3 is required to establish centromeric heterochromatin. Mol. Cell *34*, 36–46.

Smothers, J.F., and Henikoff, S. (2000). The HP1 chromo shadow domain binds a consensus peptide pentamer. Curr. Biol. *10*, 27–30.

Volk, J., Herrmann, T., and Wüthrich, K. (2008). Automated sequence-specific protein NMR assignment using the memetic algorithm MATCH. J. Biomol. NMR *41*, 127–138.

Wang, K.C., and Chang, H.Y. (2011). Molecular mechanisms of long noncoding RNAs. Mol. Cell *43*, 904–914.

Wang, G., Ma, A., Chow, C.M., Horsley, D., Brown, N.R., Cowell, I.G., and Singh, P.B. (2000). Conservation of heterochromatin protein 1 function. Mol. Cell. Biol. *20*, 6970–6983.

Wang, S.W., Stevenson, A.L., Kearsey, S.E., Watt, S., and Bähler, J. (2008). Global role for polyadenylation-assisted nuclear RNA degradation in posttranscriptional gene silencing. Mol. Cell. Biol. *28*, 656–665.

Win, T.Z., Draper, S., Read, R.L., Pearce, J., Norbury, C.J., and Wang, S.W. (2006). Requirement of fission yeast Cid14 in polyadenylation of rRNAs. Mol. Cell. Biol. *26*, 1710–1721.

Woods, A., Sherwin, T., Sasse, R., MacRae, T.H., Baines, A.J., and Gull, K. (1989). Definition of individual components within the cytoskeleton of Trypanosoma brucei by a library of monoclonal antibodies. J. Cell Sci. *93*, 491–500.

Woolcock, K.J., Gaidatzis, D., Punga, T., and Bühler, M. (2011). Dicer associates with chromatin to repress genome activity in Schizosaccharomyces pombe. Nat. Struct. Mol. Biol. *18*, 94–99.

Molecular Cell, Volume *47*

Supplemental Information

HP1^{Swi6} Mediates the Recognition and Destruction of Heterochromatic RNA Transcripts

Claudia Keller, Ricardo Adaixo, Rieka Stunnenberg, Katrina J. Woolcock, Sebastian Hiller, and Marc Bühler

Supplemental Data

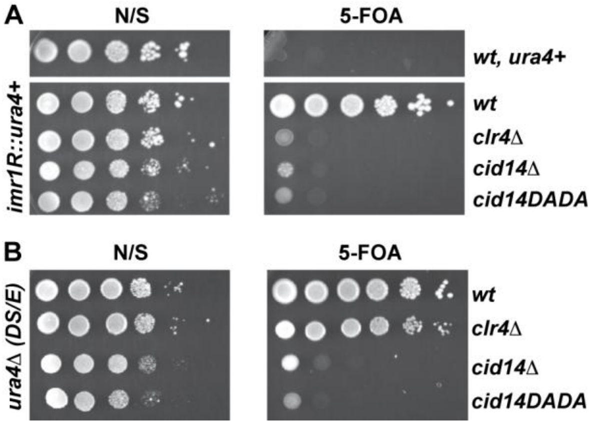

Figure S1, Related to Figure1. The Noncanonical PolyA-polymerase Cid14 Confers Resistance to 5-FOA
(A and B) Cells were spotted on PMG agar plates containing either 0 or 2 mg/L 5-FOA. The *ura4*+ gene encodes orotidine 5'-phosphate decarboxylase, which converts 5-FOA to toxic 5-fluorouracil. Therefore, cells can only grow on 5-FOA containing medium if the *ura4*+ gene is absent or silenced.
(A) Growth on 5-FOA containing medium indicates that the centromeric *ura4*+ reporter (*imr1R::ura4*+) is efficiently silenced by heterochromatin. Deletion of the gene encoding the histone H3 methyltransferase Clr4 (*clr4*Δ) disrupts heterochromatin and silencing of *imr1R::ura4*+ is lost. Similar to *clr4*Δ cells, cells lacking the *cid14*+ gene or cells expressing a catalytically inactive Cid14 (*cid14DADA*) cannot grow on 5-FOA.
(B) Cells lacking a functional *ura4*+ gene (*ura4DS/E*) grow on 5-FOA media in the absence of heterochromatin (*clr4*Δ), but not in the absence of Cid14 (*cid14*Δ) or if Cid14 has lost its polyadenylation activity (*cid14DADA).* Therefore, the inability of *imr1R::ura4*+ cells to grow on 5-FOA when expressing *cid14*$^{+}$ mutants (A) is unlikely to result from defective heterochromatin silencing. Rather, 5-FOA is converted into 5-fluorouracil or another toxic substance by a *ura4*+-independent, endogenous pathway that becomes activated in the absence of Cid14. Alternatively, 5-FOA itself is toxic, but is usually degraded by an enzyme that is only expressed in the presence of functional Cid14.

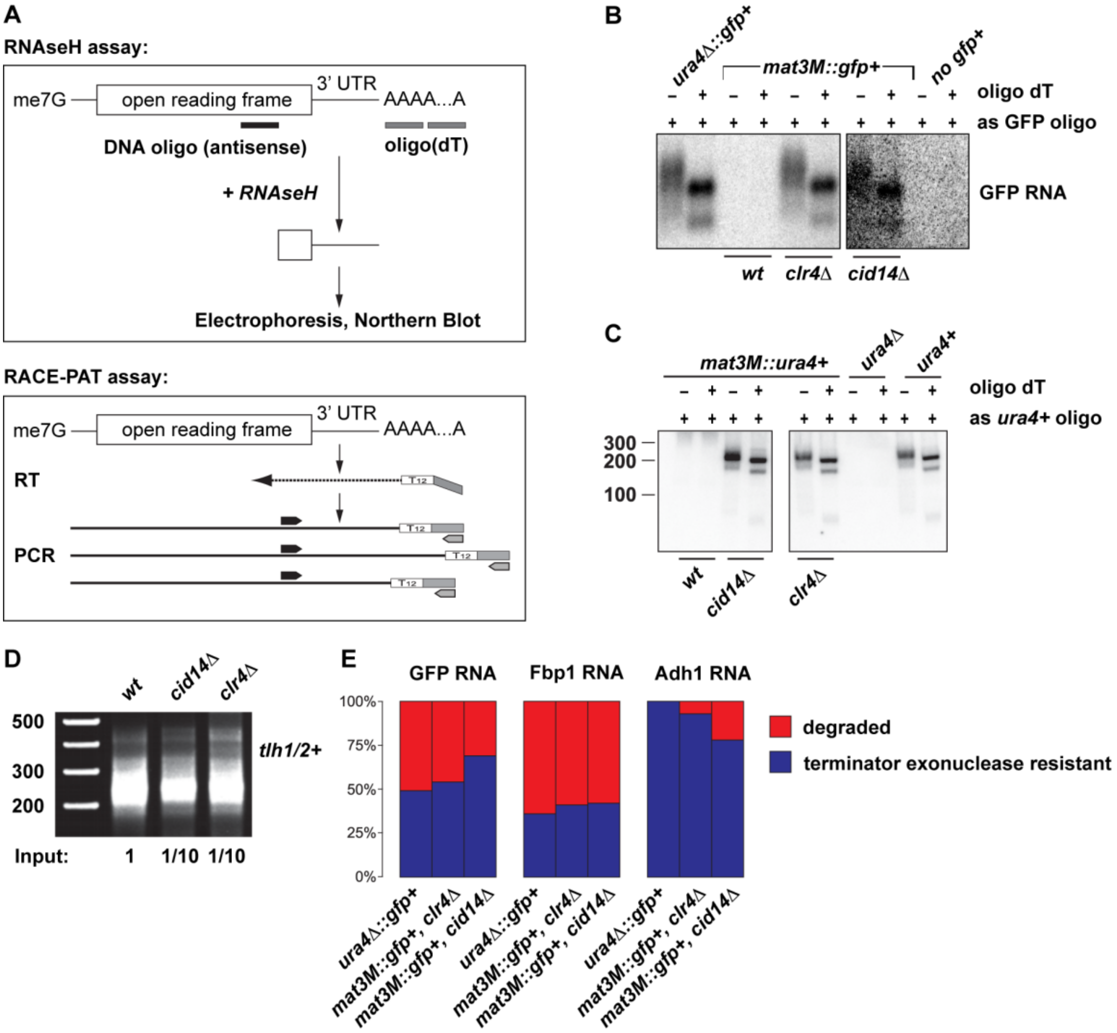

Figure S2, Related to Figure 2. Heterochromatic mRNAs Are Properly Processed
(A) Schematic diagram outlining RNAseH and RACE-PAT assays, which were used to assess the polyadenylation status of heterochromatic RNAs in different mutants.
(B) Evaluation of the polyadenylation status of heterochromatic *mat3M::gfp+* mRNAs by the RNaseH assay. Total RNA was separated on an agarose gel and transferred to a nylon membrane. GFP RNA was detected using specific ^{32}P-labelled DNA oligos. In the presence of oligodT (+oligodT), polyA tails are degraded by RNAseH. The appearance of two bands upon polyA tail removal is consistent with the presence of two major polyadenylation sites in the Tadh1 terminator present in this *gfp+* reporter. As expected, the distal site is used more frequently. The smear in the -oligodT lanes indicates the heterogenous polyA tail length of the GFP mRNA. Importantly, no major qualitative differences can be observed for euchromatic or heterochromatic GFP mRNAs in *wt, clr4Δ, or cid14Δ* cells.
(C) The polyadenylation status of heterochromatic *mat3M::ura4+* mRNAs was assessed as in B. Instead of agarose, polyacrylamide was used to separate RNAseH treated RNA.
(D) RACE-PAT assay to determine the polyadenylation state of *tlh1/2+* mRNAs. 1/10th of the RT reaction was used as input for the PCR in *cid14Δ* and *clr4Δ* cells.
(E) Total RNA was extracted from cells expressing either *gfp+* from a euchromatic (*ura4Δ::gfp+*) or heterochromatic (*mat3M::gfp+*) locus. The RNA was subsequently treated with terminator 5'-phosphate dependent exonuclease, which selectively degrades 5'-monophosphorylated RNA, while leaving 5'-me7G-capped RNA intact. The efficiency of the reaction was determined by comparing the amount of degraded 25S and 18S RNA (5'-monophosphorylated) versus 5S RNA (stable) on a Agilent Total RNA Nano Chip. The relative amount of a given RNA was quantified in untreated and exonuclease-treated samples by quantitative real-time RT-PCR. The terminator exonuclease resistant population reflects the relative amount of 5'-me7G-capped RNA.

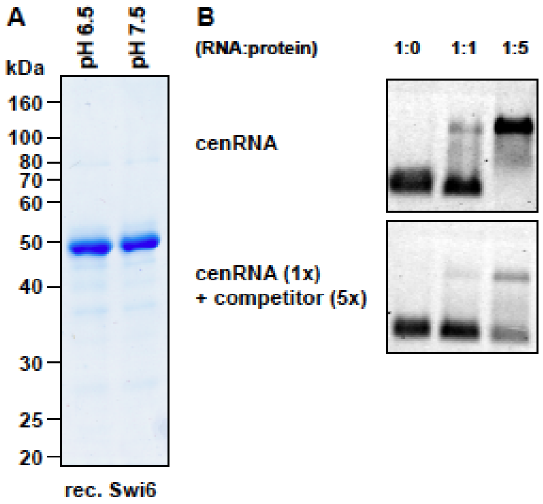
A
pH 6.5
pH 7.5
kDa
160
100
80
70
60
50
40
30
25
20
rec. Swi6
B
(RNA:protein)
1:0
1:1
1:5
cenRNA
cenRNA (1x)
+ competitor (5x)

Figure S3, Related to Figure 3. HP1^{Swi6} Is an RNA-Binding Protein
(A) SDS-PAGE of the recombinant HP1^{Swi6} proteins that were used for NMR and SPR (pH 6.5), or EMSA (pH 7.5).
(B) EMSA demonstrating that binding of HP1^{Swi6} to a fluorescently labelled RNA probe can be competed by an unlabelled RNA probe.

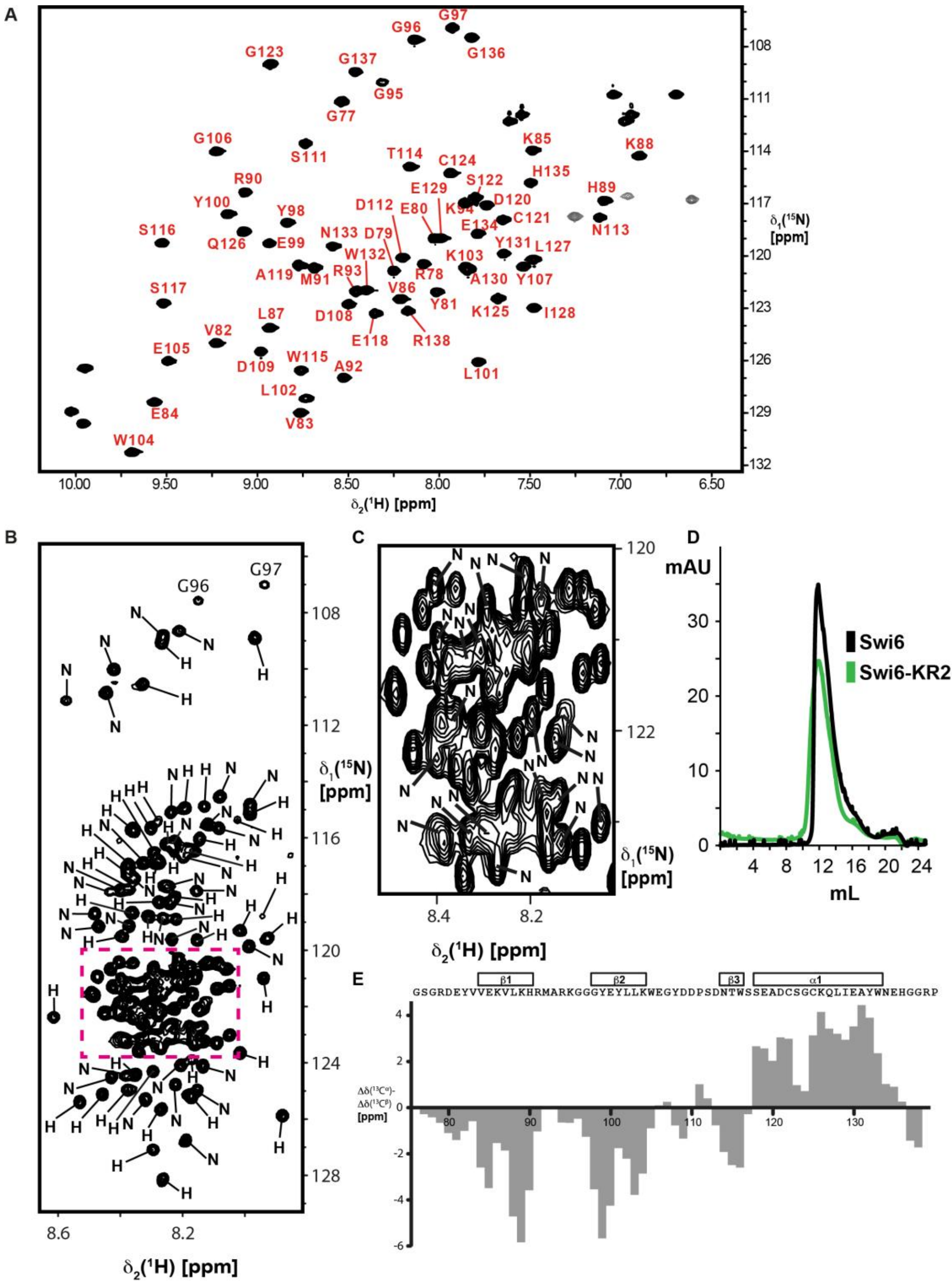

Figure S4, Related to Figure 4. Creation of a Mutant HP1^{Swi6} that Fails to Bind RNA but Keeps Its Other Molecular Properties

(A) 2D [^{15}N,^{1}H]-HSQC spectrum of the isolated CD (residues 75–139). Sequence-specific resonance assignments are indicated.

(B) Domain-specific assignments for the amide resonances arising from flexibly disordered segments of the polypeptide chain. On a 2D [^{15}N,^{1}H]-TROSY spectrum of full-length HP1^{Swi6}, the residues are identified which are part of the hinge region (“H”) and the N-terminal domain (“N”). The part in red dashed lines is shown enlarged in (C).

(C) Enlargement of the central part of the spectrum (B). Resonances from the N-terminal domain are indicated “N”. All other resonances belong to the hinge region.

(D) The chromatograms of HP1^{Swi6} and HP1^{Swi6}-KR25A that were loaded onto a Superdex200 size exclusion column show that the KR25A mutation does not affect the dimeric state of protein.

(E) Secondary chemical shifts for the $^{13}C^{\alpha}$ and $^{13}C^{\beta}$ chemical shifts of the isolated CD (residues 75–139) relative to random coil values. Above the amino acid sequence of the domain, the secondary structure elements inferred from these shifts, three β-strands and one α-helix, are indicated.

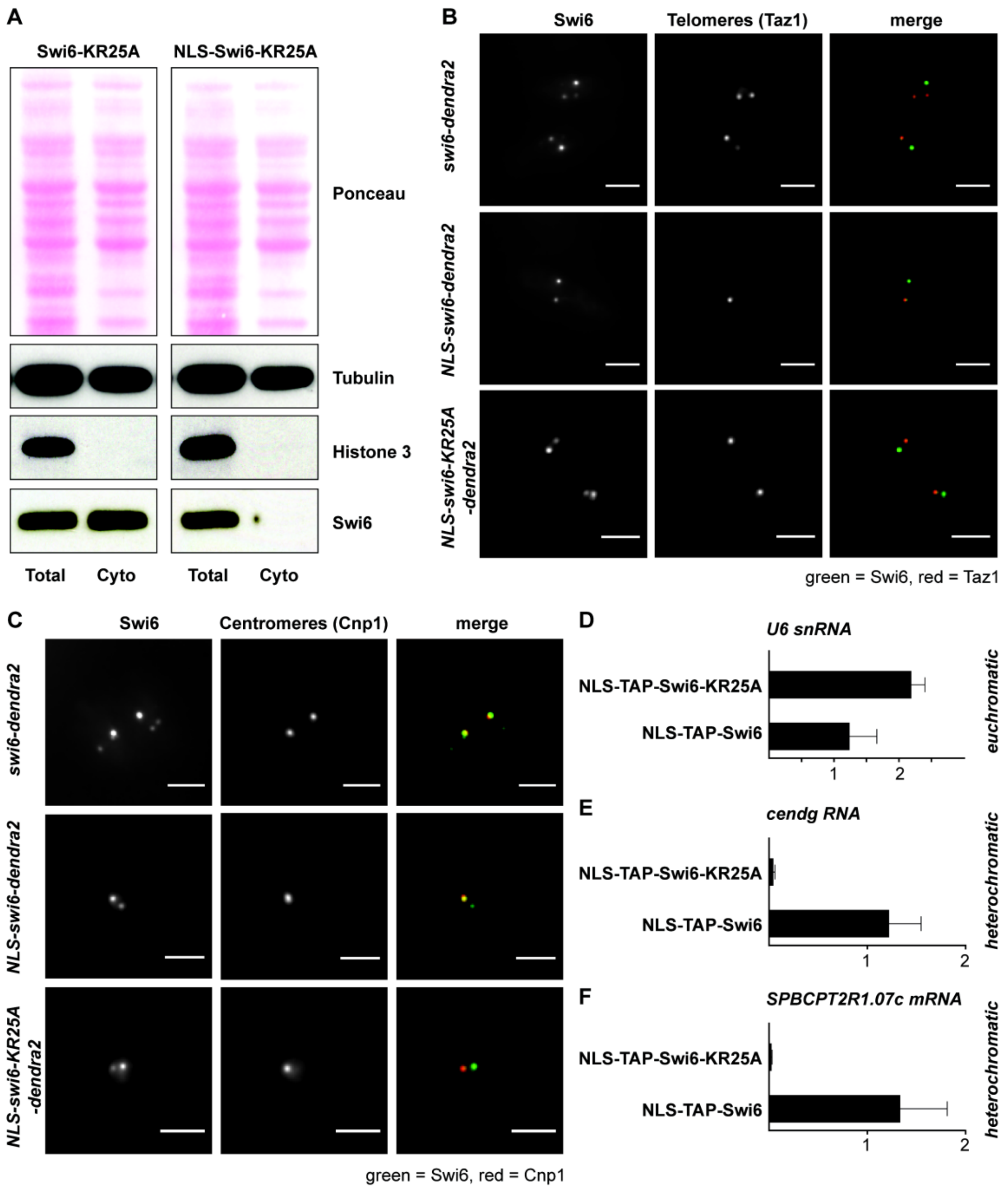

Figure S5, Related to Figure 5. RNA Binding through the Hinge Region of HP1^{Swi6} Is Required for Silencing but Not Maintenance of Heterochromatin

(A) Cells expressing HP1^{Swi6}-KR25A with or without an SV40 NLS were fractionated into total and cytoplasmic fractions. Proteins were separated by SDS-PAGE and detected by Western blot. Cytoplasmic Tubulin and nuclear Histone H3 serve as fractionation controls.

(B) Microscopy of living *S. pombe* cells co-expressing C-terminally Dendra2-tagged HP1^{Swi6} variants and C-terminally mCherry-tagged Taz1 driven from their endogenous promoters. Cells were grown in YES medium at 30°C. To restore nuclear localization of the HP1^{Swi6}-KR25A mutant (Figure S4), a SV40 NLS was added N-terminally.

(C) Microscopy of living *S. pombe* cells co-expressing C-terminally Dendra2-tagged HP1^{Swi6} variants and C-terminally mCherry-tagged Cnp1 driven from their endogenous promoters. Cells were grown in YES medium at 30°C. To restore nuclear localization of the HP1^{Swi6}-KR25A mutant (Figure S4), a SV40 NLS was added N-terminally.

(D-F) RIP experiment demonstrating that HP1^{Swi6} but not HP1^{Swi6}-KR25A interacts with heterochromatic RNA in vivo. TAP-tagged Swi6 was immunoprecipitated and the RNA was isolated followed by cDNA synthesis. The amount of co-immunoprecipitated RNA was quantified by quantitative real-time RT-PCR and normalized to act1+ mRNA. The amount of RNA co-immunoprecipitated with HP1^{Swi6}-KR25A is shown relative to the amount of RNA that co-immunoprecipitates with HP1^{Swi6}. As a control for unspecific background RNA binding in this pulldown experiment, U6 snRNA levels were measured (D).

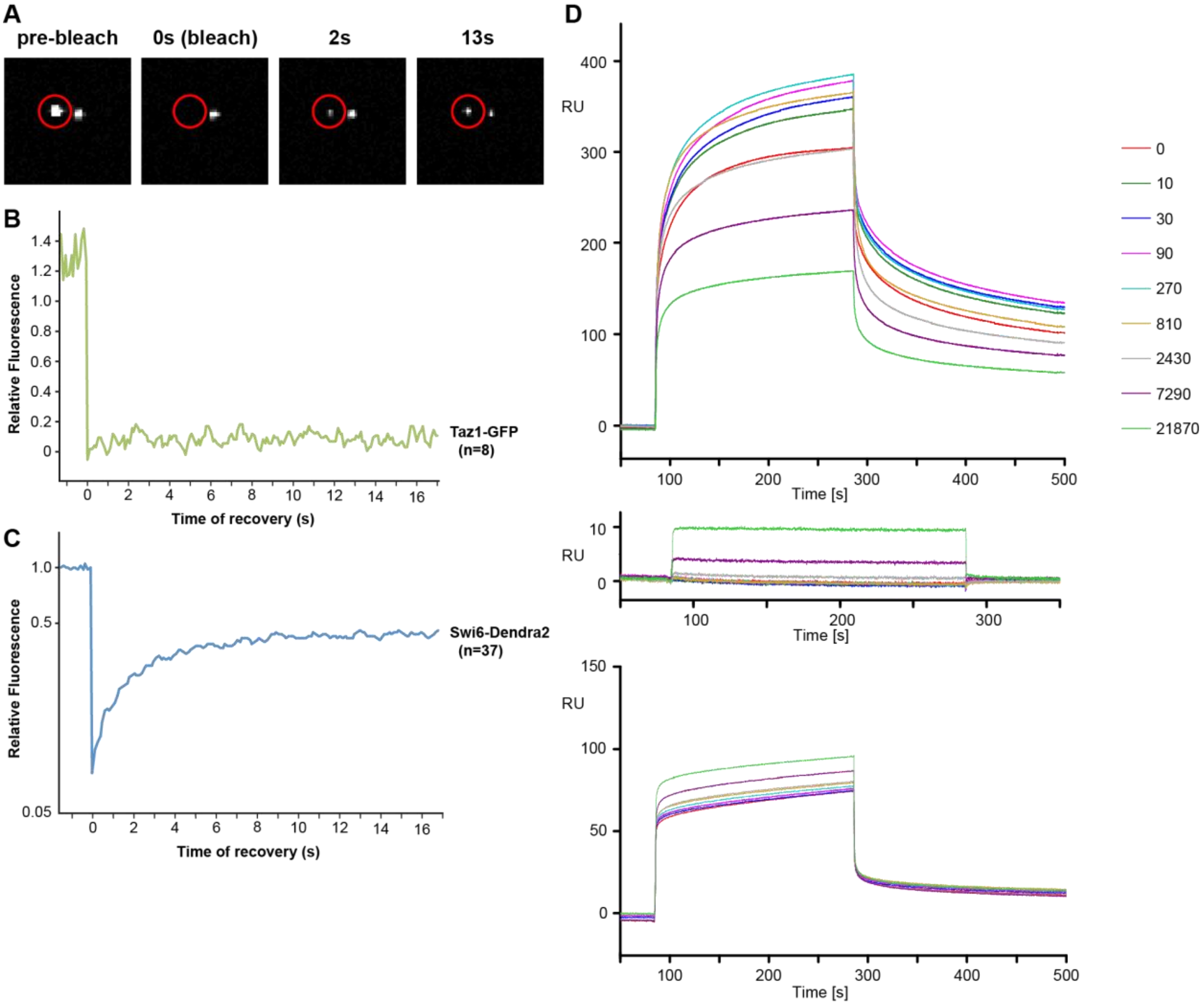

Figure S6, Related to Figure 6. Dynamic Exchange of HP1^{Swi6} from Chromatin on the Ensemble Level In Vivo and the Influence of RNA Binding on H3K9me Binding Properties

(A) Representative images of Fluorescence Recovery After Photobleaching (FRAP) performed with a cell expressing HP1^{Swi6}-Dendra2. Pictures were taken before, immediately after, 2 seconds after, and 13 seconds after photobleaching. Red circle indicates the heterochromatin focus subjected to photobleaching.

(B) FRAP analysis of cells expressing Taz1-GFP. Average relative fluorescence intensities of 8 bleached foci (cells) with a gliding time-average of 3 frames are shown.

(C) FRAP analysis of cells expressing HP1^{Swi6}-Dendra2. The fluorescence intensities were normalized to an unbleached focus in the same image. Average relative fluorescence intensities of 37 bleached foci (cells) with a gliding time-average of 3 frames are shown.

(D) SPR responses for competitive binding of H3K9me3 and RNA to HP1^{Swi6}. Top panel: A constant concentration of 1 μM HP1^{Swi6} with increasing concentrations of 20mer GFP-RNA was injected to an H3K9me3 surface for 200 s. The color code indicates the RNA concentrations in nM. Middle panel: same experiment without HP1^{Swi6}, showing that RNA does not bind to the peptide surface under the experimental conditions used. Bottom panel: same experiment as in the top panel but using 5 μM HP1^{Swi6} KR25A instead of 1 μM HP1^{Swi6} wild-type.

Supplemental Experimental Procedures

Strains and Plasmids

Fission yeast strains were grown at 30°C in YES. All strains were constructed following a PCR-based protocol (Bahler et al., 1998) or standard mating and sporulation. Point mutations were created using the QuickChange Lightning Site-directed mutagenesis kit (Stratagene).
The Swi6-KR25A hinge region fragment was created by gene synthesis (Integrated DNA Technologies, Inc.) and linked by a fusion PCR strategy to give rise to Swi6-KR25A. This was then cloned into a bacterial GST-expression vector. This plasmid was either transformed into bacteria for recombinant protein expression or used as a template for PCR-based gene targeting in *S. pombe*. All Swi6 mutant strains were created by transformation into a *swi6Δ::ura3*+ (c.a.) strain (ORF deletion) followed by counterselection on 5-FOA. The Dendra2 protein sequence (Chudakov et al., 2007) was reverse translated *in silico* using yeast codons. The template for PCR-based gene targeting was created by gene synthesis (Integrated DNA Technologies, Inc.) followed by cloning into a pFA6a-link-plasmid series vector (Sheff and Thorn, 2004),
All strains were confirmed by sequencing. Plasmid sequences and detailed maps are available upon request.

Silencing Assays

Serial 10-fold dilutions of the strains indicated were plated on PMGc (nonselective, NS) or on PMGc plates containing 2 mg/mL 5-Fluoroorotic Acid. For ade6-reporter strains, the cells were spotted on YES, YE low ade (22.5 mg/L adenine). For TBZ assays, the cells were spotted on YES plates containing 14 µg/mL Thiabendazole (TBZ) (Sigma T5535).

RNA Probe Labelling for EMSA

DNA templates were generated by PCR on *S. pombe* genomic DNA using primers containing T7 polymerase promoter sequences. In-vitro transcription was performed using the T7 RNA polymerase MEGA script kit (Ambion). For the synthesis of labeled probes, a mix of 0.6 mM UTP and 0.4 mM Fluorescin-UTP (Roche, 2.5 mM) was used. The reaction was carried out for 1h at 37°C followed by a 15 min incubation with 1 µL Turbo DNaseI (37°C). The reaction was phenol-chloroform extracted and purified over G50 spin columns (Amersham) to remove unincorporated nucleotides.

Recombinant Protein Expression and Purification

Recombinant proteins were expressed as N-terminal GST-fusion proteins in Rosetta (BL21) bacteria. A 1L culture was grown in LB + antibiotics until OD_{600}=0.4. The cells were grown for another 2h at 20°C (OD_{600} around 0.6), followed by induction of expression of the GST-fusion proteins with 0.5 mM IPTG. The culture was grown o/n at 20°C. The cells were pelleted, washed and frozen in N_2(l). For protein purification, the cell pellet was resuspended in 5 pellet volumes of lysis buffer (25 mM Tris-HCl (pH 7.5), 500 mM NaCl, 1% Triton-X100 + Protease Inhibitors) and sonicated 6 x 30 sec at 50%. The lysate was spun at 16’000 rpm, 4°C for 30 minutes and cleared by filtration (0.45 µm). The extract was incubated with 1 mL of glutathione-agarose (Sigma) and rotated for 2h at 4°C. After 3 washes (25 mM Tris-HCl (pH 7.5), 500 mM NaCl, 0.1% Triton-X100) the protein was eluted using 50 mM reduced glutathione. The eluate was dialysed o/n into 50 mM HEPES (pH 7.5), 200 mM KCl, 10% Glycerol. This recombinant protein was used for EMSA.

Polysome Profiling

A detailed protocol for polysome profiling in *S. pombe* is available upon request. Briefly, 50 mL of cells were grown to an OD of 0.5-0.6. Cycloheximide was added to a final concentration of 100 µg/µL and the culture was incubated for another 10 min at 30°C. The cells were pelleted and flash frozen in N_2(l). Lysis was performed by bead-beating in 200 µL of lysis buffer and 500 µL glass beads followed by removing insoluble material by centrifugation. 140 OD_{260} were loaded onto a 15-60% sucrose gradient and separated by ultracentrifugation for 2h at 39’000 rpm (Beckman SW40 rotor). The gradient was unloaded from the bottom with 70% sucrose. Fractions were collected while monitoring the absorbance at 254 nm. RNA was isolated from the fractions using phenol-chloroform extraction followed by isopropanol precipitation. RNA recovery was determined by UV absorbance. cDNA was synthesized from 500 ng RNA using the Affinity Script Multiple Temperature cDNA synthesis kit (Stratagene) and subsequently quantified by qRT-PCR. The data was analyzed as described in (Ding and Grosshans, 2009), calculating the RNA enrichment relative to the total amount of RNA in a given fraction.

mRNA Polyadenylation State Assays

The polyadenylation state of mRNAs was assayed by RACE-PAT or oligo(dT)/RNase H-Northern analysis as described in (Salles et al., 1999). To increase resolution in the RNAseH-Northern assay, an oligo (mb1314) that anneals 100 bp before the STOP codon of the GFP ORF was included in the RNaseH cleavage reaction. RNA was isolated from 50 mL of exponentially growing cells using the hot phenol method. 50 µg of total RNA was incubated with 2 uL mb1314 (100 µM) and with or without oligo dT (10 µL of 100 ng/µL) in a total volume of 68 µL. This was incubated at 65°C for 5 min and slowly cooled down to RT. 8 µL of 10 x buffer, 1 µL RNasIn Plus (Promega) and 1.5 µL RNaseH (New England Biolabs) were added followed by a 30 min incubation at 37°C. The RNA was phenol-chloform extracted followed by ethanol precipitation. The pellet was resuspended in 20 µL of 100% formamide, denatured and separated on a 2.4% MOPS-agarose gel. After capillary transfer in 20 x SSC to a positively charged nylon membrane and UV crosslinking, PNK-labelled oligos (mb1315/mb1316) were hybridized o/n at 35°C. The membrane was washed 3 x 15 min in 0.5 x SSC, 0.1% Triton-X100 at 35°C. Signal was detected using a Phosphorscreen.

5'-Dependent Terminator Exonuclease Assay

Total RNA was isolated using the hot phenol method. The RNA was subjected to DNase digestion using the Absolutely RNA Miniprep Kit (Stratagene). 1 µg RNA was treated with 1 µL of terminator 5'phosphate-dependent exonuclease (Epicentre) for 2h at 30°C. Control reactions were incubated for 2h at 30°C in the absence of the enzyme. The reaction was terminated by phenol-chloroform extraction followed by isopropanol precipitation.1/10th of the reaction was analyzed on a Agilent Bioanalyzer 2100 (Eukaryote Total RNA Nano Chip). 500 ng of RNA was used for cDNA synthesis and quantification by qRT-PCR.

Live Cell Imaging and FRAP Analysis

Imaging was performed on an Olympus IX81 microscope equipped with a Yokogawa CSU-X1 spinning disk, a UPlanFLN 40x/1.3 objective, a CascadeII camera (Photometrics, AZ), a 491nm laser line (Cobolt, Sweden), a Semrock Di01-T488/568 dichroic and a Semrock FF01-525/40-25 emission filter. All devices were piloted with the software Metamorph (Molecular Devices Inc, CA). For FRAP experiments, a UGA-40 module (Rapp-Optoelectronics, Hamburg) equipped with a 473nm laser line and a chroma Z405/473rpc-xt dichroic was installed on the setup. In Metamorph, image acquisition was done using the live replay menu with an exposure time of 100ms and binning 2 for the camera. The bleaching region was a diffraction-limited spot, bleach time was 20ms. The acquired images were analyzed using the open source Fiji software (Walter et al., 2010). The fluorescence intensities were normalized to an unbleached focus in the same image and pre-bleach intensities were averaged and set to 1. Growth conditions for live cell microscopy were described in (Emmerth et al., 2010). Images were acquired at room temperature.

Solution NMR Spectroscopy

The sequence-specific resonance assignments for the isolated HP1^{Swi6} CD (residues 75–140) were obtained using a 750 µM sample of [U-^{13}C,^{15}N]-labeled CD sample in 50 mM MES-KOH pH 6.5 buffer with 100 mM KCl, 5 mM DTT and 5%/95% D_2O/H_2O. The assignments were obtained from the two triple-resonance APSY-type experiments 4D APSY-HNCACB (15 projections) and 5D APSY-HNCOCACB (16 projections) (Gossert et al., 2010; Hiller et al., 2005; Hiller et al., 2007) and subsequent automated backbone assignment by the algorithm MATCH (Volk et al., 2008). These experiments were recorded at 25°C on a Bruker 600 MHz spectrometer equipped with a room-temperature triple-resonance probe in a total experiment time of 63 h. The assignments of the CD were transferred to full-length HP1^{Swi6} by a comparison of the [^{15}N,^{1}H]-correlation patterns, which were found to be highly similar (Figs. 4 & S4). The domain-specific resonance assignments of the NTD, the hinge region and the CSD were obtained by identifying the individual substracta from HP1^{Swi6} subconstructs: isolated CD, CD+hinge, CD+hinge+CSD, NTD+CD+hinge.

The NMR titration experiments were performed at 25°C on a Bruker 800 MHz spectrometer equipped with a cryogenic triple-resonance probe. 2D [^{15}N,^{1}H]-TROSY experiments

(Pervushin et al., 1997) of 50–120 μM samples of [*U*-^{15}N]-Swi6 in 50 mM MES-KOH pH 6.5 buffer with 100 mM KCl, 5 mM DTT and 5%/95% D_2O/H_2O were recorded. Typically, 1024 and 90 complex points were recorded in the direct and indirect dimension, respectively in total experiment times of 8–12 h for each spectrum. H3K9me3 peptide from a 1 mM stock solution or 20mer GFP-RNA from a 3 mM stock solution of the same buffer were added.

Surface Plasmon Resonance (SPR)

Samples were analyzed using a Biacore T-100 instrument (GE Healthcare). H3K9me3 peptide was covalently bound to a CM5 chip by amine coupling achieving a final density of 1985 RU. All measurements were recorded as subtracted sensorgrams relative to a flow channel with blank amine immobilisation. Sensorgrams were recorded at 25 °C and flow rate of 50μl min^{-1} using 25 mM NaP_i pH 7.0, 150 mM KCl, 5mM DTT, 0.1% P20, 62.5 μg ml^{-1} BSA and 5% Glycerol as running buffer. All samples were diluted in running buffer prior to injection. Each sample was injected for 200 sec and dissociation was recorded for 300 sec. A regeneration step was performed at the end of each cycle by injecting 5 mM NaOH for 30 sec followed by a stabilization period of 50 sec. For the determination of binding constants, increasing concentrations of HP1^{Swi6} or HP1^{Swi6}-KR25A were injected. For the competition assay, samples of 1 μM Swi6 with increasing amounts of RNA were injected.

Dam-ID

DamID was carried out as previously published (Woolcock et al., 2011). Average enrichment values were calculated for all the oligos overlapping the major heterochromatic regions: mating type locus (chromosome 2, 2114000-2137000), telomeres (chromosome 1, 1-20000 and 5571500-5579133; chromosome 2, 4516200-4539804), and centromeres (chromosome 1, 3753687-3789421, chromosome 2, 1602264-1644747, chromosome 3, 1070904-1137003).

RNA Immunoprecipitation (RIP)

RIP was performed essentially as described in (Gilbert and Svejstrup, 2006). IgG-dynabeads (expoxy-coupled) that have been pre-blocked using E.coli tRNA were used for the immunoprecipitation of the TAP-tagged proteins. An additional DNaseI-digestion step was included before the cDNA synthesis with random primers.

Supplemental References

Bahler, J., Wu, J.Q., Longtine, M.S., Shah, N.G., McKenzie, A., III, Steever, A.B., Wach, A., Philippsen, P., and Pringle, J.R. (1998). Heterologous modules for efficient and versatile PCR-based gene targeting in Schizosaccharomyces pombe. Yeast *14*, 943-951.

Chudakov, D.M., Lukyanov, S., and Lukyanov, K.A. (2007). Tracking intracellular protein movements using photoswitchable fluorescent proteins PS-CFP2 and Dendra2. Nat. Protocols *2*, 2024-2032.

Ding, X.C., and Grosshans, H. (2009). Repression of C. elegans microRNA targets at the initiation level of translation requires GW182 proteins. EMBO J. *28*, 213-222.

Emmerth, S., Schober, H., Gaidatzis, D., Roloff, T., Jacobeit, K., and Bühler, M. (2010). Nuclear retention of fission yeast dicer is a prerequisite for RNAi-mediated heterochromatin assembly. Dev. Cell *18*, 102-113.

Gilbert, C., and Svejstrup, J.Q. (2006). RNA immunoprecipitation for determining RNA-protein associations in vivo. Curr. Protoc. Mol. Biol. *Chapter 27*, Unit 27 24.

Gossert, A.D., Hiller, S., and Fernández, C. (2010). Automated NMR resonance assignment of large proteins for protein-ligand interaction studies. J. Am. Chem. Soc. *133*, 210-213.

Hiller, S., Fiorito, F., Wüthrich, K., and Wider, G. (2005). Automated projection spectroscopy (APSY). Proc. Natl. Acad. Sci. USA *102*, 10876-10881.

Hiller, S., Wasmer, C., Wider, G., and Wüthrich, K. (2007). Sequence-specific resonance assignment of soluble nonglobular proteins by 7D APSY-NMR spectroscopy. J. Am. Chem. Soc. *129*, 10823-10828.

Pervushin, K., Riek, R., Wider, G., and Wüthrich, K. (1997). Attenuated T_2 relaxation by mutual cancellation of dipole-dipole coupling and chemical shift anisotropy indicates an avenue to NMR structures of very large biological macromolecules in solution. Proc. Natl. Acad. Sci. USA *94*, 12366-12371.

Salles, F.J., Richards, W.G., and Strickland, S. (1999). Assaying the polyadenylation state of mRNAs. Methods *17*, 38-45.

Sheff, M.A., and Thorn, K.S. (2004). Optimized cassettes for fluorescent protein tagging in Saccharomyces cerevisiae. Yeast *21*, 661-670.

Volk, J., Herrmann, T., and Wüthrich, K. (2008). Automated sequence-specific protein NMR assignment using the memetic algorithm MATCH. J. Biomol. NMR *41*, 127-138.

Walter, T., Shattuck, D.W., Baldock, R., Bastin, M.E., Carpenter, A.E., Duce, S., Ellenberg, J., Fraser, A., Hamilton, N., Pieper, S., *et al.* (2010). Visualization of image data from cells to organisms. Nat. Methods *7*, S26-41.

Woolcock, K.J., Gaidatzis, D., Punga, T., and Bühler, M. (2011). Dicer associates with chromatin to repress genome activity in Schizosaccharomyces pombe. Nat. Struct. Mol. Biol. *18*, 94-99.

Supplemental Tables

Table S1. Plasmids

pMB247	pFA6a-Cid14DADA-TAP-hphMX6	Template for PCR based gene targeting (Creation of Cid14DADA::TAP allele)
pMB680	pGEX	empty n-term GST fusion vector with TEV and Thrombin cleavage site
pMB714	pGEX-Swi6	Swi6 purification (N-term GST, TEV and Thrombin cleavage site)
pMB715	pGEX-Swi6-KR25A	Swi6-KR25A purification (N-term GST, TEV and Thrombin cleavage site)
pMB776	pGEX-Swi6-CD	Swi6-Chromodomain purification (N-term GST, TEV and Thrombin cleavage site)
pMB768	pFA6a-link-Dendra2-hphMX	Template for PCR based gene targeting (C-term Dendra2 tagging)

Table S2. Primers for Real-Time PCR

		Forward Primer	***Reverse Primer***
cendg	mb549/mb550	AAGGAATGTGCCTCGTCAAATT	TGCTTCACGGTATTTTTTGAAATC
cendh	mb551/mb552	GTATTTGGATTCCATCGGTACTATGG	ACTACATCGACACAGAAAAGAAAACAA
gfp+	mb820/mb821	CGAAAGATCCCAACGAAAAGAG	TCCCAGCAGCTGTTACAAACTC
ura4+	mb553/554	TACAAAATTGCTTCTTGGGCTCAT	AGACCACGTCCCAAAGGTAAAC
tlh1/2+	mb682/683	CGTGTGCAAGCCGTCAAA	GCTCGAGTTGTGCTGAAATGTC
SPBCPT2R1.07c	mb3006/mb3007	TGGTGTTGCTCCAAAGTGTAGTGGA	GACAGTTGCCTCCGGTAAATGGATTC
Control Genes			
U6 snRNA	mb1281/mb1282	GATCTTCGGATCACTTTGGTCAA	TGTCGCAGTGTCATCCTTGTG
act1+	mb555/mb556	TCCTCATGCTATCATGCGTCTT	CCACGCTCCATGAGAATCTTC
fbp1+	mb557/mb558	CTGGCCAGCTTATTCAACTTCAT	GATTTCGTCGAGATCTTTTTTCATG

Table S3. Primers for RNaseH Assays

		Target	***Purpose***
mb1315	TTACAAACTCAAGAAGGACCATGTGGTCTCTC	GFP	probe
mb1316	TTTGTATAGTTCATCCATGCCATGTGTAATCCCA	GFP	probe
mb1314	GATTGTGTGGACAGGTAATGG	GFP	cleavage

Table S4. RNA Probes

		Length	***Purpose***
20-GFP-RNA	AUGGGUAAAGGAGAAGAACU	20nt	NMR
150-GFP-RNA	ggAGUAAAGGAGAAGAACUUUUCACUGGAGUUGUCCCAAUUCUUGUUGAAUUAGA UGGUGAUGUUAAUGGGCACAAAUUUUCUGUCAGUGGAGAGGGUGAAGGUGAUGC AACAUACGGAAAACUUACCCUUAAAUUUAUUUGCACUACUG	150nt	EMSA
700-GFP-RNA	ggAGUAAAGGAGAAGAACUUUUCACUGGAGUUGUCCCAAUUCUUGUUGAAUUAGA UGGUGAUGUUAAUGGGCACAAAUUUUCUGUCAGUGGAGAGGGUGAAGGUGAUGC AACAUACGGAAAACUUACCCUUAAAUUUAUUUGCACUACUGGAAAACUACCUGUU CCAUGGCCAACACUUGUCACUACUUUCACUUAUGGUGUUCAAUGCUUUUCAAGAU ACCCAGAUCAUAUGAAACGGCAUGACUUUUUCAAGAGUGCCAUGCCCGAAGGUUA UGUACAGGAAAGAACUAUAUUUUUCAAAGAUGACGGGAACUACAAGACACGUGCU GAAGUCAAGUUUGAAGGUGAUACCCUUGUUAAUAGAAUCGAGUUAAAAGGUAUUG AUUUUAAAGAAGAUGGAAACAUUCUUGGACACAAAUUGGAAUACAACUAUAACUC ACACAAUGUAUACAUCAUGGCAGACAAACAAAAGAAUGGAAUCAAAGUUAACUUCA AAAUUAGACACAACAUUGAAGAUGGAAGCGUUCAACUAGCAGACCAUUAUCAACA	711nt	EMSA

	AAAUACUCCAAUUGGCGAUGGCCCUGUCCUUUUACCAGACAACCAUUACCUGUCCACACAAUCUGCCCUUUCGAAAGAUCCCAACGAAAAGAGAGACCACAUGGUCCUUCUUGAGUUUGUAACAGCUGCUGGGAUUACACAUGGCAUGGAUGAACUAUACAAA		
100-cen-RNA	ggCGUGCGAUCGGGCCGCGACUGGCCAUUUUCAAGGAUAUAUCGAAUCAAAUUUAGGUAUUGCUCUUCUUCUGUAUUUCUAUAUUCGGAGGAAGUAAAU	99nt	EMSA

Table S5. Strain Table

		Figure	Genotype	Source	Comment
spb28	wt	1	h+ leu1-32 ura4D18 oriI ade6-M216 imr1R(Nco1)::gfp+::natMX	*	gfp+ driven by ura4+ promoter
spb38	clr4Δ	1	h+ leu1-32 ura4D18 oriI ade6-M216 imr1R(Nco1)::gfp+::natMX clr4Δ::kanMX	*	gfp+ driven by ura4+ promoter
spb36	dcr1Δ	1	h+ leu1-32 ura4D18 oriI ade6-M216 imr1R(Nco1)::gfp+::natMX dcr1Δ::kanMX	*	gfp+ driven by ura4+ promoter
spb313	cid14Δ	1	h+ leu1-32 ura4D18 oriI ade6-M216 imr1R(Nco1)::gfp+::natMX cid14Δ::kanMX	*	gfp+ driven by ura4+ promoter
spb342	wt	1	h90 mat3M(EcoRV)::gfp+::natMX ura4-DS/E leu1-32 ade6-M210	*	gfp+ driven by ura4+ promoter
spb360	clr4Δ	1	h90 mat3M(EcoRV)::gfp+::natMX ura4-DS/E leu1-32 ade6-M210 clr4Δ::kanMX	*	gfp+ driven by ura4+ promoter
spb361	dcr1Δ	1	h90 mat3M(EcoRV)::gfp+::natMX ura4-DS/E leu1-32 ade6-M210 dcr1Δ::kanMX	*	gfp+ driven by ura4+ promoter
spb374	cid14Δ	1	h90 mat3M(EcoRV)::gfp+::natMX ura4-DS/E leu1-32 ade6-M210 cid14Δ::kanMX	*	gfp+ driven by ura4+ promoter
spb342	wt	2	h90 mat3M(EcoRV)::gfp+::natMX ura4-DS/E leu1-32 ade6-M210	*	gfp+ driven by ura4+ promoter
spb374	cid14Δ	2	h90 mat3M(EcoRV)::gfp+::natMX ura4-DS/E leu1-32 ade6-M210 cid14Δ::kanMX	*	gfp+ driven by ura4+ promoter
spb360	clr4Δ	2	h90 mat3M(EcoRV)::gfp+::natMX ura4-DS/E leu1-32 ade6-M210 clr4Δ::kanMX	*	gfp+ driven by ura4+ promoter
spb535	cid14Δ clr4Δ	2	h90 mat3M(EcoRV)::gfp+::natMX ura4- leu1-32 ade6- clr4D::hph cid14Δ::kanMX	*	gfp+ is driven by ura4+ promoter; ura4D18 or DS/E; ade6-M210 or 216
spb721	swi6Δ	2	h90 mat3M(EcoRV)::gfp+::natMX ura4-DS/E leu1-32 ade6-M210 swi6Δ::ura3+	*	gfp+ driven by ura4+ promoter
spb723	cid14Δ swi6Δ	2	h90 mat3M(EcoRV)::gfp+::natMX ura4-DS/E leu1-32 ade6-M210 swi6Δ::ura3+ cid14Δ::kan	*	gfp+ driven by ura4+ promoter
spb1071	swi6-Dendra2	4	h90 mat3M(EcoRV)::gfp+::natMX ura4-DS/E leu1-32 ade6-M210 swi6-Dendra2::hphMX	*	gfp+ driven by ura4+ promoter
spb1240	nls-swi6-Dendra2	4	h90 mat3M(EcoRV)::gfp+::natMX ura4-DS/E leu1-32 ade6-M210 nls-swi6-Dendra2::hphMX	*	gfp+ driven by ura4+ promoter
spb1241	nls-swi6-KR25A-Dendra2	4	h90 mat3M(EcoRV)::gfp+::natMX ura4-DS/E leu1-32 ade6-M210 nls-swi6-KR25A-Dendra2::hphMX	*	gfp+ driven by ura4+ promoter
spb342	wt	4	h90 mat3M(EcoRV)::gfp+::natMX ura4-DS/E leu1-32 ade6-M210	*	gfp+ driven by ura4+ promoter
spb360	clr4Δ	4	h90 mat3M(EcoRV)::gfp+::natMX ura4-DS/E leu1-32 ade6-M210 clr4Δ::kanMX	*	gfp+ driven by ura4+ promoter
spb939	swi6Δ	4	h90 mat3M(EcoRV)::gfp+::natMX ura4-DS/E leu1-32 ade6-M210 swi6Δ::ura3+ (ORF deletion only)	*	gfp+ driven by ura4+ promoter
spb1226	nls-swi6	4	h90 mat3M(EcoRV)::gfp+::natMX ura4-DS/E leu1-32 ade6-M210 nls-swi6	*	gfp+ driven by ura4+ promoter
spb1227	nls-swi6-KR25A	4	h90 mat3M(EcoRV)::gfp+::natMX ura4-DS/E leu1-32 ade6-M210 nls-swi6-KR25A	*	gfp+ driven by ura4+ promoter

spb435	dam	6	h+ leu1-32 ade6-M216 ura4Δ::nmt1(81x)-dam-myc-kan		
spb436	dam-cid14	6	h+ leu1-32 ade6-M216 ura4Δ::nmt1(81x)-dam-myc-cid14-kan		
spb1386	dam swi6Δ	6	h+ leu1-32 ade6-M216 ura4Δ::nmt1(81x)-dam-myc-kan swi6Δ::ura3+ (ORF deletion only)		
spb1387	dam-cid14 swi6Δ	6	h+ leu1-32 ade6-M216 ura4Δ::nmt1(81x)-dam-myc-cid14-kan swi6Δ::ura3+ (ORF deletion only)		

spb65	wt, ura4+	S1	972h-	1	
spb221	wt	S1	h- imr1R(Nco1)::gfp+::natMX	*	gfp+ driven by ura4+ promoter
spb295	clr4Δ	S1	h- imr1R(Nco1)::gfp+::natMX clr4Δ::kanMX	*	gfp+ driven by ura4+ promoter
spb294	cid14Δ	S1	h- imr1R(Nco1)::gfp+::natMX cid14Δ::kanMX	*	gfp+ driven by ura4+ promoter
spb373	cid14DADA	S1	h- imr1R(Nco1)::gfp+::natMX cid14DADA-TAP::hphMX	*	gfp+ driven by ura4+ promoter
spb342	wt	S1	h90 mat3M(EcoRV)::gfp+::natMX ura4-DS/E leu1-32 ade6-M210	*	gfp+ driven by ura4+ promoter
spb360	clr4Δ	S1	h90 mat3M(EcoRV)::gfp+::natMX ura4-DS/E leu1-32 ade6-M210 clr4Δ::kanMX	*	gfp+ driven by ura4+ promoter
spb374	cid14Δ	S1	h90 mat3M(EcoRV)::gfp+::natMX ura4-DS/E leu1-32 ade6-M210 cid14Δ::kanMX	*	gfp+ driven by ura4+ promoter
spb739	cid14DADA	S1	h90 mat3M(EcoRV)::gfp+::natMX ura4-DS/E leu1-32 ade6-M210 cid14DADA-TAP::hphMX	*	gfp+ driven by ura4+ promoter

spb29	wt, ura4+	S2	h+ otr1R(SphI)::ura4+ leu1-32 ade6-M210 ura4Δ::gfp::natMX	*	end. ura+ ORF replaced with gfp+
spb342	wt	S2	h90 mat3M(EcoRV)::gfp+::natMX ura4-DS/E leu1-32 ade6-M210	*	gfp+ driven by ura4+ promoter
spb360	clr4Δ	S2	h90 mat3M(EcoRV)::gfp+::natMX ura4-DS/E leu1-32 ade6-M210 clr4Δ::kanMX	*	gfp+ driven by ura4+ promoter
spb374	cid14Δ	S2	h90 mat3M(EcoRV)::gfp+::natMX ura4-DS/E leu1-32 ade6-M210 cid14Δ::kanMX	*	gfp+ driven by ura4+ promoter
spb76	no gfp	S2	h90 mat3M(EcoRV)::ura4+ ura4-DS/E leu1-32 ade6-M210	2	

spb342	wt	S5	h90 mat3M(EcoRV)::gfp+::natMX ura4-DS/E leu1-32 ade6-M210	*	gfp+ driven by ura4+ promoter
spb1055	swi6-KR25A	S5	h90 mat3M(EcoRV)::gfp+::natMX ura4-DS/E leu1-32 ade6-M210 swi6-KR25A	*	gfp+ driven by ura4+ promoter
spb1468	swi6-Dendra2 cnp1-mCherry	S5	h90 mat3M(EcoRV)::gfp+::natMX ura4-DS/E leu1-32 ade6-M210 swi6-Dendra2::hphMX cnp1-mCherry::kanMX	*	gfp+ driven by ura4+ promoter
spb1450	nls-swi6-Dendra2 cnp1-mCherry	S5	h90 mat3M(EcoRV)::gfp+::natMX ura4-DS/E leu1-32 ade6-M210 nls-swi6-Dendra2::hphMX cnp1-mCherry::kanMX	*	gfp+ driven by ura4+ promoter
spb1469	nls-swi6-KR25A-Dendra2 cnp1-mCherry	S5	h90 mat3M(EcoRV)::gfp+::natMX ura4-DS/E leu1-32 ade6-M210 nls-swi6-KR25A-Dendra2::hphMX cnp1-mCherry::kanMX	*	gfp+ driven by ura4+ promoter
spb1439	NLS-TAP-Swi6	S5	h90 mat3M(EcoRV)::gfp+::natMX ura4-DS/E leu1-32 ade6-M210 NLS-TAP-Swi6	*	gfp+ driven by ura4+ promoter
Spb1493	NLS-TAP-Swi6-KR25A	S5	h90 mat3M(EcoRV)::gfp+::natMX ura4-DS/E leu1-32 ade6-M210 NLS-TAP-Swi6-KR25A	*	gfp+ driven by ura4+ promoter

Source: *this study, [1]Charles Hoffmann, [2]Danesh Moazed

Oberti et al., 2015

Cell Reports

Cell Reports

Article

Dicer and Hsp104 Function in a Negative Feedback Loop to Confer Robustness to Environmental Stress

Graphical Abstract

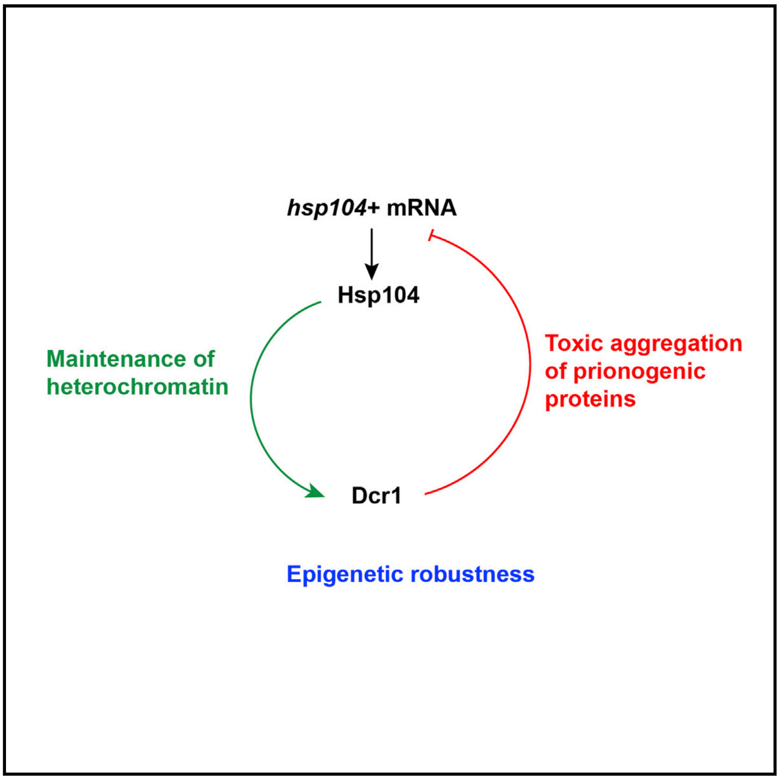
hsp104+ mRNA
Hsp104
Maintenance of heterochromatin
Toxic aggregation of prionogenic proteins
Dcr1
Epigenetic robustness

Authors

Daniele Oberti, Adriano Biasini, ...,
Yukiko Shimada, Marc Bühler

Correspondence

marc.buehler@fmi.ch

In Brief

Environmental changes can impact epigenetic mechanisms and thus evoke phenotypic variation. In this study, Oberti et al. reveal a negative feedback loop involving the RNase Dicer and the protein disaggregase Hsp104 that buffers environmentally induced stochastic epigenetic variation and toxic aggregation of exogenous prionogenic proteins.

Highlights

- Dicer aggregates are recycled in a specialized cytoplasmic compartment
- Hsp104 and Dicer function in a negative feedback loop
- Hsp104 buffers environmentally induced epigenetic variation
- Dicer averts toxic aggregation of a prionogenic protein

Accession Numbers

GSE60640

Oberti et al., 2015, Cell Reports *10*, 47–61
January 6, 2015 ©2015 The Authors
http://dx.doi.org/10.1016/j.celrep.2014.12.006

Cell Reports
Article

OPEN
ACCESS
CellPress

Dicer and Hsp104 Function in a Negative Feedback Loop to Confer Robustness to Environmental Stress

Daniele Oberti,[1,2] Adriano Biasini,[1,2] Moritz Alexander Kirschmann,[1,2] Christel Genoud,[1,2] Rieka Stunnenberg,[1,2]
Yukiko Shimada,[1,2] and Marc Bühler[1,2,*]
[1]Friedrich Miescher Institute for Biomedical Research, Maulbeerstrasse 66, 4058 Basel, Switzerland
[2]University of Basel, Petersplatz 10, 4003 Basel, Switzerland
*Correspondence: marc.buehler@fmi.ch

http://dx.doi.org/10.1016/j.celrep.2014.12.006

This is an open access article under the CC BY-NC-ND license (http://creativecommons.org/licenses/by-nc-nd/3.0/).

SUMMARY

Epigenetic mechanisms can be influenced by environmental cues and thus evoke phenotypic variation. This plasticity can be advantageous for adaptation but also detrimental if not tightly controlled. Although having attracted considerable interest, it remains largely unknown if and how environmental cues such as temperature trigger epigenetic alterations. Using fission yeast, we demonstrate that environmentally induced discontinuous phenotypic variation is buffered by a negative feedback loop that involves the RNase Dicer and the protein disaggregase Hsp104. In the absence of Hsp104, Dicer accumulates in cytoplasmic inclusions and heterochromatin becomes unstable at elevated temperatures, an epigenetic state inherited for many cell divisions after the heat stress. Loss of Dicer leads to toxic aggregation of an exogenous prionogenic protein. Our results highlight the importance of feedback regulation in building epigenetic memory and uncover Hsp104 and Dicer as homeostatic controllers that buffer environmentally induced stochastic epigenetic variation and toxic aggregation of prionogenic proteins.

INTRODUCTION

Epigenetics is the study of heritable changes in gene expression and phenotypic states that occur without a change in DNA sequence (Gottschling, 2004). Instead, chemical modifications such as methylation of DNA and histone proteins can act as epigenetic marks that stably affect gene expression and can be passed on to subsequent generations. Besides chromatin-dependent mechanisms, epigenetic information can also be transmitted by protein-based elements such as prions (Grossniklaus et al., 2013). Although epigenetic changes can be stably inherited, they are also reversible. Indeed, there can be considerable stochastic fluctuations between epigenetic states, which can potentially alter cellular and organismal phenotypes (Fraga et al., 2005; Wong et al., 2010).

Stochastic fluctuations between epigenetic states are thought to be mediated both by extrinsic and intrinsic factors. In particular, the impact of the environment on epigenetic genome regulation has attracted considerable interest. However, apart from a few well-studied natural processes such as vernalization whereby plants acquire the ability to flower in the spring upon cold exposure in winter (Song et al., 2013), it remains largely unknown if and how environmental cues like temperature trigger alterations in the epigenome (Feil and Fraga, 2011).

Heterochromatin also plays an essential role in epigenetic gene silencing in organisms ranging from yeast to humans. A classical example of heritable gene regulation mediated by heterochromatin is position effect variegation (PEV), a universally conserved epigenetic phenomenon where the expression of inserted or translocated genes is influenced by nearby heterochromatin. In *Schizosaccharomyces pombe*, genes placed within any of the three heterochromatic centromeres are repressed (Allshire, 1995; Allshire et al., 1994). However, the degree of repression depends upon the centromeric region. *S. pombe* centromeres are composed of a nonrepetitive central domain (*cnt*) around which outer repeat (*otr*) domains are symmetrically arranged (Chikashige et al., 1989). The *otr* domains are composed of *dg*/*dh* repeats that, like centromeres of higher eukaryotes, assemble into constitutive heterochromatin. Marker genes inserted into the *cnt* domain display a mosaic gene expression pattern reminiscent of PEV, whereas gene repression in the *otr* domain is remarkably strong without noticeable phenotypic variegation (Allshire et al., 1994; this study). Thus, the mechanisms that propagate the epigenetic state of the *otr* regions of *S. pombe* centromeres are highly effective.

Although it seems paradoxical, transcription of the *otr* region is necessary to stably propagate centromeric heterochromatin by a mechanism that engages the RNAi pathway (Castel and Martienssen, 2013). Indeed, centromeres of *S. pombe* cells with a nonfunctional RNAi pathway have severely impaired heterochromatin, causing chromosome segregation problems and derepression of centromeric sequences (Volpe et al., 2002, 2003).

Besides its critical role in the maintenance of centromeric heterochromatin, the *S. pombe* RNAi pathway also contributes to the tight repression of a class of euchromatic protein-coding genes referred to as ‘‘bound by Atf1 under normal conditions’’ (BANC) (Woolcock et al., 2012). BANCs are stress-response genes such as those encoding heat shock proteins that are

CrossMark

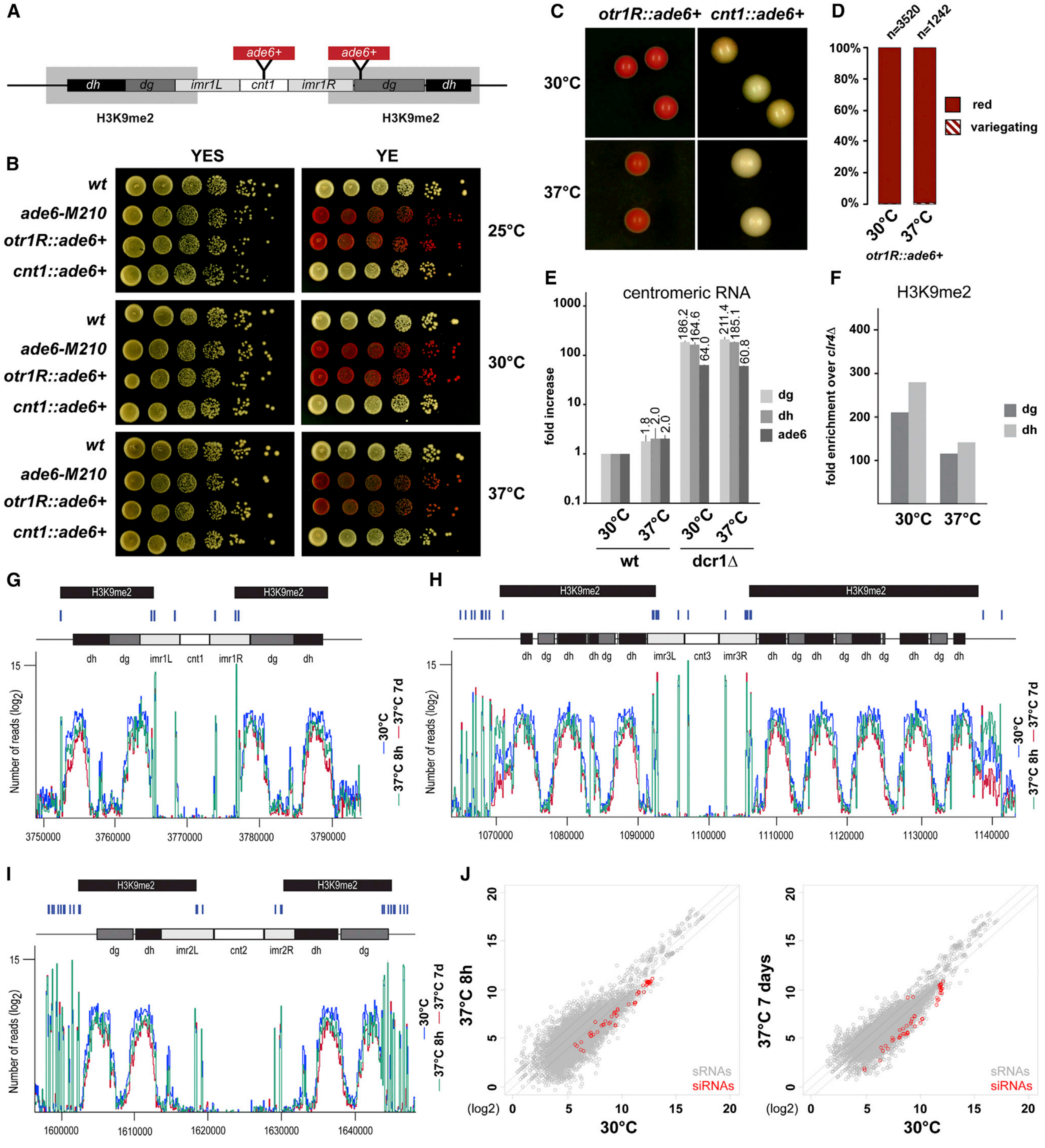

Figure 1. Centromeric Silencing Is Maintained at Elevated Temperatures

(A) Schematic of the centromeric region of chromosome I, highlighting the positions of the *ade6*+ reporter used in (B) and (C).

(B) Silencing assays of strains bearing the *ade6*+ reporter grown on YES and YE plates. The *otr1R*::*ade6*+ reporter reveals robust silencing at all temperatures tested.

(C) Imaging of single colonies showing robust silencing of the *otr1R*::*ade6*+ reporter at 30°C and 37°C, in contrast to slight silencing of the *cnt1*::*ade6*+ reporter at 30°C and loss of silencing at 37°C.

(D) Phenotypic assessment of single colonies of *otr1R*::*ade6*+ cells.

(E) Quantitative RT-PCR of centromeric (*dg*/*dh*) and *ade6*+ transcripts showing robust silencing at 37°C in *WT* cells. In contrast, silencing is lost in *dcr1∆* cells. Levels are normalized to *WT* cells at 30°C and *act1*+ RNA.

(legend continued on next page)

constitutively bound by the transcriptional activator Atf1 (Kon et al., 1997). Upon stress, Atf1 is rapidly phosphorylated and causes strong transcriptional activation of most of its target genes (Lawrence et al., 2007). Under nonstressful conditions, the RNAi factor Dicer (Dcr1) colocalizes with BANCs at nuclear pores, contributing to their firm repression presumably by degrading nascent transcripts (Woolcock et al., 2012).

Dcr1 localization and activity is regulated in a unique temperature-dependent manner. Under normal conditions in *S. pombe*, Dcr1 is predominantly nuclear (Emmerth et al., 2010), but upon acute thermal stress, it accumulates in large cytoplasmic foci. This is controlled by the double-stranded RNA-binding domain (dsRBD) of Dcr1: proper folding of the dsRBD is required for nuclear retention of Dcr1, whereas unfolding of the dsRBD and thus loss of nuclear retention can be induced by temperatures above 34°C. In vitro, these high temperatures cause precipitation of the dsRBD and progressive loss of nuclear magnetic resonance signals, indicative of protein aggregation. Thus, the Dcr1 dsRBD constitutes a thermoswitch that controls conditional relocalization of Dcr1 and may render Dcr1 aggregation prone above 34°C (Barraud et al., 2011; Woolcock et al., 2012).

Temperature-induced loss of nuclear-pore-associated Dcr1 provides an elegant mechanism for the release of BANC genes from RNAi repression under temperature stress (Holoch and Moazed, 2012). However, it raises two important questions: how is aggregation of Dcr1 prevented and, given the loss of nuclear Dcr1, what ensures the integrity of centromeric heterochromatin at elevated temperatures? Furthermore, the physiological relevance of Dcr1-mediated BANC repression has remained elusive. Here, we demonstrate that resilience of centromeric heterochromatin critically depends on Hsp104, a protein disaggregase that dissolves Dcr1 aggregates at elevated temperatures. The BANC gene *hsp104+* itself is negatively regulated by Dcr1, which averts the toxic aggregation of a budding yeast prion protein.

RESULTS

Silencing within Constitutive Heterochromatin Is Temperature Insensitive

To investigate the robustness of centromeric heterochromatin to temperature variations, we used *S. pombe* strains in which *ade6+* reporter genes were either inserted into the central core domain *cnt1* (*cnt1*::*ade6+*) or the juxtaposed heterochromatic *dg/dh* region (*otr1*::*ade6+*; Figure 1A). In this assay, wild-type (*WT*) cells form white colonies, whereas cells with a nonfunctional *ade6-M210* allele give rise to red colonies under limiting adenine conditions (Figure 1B). *cnt1*::*ade6+* cells formed mostly white colonies at 30°C with low degrees of redness at lower temperatures and pure white color at 37°C (Figures 1B and 1C). This is consistent with reports that variegated expression of genes in *cnt* regions is sensitive to temperature changes (Allshire et al., 1994). In contrast, *otr1*::*ade6+* cells gave rise to dark red colonies at all temperatures (Figures 1B–1D). Thus, the *ade6+* gene placed within constitutive heterochromatin is strongly repressed and exhibits negligible phenotypic variation even when exposed to higher temperatures.

To assess repression of the *dg/dh* repeats in the heterochromatic *otr1* region directly, we measured *dh* and *dg* RNA levels by quantitative RT-PCR. In *dcr1Δ* cells, which have impaired heterochromatin formation, *dg/dh* RNA levels typically increase more than 100-fold. However, when *otr1*::*ade6+* cells were grown at 37°C, *dg* and *dh* RNA levels increased by only 2-fold compared to the same cells grown at 30°C (Figure 1E). Thus, consistent with the previous result, silencing of heterochromatin is not greatly affected at 37°C. Moreover, when cells were grown at 37°C, H3K9me2, a hallmark of heterochromatin, was largely maintained at both *dg* and *dh* repeats (Figure 1F), and there were no major defects in chromosome segregation, which also requires heterochromatic structures.

These results demonstrate that centromeric heterochromatin in *S. pombe* is temperature insensitive. This is in stark contrast to the repression of genes placed at the *cnt* domain of centromeres, which is completely abrogated at temperatures above 30°C.

Dcr1 Is Required for Repression of Centromeric Heterochromatin at Elevated Temperatures

A functional RNAi pathway is essential for silencing centromeric heterochromatin and maintaining high H3K9me2 levels (Volpe et al., 2002). It has been suggested that RNAi in *S. pombe* could be suppressed at higher temperatures (Kloc et al., 2008). In addition, we previously showed that, at elevated temperatures, Dcr1 translocates from the nucleus to the cytoplasm and speculated that this would abrogate the repressive activity of Dcr1, at least for BANC genes (Woolcock et al., 2012). Under these assumptions, RNAi would be expected to be dispensable for heterochromatin silencing at 37°C. However, we observed a dramatic increase in *dg/dh* transcript levels at both 30°C and 37°C upon deletion of the *dcr1+* gene (Figure 1E), demonstrating that Dcr1 is required for repression of heterochromatin also at elevated temperatures.

Dcr1 is thought to act on chromatin to cleave double-stranded RNA into short interfering RNAs (siRNAs) (Emmerth et al., 2010; Woolcock et al., 2011, 2012). Thus, the observed requirement of Dcr1 for silencing also at 37°C implies continuous generation of siRNAs. Consistent with this, deep sequencing of total small RNA libraries revealed highly abundant siRNAs also at 37°C. Although we observed a slight reduction of siRNAs at 37°C (Figure 1J), they remained high even when cells were grown at 37°C for several days (Figures 1G–1I). From these results, we conclude that siRNA biogenesis or stability is not greatly affected at elevated temperatures in *S. pombe*.

(F) ChIP experiment showing only moderate decrease of H3K9me2 enrichment at centromeric *dg* and *dh* repeats upon exposure to 37°C. The value for *clr4Δ* cells was set to 1 and fold enrichment normalized to *adh1+*.

(G–I) Small RNA reads mapping to the centromeres of the three chromosomes (G: chromosome I; I: chromosome II; H: chromosome III). Small RNAs were collected from samples grown at 30°C and from samples shifted to 37°C for 8 hr and 7 days.

(J) Scatterplot of siRNA peaks (red) and total small RNA (sRNA) peaks (gray) in cells grown at 30°C versus cells shifted to 37°C for 8 hr (left) or 7 days (right).

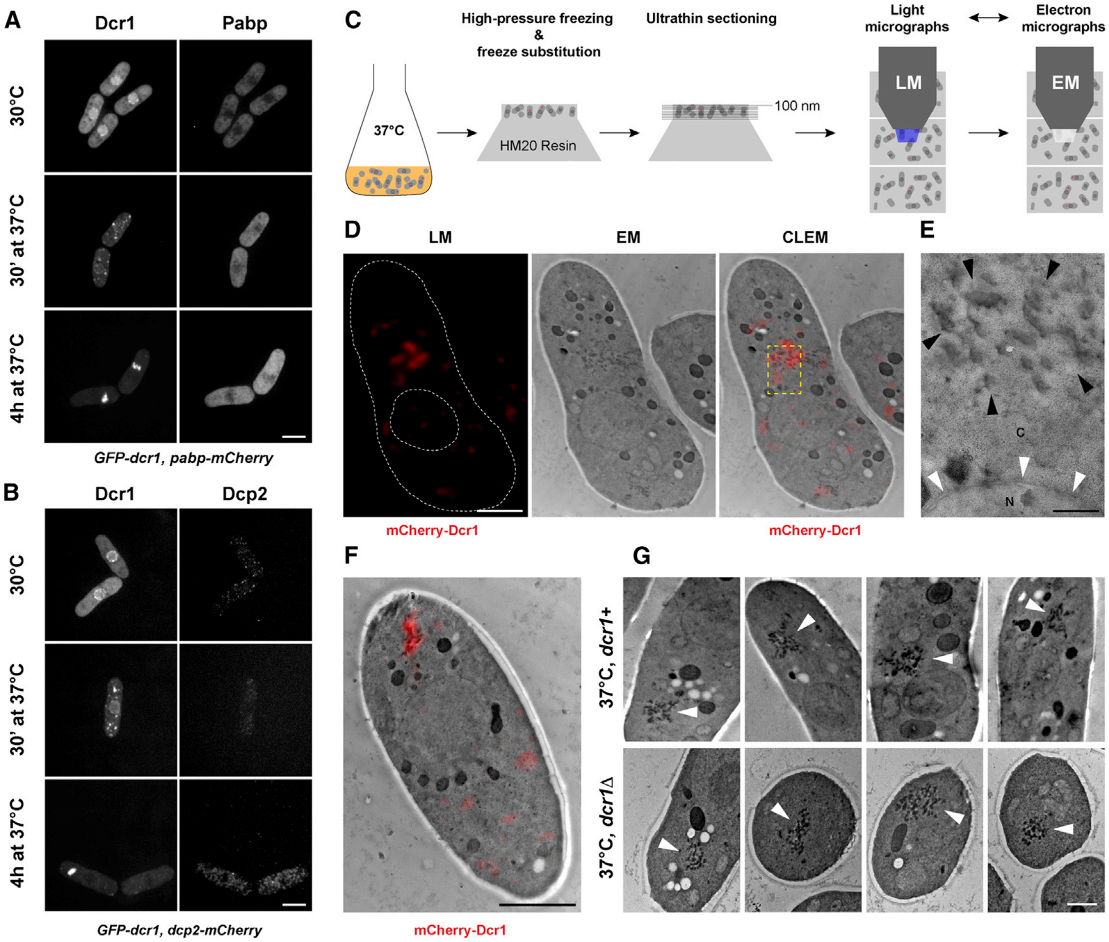
A
Dcr1
Pabp
30°C
30' at 37°C
4h at 37°C
GFP-dcr1, pabp-mCherry
B
Dcr1
Dcp2
30°C
30' at 37°C
4h at 37°C
GFP-dcr1, dcp2-mCherry
C
High-pressure freezing
&
freeze substitution
Ultrathin sectioning
Light micrographs
Electron micrographs
37°C
HM20 Resin
100 nm
LM
EM
D
LM
EM
CLEM
mCherry-Dcr1
mCherry-Dcr1
E
C
N
F
mCherry-Dcr1
G
37°C, dcr1+
37°C, dcr1Δ

Figure 2. Dcr1 Accumulates in Electron-Dense Cytoplasmic Inclusions at Elevated Temperatures

(A) Two-color live imaging of GFP-Dcr1- and Pabp-mCherry-expressing cells at different conditions reveals no specific colocalization of the two proteins. The scale bar represents 5 μm.

(B) Two-color live-cell imaging of GFP-Dcr1 and Dcp2-mCherry. The scale bar represents 5 μm.

(C) Schematic of the correlative microscopy workflow, in which the same ultrathin sections are imaged by light and transmission electron microscopy.

(D) Correlative microscopy of Dcr1 localization during heat stress. The scale bar represents 1 μm. LM, light microscopy.

(E) Enlargement of the region highlighted in (D), where Dcr1 is localized in electron-dense particles (black arrows). The nuclear envelope is also clearly visible thanks to high ultrastructure preservation (white arrows). The scale bar represents 200 nm.

(F) Another example showing Dcr1 localization in electron-dense particles. The scale bar represents 1 μm.

(G) Imaging of electron-dense particles (white arrows) in *dcr1+* and *dcr1Δ* cells at 37°C. The scale bar represents 1 μm.

Dcr1 Accumulates in Electron-Dense Cytoplasmic Inclusions at Elevated Temperatures

Thus far, we have shown that Dcr1 is required for repression of genes in the heterochromatic *otr* region of centromeres also at higher temperatures. Given that we previously observed Dcr1 accumulating in cytoplasmic foci at elevated temperatures (Woolcock et al., 2012), we further explored the nature of these cytoplasmic Dcr1 bodies (Figures 2A and 2B). As described previously, endogenous Dcr1 levels are not detectable by fluorescence microscopy (Emmerth et al., 2010). Therefore, similar to previous experiments, we used strains expressing Dcr1 to a level sufficient for detection by fluorescence microscopy (Emmerth et al., 2010; Barraud et al., 2011; Woolcock et al., 2012). We note that these conditions reflect physiological Dcr1 localization as assessed by other methods that do not rely on overexpression (Woolcock et al., 2012).

The formation of cytoplasmic structures is commonly observed when eukaryotic cells are exposed to nonphysiological growth temperatures. Under severe heat stress, general repression of translation causes a redistribution of mRNAs into stress granules (SGs) (Anderson and Kedersha, 2006). In *S. pombe*, SGs form when cells are exposed to 42°C (Dunand-Sauthier et al., 2002). Consistent with this, we did not observe formation of SGs at 37°C (Figure 2A). However, cytoplasmic Dcr1 bodies formed after only 30 min exposure to 37°C (Figures 2A and 2B). Thus, Dcr1 does not localize to SGs under mild temperature stress.

In mammalian cells, many RNAi factors can be found in processing bodies (P bodies), prompting us to look for a possible colocalization of Dcr1 with P bodies. Unlike SGs, P bodies exist even under nonstress condition (Mollet et al., 2008). Indeed, Dcp2-mCherry, a P body marker, showed punctate staining already at 30°C. Importantly, Dcr1 did not colocalize with Dcp2 either at 30°C or at 37°C (Figure 2B). Thus, the cytoplasmic Dcr1 bodies that form under mild heat stress are not SGs or P bodies.

To obtain more conclusive information about the precise cytoplasmic localization of Dcr1, we implemented correlative light and electron microscopy (CLEM). CLEM overcomes several limitations of light microscopy for analyzing the localization of fluorescently labeled proteins by combining it with electron microscopy (EM) to allow for higher resolution and to reveal the context where the protein of interest is located. The protocol we used is based on cell cryofixation, followed by freeze substitution and embedding in a Lowicryl resin, and ensures preservation of both fluorescent signal and ultrastructure as well as straightforward correlation of the two data sets (Figure 2C; Kukulski et al., 2011). In addition, by imaging sections with a thickness below the axial resolution of classical light microscopy, a higher z resolution is achieved than with confocal microscopy (Micheva and Smith, 2007).

We sequentially imaged ultrathin (<200 nm) sections from mCherry-Dcr1-expressing cells exposed for 4 hr to 37°C in a light microscope and in a transmission EM (Figure 2C). As expected from the confocal live imaging, we detected strong fluorescent mCherry-Dcr1 signal mostly in a single cytoplasmic region in every cell (Figure 2D). The signal obtained from imaging ultrathin sections however was less homogenous than whole-cell live imaging and distributed in small patches, a difference possibly due to the increased resolution. Interestingly, imaging of the same ultrathin sections in the EM and superposition of the light and electron micrographs revealed that the fluorescent signal corresponds to a cytoplasmic structure not previously described in *S. pombe* (Figures 2D–2F). This structure comprises smaller electron-dense cytoplasmic accumulations, not enclosed by membranes (Figure 2E). This structure was not observed in cells grown at 30°C but was highly characteristic of cells exposed to 37°C (Figure 2G). Moreover, these structures also formed in the absence of Dcr1 (Figure 2G). Thus, thermal stress provokes the formation of distinct electron-dense structures in the cytoplasm, in which Dcr1 accumulates during the acute phase of the stress.

Dcr1 Colocalizes with the Protein Disaggregase Hsp104 in Cytoplasmic Inclusions

The CLEM experiments were conducted on single ultrathin sections, which cover only a small cell subvolume, hindering an assessment of the number and distribution of the observed inclusions. We therefore imaged cells in their entirety using serial block-face electron microscopy (SBEM), a method that allows automated 3D imaging by combining block-face imaging with serial sectioning in a scanning EM (Denk and Horstmann, 2004). We acquired a volume encompassing several cells that had been exposed to 37°C for 4 hr before fixation and embedding. We found the electron-dense inclusions to be mostly concentrated in one region in the cytoplasm (Figures 3A, 3B, and S1; Movie S1), even in dividing cells (Figures 3C, 3D, and S1; Movie S2). 3D reconstruction confirmed that this structure is composed of many small accumulations of electron-dense material (interactive 3D model in Figure S2). In the case of the cell in Figure 3A, the cluster of electron-dense patches had a volume of around 2% of the total cell volume, but only 1/3 of it was electron dense. In this preparation, in which membranes are well stained, we again did not observe membranes enclosing the inclusion (Figures 3B and 3D).

The temperature-stress-induced electron-dense inclusions that we observed are reminiscent of heat-dependent electron-dense patches that have been associated with the protein disaggregase Hsp104 in *S. cerevisiae* (Fujita et al., 1998; Kawai et al., 1999). Hsp104 is a hexameric AAA+ ATPase that couples ATP hydrolysis to protein disaggregation (Doyle et al., 2013; Vashist et al., 2010). It mediates the resolubilization of heat-inactivated proteins from insoluble aggregates and plays an essential role in induced thermotolerance and prion propagation (Glover and Lindquist, 1998; Parsell et al., 1994; Sanchez and Lindquist, 1990). Therefore, we investigated Hsp104-mCherry localization in *S. pombe*. As observed for mCherry-Dcr1, Hsp104-mCherry accumulated in bright cytoplasmic foci at 37°C. Moreover, CLEM imaging revealed that the fluorescent Hsp104 signal corresponds to the same non-membrane-enclosed electron-dense cytoplasmic inclusion as described above (Figure 3E). Finally, labeling of Dcr1 and Hsp104 with two different fluorescent tags revealed perfect cytoplasmic colocalization of the two proteins at 37°C (Figures 3F and 3G).

Hsp104 Is Necessary to Dissolve Cytoplasmic Dcr1 Aggregates

The above results strongly suggested that the electron-dense material that we observed in the cytoplasm of cells that have been exposed to mild heat stress represent protein aggregates. Unlike most “canonical” heat shock proteins, Hsp104 disaggregates and remodels a broad repertoire of aggregated and unfolded proteins (DeSantis et al., 2012; Parsell et al., 1994). Consistent with this, we observed that the electron-dense inclusions visible during acute temperature stress progressively disappeared upon prolonged exposure to 37°C. However, they persisted in cells lacking Hsp104 (Figure 4A). We also observed a concomitant disappearance of the Hsp104-mCherry signal over time (Figures 4B and 4C). Therefore, the electron-dense cytoplasmic compartment that forms at 37°C and contains Dcr1 is likely the site where Hsp104 reactivates heat-denatured proteins.

Because we observed Hsp104 and Dcr1 colocalizing in the electron-dense cytoplasmic inclusions, we speculated that the fluorescent Dcr1 bodies observed at elevated temperatures represent aggregates of unfolded Dcr1 protein that eventually get resolubilized by Hsp104. Consistent with this compartment containing aggregated, insoluble Dcr1 molecules, fluorescence recovery after photobleaching (FRAP) experiments revealed that Dcr1 in this structure is immobile (Figure 4D). To directly test whether Hsp104 disaggregates Dcr1, we shifted cells grown at 30°C to 37°C and monitored the presence of Dcr1 aggregates in *hsp104+* and *hsp104Δ* cells over time by light microscopy (Figures 4B and 4E). In *WT hsp104+* cells, we observed the formation of a high number of small cytoplasmic Dcr1 foci during the first hour of heat stress. These then clustered in one or two large aggregates after 3 hr and subsequently disappeared progressively (Figures 4E and 4F). We also observed a high number of small Dcr1 foci during acute heat stress in *hsp104Δ* cells. These also clustered into one or two large aggregates after 3 hr, but, in contrast to the *WT* cells, they were significantly larger in size and tended to become even bigger during prolonged heat stress rather than disappearing (Figures 4E and 4F). Thus, the cytoplasmic Dcr1 bodies that form during the acute phase of temperature stress represent immobile, aggregated Dcr1 proteins, which become progressively disaggregated by Hsp104.

Recycling of Resolubilized Dcr1

Protein quality-control systems have evolved in all life kingdoms to prevent protein aggregation by facilitating either folding and refolding of misfolded proteins or their removal by proteolytic degradation (Goldberg, 2003; Tyedmers et al., 2010a). To investigate whether aggregated Dcr1 undergoes proteolysis or whether it can be properly refolded and return to the nucleus, we grew cells at 37°C for 4 hr, shifted them back to 30°C, and imaged GFP-tagged Dcr1 (Figure 5A). Similar to the result with chronic heat stress, cytoplasmic Dcr1 aggregates gradually disappeared in *WT* cells, whereas in *hsp104Δ* cells, the Dcr1 aggregates persisted during recovery (Figures 5B and 5C). Importantly, the nuclear localization of Dcr1 was rapidly restored in both *hsp104+* and *hsp104Δ* cells during recovery from heat stress (Figure 5B). To find out whether this nuclear pool of Dcr1 is exclusively newly synthesized protein or whether disaggregated Dcr1 also contributes to replenishing it, we imaged cells in which protein synthesis was blocked with cycloheximide during the recovery phase (Figure 5A). Under these conditions, nuclear Dcr1 localization was readily restored in *hsp104+* cells, but not in *hsp104Δ* cells (Figures 5D and 5E). When we photobleached Dcr1 fluorescence at the onset of recovery (Figure 5A), we could not detect any fluorescence during recovery, demonstrating that there was no new synthesis of Dcr1 protein during the course of this experiment (Figure 5D).

Thus, in the presence of Hsp104, aggregated cytoplasmic Dcr1 can be resolubilized and properly folded to re-enter the nucleus.

Hsp104 Confers Epigenetic Robustness at Elevated Temperatures

The foregoing results indicated that Hsp104 could be required to prevent loss of heterochromatin at elevated temperatures by

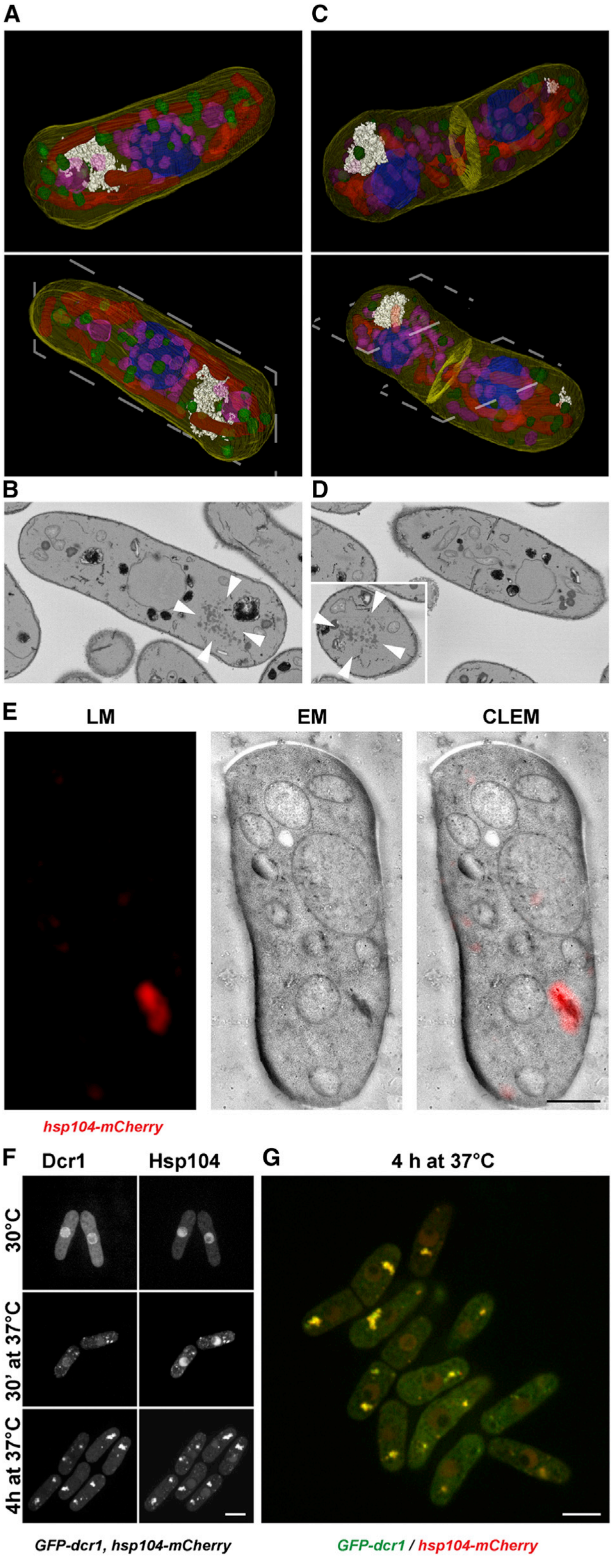

Figure 3. Dcr1 Colocalizes with Hsp104 in Electron-Dense Inclusions

(A) Reconstruction of *S. pombe* cell based on serial block-face electron microscopy imagery. White, electron-dense inclusions; blue, nucleus; red, mitochondria; pink and green, vesicles; gray dashed line, sectioning plane for (B).

(B) EM section through the cell reconstructed in (A). White arrows, electron-dense inclusion.

(C) Reconstruction of a cell undergoing mitosis. Color code as in (A); the septum is additionally shown in yellow.

(D) EM sections through the cell reconstructed in (C).

(E) Correlative microscopy imaging of hsp104-mCherry-expressing cell. The scale bar represents 1 μm.

(F) Two-color live-cell imaging of GFP-Dcr1 and hsp104-mCherry. The scale bar represents 5 μm.

(G) Two-color live-cell imaging of GFP-Dcr1 (green) and hsp104-mCherry (red). The scale bar represents 5 μm.

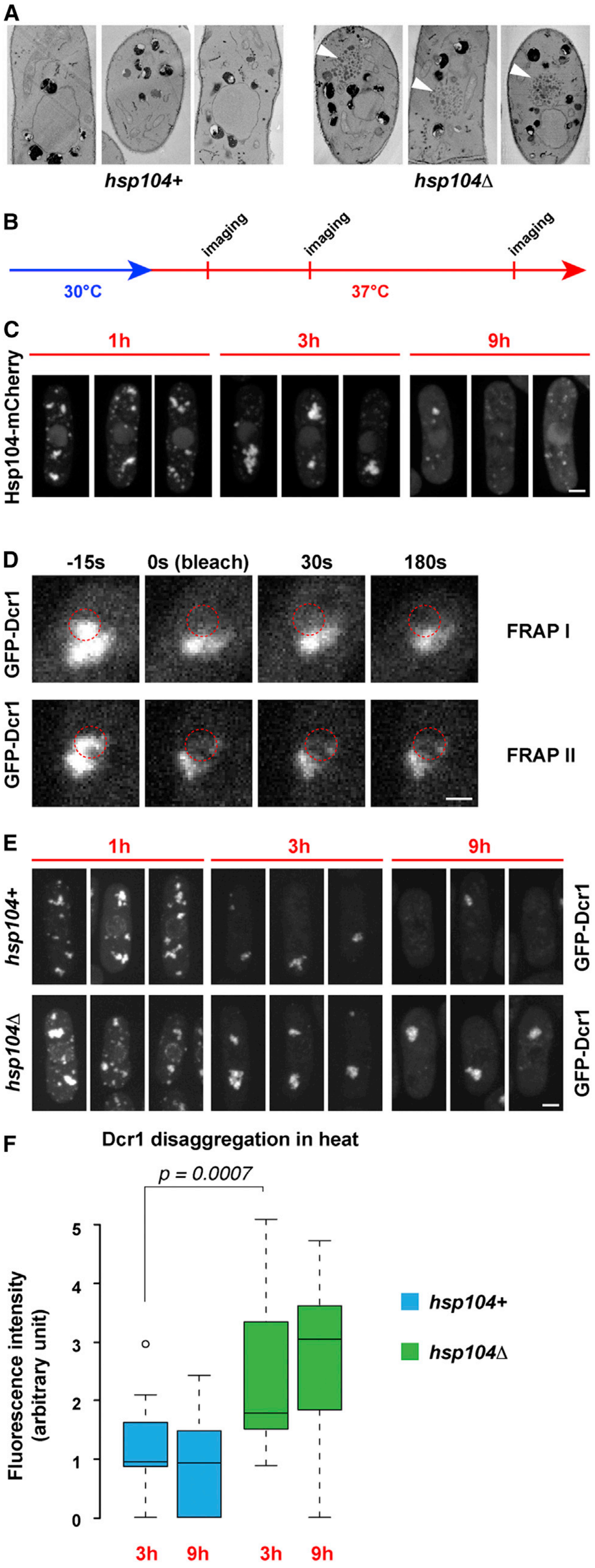

Figure 4. Disaggregation of Dcr1 Bodies Depends on Hsp104

(A) Electron microscopy imaging of *hsp104+* and *hsp104Δ* cells grown at 37°C for 10 hr. White arrows, electron-dense inclusions.

(B) Schematic of the experiment shown in (C). Cells were exposed to heat and imaged at different time points.

(C) Live-cell imaging of Hsp104-mCherry-expressing cells exposed to heat. The scale bar represents 2 μm.

(D) FRAP of GFP-Dcr1 foci. Images were acquired at the indicated time points. Two representative images are shown. Red, photobleached region. The scale bar represents 1 μm.

(E) Live-cell imaging of GFP-Dcr1 fluorescence of *hsp104+* and *hsp104Δ* cells exposed to heat. The scale bar represents 2 μm.

(F) Quantification of fluorescence in aggregates in *hsp104+* and *hsp104Δ* cells.

sustaining a sufficient amount of functional Dcr1 protein. Indeed, we observed that the repression of the heterochromatic *otr1*::*ade6+* gene became unstable in *hsp104*Δ cells at 37°C (Figures 6A and 6B). Specifically, rather than an overall loss of silencing in the entire population of cells, we observed switching between repressed and derepressed states of the *otr1*::*ade6+* gene. When we plated *hsp104*Δ cells and grew them at 37°C, we observed colonies with red and white sectors (Figure 6A). Such variegated expression of the *otr1*::*ade6+* gene hardly occurs at 30°C in either *WT* or *hsp104*Δ cells (Figures 1D and 6B). However, this phenotype was very pronounced at 37°C in *hsp104*Δ cells (Figure 6B). Notably, variegating colonies showed either fully white or dark red sectors, demonstrating that no intermediate *ade6+* expression states were established. Rather, the *otr1*::*ade6+* gene is either switched on or off in *hsp104*Δ cells at 37°C. Because all cells are genetically identical, this switch is of an epigenetic nature, and we therefore refer to *otr1*::*ade6+* "*on*" or "*off*" epialleles.

The formation of white sectors (i.e., *otr1*::*ade6+* "*on*") in *hsp104*Δ colonies indicated that thermal stress could cause a loss of heterochromatin in the absence of Hsp104. Indeed, we observed drastically reduced, yet not completely abolished, H3K9me2 levels on centromeric repeats in *hsp104*Δ cells that were grown at 37°C (Figure 6C). This experiment can only be performed with a mixed population of variegating cells, so it is possible that H3K9me2 levels are completely abolished in certain cells. Because we could not determine H3K9me2 levels on a single-cell level, we instead monitored chromosome segregation, which also requires functional heterochromatin, at the single-cell level in *hsp104Δ* cells by microscopy. Mutations that disrupt centromeric heterochromatin result in elevated rates of chromosome loss and nonsegregated, lagging chromosomes in late anaphase (Ekwall et al., 1999). We did not observe abnormal chromosome segregation patterns in *WT* cells grown at 37°C. However, we did observe lagging chromosomes in *hsp104Δ* cells at 37°C (Figure 6D). These results reveal that Hsp104 confers epigenetic robustness to *S. pombe* cells at elevated temperatures. In addition, lack of Hsp104 activity at elevated temperatures not only impacts heterochromatic gene silencing but also compromises genome stability.

Inheritance of an Environmentally Induced Epigenetic Switch

The *otr1*::*ade6+*-*off* epiallele was remarkably stable at both 30°C and 37°C in *WT* cells and at 30°C in *hsp104*Δ cells. However, an

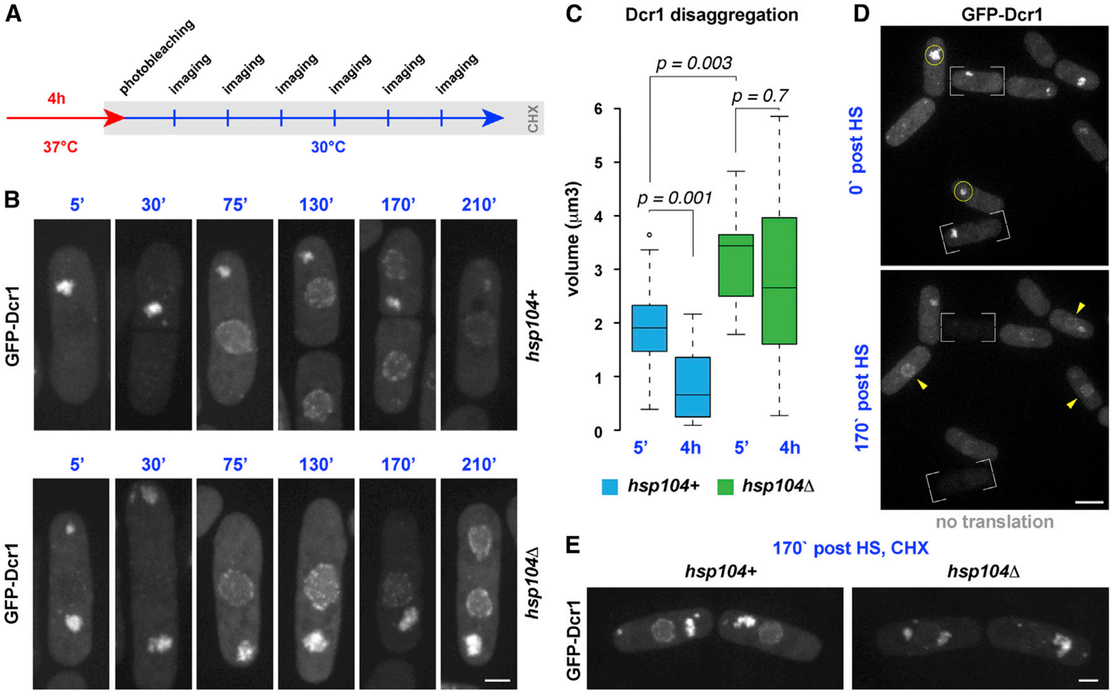

Figure 5. Disaggregated Dcr1 Re-enters the Nucleus

(A) Schematic of the experiment shown in (B). Cells pre-exposed to heat for 4 hr were shifted to 30°C and imaged at different time points.

(B) Live-cell imaging of *hsp104+* and *hsp104⊿* cells expressing GFP-Dcr1 recovering from heat condition. Different cells are shown at different time points. The scale bar represents 2 μm.

(C) Quantification of the size of GFP-Dcr1 aggregates during recovery.

(D) Live-cell imaging of *hsp104+* cells recovering from heat condition in the presence of cycloheximide. Control cells (white frames) were photobleached to confirm protein translation block. Nuclear signal is recovering after 170 min (yellow arrows), whereas cytoplasmic foci disappear (yellow circles). The scale bar represents 5 μm. HS, heat shock.

(E) Comparison of nuclear recovery in *hsp104+* and *hsp104⊿* cells treated with cycloheximide. The scale bar represents 2 μm.

increase in temperature to 37°C in *hsp104*Δ cells resulted in an unstable *otr1*::*ade6+* locus that displayed alternative silenced (*otr1*::*ade6+-off*) and expressed (*otr1*::*ade6+-on*) epigenetic states. Importantly, the *otr1*::*ade6+-on* epiallele was propagated for several cell divisions when *hsp104*Δ cells were grown at 37°C, as evidenced by the formation of white sectors within a given yeast colony (Figure 6A). Because *hsp104*Δ cells can restore the pool of functional Dcr1 by newly synthesized protein when shifted back to 30°C (Figure 5B), we predicted a rapid switch from the *otr1*::*ade6+-on* to the *otr1*::*ade6+-off* epiallele when temperature is reduced to 30°C. To test this, we selected variegating colonies at 37°C, grew them in two separate liquid cultures for about 14 divisions at 30°C or 37°C, and subsequently plated these cells to assess the epigenetic state of the *otr1*::*ade6+* allele (Figure 6E). As anticipated, we observed fully red (off) but rarely fully white (on) colonies at both temperatures, demonstrating that the *otr1*::*ade6-on* epiallele is less stable than the *otr1*::*ade6+-off* epiallele. Unexpectedly, however, we still observed a high number of white sectored colonies, although these cells had gone through at least 30 divisions at 30°C (Figure 6F). Once re-established, the *otr1*::*ade6+-off* epiallele was stably maintained (Figure S3). Thus, the *otr1*::*ade6-on* epiallele can be propagated for many divisions even in the absence of the thermal stress that initially induced the change in expression of the *otr1*::*ade6+* gene.

These results highlight that *hsp104+* mutants are predisposed to undergo temperature-induced, heritable changes in heterochromatic gene expression and reveal a phenomenon that complies with the classical definition of epigenetics (Gottschling, 2004; Ptashne, 2013).

Hsp104 and Dcr1 Function in a Negative Feedback Loop

Besides centromeric repeats, Dcr1 also physically associates with a group of stress-response genes referred to as BANCs (Woolcock et al., 2012). Under noninduced conditions, Dcr1 degrades BANC gene mRNAs cotranscriptionally, thereby assuring tight repression. Intriguingly, *hsp104+* is a BANC gene, and we have previously suggested that temperature-induced translocation of Dcr1 to the cytoplasm abrogates the repressive activity of Dcr1 on BANC gene expression (Woolcock et al., 2012).

To determine the influence of Dcr1 on the *hsp104+* expression dynamics with high temporal resolution, we measured the relative abundance of *hsp104+* mRNA in *WT* and *dcr1*Δ cells every 15 min for 3 hr, at 30°C and 37°C (Figure 7A). As expected, steady-state *hsp104+* mRNA levels were about 5- to 10-fold

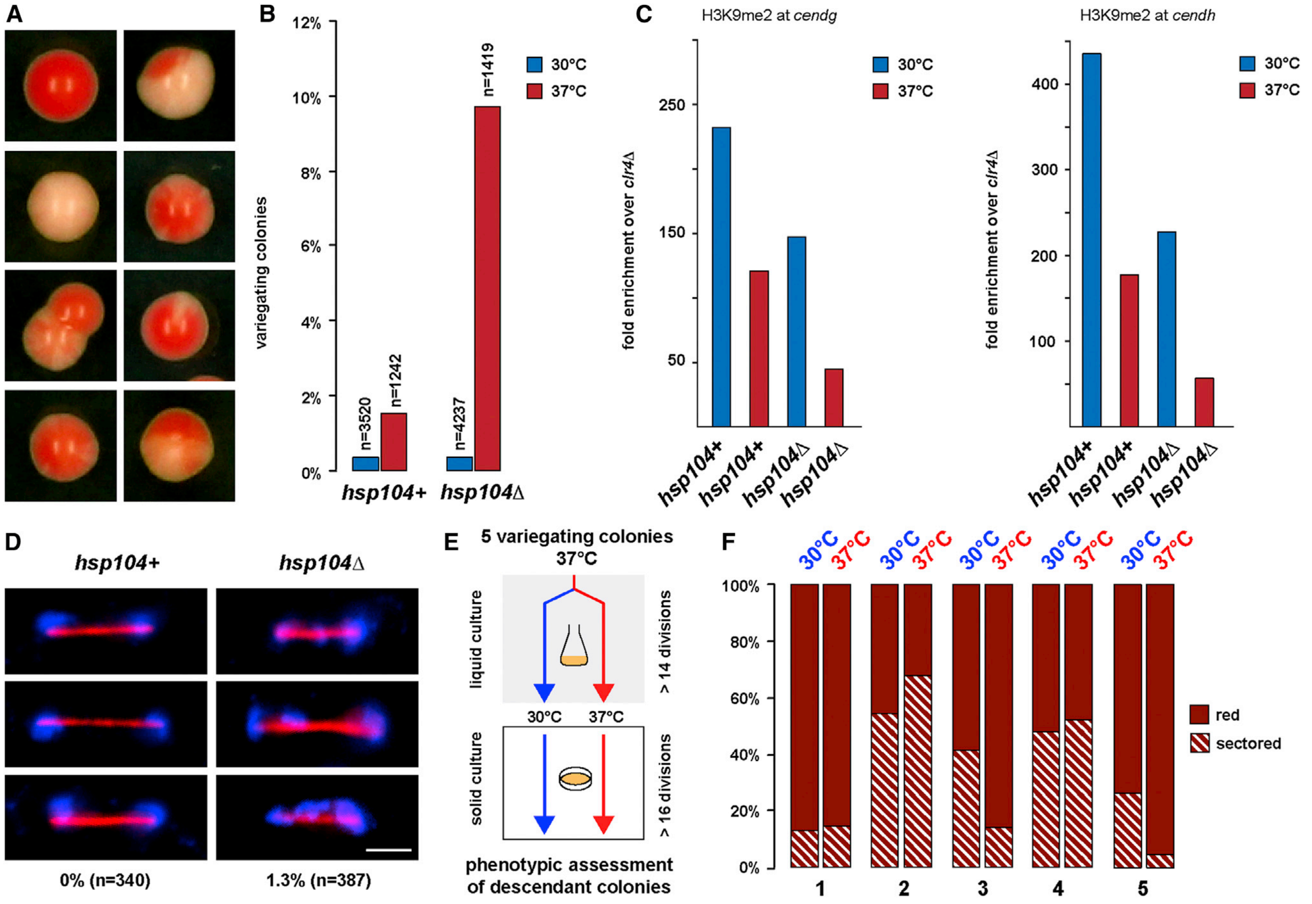

Figure 6. Hsp104 Confers Epigenetic Robustness

(A) Examples of *hsp104Δ* cells with *otr1R*::*ade6*+ reporter showing a variegating phenotype after growth at 37°C.

(B) Assessment of variegation phenotype in *hsp104*+ and *hsp104Δ* cells grown at 30°C and 37°C.

(C) ChIP experiment showing decreased H3K9me2 enrichment at centromeric (cen) *dg* and *dh* repeats in *hsp104Δ* cells at 37°C. The value for *clr4Δ* cells was set to 1 and fold enrichment normalized to *adh1*+.

(D) Lagging chromosomes in *hsp104Δ* cells. Cells grown at 37°C were stained with DAPI (blue) and α-tubulin (red). The scale bar represents 2.5 μm.

(E) Schematic of the experiment shown in (F). Variegating *hsp104Δ* colonies at 37°C were selected and further grown at 30°C or 37°C.

(F) Assessment of variegating phenotype of colonies originating from a variegating colony. Five representative examples are shown.

higher in *dcr1*Δ cells compared to *WT* cells at 30°C. When cells were shifted from 30°C to 37°C, we observed a rapid increase in *hsp104*+ expression, reaching maximal levels 30 min after the temperature shift, in both *WT* and *dcr1Δ* cells. Surprisingly, rather than constantly high or steadily decaying *hsp104*+ mRNA levels, we observed pulsatile expression patterns of *hsp104*+ when *WT* and *dcr1*Δ cells were continuously grown at 37°C. The *hsp104*+ gene cycled with a period length of approximately 30 min and synchronously in *WT* and *dcr1*Δ cells. However, *WT* cells displayed less-pronounced expression peaks than *dcr1*Δ cells, indicating that Dcr1 can still repress expression of the *hsp104*+ gene at high temperatures. Except for the first expression maximum that was similar in *WT* and *dcr1*Δ cells in most experiments, *hsp104*+ mRNA levels were always lower in *WT* compared to *dcr1*Δ cells in subsequent periods. Importantly, we observed up to 3.5-fold changes between expression maxima and minima in *dcr1Δ* cells, which were always below 2-fold in *WT* cells. Thus, elevated temperatures induce high and oscillating expression of the *hsp104*+ gene, which is dampened by Dcr1.

To investigate whether the repression of *hsp104*+ mRNA levels by Dcr1 was also reflected at the protein level, we measured total fluorescence of cells expressing Hsp104-mCherry from the endogenous locus by spinning disk microscopy. This method allows monitoring Hsp104 levels with very high temporal resolution and, by measuring the intensity of several thousand individual cells, to assess variability within the population. Similar to the mRNA behavior, average Hsp104 protein levels were constantly higher and more oscillating in *dcr1Δ* cells than in *WT* cells (Figure 7B).

Together, these results further support our model that, under elevated temperatures, Hsp104 disaggregates cytoplasmic Dcr1, which can then return to the nucleus and maintain repression of both centromeric repeats and BANC genes. It also

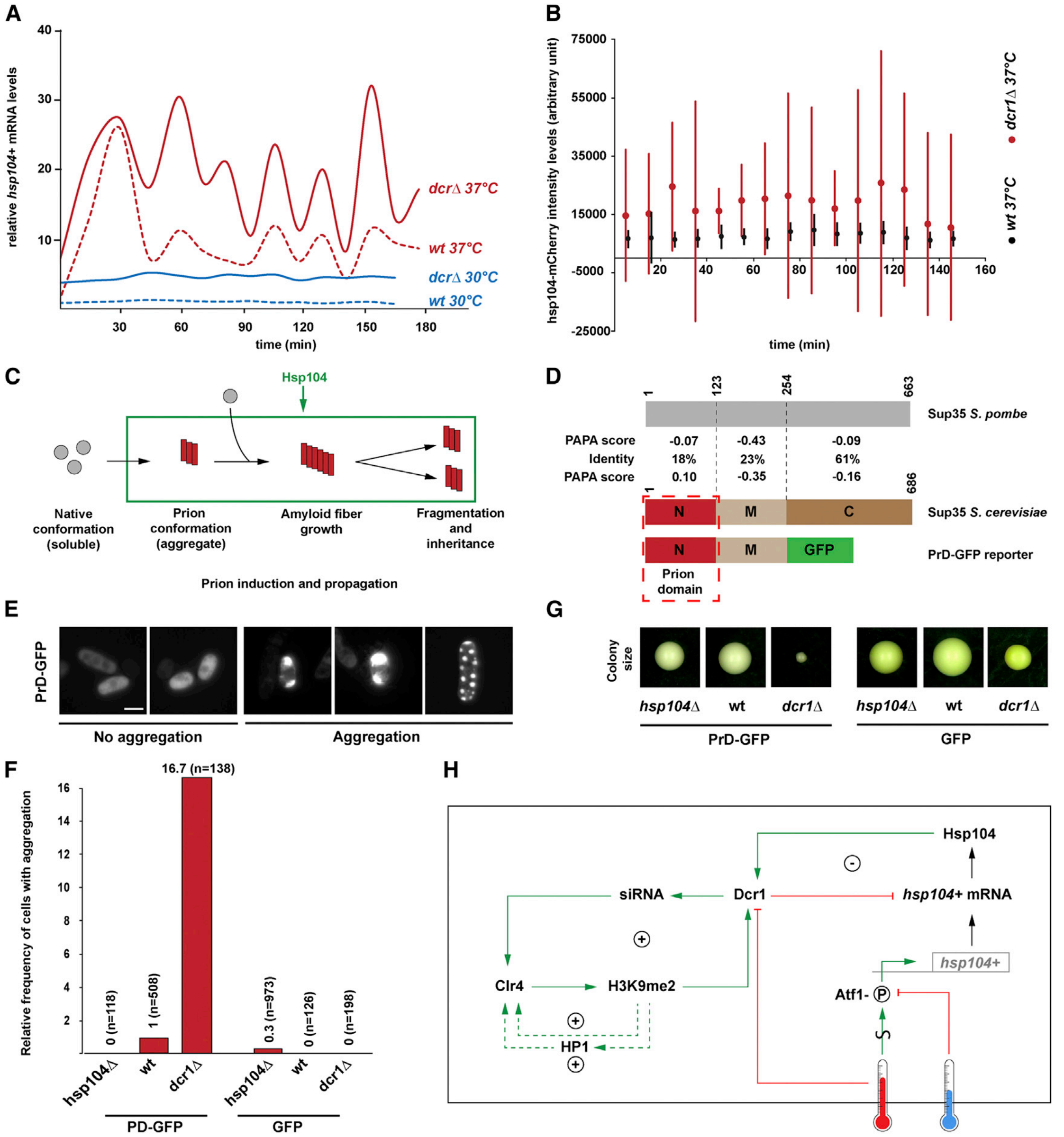

Figure 7. Dcr1 Inhibits Aggregation and Toxicity of a Prion Reporter

(A) *hsp104+* RNA levels measured every 15 min by quantitative RT-PCR in *WT* and *dcr1Δ* cells at 30°C or after shifting to 37°C.

(B) Hsp104-mCherry fluorescence levels in *WT* and *dcr1Δ* cells exposed to 37°C. Mean intensities of individual cells were measured. Averages of 10 min bins and SDs are shown.

(C) Schematic of prion induction and propagation.

(D) Domain architecture of *S. cerevisiae* Sup35, the PrD-GFP reporter used in (E)–(G) and *S. pombe* Sup35. Amino acid homology of individual domains was calculated using EMBOSS Needle, whereas prion forming propensity was calculated using the PAPA algorithm (Toombs et al., 2012).

(E) Examples of nonaggregating and aggregating phenotypes observed in different strains expressing PrD-GFP. The scale bar represents 5 μm.

(F) Frequency of aggregation in PrD-GFP- and GFP-expressing cells at 37°C (*WT*, *hsp104Δ*, and *dcr1Δ*), relative to the frequency observed in *WT* PrD-GFP-expressing cells.

(G) Colonies of PrD-GFP- and GFP-expressing strains showing strongly reduced growth in *dcr1Δ* PrD-GFP-transformed cells.

(H) Model for the formation of constitutive heterochromatin. The integration of multiple feedback motifs confers robustness to the system and buffers environmental insults. Red, >34°C; blue, <34°C. S depicts unknown oscillator; P indicates phosphorylation of Atf1.

reveals a negative feedback regulatory circuit in Dcr1-mediated control of *hsp104+* gene expression: whereas Dcr1 negatively regulates *hsp104+* expression, the Hsp104 protein positively regulates Dcr1 by keeping it in an active state.

Dcr1 Is Required to Repress Aggregation and Toxicity of a Prionogenic Protein

The forgoing results suggest that controlling the dynamics of BANC gene expression under constant thermal stress may serve as a vital buffer to prevent potentially deleterious fluctuations in heat shock gene expression. Intriguingly, in addition to its role in protein disaggregation, Hsp104 plays a crucial role in prion formation, propagation, and elimination (Figure 7C). Whereas absence of Hsp104 prevents prion formation, too high levels lead to prion curing (Chernoff et al., 1995; Shorter and Lindquist, 2004). Thus, unsteady Hsp104 levels may favor prion occurrence, and it is therefore tempting to speculate that Dcr1-mediated dampening of oscillatory *hsp104+* expression might antagonize prion formation in *S. pombe*.

To determine the rate at which prionogenic proteins might switch to the prion conformation in *S. pombe*, we exploited a widely used GFP reporter containing the prion-forming domain (PrD) of *S. cerevisiae* Sup35 (Figure 7D), one of the most well-studied fungal prions (Tessier and Lindquist, 2009; Tyedmers et al., 2010b). We transformed *WT*, *dcr1Δ*, and *hsp104Δ* cells with plasmids encoding either the PrD-GFP construct or GFP alone and monitored fluorescence localization after growth at 37°C. *WT*, *dcr1Δ*, and *hsp104Δ* cells expressing the control plasmid showed limited or no aggregation, with most or all of the cells showing diffuse staining. In contrast, PrD-GFP aggregation was significantly higher in *dcr1Δ* cells (Figure 7F) than in *WT* or *hsp104Δ* cells, revealing a link between Dcr1 and aggregation of prionogenic proteins. PrD-GFP also appeared to be toxic to *dcr1Δ* cells, as they formed much smaller colonies than *dcr1+* and *dcr1Δ* cells transformed with PrD-GFP and GFP, respectively, and could not be further expanded (Figure 7G). Both *WT* and *dcr1Δ* cells showed aggregation of PrD-GFP in different patterns, including multiple dots distributed in the cytoplasm or one single region of aggregation (Figure 7E). These patterns are typical of the switch to the prion conformation. PrD-GFP aggregation was not observed in *hsp104Δ* cells. Thus, the *S. cerevisiae* PrD forms stable aggregates and is highly toxic when expressed in *S. pombe* cells that lack Dcr1.

Although definite proof that the PrD-GFP forms a bona fide prion in *S. pombe* demands further study, our results suggest that Dcr1-mediated dampening of oscillatory expression of *hsp104+* and possibly other BANC genes might have evolved to counteract prion induction and propagation that might otherwise be toxic for the cell.

DISCUSSION

This study highlights the remarkably strong and stable repressive activity of constitutive heterochromatin, uncovers a central role for Hsp104 in buffering environmentally induced epigenetic variation, and reveals an unanticipated role for Dcr1 in averting toxic aggregation of a prionogenic protein. Below, we speculate about the physiological relevance of feedback regulation of Dcr1 and Hsp104 and discuss the implications of our findings for our understanding of RNAi-mediated heterochromatin formation and epigenetic robustness.

Recycling of Aggregated Dcr1 in a Specialized Cytoplasmic Compartment

Using CLEM, we discovered that Dcr1 colocalizes with Hsp104 in membrane-free, electron-dense, cytoplasmic inclusions at elevated temperatures. SBEM imaging and subsequent 3D reconstruction revealed the existence of one such inclusion per cell during prolonged heat, generally localizing at the cellular periphery in the vicinity of vacuoles. We never observed these structures adjacent to the nuclear membrane, and their formation required thermal stress. Interestingly, we observed a high number of small cytoplasmic Dcr1 foci during acute temperature stress, which then clustered into one large inclusion after 3 hr and subsequently disappeared progressively, indicating that formation and disintegration of these misfolded protein inclusions are both active processes. Furthermore, FRAP experiments revealed that the Dcr1 proteins in these inclusions are immobile, consistent with this compartment containing aggregated proteins.

These features are reminiscent of cytosolic protein quality-control compartments that have been described in *S. cerevisiae* and mammalian cells such as the Q bodies (Escusa-Toret et al., 2013) or the insoluble protein deposit (IPOD) (Kaganovich et al., 2008). Q bodies also contain misfolded proteins and arise in response to a temperature increase, first as several small puncta that then fuse within 30 min into few larger foci. However, proteins in Q bodies are destined for degradation. Moreover, Q bodies remain as multiple small puncta, do not coalesce in fewer bigger foci, and rapidly disappear in *hsp104Δ* cells. Dcr1 bodies instead increase in size and persist in the absence of Hsp104. Accumulation of misfolded proteins in the IPOD compartment and colocalization with Hsp104 has also been shown to be typical for stress conditions in *S. cerevisiae* (Kaganovich et al., 2008). However, it is not known whether protein disaggregation is also taking place in IPODs. Rather, it is generally assumed that IPODs contain terminally aggregated proteins (Tyedmers et al., 2010a).

Our results imply that the inclusions that form in *S. pombe* in response to acute temperature stress are not simply sequestering protein aggregates that might otherwise be toxic for the cell but are rather functional compartments in which Hsp104 exerts its functions. We show that Hsp104 actively participates in the disaggregation of proteins in this cytoplasmic compartment. As exemplified by Dcr1, these proteins are not destined for proteolysis but are rather recycled. As suggested for IPOD in budding yeast, this compartment in *S. pombe* may serve a protective function by spatially sequestering protein aggregates from the site where most proteasomal degradation takes place (Tyedmers et al., 2010a). Therefore, we propose that the large protein inclusion that forms at elevated temperatures in fission yeast constitutes a major site of protein disaggregation under acute temperature stress and serves to maintain protein homeostasis by recycling misfolded proteins.

Toxic Aggregation of Prionogenic Proteins

Prions are proteins that can exist in a soluble functional form or as amyloid fibrils. The amyloid form of prions is a self-perpetuating conformation and thus acts as a protein-based element of heredity (Shorter and Lindquist, 2005). In *S. cerevisiae*, numerous proteins are capable of forming prions that stably propagate the altered protein conformation and associated phenotypes (Alberti et al., 2009). However, there have been no reports of prion formation in *S. pombe*.

Hsp104 plays an important role in the propagation of the amyloid prion conformation in *S. cerevisiae*. It shears amyloid fibers to generate prion “seeds” or “propagons,” which facilitates the inheritance of the prion state from generation to generation (Chernoff et al., 1995). In this respect, negative feedback regulation of *hsp104+* and Dcr1 in *S. pombe* is fascinating, as it may constitute a homeostatic control mechanism that controls endogenous prion induction and propagation. Although definite proof has yet to be obtained, this hypothesis is supported by the highly increased frequency of aggregation that we observed for the exogenous PrD-GFP prion reporter in *dcr1*Δ cells. Interestingly, this aggregation is highly toxic. In contrast to *S. cerevisiae* Hsp104, *S. pombe* Hsp104 has been shown to support induction and propagation, but not curing of prions when expressed in *S. cerevisiae* (Reidy et al., 2013). It is therefore possible that PrD-GFP indeed forms prions in *dcr1*Δ cells. Because these cannot be cured in *S. pombe*, this could result in uncontrolled and irreversible propagation of aggregates, which has detrimental effects for the cell. Notably, endogenous prions have not yet been found and the number of putative prions predicted for *S. pombe* is significantly lower than for other fungi (Espinosa Angarica et al., 2013; Harrison et al., 2007). It is possible that the inability of *S. pombe* to cope with prionogenic proteins resulted in negative selection on prions while positively selecting Dcr1/Hsp104 feedback regulation.

PrD-GFP toxicity observed in this study is reminiscent of neurodegenerative diseases that share features with fungal proteins. Similar to β-sheet-rich amyloid fibrils formed by prions, many of the proteins involved in neurodegenerative conditions are deposited in insoluble, neurotoxic amyloid deposits, such as Aβ amyloid plaques in Alzheimer’s disease or Lewy bodies in Parkinson’s disease (Fraser, 2014; Halliday et al., 2014; Prusiner, 2012). *S. pombe* may therefore become an interesting model organism for studying detrimental prion-like protein aggregation in the future.

Transmission of an Epigenetic State through Successive Cell Divisions

A remarkable phenotype of *hsp104*Δ cells is that the *otr1*::*ade6+-on* epiallele can be stably maintained for more than 30 mitotic divisions, even in the absence of the stress that induced the epigenetic switch, and although normal Dcr1 distribution and BANC silencing are quickly re-established after stress removal. Thus, the descendants of the switching cells “remember” the chromatin state of the mother cell. This is reminiscent of inheritance of stress-induced disruption of heterochromatin in *Drosophila melanogaster*. When fly embryos are exposed to heat stress over multiple generations, the euchromatic chromatin state can be maintained over multiple successive generations before gradually returning to the normal state (Seong et al., 2011). The mechanism of this transgenerational inheritance of stress-induced heterochromatin disruption is unknown, and it is possible that the disrupted heterochromatin state is propagated actively. Similarly, we cannot rule out the possibility that the euchromatic state of the *otr1*::*ade6-on* epiallele is propagated by an active mechanism. However, rather than an active “memory” of the euchromatic state, we favor the idea that the long-lasting loss of *otr1*::*ade6+* repression reflects an inherent difficulty to establish heterochromatin de novo by siRNAs in the absence of preexisting H3K9 methylation. This hypothesis is consistent with various attempts to artificially induce the formation of ectopic heterochromatin by either siRNAs or tethering of the RNAi machinery to nascent transcripts, which are inefficient processes (Bühler et al., 2006; Iida et al., 2008).

Once re-established, the *otr1*::*ade6-off* epiallele is again mitotically remarkably stable under nonstressful conditions, even in *hsp104*Δ cells. Similarly, cells that are able to establish heterochromatin upon artificial tethering of the RNAi machinery to nascent transcripts stably propagate the repressed state through mitosis (Bühler et al., 2006). These results are in accordance with a model in which RNAi functions cooperatively with parentally inherited H3K9 methylated histones to re-establish heterochromatin following DNA replication. During replication of heterochromatin, the RNA-induced transcriptional silencing (RITS) complex can bind to chromatin cooperatively via siRNA-mediated base pairing with nascent transcripts and association with parental H3K9me2-marked nucleosomes. RITS-mediated recruitment of Clr4 then guarantees methylation of the newly deposited histones and thus transmission of heterochromatin from interphase to interphase (Moazed, 2011).

Stabilization of Constitutive Heterochromatin by Nested Feedback Loops

The observations discussed above exemplify the importance of positive feedback in building up epigenetic memory (Ptashne, 2013). For chromatin modifications, positive feedback can arise if nucleosomes carrying a particular modification recruit enzymes that catalyze the same modification on proximal histone tails. Therefore, methylated H3K9 could recruit the methyltransferase Clr4 directly through binding to the chromodomain or indirectly via the chromodomains of HP1 proteins or the RITS complex. However, these positive feedback loops are not sufficient to maintain heterochromatin by themselves, and it has become apparent that they must collaborate with the RNAi pathway to lock the heterochromatic state of centromeric repeats (Moazed, 2011). Therefore, we propose a model for the formation of constitutive heterochromatin that implies the integration of multiple feedback motifs to achieve robustness (Figure 7H).

In our model, Dcr1 constitutes a sensitive regulatory step that can respond to temperature changes. Without Hsp104, this step becomes ultrasensitive to thermal stress and inactivation of Dcr1 by elevated temperatures can trigger a bistable epigenetic switch. Importantly, among other factors that are required for heterochromatin repression in *S. pombe*, Hsp104 is unusual in the sense that its absence does not show complete penetrance. This suggests that the other positive feedback loops function partially redundant or that mild temperature stress inactivates Dcr1 only partly. Furthermore, switching to a euchromatic state may only occur if siRNA levels drop below a critical threshold. Thus, bistability of centromeric heterochromatin in *hsp104*Δ cells may also considerably depend on the half-life of centromeric siRNAs.

Our model predicts a concerted action of several positive feedback loops that guarantees the inheritance of the constitutive heterochromatic state of centromeric repeat sequences.

The model also highlights the importance of temperature-induced transcription of *hsp104+*, which is required for proper functioning of RNAi. But what is the role of negative regulation of *hsp104+* expression by Dcr1? Positive feedback can implement irreversible bistable switches that may only be forced back to the alternate state if coupled to negative feedback (Brandman and Meyer, 2008). Thus, negative feedback regulation of Dcr1 and *hsp104+* may have been integrated into the positive feedback core to still confer plasticity to the system. Alternatively, other processes such as the aforementioned regulation of prion induction and propagation may have been the driving force for the evolution of this negative feedback loop.

CONCLUSION

We discovered that mutating *hsp104+* predisposes *S. pombe* to undergo temperature-induced, heritable changes in heterochromatic gene expression. Although Dcr1 is certainly not the only client of Hsp104, our results strongly suggest that the bistability of centromeric heterochromatin in *hsp104Δ* cells is causally linked to malfunctioning Dcr1. Future studies with *hsp104+* mutants could reveal much hidden epigenetic variation that may or may not be linked to noncoding RNA metabolism. Similarly, Dcr1-deficient cells may enable the discovery and further characterization of endogenous prions in *S. pombe.* Finally, we hope that our proposed regulatory network model sparks future efforts to study the dynamics of the suggested feedback motifs. Combined with mathematical modeling approaches, we are convinced that this will significantly increase our understanding of epigenetic memory.

EXPERIMENTAL PROCEDURES

Extended procedures are described in the Supplemental Information.

Strains and Plasmids

S. pombe strains and plasmids used are described in the Supplemental Information.

Silencing Assays

Serial 10-fold dilutions of the strains indicated were plated on YES or YE plates and grown at the temperatures indicated. To score phenotype of individual colonies, 250–500 cells/plate were spotted and colonies were automatically counted using Matlab (MathWorks).

CLEM

Cells were prepared similar to Kukulski et al. (2011). Shortly, cells were high-pressure frozen, freeze substituted, and embedded in HM20 resin. One hundred to two hundred nanometer ultrathin sections were cut and imaged with a wide-field fluorescence microscope or spinning disk microscope, followed by transmission EM. Images were correlated with TrakEM.

SBEM

Fixed cells were prepared according to the rOTO NCMIR protocol. Embedded blocks were imaged with 3View (GATAN) in a scanning EM. Cells were digitally reconstructed using TrakEM (Fiji).

Live Fluorescence Microscopy and FRAP

S. pombe cells were imaged on agarose patches with a spinning disk microscope. For time-lapse experiments, cells were kept in culture and aliquots were taken at different time points. Intensity and volume measurement of foci was done with ImageJ. FRAP was performed on cells mounted on a Ludin chamber using a 473 nm laser.

Immunofluorescence

Synchronized cells were fixed, spheroblasted, and stained with anti-Tat1 antibody. Cells were imaged with a wide-field fluorescence microscope.

Gene Expression Analysis and Chromatin Immunoprecipitation

RNA isolation, cDNA synthesis, and quantitative RT-PCR were performed as previously described (Emmerth et al., 2010). Chromatin immunoprecipitation (ChIP) was performed as described in Bühler et al. (2006) using 2.5 μg of an antibody against dimethylated H3K9 (Kimura et al., 2008). Primers are listed in Table S3.

Generation of Small RNA Libraries for High-Throughput Sequencing

Sample libraries were prepared and analyzed as in the Supplemental Information. siRNAs were defined as reads with a decrease in number of reads of at least 8-fold between WT cells and DcrΔ cells.

ACCESSION NUMBERS

Deep sequencing data were deposited to the NCBI Gene Expression Omnibus and are available under accession number GSE60640.

SUPPLEMENTAL INFORMATION

Supplemental Information includes Supplemental Discussion, Supplemental Experimental Procedures, three figures, three tables, and two movies and can be found with this article online at http://dx.doi.org/10.1016/j.celrep.2014.12.006.

AUTHOR CONTRIBUTIONS

M.B. and D.O. conceived and designed the experiments. D.O. performed most of the experiments. A.B. performed phenotypic characterization and RNA measurements. M.A.K. wrote scripts for automated colony counting and fluorescence measurement. C.G. performed SBEM imaging. R.S. performed FRAP experiments. Y.S. performed ChIP experiments. M.B. obtained funding and oversaw the study. M.B. and D.O. wrote the manuscript.

ACKNOWLEDGMENTS

We thank Prof. Henning Stahlberg (C-CINA, Biozentrum, University of Basel) for sharing equipment and Jens Tyedmers for sharing reagents and for valuable discussions. We are grateful to Christopher Bleck for help with EM sample preparation, to Hans-Rudolf Hotz for bioinformatics support, to Wanda Kukulski for technical advices on CLEM, and to Kirsten Jacobeit for library preparation. This work was supported by funds from the European Research Council (280410). The Friedrich Miescher Institute for Biomedical Research is supported by the Novartis Research Foundation.

Received: August 18, 2014
Revised: November 6, 2014
Accepted: December 2, 2014
Published: December 24, 2014

REFERENCES

Alberti, S., Halfmann, R., King, O., Kapila, A., and Lindquist, S. (2009). A systematic survey identifies prions and illuminates sequence features of prionogenic proteins. Cell *137*, 146–158.

Allshire, R.C. (1995). Elements of chromosome structure and function in fission yeast. Semin. Cell Biol. *6*, 55–64.

Allshire, R.C., Javerzat, J.P., Redhead, N.J., and Cranston, G. (1994). Position effect variegation at fission yeast centromeres. Cell *76*, 157–169.

Anderson, P., and Kedersha, N. (2006). RNA granules. J. Cell Biol. *172*, 803–808.

Barraud, P., Emmerth, S., Shimada, Y., Hotz, H.-R., Allain, F.H.-T., and Bühler, M. (2011). An extended dsRBD with a novel zinc-binding motif mediates nuclear retention of fission yeast Dicer. EMBO J. *30*, 4223–4235.

Brandman, O., and Meyer, T. (2008). Feedback loops shape cellular signals in space and time. Science *322*, 390–395.

Bühler, M., Verdel, A., and Moazed, D. (2006). Tethering RITS to a nascent transcript initiates RNAi- and heterochromatin-dependent gene silencing. Cell *125*, 873–886.

Castel, S.E., and Martienssen, R.A. (2013). RNA interference in the nucleus: roles for small RNAs in transcription, epigenetics and beyond. Nat. Rev. Genet. *14*, 100–112.

Chernoff, Y.O., Lindquist, S.L., Ono, B., Inge-Vechtomov, S.G., and Liebman, S.W. (1995). Role of the chaperone protein Hsp104 in propagation of the yeast prion-like factor [psi+]. Science *268*, 880–884.

Chikashige, Y., Kinoshita, N., Nakaseko, Y., Matsumoto, T., Murakami, S., Niwa, O., and Yanagida, M. (1989). Composite motifs and repeat symmetry in S. pombe centromeres: direct analysis by integration of NotI restriction sites. Cell *57*, 739–751.

Denk, W., and Horstmann, H. (2004). Serial block-face scanning electron microscopy to reconstruct three-dimensional tissue nanostructure. PLoS Biol. *2*, e329.

DeSantis, M.E., Leung, E.H., Sweeny, E.A., Jackrel, M.E., Cushman-Nick, M., Neuhaus-Follini, A., Vashist, S., Sochor, M.A., Knight, M.N., and Shorter, J. (2012). Operational plasticity enables hsp104 to disaggregate diverse amyloid and nonamyloid clients. Cell *151*, 778–793.

Doyle, S.M., Genest, O., and Wickner, S. (2013). Protein rescue from aggregates by powerful molecular chaperone machines. Nat. Rev. Mol. Cell Biol. *14*, 617–629.

Dunand-Sauthier, I., Walker, C., Wilkinson, C., Gordon, C., Crane, R., Norbury, C., and Humphrey, T. (2002). Sum1, a component of the fission yeast eIF3 translation initiation complex, is rapidly relocalized during environmental stress and interacts with components of the 26S proteasome. Mol. Biol. Cell *13*, 1626–1640.

Ekwall, K., Cranston, G., and Allshire, R.C. (1999). Fission yeast mutants that alleviate transcriptional silencing in centromeric flanking repeats and disrupt chromosome segregation. Genetics *153*, 1153–1169.

Emmerth, S., Schober, H., Gaidatzis, D., Roloff, T., Jacobeit, K., and Bühler, M. (2010). Nuclear retention of fission yeast dicer is a prerequisite for RNAi-mediated heterochromatin assembly. Dev. Cell *18*, 102–113.

Escusa-Toret, S., Vonk, W.I.M., and Frydman, J. (2013). Spatial sequestration of misfolded proteins by a dynamic chaperone pathway enhances cellular fitness during stress. Nat. Cell Biol. *15*, 1231–1243.

Espinosa Angarica, V., Ventura, S., and Sancho, J. (2013). Discovering putative prion sequences in complete proteomes using probabilistic representations of Q/N-rich domains. BMC Genomics *14*, 316.

Feil, R., and Fraga, M.F. (2011). Epigenetics and the environment: emerging patterns and implications. Nat. Rev. Genet. *13*, 97–109.

Fraga, M.F., Ballestar, E., Paz, M.F., Ropero, S., Setien, F., Ballestar, M.L., Heine-Suñer, D., Cigudosa, J.C., Urioste, M., Benitez, J., et al. (2005). Epigenetic differences arise during the lifetime of monozygotic twins. Proc. Natl. Acad. Sci. USA *102*, 10604–10609.

Fraser, P.E. (2014). Prions and prion-like proteins. J. Biol. Chem. *289*, 19839–19840.

Fujita, K., Kawai, R., Iwahashi, H., and Komatsu, Y. (1998). Hsp104 responds to heat and oxidative stress with different intracellular localization in Saccharomyces cerevisiae. Biochem. Biophys. Res. Commun. *248*, 542–547.

Glover, J.R., and Lindquist, S. (1998). Hsp104, Hsp70, and Hsp40: a novel chaperone system that rescues previously aggregated proteins. Cell *94*, 73–82.

Goldberg, A.L. (2003). Protein degradation and protection against misfolded or damaged proteins. Nature *426*, 895–899.

Gottschling, D.E. (2004). Summary: epigenetics—from phenomenon to field. Cold Spring Harb. Symp. Quant. Biol. *69*, 507–519.

Grossniklaus, U., Kelly, W.G., Ferguson-Smith, A.C., Pembrey, M., and Lindquist, S. (2013). Transgenerational epigenetic inheritance: how important is it? Nat. Rev. Genet. *14*, 228–235.

Halliday, M., Radford, H., and Mallucci, G.R. (2014). Prions: generation and spread versus neurotoxicity. J. Biol. Chem. *289*, 19862–19868.

Harrison, L.B., Yu, Z., Stajich, J.E., Dietrich, F.S., and Harrison, P.M. (2007). Evolution of budding yeast prion-determinant sequences across diverse fungi. J. Mol. Biol. *368*, 273–282.

Holoch, D., and Moazed, D. (2012). RNAi in fission yeast finds new targets and new ways of targeting at the nuclear periphery. Genes Dev. *26*, 741–745.

Iida, T., Nakayama, J., and Moazed, D. (2008). siRNA-mediated heterochromatin establishment requires HP1 and is associated with antisense transcription. Mol. Cell *31*, 178–189.

Kaganovich, D., Kopito, R., and Frydman, J. (2008). Misfolded proteins partition between two distinct quality control compartments. Nature *454*, 1088–1095.

Kawai, R., Fujita, K., Iwahashi, H., and Komatsu, Y. (1999). Direct evidence for the intracellular localization of Hsp104 in Saccharomyces cerevisiae by immunoelectron microscopy. Cell Stress Chaperones *4*, 46–53.

Kimura, H., Hayashi-Takanaka, Y., Goto, Y., Takizawa, N., and Nozaki, N. (2008). The organization of histone H3 modifications as revealed by a panel of specific monoclonal antibodies. Cell Struct. Funct. *33*, 61–73.

Kloc, A., Zaratiegui, M., Nora, E., and Martienssen, R. (2008). RNA interference guides histone modification during the S phase of chromosomal replication. Curr. Biol. *18*, 490–495.

Kon, N., Krawchuk, M.D., Warren, B.G., Smith, G.R., and Wahls, W.P. (1997). Transcription factor Mts1/Mts2 (Atf1/Pcr1, Gad7/Pcr1) activates the M26 meiotic recombination hotspot in Schizosaccharomyces pombe. Proc. Natl. Acad. Sci. USA *94*, 13765–13770.

Kukulski, W., Schorb, M., Welsch, S., Picco, A., Kaksonen, M., and Briggs, J.A.G. (2011). Correlated fluorescence and 3D electron microscopy with high sensitivity and spatial precision. J. Cell Biol. *192*, 111–119.

Lawrence, C.L., Maekawa, H., Worthington, J.L., Reiter, W., Wilkinson, C.R.M., and Jones, N. (2007). Regulation of Schizosaccharomyces pombe Atf1 protein levels by Sty1-mediated phosphorylation and heterodimerization with Pcr1. J. Biol. Chem. *282*, 5160–5170.

Micheva, K.D., and Smith, S.J. (2007). Array tomography: a new tool for imaging the molecular architecture and ultrastructure of neural circuits. Neuron *55*, 25–36.

Moazed, D. (2011). Mechanisms for the inheritance of chromatin states. Cell *146*, 510–518.

Mollet, S., Cougot, N., Wilczynska, A., Dautry, F., Kress, M., Bertrand, E., and Weil, D. (2008). Translationally repressed mRNA transiently cycles through stress granules during stress. Mol. Biol. Cell *19*, 4469–4479.

Parsell, D.A., Kowal, A.S., Singer, M.A., and Lindquist, S. (1994). Protein disaggregation mediated by heat-shock protein Hsp104. Nature *372*, 475–478.

Prusiner, S.B. (2012). Cell biology. A unifying role for prions in neurodegenerative diseases. Science *336*, 1511–1513.

Ptashne, M. (2013). Epigenetics: core misconcept. Proc. Natl. Acad. Sci. USA *110*, 7101–7103.

Reidy, M., Sharma, R., and Masison, D.C. (2013). Schizosaccharomyces pombe disaggregation machinery chaperones support Saccharomyces cerevisiae growth and prion propagation. Eukaryot. Cell *12*, 739–745.

Sanchez, Y., and Lindquist, S.L. (1990). HSP104 required for induced thermotolerance. Science *248*, 1112–1115.

Seong, K.-H., Li, D., Shimizu, H., Nakamura, R., and Ishii, S. (2011). Inheritance of stress-induced, ATF-2-dependent epigenetic change. Cell *145*, 1049–1061.

Shorter, J., and Lindquist, S. (2004). Hsp104 catalyzes formation and elimination of self-replicating Sup35 prion conformers. Science *304*, 1793–1797.

Shorter, J., and Lindquist, S. (2005). Prions as adaptive conduits of memory and inheritance. Nat. Rev. Genet. *6*, 435–450.

Song, J., Irwin, J., and Dean, C. (2013). Remembering the prolonged cold of winter. Curr. Biol. *23*, R807–R811.

Tessier, P.M., and Lindquist, S. (2009). Unraveling infectious structures, strain variants and species barriers for the yeast prion [PSI+]. Nat. Struct. Mol. Biol. *16*, 598–605.

Toombs, J.A., Petri, M., Paul, K.R., Kan, G.Y., Ben-Hur, A., and Ross, E.D. (2012). De novo design of synthetic prion domains. Proc. Natl. Acad. Sci. USA *109*, 6519–6524.

Tyedmers, J., Mogk, A., and Bukau, B. (2010a). Cellular strategies for controlling protein aggregation. Nat. Rev. Mol. Cell Biol. *11*, 777–788.

Tyedmers, J., Treusch, S., Dong, J., McCaffery, J.M., Bevis, B., and Lindquist, S. (2010b). Prion induction involves an ancient system for the sequestration of aggregated proteins and heritable changes in prion fragmentation. Proc. Natl. Acad. Sci. USA *107*, 8633–8638.

Vashist, S., Cushman, M., and Shorter, J. (2010). Applying Hsp104 to protein-misfolding disorders. Biochem. Cell Biol. *88*, 1–13.

Volpe, T.A., Kidner, C., Hall, I.M., Teng, G., Grewal, S.I.S., and Martienssen, R.A. (2002). Regulation of heterochromatic silencing and histone H3 lysine-9 methylation by RNAi. Science *297*, 1833–1837.

Volpe, T., Schramke, V., Hamilton, G.L., White, S.A., Teng, G., Martienssen, R.A., and Allshire, R.C. (2003). RNA interference is required for normal centromere function in fission yeast. Chromosome Res. *11*, 137–146.

Wong, C.C.Y., Caspi, A., Williams, B., Craig, I.W., Houts, R., Ambler, A., Moffitt, T.E., and Mill, J. (2010). A longitudinal study of epigenetic variation in twins. Epigenetics *5*, 516–526.

Woolcock, K.J., Gaidatzis, D., Punga, T., and Bühler, M. (2011). Dicer associates with chromatin to repress genome activity in Schizosaccharomyces pombe. Nat. Struct. Mol. Biol. *18*, 94–99.

Woolcock, K.J., Stunnenberg, R., Gaidatzis, D., Hotz, H.-R., Emmerth, S., Barraud, P., and Bühler, M. (2012). RNAi keeps Atf1-bound stress response genes in check at nuclear pores. Genes Dev. *26*, 683–692.

Cell Reports, Volume *10*

Supplemental Information

Dicer and Hsp104 Function in a Negative Feedback Loop to Confer Robustness to Environmental Stress

Daniele Oberti, Adriano Biasini, Moritz Alexander Kirschmann, Christel Genoud, Rieka Stunnenberg, Yukiko Shimada, and Marc Bühler

Supplemental Figures

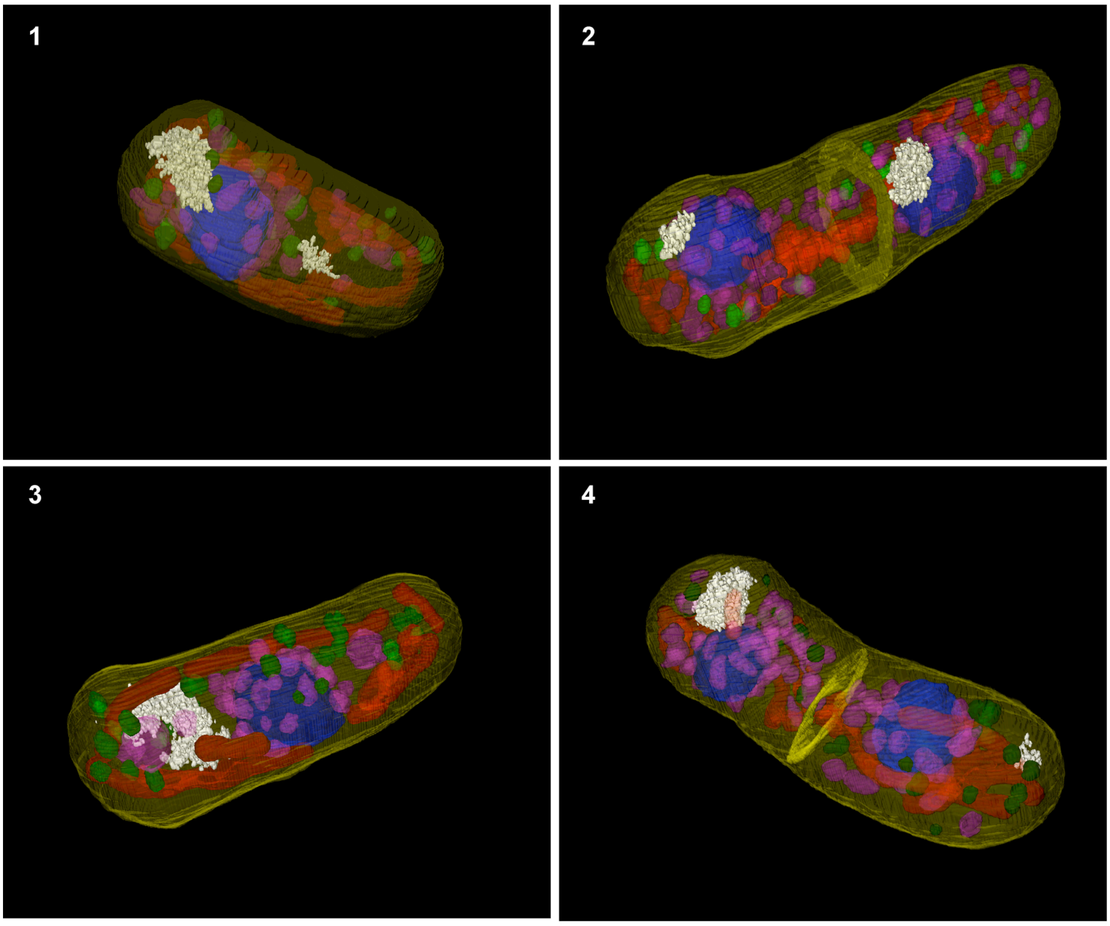

Volumes (μm^3)	**Cell 1**	**Cell 2**	**Cell 3**	**Cell 4**
Cell (yellow)	119.50	181.08	148.67	150.47
Nucleus (blue)	9.55	7.85/7.36	12.35	6.58/6.42
Mitochondria (red)	5.79	7.87	6.98	7.07
Electron-dense vesicles (pink)	3.83	6.03	5.59	6.33
Electron-light vesicles (green)	1.43	0.97	1.88	1.25
Large aggregate (white)	0.84	0.64	1.19	0.86
Small aggregate (white)	0.10	0.09	-	0.05

Figure S1. 3D-reconstruction of *S. pombe* cells with SBEM. Related to Figure 3. 3D-reconstruction based on SBEM imaging. Volumes were measured with TrakEM (Fiji). White: electron-dense inclusions; blue: nucleus; red: mitochrondria; pink and green: vesicles.

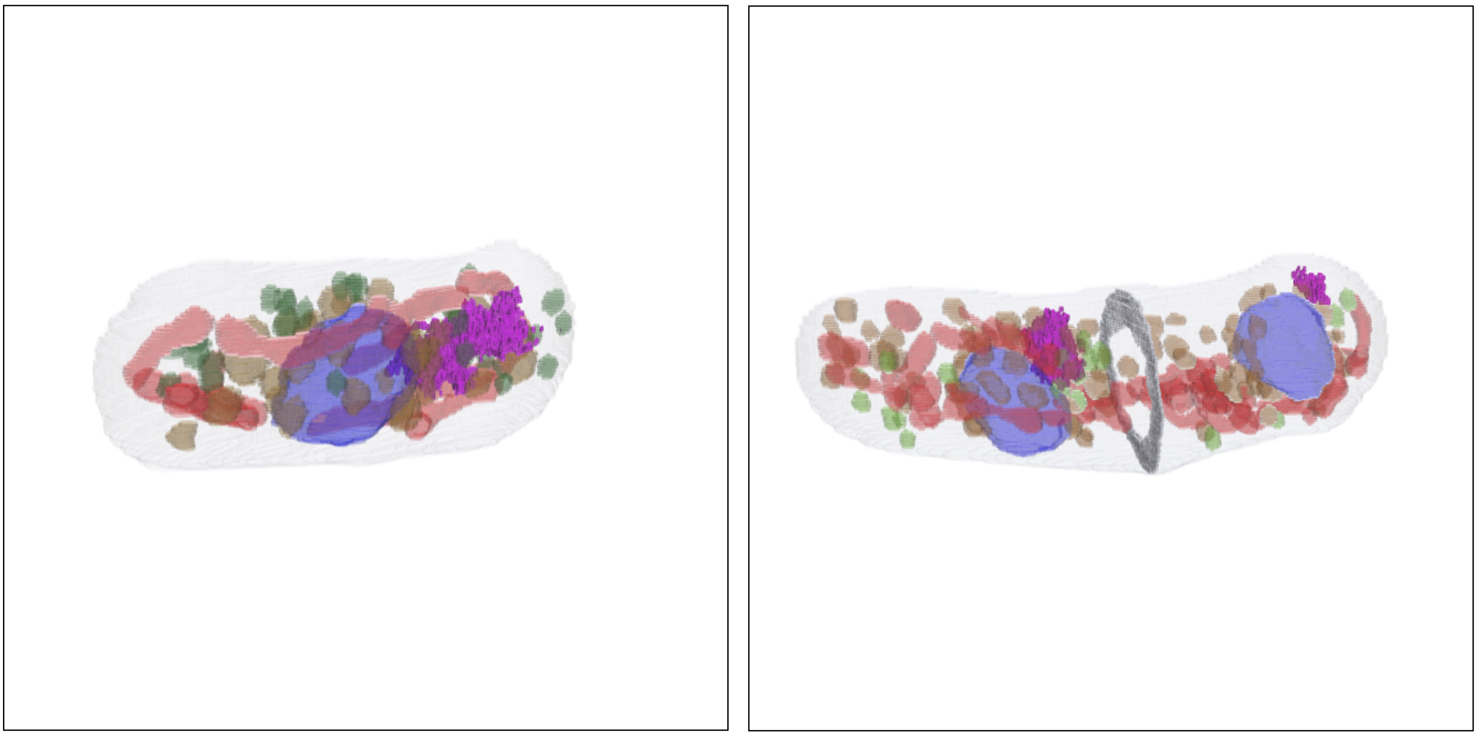

Figure S2. 3D models of S. pombe cells. Related to Figure 3.
Interactive models of S. pombe cells, viewable with Adobe Acrobat (version 7 or above).
To visualize, click once on the boxes below. Click on “View” on the appearing menu bar for preset views, or click and drag on the model to navigate it. Individual structures can be selected under “Views” menu.
Compatibilty: the models are embedded in U3D format and can be visualized with
Adobe Acrobat (version 7 or later).

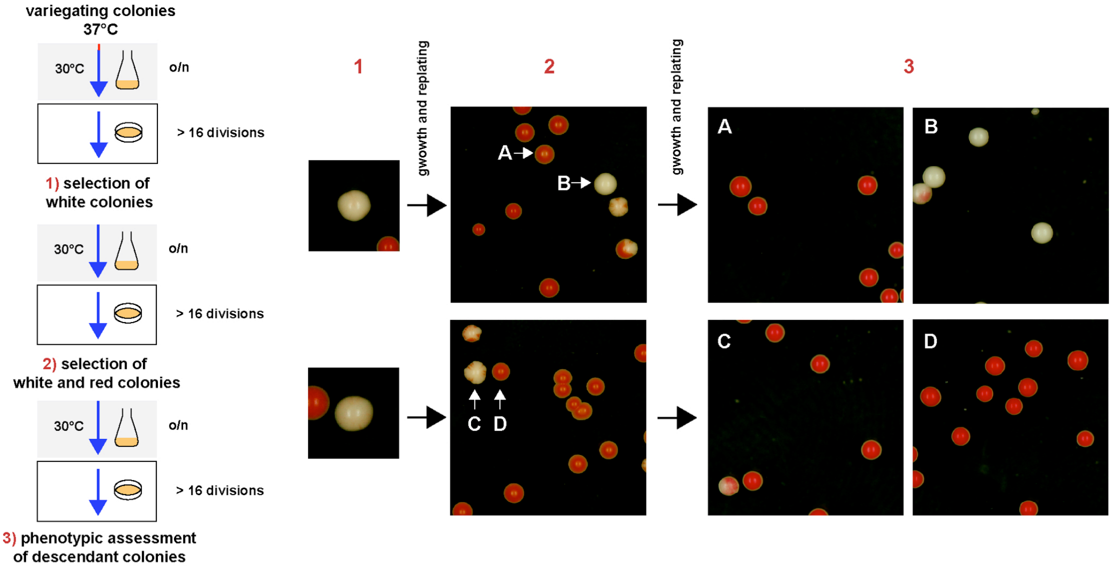
variegating colonies
37°C
30°C
o/n
> 16 divisions
1) selection of white colonies
30°C
o/n
> 16 divisions
2) selection of white and red colonies
30°C
o/n
> 16 divisions
3) phenotypic assessment of descendant colonies
1
gwowth and replating
2
A
B
C
D
gwowth and replating
3
A
B
C
D

Figure S3. Reestablishment of centromeric silencing from variegating phenotype. Related to Figure 6.
Variegating colonies were plates, white colonies selected, grown in liquid culture and plated. White and red colonies were grown further in liquid culture, plated and the phenotype was assessed.

Movie S1. 3D-reconstruction of *S. pombe* cell with SBEM. Related to Figure 3.
3D-reconstruction based on SBEM imaging. Magenta: electron-dense inclusions; blue: nucleus; red: mitochrondria; orange and green: vesicles.

Movie S2. 3D-reconstruction of mitotic *S. pombe* cell with SBEM. Related to Figure 3.
3D-reconstruction based on SBEM imaging. Magenta: electron-dense inclusions; blue: nucleus; red: mitochrondria; orange and green: vesicles; grey: septum.

Supplemental Tables

Table S1. Plasmids used in the study. Related to Experimental Procedures.
This table contains the plasmids used in the study, their name and source.

Name	Common name	
pMB1465	pRS304-GPD-NMGFP	1
pMB1468	pJR1-p3nmt1-PD-GFP	2
pMB1470	pJR1-p3nmt1-GFP	2

1. kind gift from Jens Tyedmers, used to generate pMB1468 and pMB1470
2: generated in this study

Table S2. Strains used in the study. Related to Experimental Procedures. This table contains the strains used in the study, their genotype and source.

Strain	Genotype	Source
SPB65	*972h-*	2
SPB70	*h- leu1-32 ade6-M210*	3
SPB80	*h+ imr1R(Nco1)::ura4+ leu1-32 ura4-D18 ori1 ade6-216*	3
SPB75	*h+ otr1R(SphI)::ade6+ ura4-D18 leu1-32 ade6-M210*	4
SPB309	*h+ imr1R(Nco1)::ura4+ leu1-32 ura4-D18 ori1 ade6-216 dcr1-WQI-D937A-D1127A::nat*	3
SPB1844	*h+ ade6-210 leu1-32 ura4-D18 TM1(ura4-)::ade6*	5
SPB74	*h+ otr1R(SphI)::ura4+ ura4-DS/E leu1-32 ade6-M210*	4
SPB94	*h+ otr1R(SphI)::ura4+ ura4-DS/E leu1-32 ade6-M210 dcr1Δ::nat*	3
SPB1672	*h+ otr1R(SphI)::ura4+ ura4-DS/E leu1-32 ade6-M210 kan-nmt1(3x)-GFP::dcr1 pabp::mCherry-hph*	1
SPB1673	*h+ otr1R(SphI)::ura4+ ura4-DS/E leu1-32 ade6-M210 kan-nmt1(3x)-GFP::dcr1 dcp2::mCherry-hph*	1
SPB0451	*imr1R::GFP-nat , GFP-lacI, nup107+::GFP-kan, kan-nmt1(3x)-mCherry::dcr1+*	1
SPB1458	h+ *otr1R(SphI)::ura4+ ura4-DS/E leu1-32 ade6-M210 atf31Δ::kan dcr1Δ::nat*	1
SPB1671	*h+ otr1R(SphI)::ura4+ ura4-DS/E leu1-32 ade6-M210 kan-nmt1(3x)-GFP::dcr1 hsp104::mCherry-hph*	1
SPB278	*h+ imr1R(Nco1)::ura4+ leu1-32 ura4-D18 ori1 ade6-216 kan-nmt1(3x)-GFP::dcr1*	1
SPB1470	*h+ imr1R(Nco1)::ura4+ leu1-32 ura4-D18 ori1 ade6-216 kan-nmt1(3x)-GFP::dcr1 hsp104Δ::hphMx*	1
SPB1729	*h+ otr1R(SphI)::ade6+ ura4-D18 leu1-32 ade6-M210 hsp104Δ::kan*	1
SPB1730	*h+ otr1R(SphI)::ade6+ ura4-D18 leu1-32 ade6-M210 dcr1Δ::nat*	1
SPB2189	*h+ otr1R(SphI)::ura4+ ura4-DS/E leu1-32 ade6-M210 hsp104::mCherry-kan*	1
SPB2217	*h+ otr1R(SphI)::ura4+ ura4-DS/E leu1-32 ade6-M210 hsp104::mCherry-kan dcr1Δ::nat*	1

1= this study/Bühler lab; 2 = Charles Hoffman; 3= Danesh Moazed, 4 = Karl Ekwall, 5 = Robin Allshire

Table S3. Oligos used in this study. Related to Experimental Procedures. This table contains the oligos used in the study and their sequence.

Name	Sequence
cendg for	AAGGAATGTGCCTCGTCAAATT
cendg rev	TGCTTCACGGTATTTTTTGAAATC
cendh for	GTATTTGGATTCCATCGGTACTATGG
cendh rev	ACTACATCGACACAGAAAAGAAAACAA
ade6 for	CTTCACTCTATTGTTCAGATGCC
ade6 rev	CGACAGGCTAAAATACCGGC
act for	TCCTCATGCTATCATGCGTCTT
act rev	CCACGCTCCATGAGAATCTTC
hsp104 for	CGTGAATCTCAGCCCGAAGT
hsp104 rev	TCAACGCGGAGTTGTCGAA
adh1 for	TCCGTTCCCCTCGAGGTT
adh1 rev	TCAAGGCACGATAGCAAGTGA

Extended Experimental Procedures

Strains and plasmids

Fission yeast strains used in this study are listed in Table S2 and were grown at 30°C in YES unless specified differently. All strains were constructed using a standard PCR-based protocol (Bähler et al., 1998). Constructs in yeast strains were confirmed by sequencing. Plasmids are listed in Table S1.

Silencing assays

Serial 10-fold dilutions of the strains indicated were plated on YES or YE plates and grown at the temperatures indicated. To score phenotype of individual colonies, 250-500 cells/plate were plated. All colonies were automatically segmented based on the circular shape of the colonies, via circular Hough transforms, by a Matlab script (MATLAB Release 2013b, The MathWorks, Inc.) The resulting segmentations were confirmed and the variegating colonies were counted manually.

RNA isolation and cDNA synthesis

RNA isolation, cDNA synthesis, and quantitative RT-PCR were performed as previously described (Emmerth et al., 2010). Cells were harvested at OD600=0.5, washed once with water, and flash frozen in liquid nitrogen. RNA isolation was performed with the Absolutely RNA Miniprep Kit (Agilent) with the following modification: 600 µl lysis buffer, 4.2 µl Mercaptoethanol were added to the cells which were bead-beaten with 500 µl glass beads for 1 min. RNA isolation was performed according to the supplier's protocol. cDNA was synthesized with the AffinityScript MultipleTemperature cDNA Synthesis Kit (Agilent) using random primers.

Quantitative RT-PCR

Quantitative PCR was performed on a Bio-Rad CFX96 Real-Time System using the Fast SYBR Green Master Mix as described in (Keller et al., 2012). Relative RNA levels were normalized to the mRNA levels indicated in the figures. Primers pairs used for PCR reactions are listed in Table S3.

Generation of small RNA libraries for high-throughput sequencing

Total RNA was isolated from exponentially growing cells using the hot phenol method (Leeds et al., 1991). Small RNA was enriched using the RNeasy Midi kit (Qiagen) following the RNA cleanup protocol. 18-28-nt sRNAs were separated by 17.5% PAGE. Libraries were generated using the Illumina TruSeqTM small RNA preparation protocol (Cat.# RS-930-1012). The 145- to 160-nt population was isolated and the library sequenced on an Illumina HiSeq2000. Small RNA reads were mapped as previously described

(Emmerth et al., 2010) with two mismatches allowed. siRNAs were defined as reads with a decrease in number of at least 8 fold between *wt* cells and *dcr*Δ cells.

ChIP

ChIP experiments were performed as described in (Keller et al., 2012) with minor modifications. Shortly, after fixation of *S. pombe* cells with 1% formaldehyde for 15 min, they were lysed in buffer containing 50 mM HEPES/KOH, pH 7.5, 140 mM NaCl, 1 mM EDTA, 1% Triton X-100, 0.1% Na deoxycholate, 1 mM PMSF and protease-inhibitor cocktail. Chromatin was sheared with a Bioruptor (Diagenode). An histone H3K9me2-specific mouse monoclonal antibody from Wako (clone no. MABI0307) was used.

CLEM

Cells were prepared similar to (Kukulski et al., 2011). Yeast cells were grown to log phase and high-pressure frozen with a Leica EM PACT2. Freeze substitution was done at -90°C for 48h with 0.1% (wt/vol) uranyl acetate in acetone. Temperature was subsequently increased to -45°C (5°C/h) and after washing with acetone the samples were infiltrated with increasing concentrations of Lowicryl HM20 resin in acetone (10, 20, 50, and 75%, 4 h each). After infiltrating 3 times with 100% HM20 for 10 h each time, the samples were UV polymerized at -25°C for 48 h, after which temperature was raised to 20°C (5°C/h). 100-200 nm sections were cut with a ultramicrotome (Leica EM UC7) and mounted on carbon coated grids. Sections were imaged with an AxioImager M microscope with a Yokogawa CSU-22 spinning disk and a transmission electron microscope (Philips CM10). Correlation was done with TrakEM package in Fiji software and further processed with Adobe Photoshop CS5 for visualization.

SBEM

10 ml of exponentially growing cells were fixed with 2% glutaraldehyde in 0.1M sodium phosphate buffer (pH7.0) overnight at 4°C. After washing with buffer, the cell wall was digested by respuspending in 2 ml 0.1M potassium phosphate, 1M Sorbitol and 0.25 mg Zymolase for 30 min at 30°C. They were then stained following a modified version of the rOTO NCMIR protocol (http://www.ncmir.ucsd.edu/sbfsem-protocol.pdf). They were rinsed 3x 5 min with 0.1M Na-cacodylate buffer pH 7.4 and postfixed with 1.5% potassium ferrocyanide and 1% osmium tetroxide in 0.1M Na-cacodylate buffer for 30 min. After 5 rinses in ddH2O, a solution of 1% thiocarbohydrazide in ddH2O was applied for 20 min. After thoroughly rinsing in ddH20, yeasts were stained for 30 min in 1% osmium tetroxide in ddH2O. To enhance contrast, after 5 rinses in ddH2O, they were stained *en bloc* with 1% aqueous uranyl acetate overnight. After rinsing, yeasts were stained for 20 min in Walton's lead aspartate at 60°C. Yeast were then dehydrated by successive steps in 30%, 50%, 70%, 90%, 95% and 100% ethanol, and then were embedded in Eppendorf tubes in Embed812 resin (EMS). After removal of the Eppendorf tube, a piece of the embedded pellet (approx. 1 cubic mm) was cut out of the block and glued with cyanoacrylate glue on a 3View stub (GATAN Inc, Pleasanton USA). The block was trimmed in a trapezoid shape and a layer of approx. 12 nm of gold/palladium was sputtered on the surface. After being

placed in the 3View (GATAN Inc, Pleasanton, USA) inside a scanning electron microscopy QUANTA FEG200 (FEI, Endhoven, the Netherlands), series of images were acquired at 5kV with 0.33 Torr of water pressure. Images of 5000 x 5000 pixels were acquired at 7 nm/pixel and 6 microseconds/pixel. After each image, 60 nm were cut from the surface of the block by a diamond knife and the new surface was scanned again. The cycle was repeated to obtain a stack of images allowing to visualize a volume at ultrastructural level (voxel of 6x6x60 nm). Images were finally registered using TrakEM (Fiji).

Live fluorescence microscopy

S. pombe precultures were grown in filtered YES for 8 h at 30°C, diluted and grown again overnight to log phase at 30°C. Depending on the experiments, cultures were further shifted to 37°C. For microscopy, cells were spread on agarose patches containing YES medium with 3% glucose. Images were acquired with a AxioImager M1 microscope with Yokogawa CSU-22 spinning disk. For time-lapse experiments measuring the intensity of Dcr1 foci, cells were kept in culture and aliquots were taken at different time points. Intensity values were measured by summing intensity of pixels within foci in a sum projection with ImageJ. For volume measurement of the foci, cells were imaged in the same way and volume was measured with ImageJ from z-stacks. Whole-cell fluorescence quantifications were calculated from summed intensity z-projections of z-stacks. The resulting images were segmented with the supervised machine-learning Software Ilastik into cells, background and background-around-cells. The following quantifications were calculated by a custom Imagej script. False-positive cell segments were removed by size filtering. The segments being background-around-cells were omitted from the intensity quantifications to avoid bias from stray fluorescence. Of all remaining cell segments the mean fluorescence intensities were measured and the mean image background intensity was subtracted.

Fluorescence Recovery After Photobleaching (FRAP)

For whole-cell bleaching experiments, the microscope was preheated to 37°C, cells mounted on a Ludin chamber coated with Lectin (BS-I, Sigma) and bleached twice for 10 ms with 473nm laser and imaged at different time points with an Olympus IX81 equipped with Yokogawa CSU-X1 spinning disk. Cycloheximide was added at a concentration of 100 µg/ml during the last 30 min of heat treatment and at the same concentration to fresh medium during imaging. For Dcr-1 foci bleaching experiments, cells were prepared similarly (but without the addition of cycloheximide) and foci were bleached once.

Immunofluorescence

Cells were treated with 15 mM Hydroxyurea for 4 h and released by washing twice with YES. After 2 h, cells were fixed with 3% formaldehyde and 0,2% glutaraldehyde for 90 min. Cell wall was digested with 1 mg/ml lysing enzyme from *Trichoderma harzianum* and 0.5 mg/ml Zymolyase. After permeabilization with 1% Triton, cells were incubated with anti-Tat1 antibody and 1% BSA o/n, washed three times and incubated for 4 h with AlexaFluor

564-conjugated secondary antibody. Cells were mounted in DAPI and imaged with a Zeiss Z1 microscope.

Prion induction

Cells transformed with plasmids (Table S1) were grown on PMG-leu plates at 30°C for 12 days and additional 3 days at 37°C. Phenotypes were assessed by imaging cells with a Zeiss Z1 microscope.

Supplemental Discussion

RNAi remains functional at elevated temperatures

It was previously proposed that the *S. pombe* RNAi pathway is suppressed at high temperatures but enhanced at low temperatures. This was based on the observation that levels of centromeric siRNAs in the temperature sensitive cell cycle mutant *cdc25-22* were higher at the permissive than at the restrictive temperature (Kloc et al., 2008). Two main observations made in our study demonstrate that the RNAi pathway is well functioning at elevated temperatures. Firstly, centromeric transcript levels dramatically increase in *dcr1*Δ cells at 37°C. Thus, the RNAi machinery is indispensable for heterochromatin silencing also at elevated temperatures. Secondly, we did not observe markedly different centromeric siRNA levels even when cells were incubated at 37°C for several days. Therefore, reduced levels of siRNAs observed by Kloc and colleagues cannot be explained by temperature-mediated suppression of RNAi, unless Hsp104 function was impaired in the respective cell cycle mutant strains. It will be interesting to further investigate whether reduced levels of centromeric siRNAs is a characteristic of temperature-sensitive cell cycle mutants that were used in previous studies (Chen et al., 2008; Kloc et al., 2008).

Supplemental References

Bähler, J., Wu, J.Q., Longtine, M.S., Shah, N.G., McKenzie, A., Steever, A.B., Wach, A., Philippsen, P., and Pringle, J.R. (1998). Heterologous modules for efficient and versatile PCR-based gene targeting in Schizosaccharomyces pombe. Yeast *14*, 943–951.

Bühler, M., Verdel, A., and Moazed, D. (2006). Tethering RITS to a nascent transcript initiates RNAi- and heterochromatin-dependent gene silencing. Cell *125*, 873–886.

Chen, E.S., Zhang, K., Nicolas, E., Cam, H.P., Zofall, M., and Grewal, S.I.S. (2008). Cell cycle control of centromeric repeat transcription and heterochromatin assembly. Nature *451*, 734–737.

Emmerth, S., Schober, H., Gaidatzis, D., Roloff, T., Jacobeit, K., and Bühler, M. (2010). Nuclear retention of fission yeast dicer is a prerequisite for RNAi-mediated heterochromatin assembly. Dev. Cell *18*, 102–113.

Keller, C., Adaixo, R., Stunnenberg, R., Woolcock, K.J., Hiller, S., and Bühler, M. (2012). HP1(Swi6) Mediates the Recognition and Destruction of Heterochromatic RNA Transcripts. Mol. Cell 215–227.

Kimura, H., Hayashi-Takanaka, Y., Goto, Y., Takizawa, N., and Nozaki, N. (2008). The organization of histone H3 modifications as revealed by a panel of specific monoclonal antibodies. Cell Struct. Funct. *33*, 61–73.

Kloc, A., Zaratiegui, M., Nora, E., and Martienssen, R. (2008). RNA interference guides histone modification during the S phase of chromosomal replication. Curr. Biol. *18*, 490–495.

Kukulski, W., Schorb, M., Welsch, S., Picco, A., Kaksonen, M., and Briggs, J.A.G. (2011). Correlated fluorescence and 3D electron microscopy with high sensitivity and spatial precision. J. Cell Biol. *192*, 111–119.

Leeds, P., Peltz, S.W., Jacobson, A., and Culbertson, M.R. (1991). The product of the yeast UPF1 gene is required for rapid turnover of mRNAs containing a premature translational termination codon. Genes Dev. *5*, 2303–2314.

Stunnenberg et al., 2015

EMBO Journal

Published online: October 5, 2015

Article

TRANSPARENT PROCESS

THE EMBO JOURNAL

H3K9 methylation extends across natural boundaries of heterochromatin in the absence of an HP1 protein

Rieka Stunnenberg[1,2], Raghavendran Kulasegaran-Shylini[1,†], Claudia Keller[1,2,‡], Moritz A Kirschmann[1,§], Laurent Gelman[1] & Marc Bühler[1,2,*]

Abstract

Proteins of the conserved HP1 family are elementary components of heterochromatin and are generally assumed to play a central role in the creation of a rigid, densely packed heterochromatic network that is inaccessible to the transcription machinery. Here, we demonstrate that the fission yeast HP1 protein Swi6 exists as a single highly dynamic population that rapidly exchanges *in cis* and *in trans* between different heterochromatic regions. Binding to methylated H3K9 or to heterochromatic RNA decelerates Swi6 mobility. We further show that Swi6 is largely dispensable to the maintenance of heterochromatin domains. In the absence of Swi6, H3K9 methylation levels are maintained by a mechanism that depends on polymeric self-association properties of Tas3, a subunit of the RNA-induced transcriptional silencing complex. Our results disclose a surprising role for Swi6 dimerization in demarcating constitutive heterochromatin from neighboring euchromatin. Thus, rather than promoting maintenance and spreading of heterochromatin, Swi6 appears to limit these processes and appropriately confine heterochromatin.

Keywords H3K9 methylation; heterochromatin; HP1 dynamics; Swi6; Tas3
Subject Categories Chromatin, Epigenetics, Genomics & Functional Genomics; Transcription
DOI 10.15252/embj.201591320 | Received 17 February 2015 | Revised 28 August 2015 | Accepted 3 September 2015

Introduction

Eukaryotic genomes are packaged into a complex structure known as chromatin. The basic unit of chromatin is the nucleosome, which consists of two copies each of the histone proteins H2A, H2B, H3, and H4. The flexible N-termini of histone proteins are subject to various posttranslational modifications associated with different types of chromatin. Originally defined cytologically as chromosome regions that do not undergo post-mitotic decondensation but remain condensed during interphase, a distinct type of chromatin referred to as heterochromatin is generally characterized by histone hypoacetylation and specific methylation of lysine 9 of the histone H3 tail (H3K9me). This mark is a binding site for proteins containing a so-called chromodomain (CD), such as proteins of the heterochromatin protein 1 (HP1) family that recognize and bind methylated H3K9 via their CDs (Eissenberg & Elgin, 2000; Bannister *et al*, 2001; Lachner *et al*, 2001).

HP1 proteins have long been thought to play a central role in the creation of a rigid, densely packed heterochromatic network that is inaccessible to the transcription machinery. However, several observations in the last decade have challenged this view (Buhler & Moazed, 2007; Grewal & Elgin, 2007). There have been numerous reports of low-level transcription of heterochromatic regions in various organisms (Rouleux-Bonnin *et al*, 1996, 2004; Lorite *et al*, 2002; Azzalin *et al*, 2007; Li *et al*, 2008; Pezer & Ugarkovic, 2008), and *Schizosaccharomyces pombe* mutants have been identified in which heterochromatic reporter genes are expressed without notable differences in H3K9 methylation or HP1 association (Buhler *et al*, 2007; Keller *et al*, 2012). Furthermore, genomewide studies of chromatin accessibility using *in vivo* methylation by the DNA adenine methyltransferase (Dam) in *C. elegans* showed only little variation (Sha *et al*, 2010), and DNA-binding factors seem to have normal access to repressed sites, even in highly compacted mitotic chromosomes (Verschure *et al*, 2003; Chen *et al*, 2005). Finally, fluorescence recovery after photobleaching (FRAP) experiments in mammalian and *S. pombe* cells revealed that HP1 proteins are mobile molecules (Cheutin *et al*, 2003, 2004; Festenstein *et al*, 2003). Previous kinetic modeling indicated the existence of at least two kinetically distinct populations of the *S. pombe* HP1 protein Swi6 in heterochromatin, arguing for a stochastic model of heterochromatin in which Swi6 acts not solely by forming static

---

1 Friedrich Miescher Institute for Biomedical Research, Basel, Switzerland
2 University of Basel, Basel, Switzerland
*Corresponding author. Tel: +41 61 696 04 38; E-mail: marc.buehler@fmi.ch
[†] Present address: Wellcome Trust Centre for Cell Biology, Institute of Cell Biology, School of Biological Sciences, The University of Edinburgh, Edinburgh, UK
[‡] Present address: Max Planck Institute of Immunobiology and Epigenetics, Freiburg, Germany
[§] Present address: Center for Microscopy and Image Analysis, University of Zurich, Zurich, Switzerland

© 2015 The Authors

Published online: October 5, 2015

oligomeric networks. These studies were performed in *swi6*Δ cells in which GFP-Swi6 was ectopically expressed under the control of a thiamine-repressible promoter (Cheutin *et al*, 2004). Whether Swi6 kinetics differ when Swi6 is expressed from its endogenous locus is not known.

In *S. pombe*, transcriptional activity within heterochromatin is particularly evident at pericentromeric repeat sequences, where RNA polymerase II is essential for RNA-interference (RNAi)-mediated assembly and silencing of heterochromatin (Volpe *et al*, 2002; Djupedal *et al*, 2005; Kato *et al*, 2005). Moreover, siRNAs homologous to centromeric sequences accumulate to relatively high levels (Reinhart & Bartel, 2002; Buhler *et al*, 2008; Halic & Moazed, 2010). A key factor for RNAi-mediated deposition of H3K9me2 is the RNA-induced transcriptional silencing (RITS) complex. RITS is composed of Tas3, the CD containing protein Chp1, and the siRNA-binding protein Ago1 (Verdel *et al*, 2004). Together with long chromatin-associated transcripts, RITS acts as a hub for the assembly of machineries that amplify heterochromatic siRNAs, modify histones, and silence gene expression (Holoch & Moazed, 2015). Besides centromeres, constitutive heterochromatin is also found at telomeres and the silent mating type locus in *S. pombe*. However, in contrast to centromeric heterochromatin, the RNAi machinery is dispensable to the maintenance of the repressed state at these regions (Jia *et al*, 2004; Kanoh *et al*, 2005). Instead, the non-canonical polyA-polymerase Cid14 and Swi6 are essential to the elimination of heterochromatic RNA transcripts (Buhler *et al*, 2007; Keller *et al*, 2010). We have recently demonstrated that Swi6 efficiently captures heterochromatic RNAs, which thereby become translationally incompetent and are eventually degraded. Importantly, RNA binding to the hinge region of Swi6 competes with methylated H3K9 for binding to the CD, predicting that Swi6 dynamics *in vivo* might be influenced by RNA (Keller *et al*, 2012).

The requirement for transcription in heterochromatin assembly seems difficult to reconcile with the silencing of heterochromatic genes. One possible solution to this paradox is the need for a pioneering round of transcription to initiate heterochromatin assembly. It has been suggested that Swi6 dissociates from chromatin due to H3S10 phosphorylation during M and S phase, opening up a window of opportunity for the transcription of centromeric repeats. Once assembled, transcription would be silenced by heterochromatin throughout the remainder of the cell cycle (Kloc & Martienssen, 2008). Consistent with this, RNA polymerase II occupancy on centromeric repeats is highest in S phase and transcripts corresponding to centromeric repeat sequences accumulate (Chen *et al*, 2008; Kloc *et al*, 2008). Alternatively, transcription could also occur outside S phase, with the resulting RNA immediately degraded co-transcriptionally (Buhler, 2009; Castel & Martienssen, 2013). However, such highly unstable RNA is difficult to demonstrate biochemically. Thus, although pericentromeric heterochromatin becomes more permissive to transcription in S phase (Chen *et al*, 2008), the actual transcriptional status of heterochromatin, particularly in the G2 phase of the *S. pombe* cell cycle when H3K9me2 levels are the highest, has remained elusive due to technical limitations.

Here, we demonstrate that Swi6 exists as a single dynamic population in constitutive heterochromatin when expressed from its endogenous locus, with little if any Swi6 molecules persistently bound to heterochromatin. Swi6 rapidly exchanges *in cis* and *in trans* between different heterochromatic regions and is not obligatory for the maintenance and spreading of H3K9 methylation. Instead, our results disclose an unexpected activity of Swi6 in demarcating constitutive heterochromatin from neighboring euchromatin. Our results support a model in which Swi6 dimer formation is important in counteracting the spread of H3K9 methylation, which is mediated by a mechanism that requires polymeric self-association properties of the Tas3 subunit of the RITS complex.

Results

Transient association of Swi6 with constitutive heterochromatin

Schizosaccharomyces pombe encodes two HP1 proteins, Chp2 and Swi6. We have previously shown that RNA binds to Swi6, involving the hinge, CD, and the N-terminus, which impedes binding of full-length Swi6 to an immobilized peptide corresponding to residues 1–20 of a K9 trimethylated histone H3 tail (Keller *et al*, 2012). To study the impact of Swi6-RNA interactions on Swi6 dynamics *in vivo*, we created an *S. pombe* strain in which the endogenous *swi6+* gene was tagged C-terminally with a codon-optimized EGFP tag (Sheff & Thorn, 2004) by homologous recombination. Importantly, the Swi6 and EGFP moieties were separated by a GDGAGLIN linker sequence, rendering the Swi6-EGFP fusion protein fully functional (Keller *et al*, 2013). Furthermore, Swi6-EGFP and endogenous Swi6 were expressed at similar levels within the cell (Fig EV1A and B). Thus, in contrast to previous kinetic measurements performed with N-terminally tagged and ectopically expressed, plasmid-borne GFP-Swi6 (Cheutin *et al*, 2004), our approach allowed us to assess heterochromatin dynamics under near physiological Swi6 expression conditions.

In fluorescence recovery after photobleaching (FRAP) experiments, a fluorescent region is irreversibly bleached by a short laser pulse and the recovery of the fluorescence signal measured over time (Carisey *et al*, 2011). We first performed FRAP on Swi6-EGFP heterochromatic loci in exponentially growing cells and acquired single focal plane images every 60 milliseconds (ms) (Fig 1A and Movie EV1). The bleached regions comprised centromeres, telomeres, or the mating type locus. For proteins bound tightly to chromatin, recovery kinetics are expected to be slow or not detectable, as observed for the telomere-binding protein Taz1 (Keller *et al*, 2012). The fluorescence signal for Swi6-EGFP, however, recovered within 3 s with an average half-recovery time ($t_{1/2}$) of 535 ms (Fig 1B and C). The recovery curve holding the average intensities of 31 FRAP experiments fits best to a one-component model ($y(x) = a(1 - \exp(-bx))$) with an R-squared value of 0.9964 (Fig 1B). Addition of a second component did not significantly improve the fit (Fig EV1D and E). Importantly, FRAP performed with cells that express Swi6-EGFP from a plasmid using the same conditions as Cheutin *et al* (0.4 μg/ml thiamine) resulted in a good fit to a two-component model with $t_{1/2}$ values of the individual components in a physiological range (Fig EV1F–H). These results imply the presence of one major population of Swi6 that binds heterochromatin highly dynamically if expressed from the endogenous locus.

To further test whether Swi6 exists in a single population or as two high- and low-mobility fractions (F_M and F_I, respectively), we

© 2015 The Authors

Published online: October 5, 2015

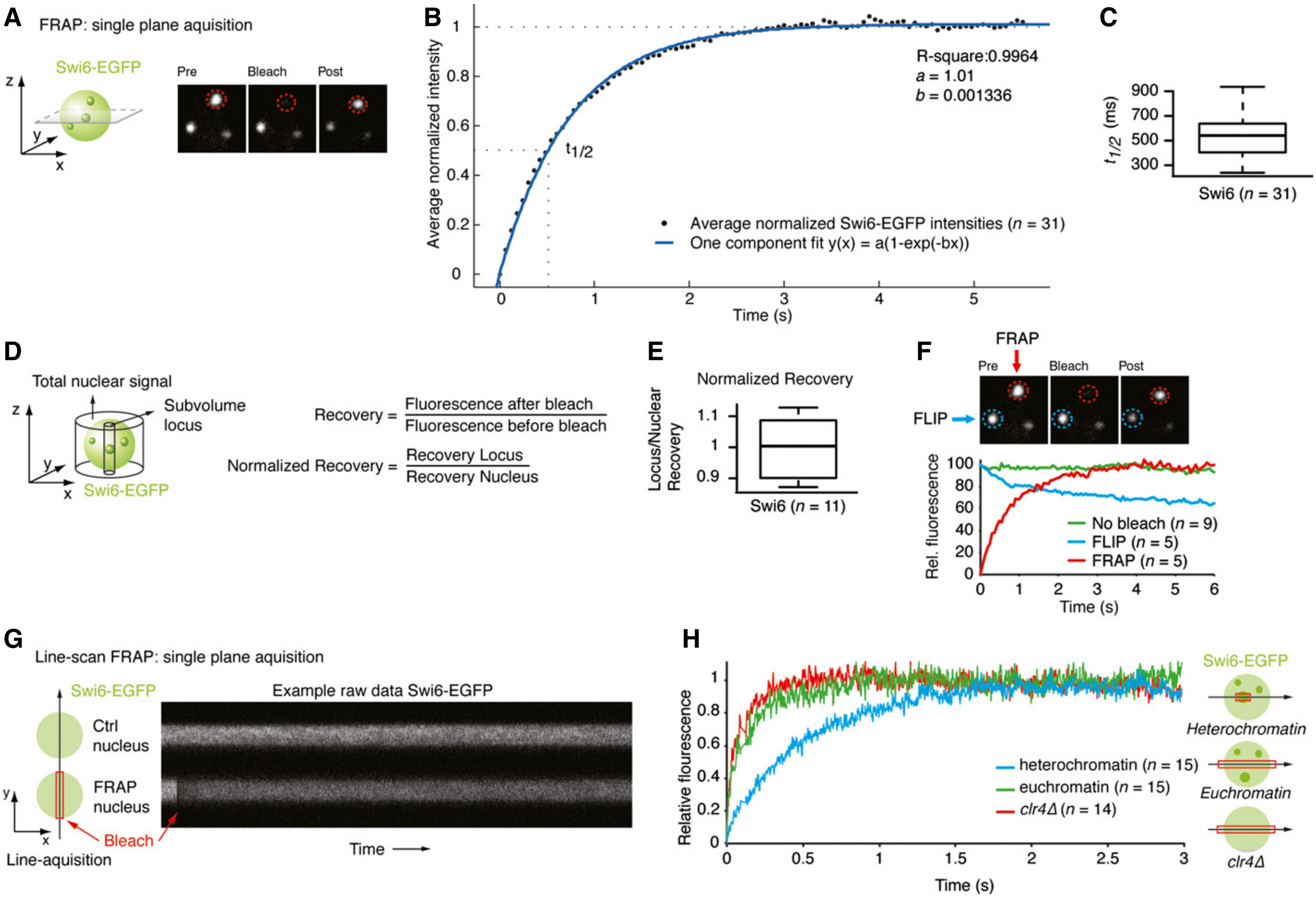

Figure 1. Swi6 is highly mobile.

- A Schematic of single-plane acquisition FRAP on endogenously tagged Swi6-EGFP. Representative still images of a FRAP experiment are shown. See also Movie EV1. Green sphere: yeast nucleus containing Swi6-EGFP; green dots: heterochromatic Swi6-EGFP; red circle: bleached area.
- B Normalized average intensities (black dots) of FRAP on Swi6-EGFP heterochromatic loci ($n = 31$) fitted to a one-component model (blue line). The dashed lines indicate the final relative intensity that is set to 1 and the fluorescence half-recovery time ($t_{1/2}$).
- C Fluorescence $t_{1/2}$ values of FRAP on Swi6-EGFP heterochromatic loci. The box bounds the interquartile range (IQR) divided by the median, and whiskers extend to a maximum of 1.5 × IQR beyond the box.
- D Schematic indicating the volumes measured to calculate the normalized fluorescence recovery of a locus relative to the entire nucleus.
- E Normalized fluorescence recovery values of FRAP on Swi6-EGFP heterochromatic loci. The box bounds the interquartile range (IQR) divided by the median, and whiskers extend to a maximum of 1.5 × IQR beyond the box.
- F FLIP experiment showing a bleached (FRAP, red circle) and unbleached, adjacent locus (FLIP, blue circle) in the same nucleus. The graph displays average relative fluorescence of FLIP (blue), FRAP (red), and control loci (no bleach, green) in other non-bleached cells.
- G Schematic of a line-scan FRAP experiment. Fluorescence intensities are measured along a line of a non-bleached nucleus (Ctrl nucleus) and a bleached nucleus (FRAP nucleus) in Swi6-EGFP *clr4Δ* cells. Red box: bleached region. Right: raw data example.
- H Average relative intensities of a line-scan FRAP experiment on Swi6-EGFP in heterochromatin (blue line), euchromatin (green line), and *clr4Δ* (red line). The curves have a gliding average of 40.

investigated percentage recovery after photobleaching. F_M is the proportion of bleached proteins replaced by unbleached proteins during the experiment. Thus, F_M at a given locus can be determined by dividing fluorescence intensity at the end of the time lapse (F_∞) by fluorescence intensity before the bleaching event (F_{initial}). If a second, static or low-mobility population of Swi6 existed, F_M should be less than 1. However, several experimental artifacts can bias estimation of this ratio and need to be taken into account for a precise determination of F_M. First, and consistent with a previous report, we observed that heterochromatin domains are highly mobile in *S. pombe* (Cheutin *et al*, 2004) and give a fainter signal when moving out of the focal plane. This leads to an underestimation of the total recovery if acquisition is made only at single focal planes (Fig EV1I–L). Second, because 20–35% of total fluorescence in the nucleus is lost when bleaching a single locus, the remaining fluorescence available for recovery must be evaluated. We therefore acquired stacks of the whole nucleus before photobleaching and after recovery and calculated the loss of total fluorescence in the whole nucleus to correct the F_M ratio (Fig 1D). This analysis revealed full recovery of the Swi6-EGFP signal by 3–4 s after photobleaching (Fig 1E), suggesting that there is no static or slow recovering population of Swi6 within heterochromatin.

© 2015 The Authors

Published online: October 5, 2015

In summary, Swi6-EGFP expressed from its endogenous locus manifests a single, highly dynamic population on heterochromatic domains with an average $t_{1/2}$ of 535 ms in exponentially growing cells. Although we cannot rule out the possibility that a small population of stably associated Swi6-EGFP molecules remained undetected in our analyses, our results demonstrate that the vast majority of Swi6 rapidly exchanges on heterochromatin.

Swi6 exchanges between independent heterochromatic domains

Swi6-EGFP is highly concentrated in two to six bright foci, with most of the cells containing three foci (Cheutin *et al*, 2004). The amount of Swi6-EGFP outside these foci is marginal. Hence, full recovery of fluorescence after photobleaching in these foci can only be explained if Swi6-EGFP exchanges between the different heterochromatin domains. Our experimental FRAP setup allowed us also to monitor fluorescence loss in photobleaching (FLIP) in the non-bleached heterochromatic foci. Photobleaching of one heterochromatic focus caused a significant loss of fluorescence in the non-bleached foci (Fig 1F), demonstrating that Swi6 does indeed rapidly exchange not only on heterochromatin *in cis* but also between heterochromatic domains *in trans*.

These results imply that Swi6 very rapidly transfers between heterochromatic domains via the nucleoplasm. Because our standard FRAP setup is limited to image acquisition rates of 1 per 60 ms, we switched to a high-speed confocal line-scan microscopy approach, allowing measurement of fluorescence intensities along a single line with a time resolution of ±2 ms (Fig 1G). The results revealed full fluorescence recovery in < 1 s, with an average $t_{1/2}$ of approximately 89 ms in non-heterochromatic areas of the nucleus (Fig 1H). Even faster Swi6-EGFP kinetics of approximately 49 ms were obtained by repeating the same experiments in cells lacking Clr4, the sole histone methyltransferase that methylates H3K9 in *S. pombe*. As expected, line-scan FRAP in heterochromatic loci revealed slower Swi6-EGFP kinetics than in the nucleoplasm or in *clr4Δ* cells (Fig 1H).

In summary, Swi6 is highly mobile throughout the nucleus, exchanging between different heterochromatic domains via the nucleoplasm. As expected for a heterochromatin-binding protein, Swi6 dynamics are influenced by H3K9 methylation.

Swi6 *in vivo* dynamics are slowed down by heterochromatic RNA

We previously demonstrated that the kinetic off-rate constant for dissociation of the Swi6-H3K9me3 complex *in vitro* is in the range of 10–1,000/s, corresponding to a lifetime of 1–100 ms (Keller *et al*, 2012). These data are consistent with the $t_{1/2}$ values obtained in our FRAP experiments. Importantly, Swi6-RNA and Swi6-H3K9me3 interactions are mutually exclusive *in vitro* and we therefore predicted that RNA influences Swi6 dynamics. To test this hypothesis, we performed FRAP experiments with cells expressing either wild-type Swi6 or Swi6 that does not bind RNA (NLS-Swi6-EGFP or NLS-Swi6-KR25A-EGFP, respectively). The KR25A mutation in the hinge region of Swi6 does not affect H3K9 binding but abolishes RNA binding and nuclear import of Swi6. Therefore, fusion of an SV40 nuclear localization signal (NLS) to the N-terminus of the Swi6-KR25A is required (Keller *et al*, 2012). The NLS fused to the N-terminus of Swi6 caused an increase in $t_{1/2}$ values from ±535 ms to ±790 ms (Fig EV2B). In contrast, $t_{1/2}$ values decreased from ±790 ms for NLS-Swi6-EGFP to ±270 ms for NLS-Swi6-KR25A-EGFP (Figs 2A and B, and EV2A and B).

The observed faster recovery kinetics of the Swi6-KR25A mutant strongly suggested that RNA binding to Swi6 slows its mobility. To rule out the possibility that the effect was due to the KR25A mutations *per se* rather than the inability to bind RNA, we monitored fluorescence recovery kinetics of wild-type Swi6 in *cid14Δ* cells. Cid14 facilitates the removal and subsequent degradation of Swi6-bound RNAs (Buhler *et al*, 2007; Keller *et al*, 2012). Consistent with elevated heterochromatic RNA levels upon deletion of *cid14+*, $t_{1/2}$ values for Swi6-EGFP increased significantly in *cid14Δ* relative to *cid14+* cells (Fig 2C and D). However, $t_{1/2}$ values for the NLS-Swi6-KR25A RNA-binding mutant did not differ between *cid14+* and *cid14Δ* cells (Fig 2E and F). These results demonstrate that Swi6-RNA interactions slow Swi6 mobility in the nucleus and suggest that Cid14-mediated release of heterochromatic RNAs from Swi6 is the rate-limiting step in the Swi6 exchange cycle.

Swi6 dynamics are influenced by RNA throughout the cell cycle at centromeres and are similar at telomeres

The FRAP experiments described could not address the question of whether heterochromatin at centromeres or telomeres could differently influence Swi6 dynamics. Furthermore, Swi6 dynamics might differ in particular phases of the cell cycle. To specifically visualize and photobleach telomeric or centromeric heterochromatin, we generated strains expressing Taz1-mCherry or Cnp1-mCherry, respectively, in addition to Swi6-EGFP (Fig 3A). FRAP experiments on Cnp1-marked centromeric heterochromatin revealed average $t_{1/2}$ values for Swi6-EGFP of approximately 520 ms, very similar to the values obtained from FRAP experiments that were not centromere specific (Figs 1B and 3D). Very similar fluorescence recovery kinetics for telomeric heterochromatin were recorded (Fig 3D) and, thus, both constitutive heterochromatin regions are equally accessible to incoming fluorescent Swi6 protein. Both regions also appear permissive to low-level transcription. Consistent with RNA production, we observed significantly lower $t_{1/2}$ values for NLS-Swi6-KR25A-EGFP than for NLS-Swi6-EGFP at both centromeres and telomeres (Fig 3B and C).

In asynchronous *S. pombe* cultures, most cells are in the G2 phase of the cell cycle. Biochemical experiments performed with unsynchronized populations of *S. pombe* thus mainly represent G2. In contrast, our live cell imaging approach allowed us to look at individual cells representing different cell cycle stages. To examine whether Swi6 dynamics change during the cell cycle, we performed FRAP on individual cells residing in G1, S, or G2. Values of $t_{1/2}$ for NLS-Swi6-EGFP ranged from 300- to 2,200 ms throughout the entire cell cycle (Fig 3E). This high variability of $t_{1/2}$ remained constant over the entire time course. The $t_{1/2}$ values for the RNA-binding mutant NLS-Swi6-KR25A also remained the same throughout the entire cell cycle. However, the dynamic range of the $t_{1/2}$ values for NLS-Swi6-KR25A-EGFP was much smaller than for NLS-Swi6-EGFP (Fig 3E). Interestingly, the average $t_{1/2}$ values for NLS-Swi6-EGFP in G2 and S cells were not significantly different but in G1 were significantly lower (Fig 3F). Moreover, Swi6 mobility was greater in the absence of RNA binding, including the cells residing in G2 (Fig 3E and G).

© 2015 The Authors

Published online: October 5, 2015

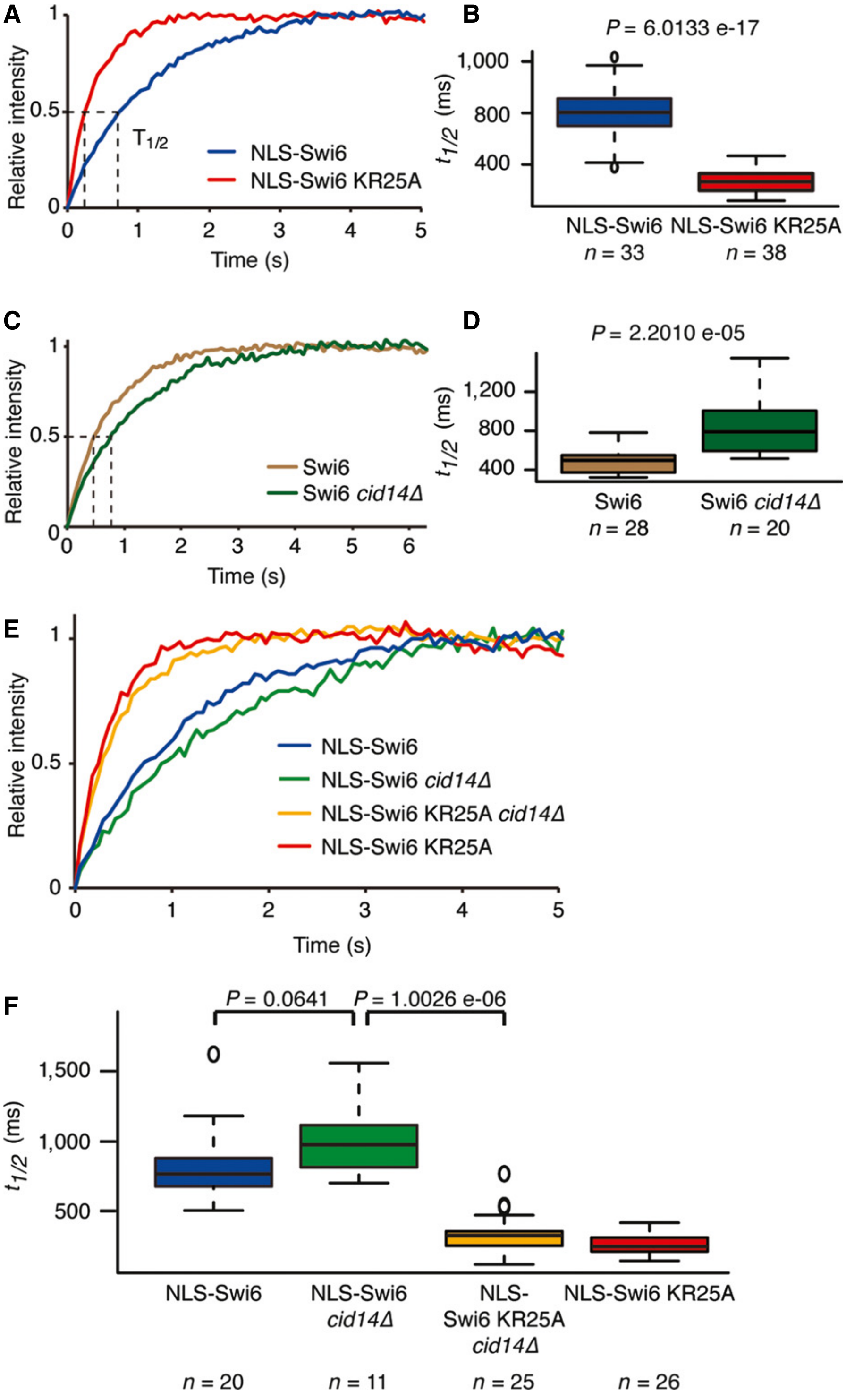

Figure 2. RNA decelerates Swi6 dynamics.

A, B Average relative intensities over time and corresponding fluorescence $t_{1/2}$ values of heterochromatic Swi6 obtained from FRAP experiments performed with cells expressing NLS-Swi6-EGFP (blue) or NLS-Swi6-KR25A-EGFP (red).

C, D Average relative intensities over time and corresponding fluorescence $t_{1/2}$ values of heterochromatic Swi6 obtained from FRAP experiments performed with wild-type (brown) or *cid14*Δ (dark green) cells expressing Swi6-EGFP.

E, F Average relative intensities over time and corresponding fluorescence $t_{1/2}$ values of heterochromatic Swi6 obtained from FRAP experiments performed with wild-type cells expressing heterochromatic NLS-Swi6-EGFP (blue) or NLS-Swi6 KR25A-EGFP (red), or *cid14*Δ cells expressing NLS-Swi6-EGFP (green) or NLS-Swi6-KR25A-EGFP (yellow).

Data information: In (B), (D) and (F), the box bounds the interquartile range (IQR) divided by the median, and whiskers extend to a maximum of 1.5 × IQR beyond the box.

© 2015 The Authors

Published online: October 5, 2015

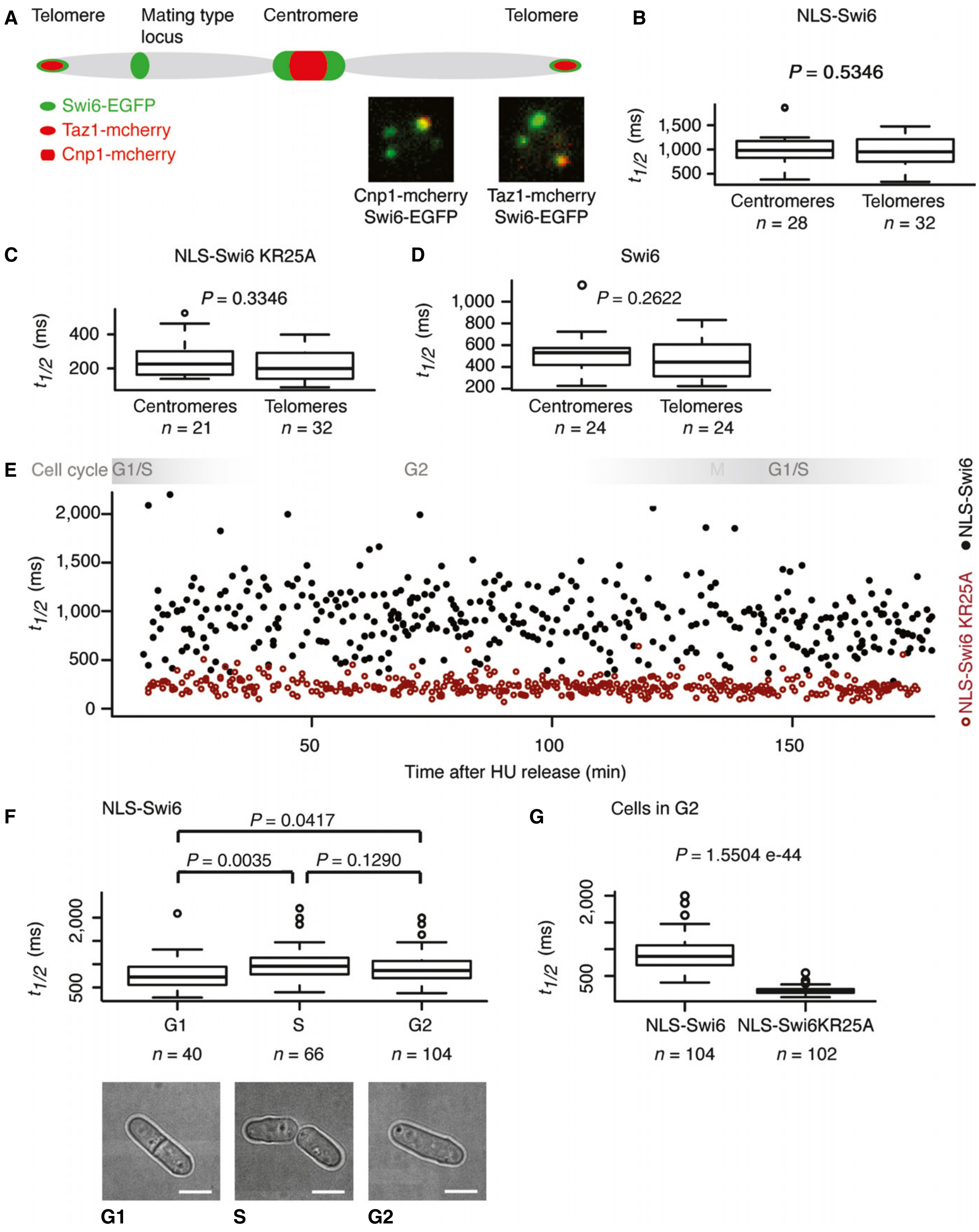

Figure 3.

Published online: October 5, 2015

Figure 3. Swi6 dynamics remain the same throughout the cell cycle.

A Schematic of a chromosome indicating Swi6-EGFP heterochromatic domains (green). Cnp1-mCherry and Taz1-mCherry (red) mark centromeres and telomeres, respectively. Representative images demonstrating Swi6-EGFP co-localization with centromeres (Cnp1-mCherry) and telomeres (Taz1-mCherry) are shown.

B Fluorescence $t_{1/2}$ values of centromeric or telomeric Swi6 obtained from FRAP experiments performed with cells expressing NLS-Swi6-EGFP.

C Fluorescence $t_{1/2}$ values of centromeric or telomeric Swi6 obtained from FRAP experiments performed with cells expressing the RNA-binding mutant NLS-Swi6-KR25A-EGFP.

D Fluorescence $t_{1/2}$ values of centromeric or telomeric Swi6 obtained from FRAP experiments performed with cells expressing Swi6-EGFP.

E Fluorescence $t_{1/2}$ values of centromeric Swi6 obtained from FRAP experiments performed after release of cells expressing NLS-Swi6-EGFP (black dots) or the RNA-binding mutant NLS-Swi6-KR25A-EGFP (red dots) from G1/S cell cycle arrest. Each dot represents one FRAP experiment at the respective time after release from cell cycle arrest. Swi6 is dispersed in M phase due to H3S10 phosphorylation, and M phase was therefore not included in the FRAP analysis.

F Fluorescence $t_{1/2}$ values obtained from FRAP experiments performed on centromeric Swi6. A total of 40, 66, and 104 individual cells residing in the G1, S, and G2 phases of the cell cycle were analyzed, respectively. Representative bright-field images of cells in G1, S, or G2 are shown. Scale bars = 2 μm.

G Fluorescence $t_{1/2}$ values obtained from FRAP experiments performed on centromeric Swi6 of cells expressing NLS-Swi6-EGFP and NLS-Swi6-KR25A-EGFP that reside in the G2 of the cell cycle.

Data information: In (B–D), (F) and (G), the box bounds the interquartile range (IQR) divided by the median, and whiskers extend to a maximum of 1.5 × IQR beyond the box.

Together these results show that Swi6 dynamics in heterochromatin do not differ significantly at centromeres compared with telomeres and respond equally to RNA binding at these heterochromatin regions. Thus, similar to centromeric repeats, telomeric heterochromatin also appears permissive for RNA synthesis. Consistent with this, transcripts originating from the subtelomeric *tlh1+* gene were clearly detected in wild-type cells (Fig EV1C). Interestingly, Swi6 mobility is markedly influenced by RNA binding throughout the cell cycle, suggesting that heterochromatic RNA production is not restricted to G1/S. Yet, the high dynamic range and random distribution of $t_{1/2}$ values for wild-type Swi6 indicate widely fluctuating and stochastic production of RNA within *S. pombe* heterochromatin.

Swi6 dimerization prevents spreading of centromeric H3K9 methylation

A characteristic, conserved feature of heterochromatin is that it spreads along chromatin from specific nucleation sites (Grewal & Moazed, 2003). Current models for heterochromatin spreading in *S. pombe* assign Swi6 a central role. It is generally assumed that it acts via a stepwise higher-order oligomerization process and recruitment of histone-modifying activities (Canzio *et al*, 2014). Therefore, our observation that Swi6 exists as one single dynamic population in heterochromatin is surprising, as a slowly exchanging fraction of Swi6 would be expected upon formation of an oligomeric network. We reasoned that such stably bound Swi6 molecules are at very low abundance and remained undetected in our FRAP experiments.

If a minor subpopulation of Swi6 that promotes spreading by oligomerization existed, defects in the spreading of H3K9 methylation in the absence of Swi6 would be expected. To test this hypothesis, we performed ChIP sequencing (ChIP-seq) with *swi6+* and *swi6Δ* cells and an antibody specifically recognizing H3K9me2. Consistent with the above hypothesis, we observed partially disrupted H3K9me2 in subtelomeric regions (Fig EV3A), as well as partial loss of H3K9me2 at the silent mating type locus, as previously reported (Hall *et al*, 2002) (Fig EV3B). However, in contrast to *chp2Δ* cells (Fig EV4B), levels of H3K9me2 were not reduced at any of the pericentromeric repeat regions in cells lacking Swi6 (Figs 4A and EV3E and F). This is consistent with a previous report of no significant reduction in H3K9me2 levels at specific centromeric sites in *swi6Δ* cells as measured by regular ChIP–PCR (Sadaie *et al*, 2004). However, we observed unexpected spreading of H3K9me2 beyond normal boundaries of heterochromatin in the absence of Swi6, most pronounced at the inverted repeat element IRC1R boundary region of centromere 1 (Fig 4A) and in the subtelomeric region of the right arm of chromosome 1 (Fig 4B). Similarly, we observed increased H3K9 methylation levels on the subtelomeric *tlh1+* and *tlh2+* genes in *swi6Δ* cells (Fig EV3A and D).

Thus, Swi6 is not obligatory for spreading of centromeric heterochromatin but is required for the demarcation of heterochromatin at the IRC1 boundaries of centromere 1. This is highly unexpected and raises the question of whether we are seeing an indirect consequence of the complete loss of Swi6 or whether Swi6 acts *per se* in blocking the propagation of H3K9 methylation. Therefore, we assessed by ChIP–PCR H3K9 methylation at the IRC1R boundary in cells that express Swi6 bearing single point mutations in either the CSD (*swi6L315E*), which abolish dimerization of Swi6 (Cowieson *et al*, 2000; Canzio *et al*, 2011), or the CD (*swi6W104A*), which abolish H3K9me2 binding (Jacobs & Khorasanizadeh, 2002; Canzio *et al*, 2013). Consistent with our ChIP-seq results, H3K9me2 in the centromeric repeat region (dh/dg) was not significantly different in wild-type and *swi6Δ* cells but was markedly increased on the neighboring *emc5+* and *rad50+* genes (Fig 5B and C). Likewise, H3K9me2

Figure 4. Methylation of H3K9 spreads across natural boundaries and heterochromatin becomes derepressed in *swi6Δ* cells.

A H3K9me2 ChIP-seq enrichment profiles for *swi6+* and *swi6Δ* cells on centromere 1. Centromeric repeat elements (dg/dh) are indicated. Inverted repeats (IRC1) constitute heterochromatin boundaries in wild-type cells (Cam *et al*, 2005). The *y*-axes represent $\log_2$ ChIP-seq enrichments in 200-bp genomically tiled windows calculated over *clr4Δ* cells. Two independent biological replicates for each genotype were performed (replicates 1 and 2). Positions of genomic elements on the plus and minus strands are indicated. Blue, protein-coding genes; white, repeats; green, long terminal repeat (LTR).

B H3K9me2 ChIP-seq enrichment profiles for *swi6+* and *swi6Δ* cells on the telomere of the right arm of chromosome 1. Two independent biological replicates for each genotype were performed (replicates 1 and 2).

C Differential expression of transcripts coming from centromere 1 assessed by tiling microarray gene expression analysis. Expression data for *swi6+* and *swi6Δ* cells were taken from a previous publication (Woolcock *et al*, 2012).

Published online: October 5, 2015

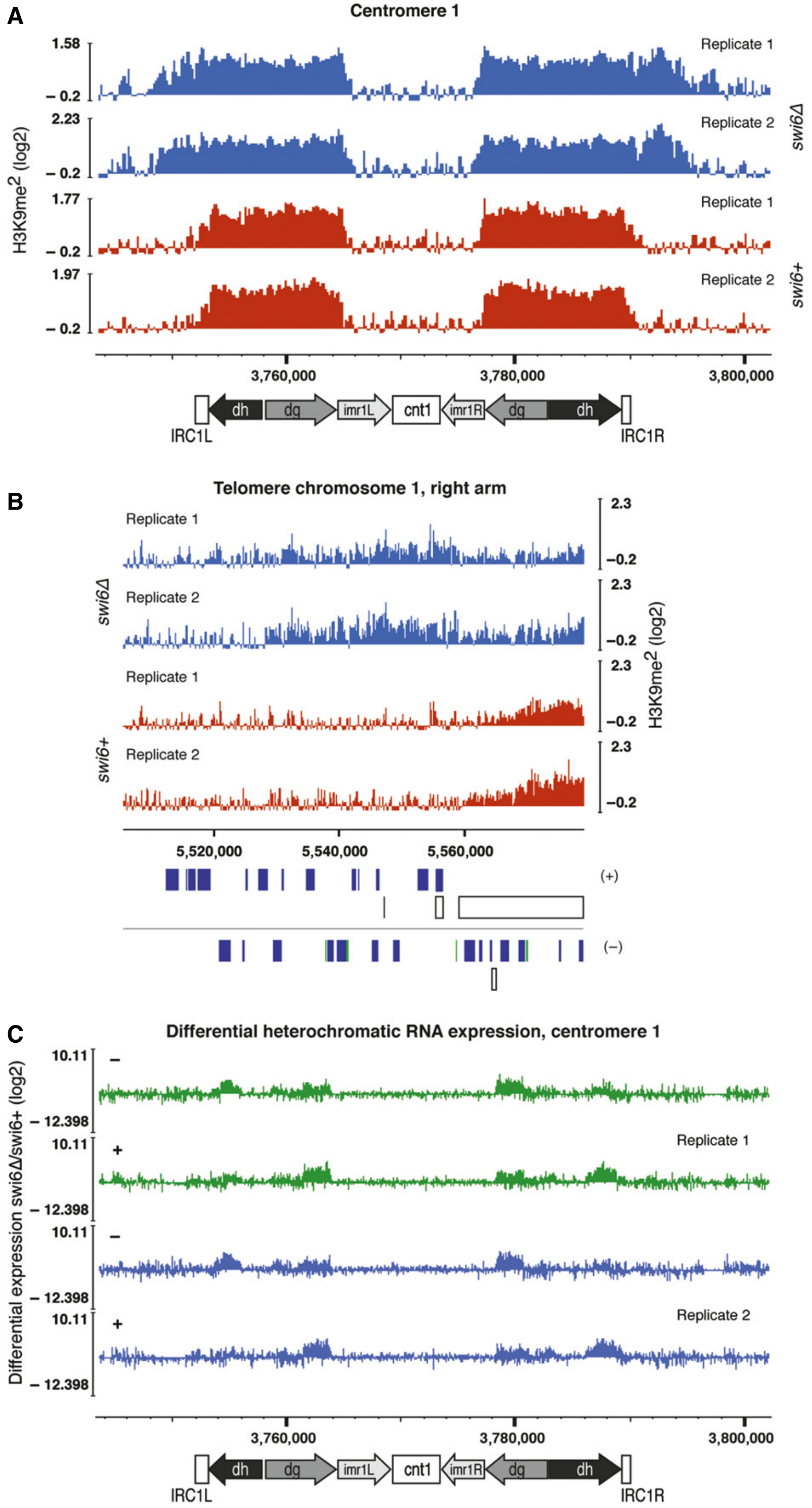

Figure 4.

© 2015 The Authors

Published online: October 5, 2015

spread beyond the IRC1R boundary in both *swi6L315E* and *swi6W104A* cells (Fig 5A–D). Hence, Swi6 dimerization and H3K9me2 binding are both critical for limiting the spreading of H3K9 methylation.

The results so far indicate that Swi6 is directly involved in counteracting spreading of H3K9 methylation. Importantly, the anti-silencing factor Epe1 has been reported also to limit the spreading of H3K9 methylation (Ayoub *et al*, 2003; Zofall & Grewal, 2006; Trewick *et al*, 2007). Thus, as Epe1 recruitment to heterochromatin depends on Swi6, spreading of H3K9 methylation in the absence of Swi6, or Swi6 binding to H3K9me2, could be explained by failure to recruit Epe1 (Zofall & Grewal, 2006). To test this hypothesis directly, we measured H3K9me2 levels in wild-type, *epe1*Δ, and *swi6*Δ cells. The levels of H3K9me2 in *epe1*Δ were slightly higher than in wild-type cells but not statistically significant and never as high as H3K9me2 in *swi6*Δ cells (Fig 5E). Therefore, spreading of H3K9 methylation in the absence of Swi6 cannot be explained solely by impaired Epe1 recruitment.

In conclusion, our results reveal that Swi6 dimerization is crucial for the prevention of H3K9 methylation spreading beyond the IRC1R boundary region of centromere 1. Although we cannot rule out Swi6-mediated recruitment of further anti-silencing factors that may act redundantly with Epe1, we favor a model in which heterochromatin spreading is counteracted by a previously described distinct conformational state of Swi6 dimers (see Discussion).

Tas3 self-association is required for H3K9 methylation in the absence of Swi6

Besides that of the precise contribution of Swi6 to the restriction of H3K9me2 to its natural boundaries, the question arises as to what mechanism propagates H3K9me2 beyond the IRC1R boundary in the absence of Swi6. To test the possible involvement of the RNAi pathway, which is essential for the assembly and maintenance of centromeric heterochromatin, we profiled small interfering RNAs (siRNAs) in wild-type and *swi6*Δ cells by deep sequencing. Instead of finding additional siRNAs mapping to the heterochromatin flanking regions, we observed slightly reduced levels of canonical centromeric siRNAs and loss of border RNAs (brdrRNAs) (Keller *et al*, 2013) that map to the IRC1R boundary (Fig 6A).

The absence of siRNAs mapping to the region that becomes H3K9 methylated in *swi6*Δ cells argues against the deposition of H3K9me2 through the canonical RNAi-mediated heterochromatin assembly pathway (Holoch & Moazed, 2015). However, the RNA-induced transcriptional silencing (RITS) complex was shown previously to spread from siRNA-producing centromeric heterochromatin nucleation sites to regions with few or no siRNAs (Li *et al*, 2009). Therefore, we hypothesized that spreading of H3K9me2 in the absence of Swi6 is caused by spreading of the RITS complex independently of siRNAs. RITS spreading *in cis* depends on

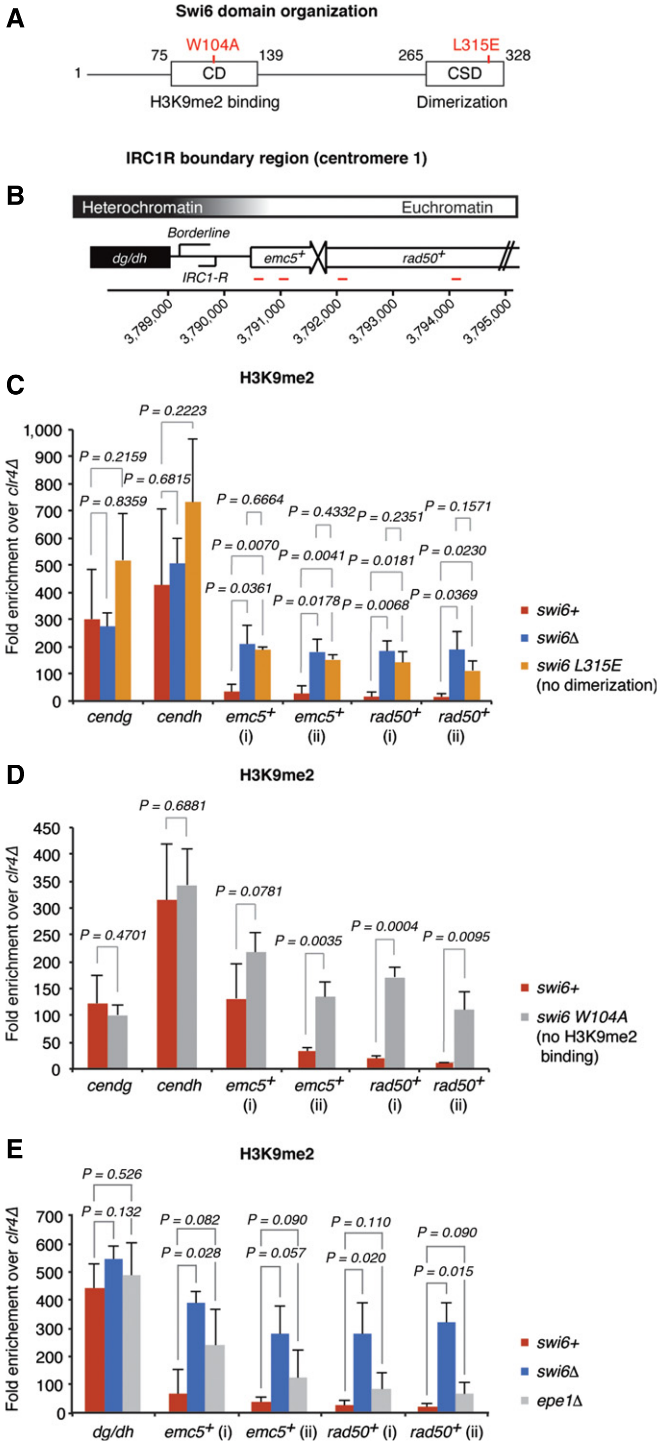

Figure 5. Swi6 dimerization and H3K9me2 binding are required for the prevention of H3K9me2 spreading.

- A Domain architecture of full-length Swi6. The indicated mutations in red disrupt the dimerization property of the CSD (L315E) or the ability of the CD to bind H3K9me2 (W104A).
- B Schematic of the IRC1R boundary region. IRC1R partially overlaps with the region that expresses the noncoding RNA borderline (Keller *et al*, 2013). Positions of the quantitative RT–PCR primers are indicated in red.
- C–E H3K9me2 levels on heterochromatin-adjacent genes assessed by ChIP–PCR in *swi6+*, *swi6*Δ, and *swi6-L315E* (CSD dimerization mutant) (C), *swi6-W104A* (H3K9me2 binding mutant) (D), and *epe1*Δ (E) cells. Enrichments over *clr4*Δ are normalized to *adh1+*. Average fold enrichment with s.d. is shown for three (C and E) or four (D) independent experiments. *P*-values were generated by the Student's *t*-test (two-tailed distribution, two-sample, unequal variance).

© 2015 The Authors

Published online: October 5, 2015

a C-terminal Tas3 α-helical motif (TAM) that can undergo polymeric self-association *in vitro* (Li *et al*, 2009). Because Tas3–Tas3 interactions mediated by TAM have been proposed to be especially important for RITS spreading into regions with few or no siRNAs, we speculated that Tas3-TAM plays a critical role in H3K9me2 spreading from centromeric repeats into the region flanking the IRC1R boundary in the absence of Swi6. To test this, we introduced a single amino acid substitution (L479E, Fig 6B) that abrogates Tas3–TAM polymerization (Li *et al*, 2009) in *swi6+* and *swi6Δ* cells and assessed H3K9me2 levels by ChIP (Fig 6C). H3K9me2 levels were mildly affected in *tas3-L479E* cells but completely eradicated in *tas3-L479E swi6*Δ double-mutant cells (Fig 6D). Thus, upon removal of Swi6, Tas3 self-association becomes absolutely essential to the maintenance of H3K9 methylation within centromeric repeat sequences. This strongly suggests that centromeric H3K9me2 spreading in *swi6*Δ cells is mediated by self-association of Tas3. The importance of Tas3 self-association to the maintenance of H3K9 methylation at other heterochromatin regions awaits further investigations.

Discussion

In this study, we have reanalyzed the dynamics of the *S. pombe* HP1 protein Swi6 in living cells and investigated its contribution to the maintenance and spreading of heterochromatin. We found that Swi6 rapidly exchanges *in cis* and *in trans* between different heterochromatic regions and that Swi6 mobility is decelerated by methylated histone H3K9 and RNA. Although we show that Swi6 could in principle exist in at least three kinetically distinct populations (Fig 7), we found that most if not all Swi6 molecules exchange between the RNA and heterochromatin-bound form under physiological conditions. Our results are consistent with a stochastic model of heterochromatin (Cheutin *et al*, 2004) and suggest that (i) heterochromatin in *S. pombe* is permissive for transcription throughout the cell cycle, (ii) only very few Swi6 molecules are engaged in heterochromatin spreading by oligomerization at telomeres, and (iii) Swi6 is dispensable to the expansion of centromeric heterochromatin. Rather, it appears to be involved in the demarcation of centromeric heterochromatin from neighboring euchromatin by a mechanism that remains to be fully elucidated. We discuss below the implications of these findings for the mechanisms of heterochromatin formation and repression in fission yeast.

The role of Swi6 in maintenance and spreading of heterochromatin

Iterative HP1 binding to methylated H3K9 and recruitment of HMTase activity is the prevalent model for heterochromatin spreading (Eissenberg & Elgin, 2014). The involvement of Swi6 in heterochromatin spreading is strongly supported by *in vivo* experiments using Swi6 overexpression to force the expansion of heterochromatin (Noma *et al*, 2006; Wang *et al*, 2013). *In vitro* data on Swi6-nucleosome interactions further imply a direct role of Swi6 in spreading along the chromatin fiber through a process of stepwise higher-order oligomerization (Canzio *et al*, 2011, 2013). The Swi6 dynamics determined in this study imply that such

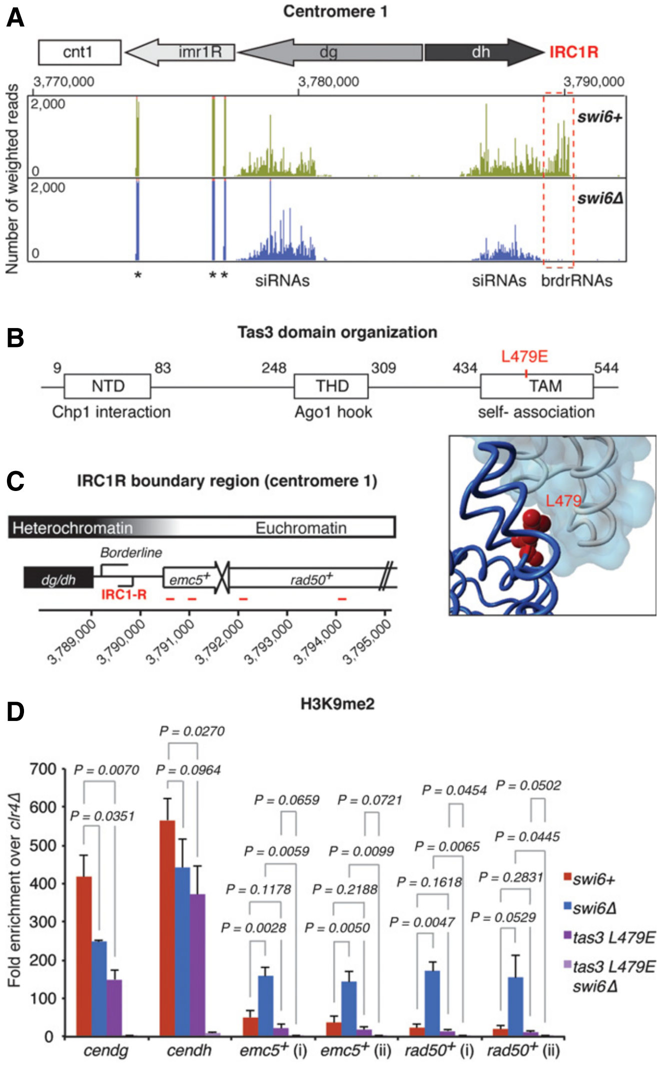

Figure 6. Tas3 self-association is required for H3K9 methylation at centromeric repeats in the absence of Swi6.

A sRNA reads mapping to centromere 1 in *swi6+* (green) and *swi6*Δ (blue) cells. The dashed red box highlights the loss of brdrRNAs at the IRC1R in the absence of Swi6. Centromeric repeat elements and the central core are indicated. Counts were normalized to the library size. Asterisks denote tRNA fragments. Note that tRNA genes flank IRC3 (Fig EV4) but not IRC1R.

B Domain architecture of full-length Tas3, adapted from Li *et al* (2009). The N-terminal domain (NTD) and the Tas3-homology domain (THD) are responsible for the interactions with Chp1 and Ago1, respectively. Tas3 self-association is mediated through the TAM motif, which is disrupted by the point mutation L497E, indicated in red. The location of residue L479 (red) is highlighted in the tube representation of two Tas3 molecules (dark blue and gray) with one surface view (light blue). Created from structure 3D1D of the PDB database.

C Schematic of the IRC1R boundary region. IRC1R partially overlaps with the region that expresses the noncoding RNA borderline (Keller *et al*, 2013). The positions of the primers used for quantitative RT–PCR are indicated in red.

D H3K9me2 levels on heterochromatin-adjacent genes assessed by ChIP–PCR in *swi6+*, *swi6*Δ, *tas3 L479E,* and *tas3 L479E swi6*Δ cells. Enrichments over *clr4*Δ are normalized to *adh1+*. Average fold enrichment with s.d. is shown for three independent experiments. *P*-values were generated by Student's *t*-test (two-tailed distribution, two-sample, unequal variance).

© 2015 The Authors

Published online: October 5, 2015

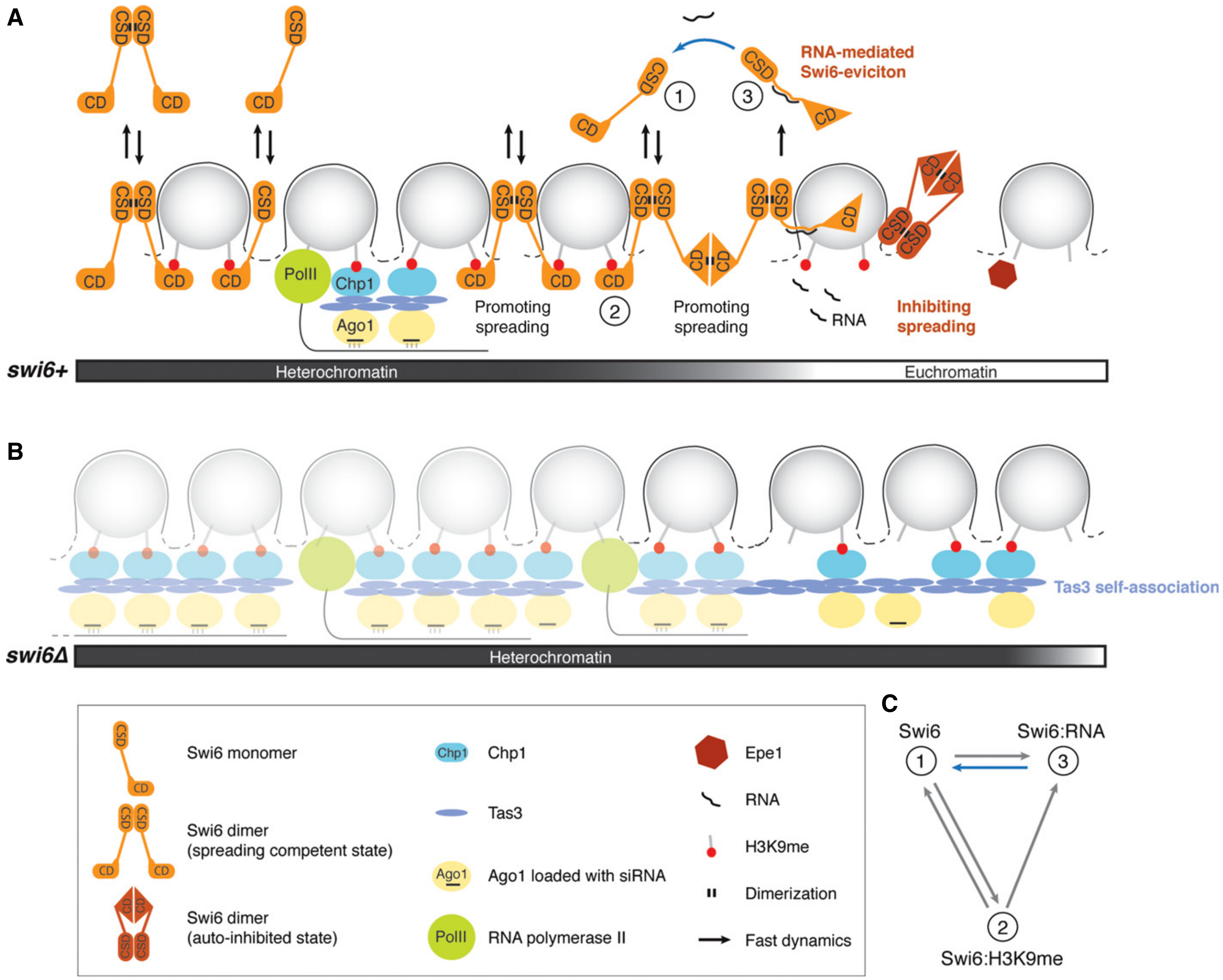
A
CSD
CD
RNA-mediated Swi6-eviciton
1
2
3
PolII
Chp1
Ago1
Promoting spreading
Promoting spreading
RNA
Inhibiting spreading
swi6+
Heterochromatin
Euchromatin
B
Tas3 self-association
swi6Δ
Heterochromatin
Swi6 monomer
Swi6 dimer (spreading competent state)
Swi6 dimer (auto-inhibited state)
Chp1
Tas3
Ago1 loaded with siRNA
RNA polymerase II
Epe1
RNA
H3K9me
Dimerization
Fast dynamics
C
Swi6
Swi6:RNA
Swi6:H3K9me

Figure 7. Regulation of Swi6 dynamics and the role of Swi6 in heterochromatin spreading, boundary formation, and repression.

A Model for the formation of a distinct heterochromatic domain. The spreading-competent open conformation of Swi6 dimers is fully dispensable or acts redundantly with RNAi-mediated spreading mechanisms in the formation of constitutive heterochromatin. The spreading of heterochromatin into neighboring euchromatin in the absence of DNA-encoded boundary elements, such as TFIIIC binding sites, can be stopped by the spreading-incompetent closed conformation of Swi6 dimers, RNA-mediated eviction of spreading-competent Swi6, or Epe1 activity. Swi6 molecules interact with H3K9me2 only transiently and exchange between free and RNA-bound forms (2, 1, or 3, respectively; see also C). Removal of RNA from Swi6 constitutes a rate-limiting step in the Swi6 exchange cycle (blue arrow) and contributes to tight repression of heterochromatin.

B In the absence of Swi6, H3K9 methylation is mediated by the RITS complex (Ago1, Chp1, Tas3) and can spread beyond natural boundaries via self-associating Tas3. This might occur independently of siRNAs.

C In theory, Swi6 can exist in at least three kinetically distinct populations: 1) freely diffusible Swi6, 2) Swi6 bound to H3K9me2, and 3) Swi6 bound to RNA; 3 is the least and 1 the most mobile population. The blue arrow indicates the rate-limiting step in the Swi6 exchange cycle. Under physiological conditions, most Swi6 molecules exchange between the RNA- and H3K9me2-bound forms.

oligomeric networks, if indeed they exist *in vivo* under natural conditions, are not inert but rather exist as a steady-state equilibrium of association and dissociation of Swi6 molecules with nucleosomes and themselves. We postulate that only very few if any Swi6 molecules remain stably bound to chromatin under physiological conditions; the majority are in a dynamic equilibrium. Only Swi6 overexpression results in stable association with chromatin and may enhance heterochromatin spreading. This may explain why strains with additional copies of the *swi6+* gene were employed in previous investigations of heterochromatin boundaries (Noma *et al*, 2001, 2006; Wang *et al*, 2013; Verrier *et al*, 2015).

Our ChIP-seq results suggest that Swi6-mediated spreading contributes partially to the propagation and spreading of the H3K9me2 mark at some telomeric regions of *S. pombe* chromosomes under physiological conditions. In contrast, Swi6 is fully

Published online: October 5, 2015

dispensable to the maintenance of H3K9me2 at centromeres. However, we found that Swi6 is required for the restriction of H3K9me2 to the pericentromeric repeat region and the prevention of spreading into neighboring euchromatin. This unanticipated finding highlights the functional promiscuity of HP1 proteins and raises the question of how Swi6 participates in counteracting heterochromatin spreading. Our results show that it cannot simply be recruitment of the anti-silencing factor Epe1, because H3K9 methylation in *epe1Δ* cells does not phenocopy the spreading we observed in *swi6Δ* cells (Fig 5E). This is further supported by a recent study demonstrating that H3K9me2 levels around the IRC1 boundary regions of centromere 1 in *epe1Δ* cells are similar to those of wild-type cells, unless Swi6 is overexpressed (Wang *et al*, 2013). Furthermore, Epe1 binding at the IRC1 boundary element was reported in Swi6-defective cells (Zofall & Grewal, 2006). Thus, the spreading we observed in *swi6Δ* cells cannot be explained by a failure to recruit Epe1 to the boundary. Therefore, further properties of Swi6 are likely to contribute to boundary formation. Intriguingly, Swi6 dimers that form through CSD interactions have recently been demonstrated to exist in closed and open states *in vitro*. The closed state is mediated by interaction between the two CDs of a Swi6 dimer and inhibits binding of the H3K9me2 mark. Furthermore, this conformation cannot participate in the Swi6 oligomerization process and could therefore stop spreading of heterochromatin (Canzio *et al*, 2013). Supporting such a model, we found that dimerization is crucial to Swi6 activity in boundary protection (Fig 5C). It is possible that proteins bound at heterochromatin–euchromatin transitions can induce and stabilize the closed state of Swi6 dimers and thereby stop encroachment of heterochromatin into neighboring regions. Similarly, RNA could also drive Swi6 into the closed state. Consistent with this model is our previous observation that heterochromatin spreads into neighboring euchromatin if Swi6 fails to bind RNA (Keller *et al*, 2013). Thus, in addition to evicting spreading-competent Swi6 from the chromatin template, as we have previously suggested, ncRNAs may also switch Swi6 into the closed Swi6 conformation that stops the spreading of heterochromatin. This is an attractive hypothesis that demands further study.

We propose a model in which RNAi- and Swi6-dependent mechanisms act redundantly within centromeric repeats and maintain heterochromatin under physiological conditions (Fig 7A). Redundancy between the two mechanisms is supported by a previous study, which showed that Swi6 maintains some H3K9 methylation at centromeric repeats in the absence of RNAi (Sadaie *et al*, 2004). Similarly, we observed only slightly reduced H3K9me2 levels in *tas3L479E* and *swi6Δ* cells, but complete loss of H3K9me2 in *tas3L479E swi6Δ* double-mutant cells (Fig 6D). We envision that spreading-incompetent (closed) Swi6 dimers is an important factor in counteracting the spread of heterochromatin into the repeat proximal regions, which can be mediated either by the open conformation of Swi6 dimers or by RNAi-mediated H3K9me2 deposition. In the absence of Swi6, additional H3K9me2-binding sites are available for the Chp1 subunit of the RITS complex, which stabilizes the RNAi machinery on chromatin and thereby promotes the methylation of neighboring nucleosomes (Fig 7B). Importantly, our results highlight the importance of Tas3 self-association for such spreading of H3K9me2 and that this may occur independently of siRNAs (Fig 6).

The role of Swi6 in silencing of heterochromatin

Whereas Swi6 is dispensable to the maintenance of H3K9me2 at centromeric repeats, it is required for full repression. Previous quantitative RT–PCR analyses have demonstrated that Swi6 contributes roughly 14% and 32% to the silencing of centromeric *dg* and *dh* sequences, respectively. At telomeres of *S. pombe* chromosomes, Swi6 was shown to be required for the majority of silencing at the subtelomeric *tlh1+* gene (Motamedi *et al*, 2008). These findings are in agreement with our high-resolution gene expression data and demonstrate that complete repression of heterochromatin cannot be achieved without Swi6 (Figs 4C and EV5) (Woolcock *et al*, 2012).

We previously postulated a model for the silencing of heterochromatin in which Swi6 serves a general function linking transcription to downstream RNA degradation, rather than reducing transcription *per se*. Importantly, we have demonstrated that Swi6 complexed with RNA dissociates from H3K9-methylated nucleosomes and escorts its associated RNAs to the RNA-decay machinery, thereby contributing to tight repression of heterochromatin at a co- or post-transcriptional level (Keller *et al*, 2012). Our current study extends these findings and reveals that RNA binding to Swi6 decelerates the mobility of Swi6 on heterochromatin about three fold, suggesting that release of heterochromatic RNAs from Swi6 is the rate-limiting step in the Swi6 exchange cycle (Fig 7A and C).

In conclusion, rather than promoting the maintenance and spreading of heterochromatin, ensuring tight repression of heterochromatin seems to be the prevailing activity of Swi6. Our results are consistent with a model for heterochromatin silencing in which Swi6 assures coupling between heterochromatin transcription and RNA degradation by acting as an H3K9me2-specific checkpoint. Molecular details of RNA decay downstream of Swi6 remain elusive, and future investigations focused on RNA decay are thus required in order to achieve a better mechanistic understanding of heterochromatin silencing.

Materials and Methods

Strains and plasmids

Fission yeast strains and plasmids used in this study are described in Appendix Tables S1 and S2.

Western blot and antibodies

Total proteins from exponentially growing cells were extracted using TCA and separated on a NuPAGE 4–12% Bis–Tris gel (Invitrogen). Antibodies for Western blotting were used at the following concentrations: Swi6 (in-house generated; 1:20,000), tubulin ((Woods *et al*, 1989), 1:3,000). The Swi6 mouse monoclonal antibody was raised against full-length recombinant Swi6 and affinity-purified with Protein G.

Fluorescence recovery after photobleaching (FRAP)

Imaging was performed with an Olympus IX81 microscope equipped with a Yokogawa CSU-X1 spinning disk, a PlanApo 100×/1.45 TIRFM oil objective, two back-illuminated EM-CCD EvolveDelta

Published online: October 5, 2015

cameras (Photometrics, AZ), 491-nm and 561-nm laser lines (Cobolt, Sweden), a Semrock Di01-T488/568 dichroic, and Semrock FF01-525/40-25 and FF01-440/521/607/700-25 emission filters. All devices were piloted with the software Visiview (Visitron GmbH, Puchheim, Germany). For FRAP experiments, a VisiFRAP module (Visitron), a 473-nm laser line and a chroma Z405/473rpc-xt dichroic were installed on the setup. The bleach region was a diffraction-limited spot, and the bleach time was 20 ms.

For each FRAP experiment, a time series of 120 images of a fixed confocal plane was acquired every 60 ms, while the bleach pulse was aimed and triggered manually by mouse click. Additionally, in order to calculate the recovery percentage of the bleached foci, a stack was taken before and after the time series acquisition. All images were acquired at 30°C. Cells were grown in YES medium to exponential phase and imaged on a slide harboring an agarose patch containing YES medium with 3% glucose.

FRAP during the cell cycle

Exponentially growing cells were synchronized in G1/S phase by a 4-h treatment with 15 mM hydroxyurea and released into the cell cycle after a wash with YES medium. The cells were imaged in a Ludin Chamber with a lectin-coated glass slide (BS-I; Sigma). FRAP experiments were performed for approximately 3 h after release, each time-point representing the recovery curve of a locus from a different cell. All images were acquired at 30°C. M phase was not included in the FRAP analysis as Swi6 becomes dispersed (Ekwall *et al*, 1995; Pidoux *et al*, 2000; Li *et al*, 2013).

Line-scan FRAP

Imaging was performed on an AXIO OBSERVER Z1 equipped with an LSM 710 scanning head, a multiline Argon 458/488/514 nm (25 mW) laser and a Plan-Apochromat 63×/1.40 Oil DIC M27 objective. The devices were piloted with ZEN Black 2010 software.

Analysis of FRAP data

The acquired images were analyzed using custom script in the open-source software Fiji (Schindelin *et al*, 2012). For each FRAP time series, we manually assigned the bleached region as a region of interest (ROI) and calculated the mean intensity of the ROI. We subtracted the obtained minimal intensity from these mean intensities. To calculate the recovery half-times ($t_{1/2}$), we performed an exponential one-component curve fit based on the formula $y(x) = a(1 - \exp(-bx))$. The boxplots of the $t_{1/2}$ values were made in RStudio.

Curve fitting of mean recovery curves

To obtain mean recovery curves of the different conditions, we normalized each individual series of intensities to the mean of its last 15 time-points post-recovery. Of these normalized intensity series, aligned to the bleaching time-point, the means were calculated and loaded into the curve fitting toolbox of Matlab (MATLAB and Curve Fitting Toolbox Release 2013b; The MathWorks, Inc., Natick, USA). The one-component fits were based on the formula $y(x) = a(1 - \exp(-bx))$, while the two-component fits were based on $y(x) = a(1 - \exp(-bx)) + c(1 - \exp(-dx))$.

Chromatin immunoprecipitation (ChIP)

H3K9me2 ChIP experiments were performed with an H3K9me2-specific mouse monoclonal antibody from Wako (clone no. MABI0307; 302-32369). Anti-H3K9me antibody was used at 1 µg per mg of whole-cell extract (WCE). Cells were processed for ChIP analysis as previously described (Keller *et al*, 2013).

ChIP sequencing (ChIP-seq)

ChIP-seq libraries were generated with an Illumina-based protocol with custom reagents and bar-coded adapters as previously described (Keller *et al*, 2013). Libraries were sequenced on the Illumina HiSeq2000 system according to the manufacturer's protocols.

sRNA sequencing

RNA for sRNA sequencing was prepared as previously described (Keller *et al*, 2013). Libraries were prepared with the Illumina TruSeq sRNA preparation protocol (Cat. no. RS-930-1012). The 145- to 160-nt population was isolated and the library sequenced on an Illumina HiSeq2000. sRNA reads were aligned as described previously (Emmerth *et al*, 2010) with zero mismatch allowed.

Accession codes

The deep sequencing data are deposited under the accession code GSE70946 (NCBI Gene Expression Omnibus), which include the ChIP-seq data of the *swi6Δ* samples under the accession number GSE61136 and the small-RNA sequencing data of *swi6+* and *swi6Δ* samples under GSE70945. The ChIP-seq data of wild type were previously published and can be found under accession code GSE42850.

Expanded View for this article is available online:
http://emboj.embopress.org

Acknowledgements

We would like to thank Yukiko Shimada for excellent technical assistance, Katarzyna Kowalik for bioinformatics advice, Jeffrey Chao and Susan Gasser for constructive advice, Alex Tuck and Pat King for critical reading and editing of the manuscript, and Daniele Oberti and other laboratory members for fruitful discussions. We are grateful to T. Roloff, S. Dessus-Babus, D. Gaidatzis, and H.-R. Hotz for help with Illumina deep sequencing and advice on data analysis. We thank Danesh Moazed and Hisao Musakata for providing *S. pombe* strains. This work was supported by funds from the Swiss National Science Foundation (PP00P3_139204/1). R.K.-S. was supported by a postdoctoral fellowship from the Peter and Traudl Engelhorn Foundation. The Friedrich Miescher Institute for Biomedical Research is supported by the Novartis Research Foundation.

Author contributions

RS designed and carried out most of the experiments. RK-S performed ChIP, generated libraries for next-generation sequencing, and analyzed ChIP-seq. CK prepared RNA for sRNA deep sequencing. MAK and LG assisted with data analysis and establishment of the methods. MB obtained funding, designed experiments, and oversaw the study. MB and RS wrote the manuscript.

© 2015 The Authors

Published online: October 5, 2015

Conflict of interest

The authors declare that they have no conflict of interest.

References

Ayoub N, Noma K, Isaac S, Kahan T, Grewal SI, Cohen A (2003) A novel jmjC domain protein modulates heterochromatization in fission yeast. *Mol Cell Biol* 23: 4356 – 4370

Azzalin CM, Reichenbach P, Khoriauli L, Giulotto E, Lingner J (2007) Telomeric repeat containing RNA and RNA surveillance factors at mammalian chromosome ends. *Science* 318: 798 – 801

Bannister AJ, Zegerman P, Partridge JF, Miska EA, Thomas JO, Allshire RC, Kouzarides T (2001) Selective recognition of methylated lysine 9 on histone H3 by the HP1 chromo domain. *Nature* 410: 120 – 124

Buhler M, Haas W, Gygi SP, Moazed D (2007) RNAi-dependent and - independent RNA turnover mechanisms contribute to heterochromatic gene silencing. *Cell* 129: 707 – 721

Buhler M, Moazed D (2007) Transcription and RNAi in heterochromatic gene silencing. *NatStructMol Biol* 14: 1041 – 1048

Buhler M, Spies N, Bartel DP, Moazed D (2008) TRAMP-mediated RNA surveillance prevents spurious entry of RNAs into the Schizosaccharomyces pombe siRNA pathway. *Nat Struct Mol Biol* 15: 1015 – 1023

Buhler M (2009) RNA turnover and chromatin-dependent gene silencing. *Chromosoma* 118: 141 – 151

Cam HP, Sugiyama T, Chen ES, Chen X, FitzGerald PC, Grewal SI (2005) Comprehensive analysis of heterochromatin- and RNAi-mediated epigenetic control of the fission yeast genome. *NatGenet* 37: 809 – 819

Canzio D, Chang EY, Shankar S, Kuchenbecker KM, Simon MD, Madhani HD, Narlikar GJ, Al-Sady B (2011) Chromodomain-mediated oligomerization of HP1 suggests a nucleosome-bridging mechanism for heterochromatin assembly. *Mol Cell* 41: 67 – 81

Canzio D, Liao M, Naber N, Pate E, Larson A, Wu S, Marina DB, Garcia JF, Madhani HD, Cooke R, Schuck P, Cheng Y, Narlikar GJ (2013) A conformational switch in HP1 releases auto-inhibition to drive heterochromatin assembly. *Nature* 496: 377 – 381

Canzio D, Larson A, Narlikar GJ (2014) Mechanisms of functional promiscuity by HP1 proteins. *Trends Cell Biol* 24: 377 – 386

Carisey A, Stroud M, Tsang R, Ballestrem C (2011) Fluorescence recovery after photobleaching. *Methods Mol Biol* 769: 387 – 402

Castel SE, Martienssen RA (2013) RNA interference in the nucleus: roles for small RNAs in transcription, epigenetics and beyond. *Nat Rev Genet* 14: 100 – 112

Chen D, Dundr M, Wang C, Leung A, Lamond A, Misteli T, Huang S (2005) Condensed mitotic chromatin is accessible to transcription factors and chromatin structural proteins. *J Cell Biol* 168: 41 – 54

Chen ES, Zhang K, Nicolas E, Cam HP, Zofall M, Grewal SI (2008) Cell cycle control of centromeric repeat transcription and heterochromatin assembly. *Nature* 451: 734 – 737

Cheutin T, McNairn AJ, Jenuwein T, Gilbert DM, Singh PB, Misteli T (2003) Maintenance of stable heterochromatin domains by dynamic HP1 binding. *Science* 299: 721 – 725

Cheutin T, Gorski SA, May KM, Singh PB, Misteli T (2004) In vivo dynamics of Swi6 in yeast: evidence for a stochastic model of heterochromatin. *Mol Cell Biol* 24: 3157 – 3167

Cowieson NP, Partridge JF, Allshire RC, McLaughlin PJ (2000) Dimerisation of a chromo shadow domain and distinctions from the chromodomain as revealed by structural analysis. *Curr Biol* 10: 517 – 525

Djupedal I, Portoso M, Spahr H, Bonilla C, Gustafsson CM, Allshire RC, Ekwall K (2005) RNA Pol II subunit Rpb7 promotes centromeric transcription and RNAi-directed chromatin silencing. *Genes Dev* 19: 2301 – 2306

Eissenberg JC, Elgin SC (2000) The HP1 protein family: getting a grip on chromatin. *CurrOpinGenetDev* 10: 204 – 210

Eissenberg JC, Elgin SC (2014) HP1a: a structural chromosomal protein regulating transcription. *Trends in genetics: TIG* 30: 103 – 110

Ekwall K, Javerzat JP, Lorentz A, Schmidt H, Cranston G, Allshire R (1995) The chromodomain protein Swi6: a key component at fission yeast centromeres. *Science* 269: 1429 – 1431

Emmerth S, Schober H, Gaidatzis D, Roloff T, Jacobeit K, Buhler M (2010) Nuclear retention of fission yeast dicer is a prerequisite for RNAi-mediated heterochromatin assembly. *Dev Cell* 18: 102 – 113

Festenstein R, Pagakis SN, Hiragami K, Lyon D, Verreault A, Sekkali B, Kioussis D (2003) Modulation of heterochromatin protein 1 dynamics in primary Mammalian cells. *Science* 299: 719 – 721

Grewal SI, Moazed D (2003) Heterochromatin and epigenetic control of gene expression. *Science* 301: 798 – 802

Grewal SI, Elgin SC (2007) Transcription and RNA interference in the formation of heterochromatin. *Nature* 447: 399 – 406

Halic M, Moazed D (2010) Dicer-independent primal RNAs trigger RNAi and heterochromatin formation. *Cell* 140: 504 – 516

Hall IM, Shankaranarayana GD, Noma K, Ayoub N, Cohen A, Grewal SI (2002) Establishment and maintenance of a heterochromatin domain. *Science* 297: 2232 – 2237

Holoch D, Moazed D (2015) RNA-mediated epigenetic regulation of gene expression. *Nat Rev Genet* 16: 71 – 84

Jacobs SA, Khorasanizadeh S (2002) Structure of HP1 chromodomain bound to a lysine 9-methylated histone H3 tail. *Science* 295: 2080 – 2083

Jia S, Noma K, Grewal SI (2004) RNAi-independent heterochromatin nucleation by the stress-activated ATF/CREB family proteins. *Science* 304: 1971 – 1976

Kanoh J, Sadaie M, Urano T, Ishikawa F (2005) Telomere binding protein Taz1 establishes Swi6 heterochromatin independently of RNAi at telomeres. *CurrBiol* 15: 1808 – 1819

Kato H, Goto DB, Martienssen RA, Urano T, Furukawa K, Murakami Y (2005) RNA polymerase II is required for RNAi-dependent heterochromatin assembly. *Science* 309: 467 – 469

Keller C, Woolcock K, Hess D, Buhler M (2010) Proteomic and functional analysis of the noncanonical poly(A) polymerase Cid14. *RNA* 16: 1124 – 1129

Keller C, Adaixo R, Stunnenberg R, Woolcock KJ, Hiller S, Buhler M (2012) HP1 (Swi6) mediates the recognition and destruction of heterochromatic RNA transcripts. *Mol Cell* 47: 215 – 227

Keller C, Kulasegaran-Shylini R, Shimada Y, Hotz HR, Buhler M (2013) Noncoding RNAs prevent spreading of a repressive histone mark. *Nat Struct Mol Biol* 20: 1340

Kloc A, Martienssen R (2008) RNAi, heterochromatin and the cell cycle. *Trends Genet* 24: 511 – 517

Kloc A, Zaratiegui M, Nora E, Martienssen R (2008) RNA interference guides histone modification during the S phase of chromosomal replication. *Curr Biol* 18: 490 – 495

Lachner M, O'Carroll D, Rea S, Mechtler K, Jenuwein T (2001) Methylation of histone H3 lysine 9 creates a binding site for HP1 proteins. *Nature* 410: 116 – 120

Li F, Sonbuchner L, Kyes SA, Epp C, Deitsch KW (2008) Nuclear non-coding RNAs are transcribed from the centromeres of Plasmodium falciparum

© 2015 The Authors

Published online: October 5, 2015

and are associated with centromeric chromatin. *J Biol Chem* 283: 5692 – 5698

Li H, Motamedi MR, Yip CK, Wang Z, Walz T, Patel DJ, Moazed D (2009) An alpha motif at Tas3 C terminus mediates RITS cis spreading and promotes heterochromatic gene silencing. *Mol Cell* 34: 155 – 167

Li PC, Green MD, Forsburg SL (2013) Mutations disrupting histone methylation have different effects on replication timing in S. pombe centromere. *PLoS ONE* 8: e61464

Lorite P, Renault S, Rouleux-Bonnin F, Bigot S, Periquet G, Palomeque T (2002) Genomic organization and transcription of satellite DNA in the ant Aphaenogaster subterranea (Hymenoptera, Formicidae). *Genome* 45: 609 – 616

Motamedi MR, Hong EJ, Li X, Gerber S, Denison C, Gygi S, Moazed D (2008) HP1 proteins form distinct complexes and mediate heterochromatic gene silencing by nonoverlapping mechanisms. *Mol Cell* 32: 778 – 790

Noma K, Allis CD, Grewal SI (2001) Transitions in distinct histone H3 methylation patterns at the heterochromatin domain boundaries. *Science* 293: 1150 – 1155

Noma K, Cam HP, Maraia RJ, Grewal SI (2006) A role for TFIIIC transcription factor complex in genome organization. *Cell* 125: 859 – 872

Pezer Z, Ugarkovic D (2008) RNA Pol II promotes transcription of centromeric satellite DNA in beetles. *PLoS ONE* 3: e1594

Pidoux AL, Uzawa S, Perry PE, Cande WZ, Allshire RC (2000) Live analysis of lagging chromosomes during anaphase and their effect on spindle elongation rate in fission yeast. *J Cell Sci* 113(Pt 23): 4177 – 4191

Reinhart BJ, Bartel DP (2002) Small RNAs correspond to centromere heterochromatic repeats. *Science* 297: 1831

Rouleux-Bonnin F, Renault S, Bigot Y, Periquet G (1996) Transcription of four satellite DNA subfamilies in Diprion pini (Hymenoptera, Symphyta, Diprionidae). *Eur J Biochem* 238: 752 – 759

Rouleux-Bonnin F, Bigot S, Bigot Y (2004) Structural and transcriptional features of Bombus terrestris satellite DNA and their potential involvement in the differentiation process. *Genome* 47: 877 – 888

Sadaie M, Iida T, Urano T, Nakayama J (2004) A chromodomain protein, Chp1, is required for the establishment of heterochromatin in fission yeast. *EMBO J* 23: 3825 – 3835

Schindelin J, Arganda-Carreras I, Frise E, Kaynig V, Longair M, Pietzsch T, Preibisch S, Rueden C, Saalfeld S, Schmid B, Tinevez JY, White DJ, Hartenstein V, Eliceiri K, Tomancak P, Cardona A (2012) Fiji: an open-source platform for biological-image analysis. *Nat Methods* 9: 676 – 682

Sha K, Gu SG, Pantalena-Filho LC, Goh A, Fleenor J, Blanchard D, Krishna C, Fire A (2010) Distributed probing of chromatin structure in vivo reveals pervasive chromatin accessibility for expressed and non-expressed genes during tissue differentiation in C. elegans. *BMC Genom* 11: 465

Sheff MA, Thorn KS (2004) Optimized cassettes for fluorescent protein tagging in Saccharomyces cerevisiae. *Yeast* 21: 661 – 670

Trewick SC, Minc E, Antonelli R, Urano T, Allshire RC (2007) The JmjC domain protein Epe1 prevents unregulated assembly and disassembly of heterochromatin. *The EMBO journal* 26: 4670 – 4682

Verdel A, Jia S, Gerber S, Sugiyama T, Gygi S, Grewal SI, Moazed D (2004) RNAi-mediated targeting of heterochromatin by the RITS complex. *Science* 303: 672 – 676

Verrier L, Taglini F, Barrales RR, Webb S, Urano T, Braun S, Bayne EH (2015) Global regulation of heterochromatin spreading by Leo1. *Open Biol* 5: 150045

Verschure PJ, van der Kraan I, Manders EM, Hoogstraten D, Houtsmuller AB, van Driel R (2003) Condensed chromatin domains in the mammalian nucleus are accessible to large macromolecules. *EMBO Rep* 4: 861 – 866

Volpe TA, Kidner C, Hall IM, Teng G, Grewal SI, Martienssen RA (2002) Regulation of heterochromatic silencing and histone H3 lysine-9 methylation by RNAi. *Science* 297: 1833 – 1837

Wang J, Tadeo X, Hou H, Tu PG, Thompson J, Yates JR 3rd, Jia S (2013) Epe1 recruits BET family bromodomain protein Bdf2 to establish heterochromatin boundaries. *Genes Dev* 27: 1886 – 1902

Woods A, Sherwin T, Sasse R, MacRae TH, Baines AJ, Gull K (1989) Definition of individual components within the cytoskeleton of Trypanosoma brucei by a library of monoclonal antibodies. *J Cell Sci* 93(Pt 3): 491 – 500

Woolcock KJ, Stunnenberg R, Gaidatzis D, Hotz HR, Emmerth S, Barraud P, Buhler M (2012) RNAi keeps Atf1-bound stress response genes in check at nuclear pores. *Genes Dev* 26: 683 – 692

Zofall M, Grewal SI (2006) Swi6/HP1 recruits a JmjC domain protein to facilitate transcription of heterochromatic repeats. *Mol Cell* 22: 681 – 692

© 2015 The Authors

Expanded View Figures

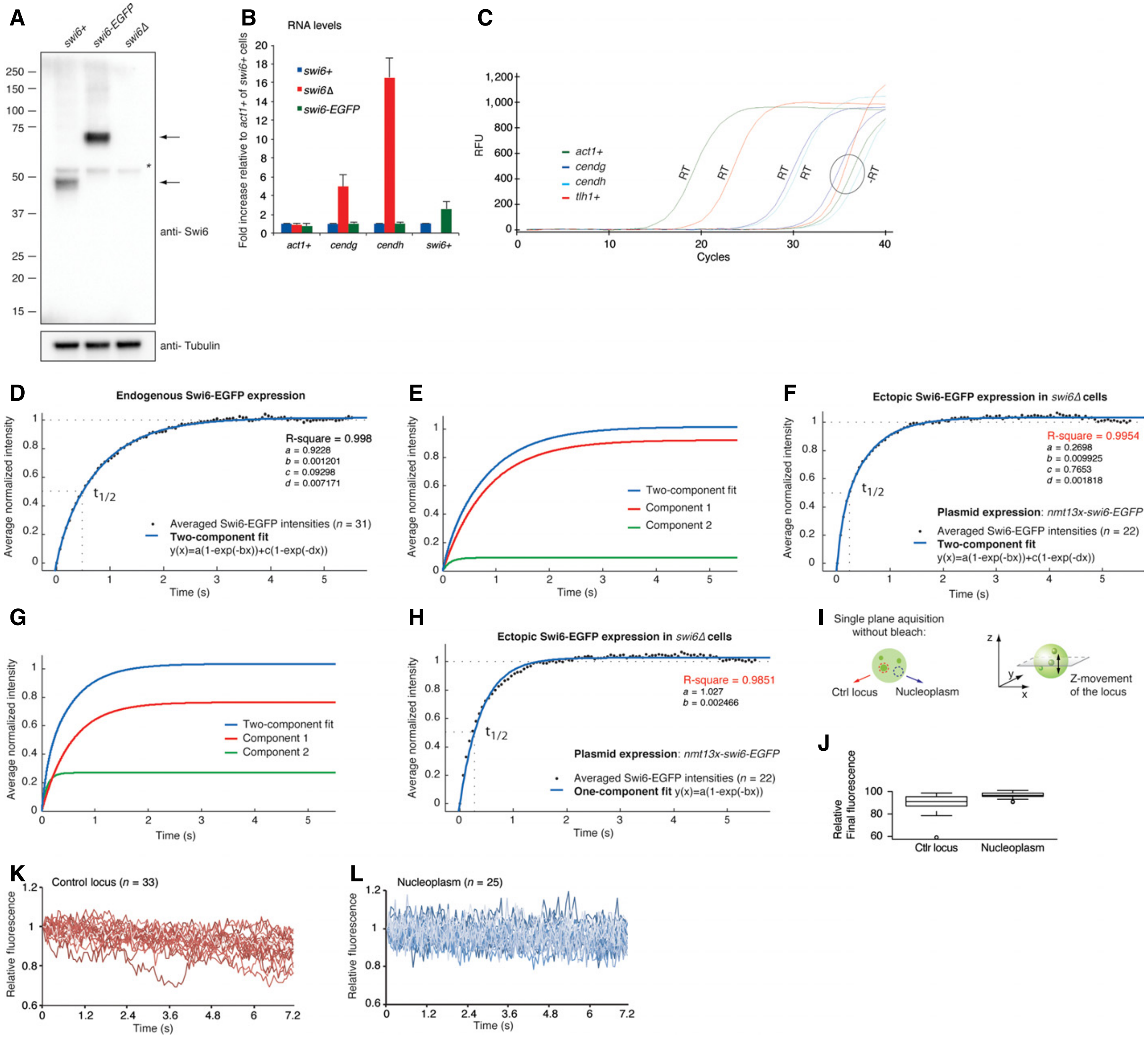

© 2015 The Authors

Figure EV1. Dynamics of endogenously and ectopically expressed Swi6-EGFP.

A Western blot showing protein levels of endogenous Swi6 and Swi6-EGFP (denoted by arrows). The blot was probed sequentially with antibodies recognizing Swi6 and tubulin, which serves as a loading control. The asterisk indicates an unspecific band.

B Fold increase in *cendg*, *cendh*, and *swi6+* RNA levels in *swi6-EGFP* and *swi6Δ* cells compared with wild-type cells, relative to *act1+ mRNA*. Error bars denote s.d. from three independent experiments.

C Representative plot of real-time PCR amplification curves obtained for *act1+*, *cendg*, *cendh*, and *tlh1+* cDNA (RT) generated from RNA that was isolated from wild-type cells. −RT serves as a DNA contamination control (no reverse transcriptase added to the cDNA synthesis reaction). RFU, relative fluorescence units.

D Two-component fit (blue line) of normalized average FRAP intensities (black dots) obtained for endogenously tagged Swi6-EGFP at heterochromatic loci. Dashed lines indicate the final relative fluorescence intensity that is set to 1 and the fluorescence half-recovery time ($t_{1/2}$).

E Plot of individual components of the FRAP curve fit in (A). Component 1: $a(1\text{-}\exp(\text{-}bx))$, Component 2: $c(1\text{-}\exp(\text{-}dx))$.

F Two-component fit (blue line) of normalized average FRAP intensities (black dots) obtained for plasmid-borne ectopically expressed Swi6-EGFP at heterochromatic loci.

G Plot of individual components of the curve fit in (D). Component 1: $a(1-\exp(-bx))$, Component 2: $c(1-\exp(-dx))$.

H One-component fit (blue line) of normalized average FRAP intensities (black dots) obtained for plasmid-borne ectopically expressed Swi6-EGFP at heterochromatic loci.

I Schematics of a single-plane acquisition of a heterochromatic Swi6-EGFP locus (red, control locus) and a region in the nucleoplasm (blue). Movement of the locus out of the focal plane is depicted on the right.

J Relative final fluorescence signal after photobleaching obtained for heterochromatic and nucleoplasmic Swi6-EGFP. The box bounds the interquartile range (IQR) divided by the median, and whiskers extend to a maximum of 1.5 × IQR beyond the box.

K, L Relative fluorescence of heterochromatic Swi6-EGFP (red) (K) and nucleoplasmic Swi6-EGFP (blue) (L) acquired on a single plane in living cells over time. Fluorescence intensity at the beginning of image acquisition was set to 1.

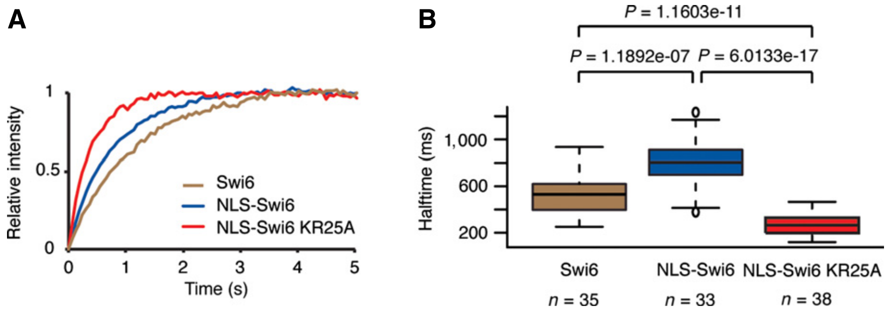

Figure EV2. Dynamics of NLS-Swi6-EGFP.

A, B Average relative intensities over time (A) and corresponding fluorescence $t_{1/2}$ values (B) of heterochromatic Swi6 obtained from FRAP experiments performed with cells expressing Swi6-EGFP (blue), NLS-Swi6-EGFP (green), or NLS-Swi6-KR25A-EGFP (red).

Data information: In (B), the box bounds the interquartile range (IQR) divided by the median, and whiskers extend to a maximum of 1.5 × IQR beyond the box.

© 2015 The Authors

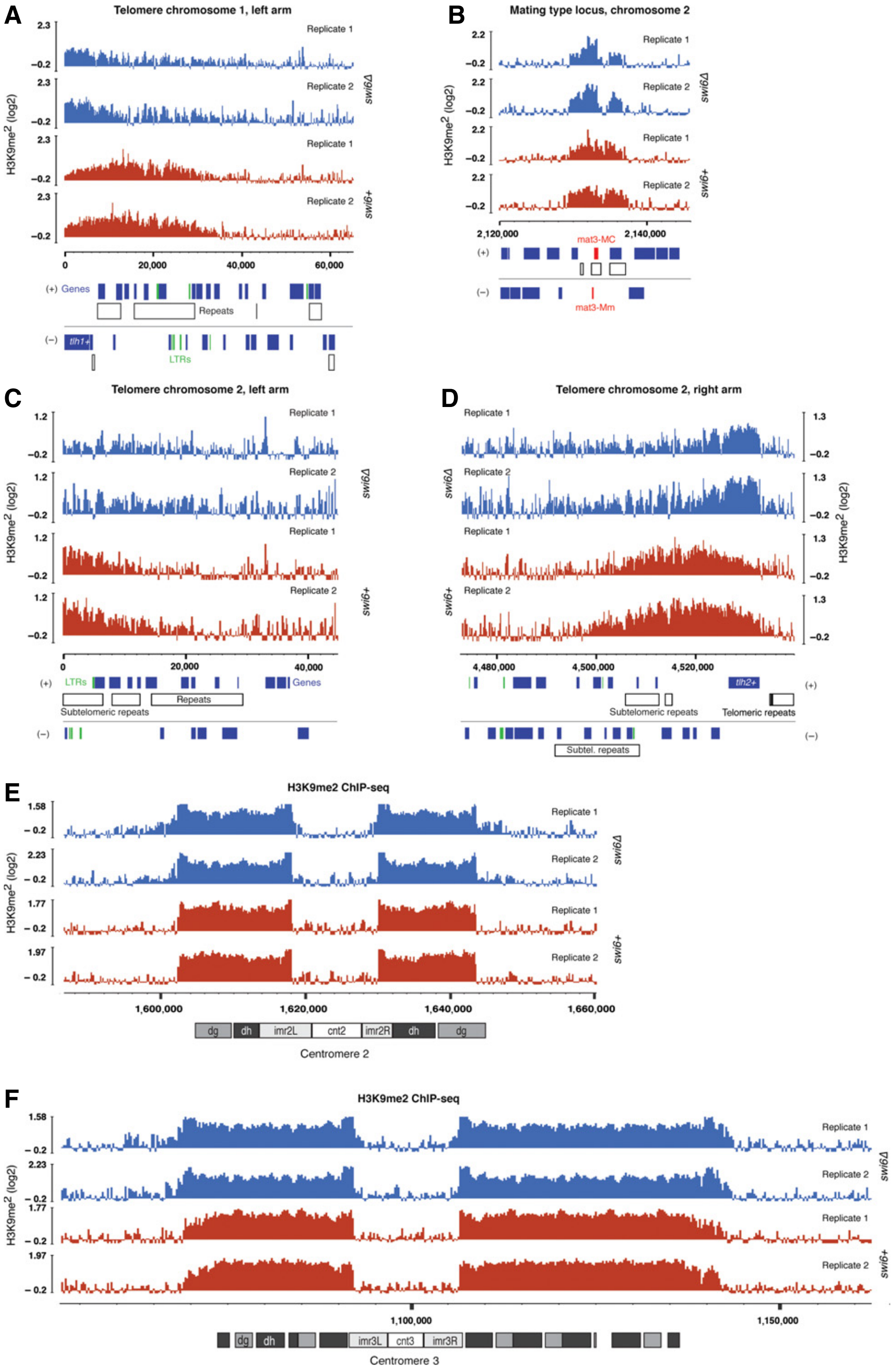

Figure EV3. H3K9 methylation in the absence of Swi6.

A, B H3K9me2 ChIP-seq enrichment profiles for *swi6*+ (red) and *swi6*Δ (blue) cells at the telomere of the left arm of chromosome 1 (A) and the silent mating type locus on chromosome 2 (B).

C, D H3K9me2 ChIP-seq enrichment profiles for *swi6*+ (red) and *swi6*Δ (blue) cells at the telomeres of the left (C) and right (D) arms of chromosome 2.

E, F H3K9me2 ChIP-seq enrichment profiles for *swi6*+ (red) and *swi6*Δ (blue) cells at centromere 2 (E) and centromere 3 (F).

Data information: The *y*-axes represent $\log_2$ ChIP-seq enrichments in 200-bp genomically tiled windows calculated over *clr4*Δ cells. Two independent biological replicates for each genotype were performed (replicates 1 and 2). Positions of genomic elements on the plus and minus strands are indicated. Blue, protein-coding genes; white, repeats; green, long terminal repeat (LTR).

© 2015 The Authors

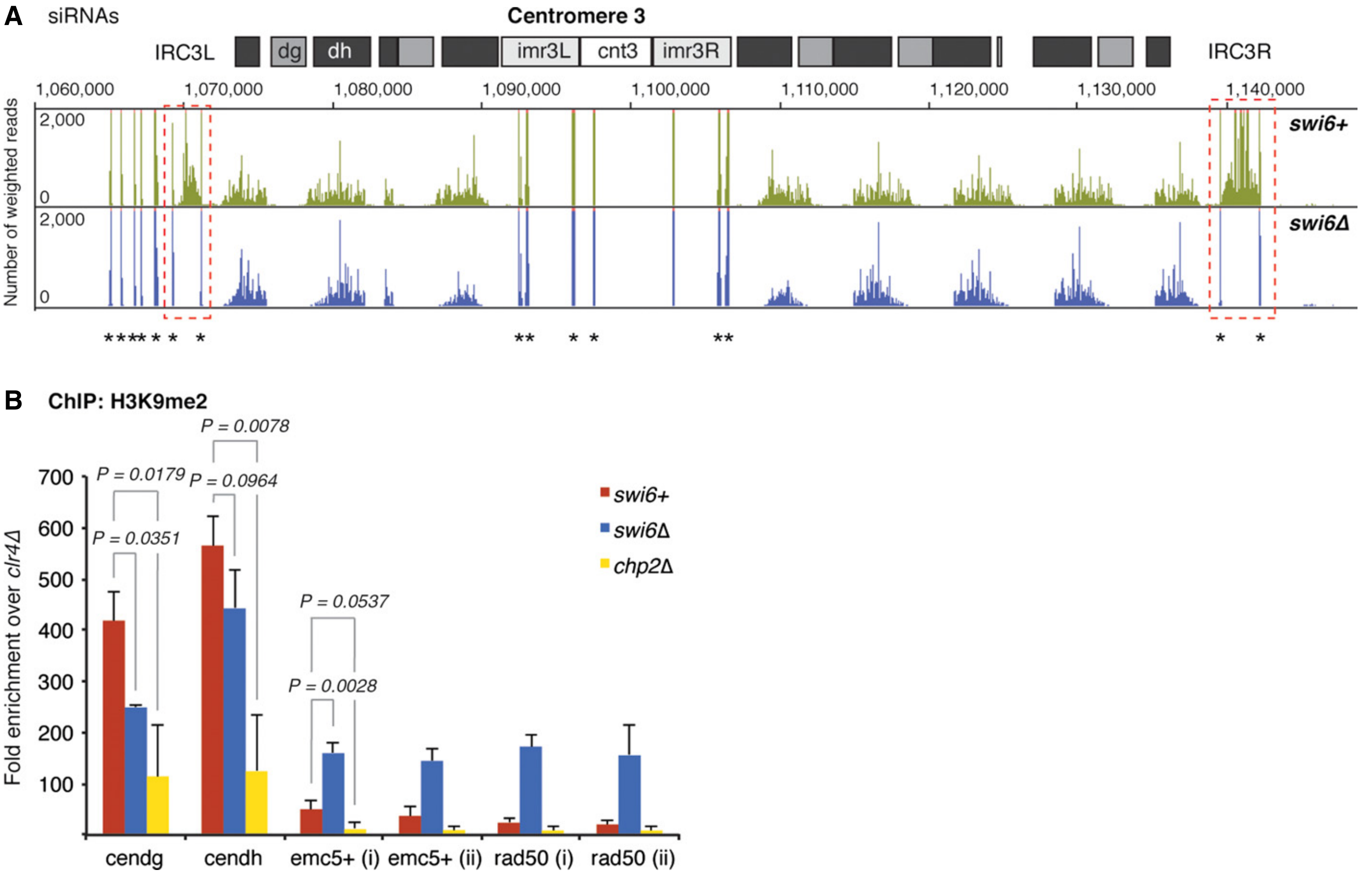

Figure EV4. siRNA levels and spreading of H3K9me at centromere 3 in the absence of Swi6.

A Small RNA reads mapping to centromere 3 in *swi6+* (green) and *swi6*Δ (blue) cells. The dashed red box points out the loss of siRNAs mapping to IRC3 elements in the absence of Swi6. Centromeric repeat elements and the central core are indicated. Counts were normalized to the library size. Asterisks denote tRNA fragments. Note that tRNA genes flank IRC3 but not IRC1 (Fig 6).

B H3K9me2 levels on heterochromatin-adjacent genes assessed by ChIP–PCR in *swi6+*, *swi6*Δ, and *chp2*Δ cells. Enrichments over *clr4*Δ were normalized to *adh1+*. Average fold enrichment with s.d. is shown for three independent experiments. *P*-values were generated by the Student's *t*-test (two-tailed distribution, two-sample, unequal variance).

© 2015 The Authors

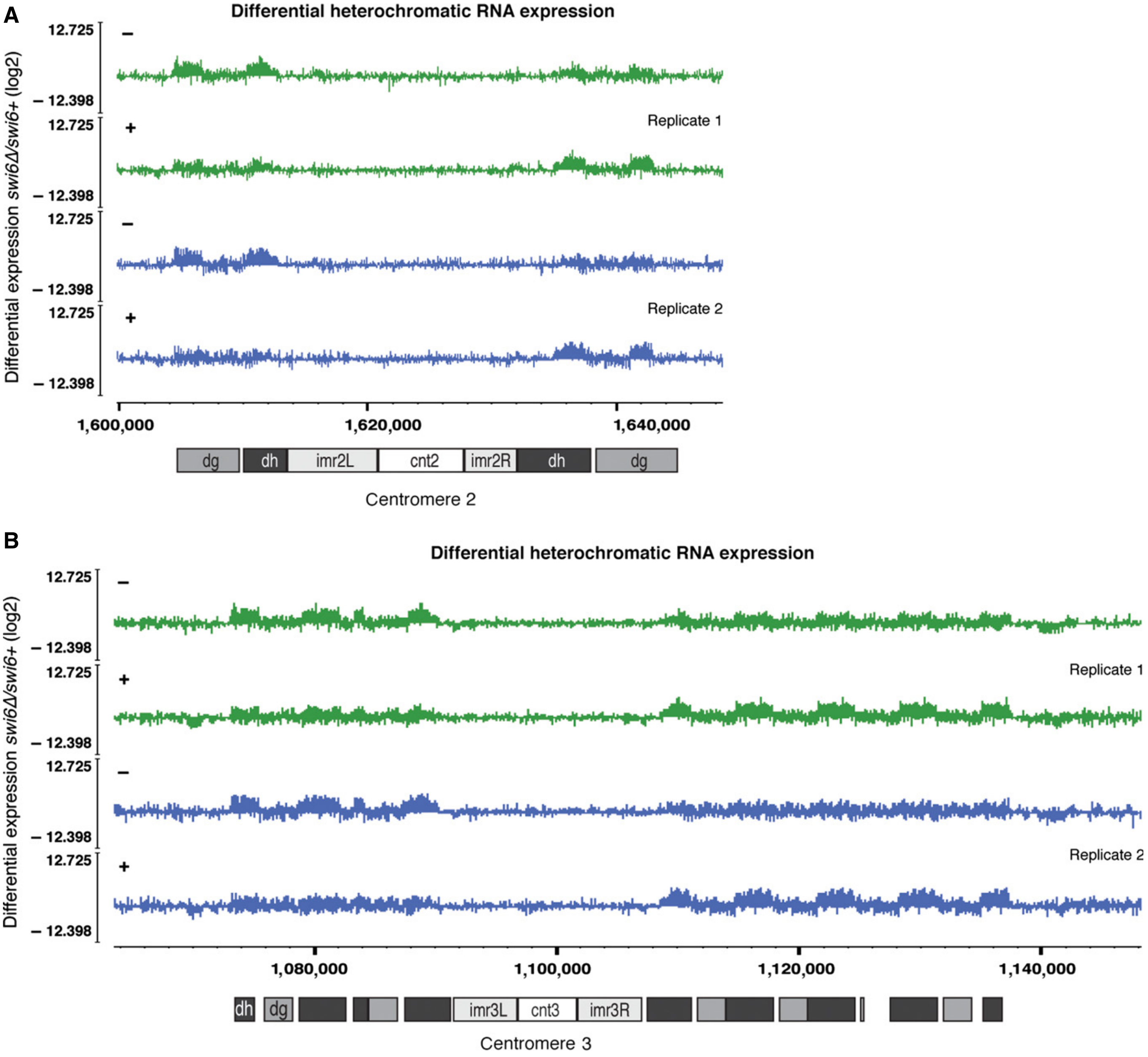

Figure EV5. Derepression of heterochromatin in the absence of Swi6.

A, B Differential expression of centromeric transcripts assessed by tiling microarray gene expression analysis. Expression data for *swi6*+ and *swi6*Δ cells were taken from a previous publication (Woolcock *et al*, 2012). A, centromere 2; B, centromere 3. Different genomic elements in these regions are indicated.

© 2015 The Authors

APPENDIX

Appendix Table S1 - Strains used in this study

Strain	Genotype	Source
SPB88*	*h+ leu1-32 ura4-D18 ori1 ade6-216 imr1R(Nco1)::ura4+ swi6D::natMX*	1
SPB1779	*h90 mat3::ura4+ ura4-DS/E leu1-32 ade6-M210 swi6-linker-EGFP::hphMX*	1
SPB1780	*h90 mat3::ura4+ ura4-DS/E leu1-32 ade6-M210 nls-swi6-linker-EGFP::hphMX*	1
SPB1781	*h90 mat3::ura4+ ura4-DS/E leu1-32 ade6-M210 nls-swi6-KR25A-linker-EGFP::hphMX*	1
SPB1782	*h90 mat3::ura4+ ura4-DS/E leu1-32 ade6-M210 nls-swi6-KR25A-linker-EGFP::hphMX cnp1::mcherry::kanMX*	1
SPB1785	*h90 mat3::ura4+ ura4-DS/E leu1-32 ade6-M210 swi6-linker-EGFP::hphMX taz1::mcherry::KanMX*	1
SPB1811	*h90 mat3::ura4+ ura4-DS/E leu1-32 ade6-M210 swi6-linker-EGFP::hphMX cid14D::natMX*	1
SPB1923	*h90 mat3::ura4+ ura4-DS/E leu1-32 ade6-M210 swi6-linker-EGFP::hphMX cnp1::mcherry::kanMX*	1
SPB2001	*h90 mat3::ura4+ ura4-DS/E leu1-32 ade6-M210 nls-swi6-KR25A-linker-EGFP::hphMX taz1::mcherry::kanMx*	1
SPB2026	*h90 mat3::ura4+ ura4-DS/E leu1-32 ade6-M210 nls-swi6-linker-EGFP::hphMX cnp1::mcherry::kanMX*	1
SPB2027	*h90 mat3::ura4+ ura4-DS/E leu1-32 ade6-M210 nls-swi6-linker-EGFP::hphMX taz1::mcherry::kanMX*	1
SPB2050	*h90 mat3::ura4+ ura4-DS/E leu1-32 ade6-M210 swi6-linker-EGFP::hphMX clr4D::kanMX*	1
SPB342	*h90 mat3M(EcoRV)::gfp+::natMX ura4-DS/E leu1-32 ade6-M210*	2
SPB360	*h90 mat3M(EcoRV)::gfp+::natMX ura4-DS/E leu1-32 ade6-M210 clr4Δ::kanMX*	2
SPB939	*h90 mat3M(EcoRV)::gfp+::natMX ura4-DS/E leu1-32 ade6-M210 swi6 Δ ::ura3+*	2
SPB2361	*h90 mat3M(EcoRV)::gfp+::natMX ura4-DS/E leu1-32 ade6-M210 epe1Δ::kanMX*	1
SPB2571	*h+ leu1-32 ade6-216 ura4-D18 imr1R(NcoI)::ura4+ oriI tas3L479E-TAP-natMX*	3
SPB2594	*h90 mat3M(EcoRV)::gfp+::natMX ura4-DS/E leu1-32 ade6-M210 chp2Δ::kanMX*	1
SPB2604	*h+ leu1-32 ade6-216 ura4-D18 imr1R(NcoI)::ura4+ oriI tas3L479E-TAP-natMX swi6Δ::hphMX*	1

SPB2605	*h90 mat3M(EcoRV)::gfp+::natMX ura4-DS/E leu1-32 ade6-M210 swi6L315E*	1
SPB2610	*h90 ura4-DS/E Kint2::ura4+ swi6D::kanMX6::(swi6W104A hphMX6)*	4
SPB2611	*h90 ura4-DS/E Kint2::ura4+*	4

1 = this study, 2 = (Keller et al, 2012); *Used for plasmid expression of pmb1474 Linker amino acids in Swi6-linker-EGFP: GDGAGLIN, 3 = obtained from Danesh Moazed (Li et al, 2009), 4 = obtained from Hisao Musakata (Hayashi et al, 2009).

Appendix Table S2 - Plasmids used in this study

Name	Common name	Source
pmb85	pJR1-3xL	2
pmb1474*	pJR3xL -Swi6-linker-EGFP	1
pmb851	**pGEX - Swi6 L315E**	1

1 = this study, 2 = (Moreno et al, 2000)

* pmb1474: Swi6-linker-EGFP was cloned into pmb85 at Xho I and Spe I site. Linker amino acids: GDGAGLIN

Appendix Table S3 - Primers used in this study for ChIP-qPCR

Name	Target	Sequence	Source
mb566	*adh1+*	TCCGTTCCCCTCGAGGTT	1
mb567	*adh1+*	TCAAGGCACGATAGCAAGTGA	1
mb549	*cendg*	AAGGAATGTGCCTCGTCAAATT	1
mb550	*cendg*	TGCTTCACGGTATTTTTGAAATC	1
mb551	*cendh*	GTATTTGGATTCCATCGGTACTATGG	1
mb552	*cendh*	ACTACATCGACACAGAAAAGAAAACAA	1
mb4719	*5' of emc5+*	ATGCGTTTGCGATTCTCTGC	1
mb4720	*5' of emc5+*	GTGTGAGCGCTAACTTTTGCT	1
mb4721	*emc5+*	ACACTGCTTATTCTGCACATGA	1
mb4722	*emc5+*	TGCCGCATGTGGTAAAGACA	1
mb4509	*rad50+ (i)*	AGCCAAACTACATATATTCTCTTCATCG	1
mb4510	*rad50+ (i)*	TTGGCAGAATGTCTAGGTGTAAACTGTG	1
mb4539	*rad50+ (ii)*	ACGTACATCTTCGACTAGTTTATCCA	1
mb4540	*rad50+ (ii)*	CTATACTGGCTAACCAACTGATGACATTG	1

1 = (Keller et al, 2013)

References

Hayashi MT, Takahashi TS, Nakagawa T, Nakayama J, Masukata H (2009) The heterochromatin protein Swi6/HP1 activates replication origins at the pericentromeric region and silent mating-type locus. *Nat Cell Biol* **11:** 357-362

Keller C, Adaixo R, Stunnenberg R, Woolcock KJ, Hiller S, Buhler M (2012) HP1(Swi6) Mediates the Recognition and Destruction of Heterochromatic RNA Transcripts. *Molecular cell* **47:** 215-227

Keller C, Kulasegaran-Shylini R, Shimada Y, Hotz HR, Buhler M (2013) Noncoding RNAs prevent spreading of a repressive histone mark. *Nature structural & molecular biology* **20:** 1340

Li H, Motamedi MR, Yip CK, Wang Z, Walz T, Patel DJ, Moazed D (2009) An alpha motif at Tas3 C terminus mediates RITS cis spreading and promotes heterochromatic gene silencing. *Mol Cell* **34:** 155-167

Moreno MB, Duran A, Ribas JC (2000) A family of multifunctional thiamine-repressible expression vectors for fission yeast. *Yeast* **16:** 861-872

Manuscript EMBO-2015-91320

H3K9 methylation extends across natural boundaries of heterochromatin in the absence of an HP1 protein

Rieka Stunnenberg, Raghavendran Kulasegaran, Claudia Keller, Moritz A. Kirschmann, Laurent Gelman and Marc Buehler

Corresponding author: Marc Buehler, Friedrich Miescher Institute For Biomedical Research

---

Review timeline:

	Submission date:	17 February 2015
	Editorial Decision:	09 April 2015
	Revision received:	28 July 2015
	Editorial Decision:	23 August 2015
	Revision received:	28 August 2015
	Accepted:	03 September 2015

Transaction Report:

(Note: With the exception of the correction of typographical or spelling errors that could be a source of ambiguity, letters and reports are not edited. The original formatting of letters and referee reports may not be reflected in this compilation.)

Editor: Anne Nielsen

1st Editorial Decision 09 April 2015

1st editorial decision 9th April 2015

Thank you again for submitting your manuscript for consideration here and my sincere apologies for the highly unusual duration of the review process. Your manuscript has now been seen by three referees whose comments are included below. As you will see, while the referees do highlight the interest and potential impact of your findings they also raise a number of rather major concerns that would have to be addressed before they can support publication in The EMBO Journal.

More specifically, you will see that while ref#1 is the more positive one, ref#2 is rather critical and finds that the second half of the manuscript would have to be extensively developed in order for the manuscript to be suitable for publication in The EMBO Journal. Ref #3 is largely positive, but does point out the need to provide further functional insight on the proposed role for Swi6 in limiting heterochromatin spreading.

Given the divergent recommendations from referees #1 and #2 I ran an additional round of consultation with ref#3 who provided the following comments:

' Referee 1: In general, I agree with the comments from this referee. I particularly agree with Major point 1 (a point also made myself) that it is essential to show that Swi6-EGFP is fully functional. I believe the western blot requested by referee 1 is essential for this.

Referee 2: Argues that most of the paper has little to offer over that which is already known. However, I believe the observation that expression of Swi6 from its endogenous locus (ie. not over expressed) indicates a predominantly single kinetic population of Swi6 is important as over-expression studies indicated at least two populations with different kinetics. Notwithstanding this, I do have some sympathy with his/her belief that the K9me spreading at centromeric positions in the absence of Swi6 is rather preliminary. Perhaps, the authors could enhance this section with additional data, maybe by exploring the effect of Swi6 mutants as I suggested. '

Having discussed the reports and additional comments with my colleagues in the editorial team once more, it is clear that extensive revision of your manuscript would be required to convince the referees and bring the study to the level of insight required for publication here. Given the general support from both ref #1 and #3 I would invite you to submit a revised manuscript addressing the concerns raised; however, I do also understand if you would at this stage rather prefer to seek rapid publication of the current manuscript elsewhere. In order to better define the revisions required to satisfy the referees it would be helpful if you could already at this stage provide me with an outline of the experiments that could be included in a revised manuscript. Please feel free to contact me with any questions regarding this.

In conclusion, given the referees' overall positive recommendations, I would like to invite you to submit a revised version of the manuscript, addressing the comments of all three reviewers. I should add that it is EMBO Journal policy to allow only a single round of revision, and acceptance of your manuscript will therefore depend on the completeness of your responses in this revised version. In light of the extensive, additional work required in the present case we could offer to extend the deadline for the revised manuscript.

When preparing your letter of response to the referees' comments, please bear in mind that this will form part of the Review Process File, and will therefore be available online to the community. For more details on our Transparent Editorial Process, please visit our website: http://emboj.embopress.org/about#Transparent_Process

We generally allow three months as standard revision time. As a matter of policy, competing manuscripts published during this period will not negatively impact on our assessment of the conceptual advance presented by your study. However, we request that you contact the editor as soon as possible upon publication of any related work, to discuss how to proceed. Should you foresee a problem in meeting this three-month deadline, please let us know in advance and we may be able to grant an extension.

Thank you for the opportunity to consider your work for publication. I look forward to your revision.

REFEREE COMMENTS

Referee #1:

Heterochromatin, one of the two major states of chromatin present in eukaryotic cells, was believed for decades to be static. However, live microscopy analyses together with studies on RNA-mediated heterochromatin formation have demonstrated recently that heterochromatin is a rather dynamic state. Heterochromatin Protein 1 (HP1) type proteins are chromodomain-containing proteins binding to methylated lysine 9 of histone H3 (H3K9) and are considered to be building blocks of heterochromatin. In this manuscript, entitled "H3K9 methylation extends across natural boundaries of heterochromatin in the absence of an HP1 protein", Stunnenberg and co-workers report that, in the yeast S. pombe, the HP1 protein Swi6 exists mostly as a single nuclear population rapidly moving on and out of heterochromatin, as well as from one site of heterochromatin to another. By using different mutant cells, it is shown that Swi6 mobility is slowed down by its binding to either methylated lysine 9 of histone H3 or RNA. Moreover, Swi6 mobility at pericentromeric and subtelomeric heterochromatin stays the same in G1, S and G2 phases of the cell cycle. Surprisingly, using H3K9 methylation chromatin immunoprecipitation (ChIP) combined to massive sequencing, it is shown that Swi6, which plays only a minor role in maintaining a high level of H3K9 methylation at pericentric heterochromatin region, is actually required to avoid propagation of this epigenetic mark above the natural borders of this region. The requirement for Swi6 in restricting the spreading of H3K9 methylation over natural barriers is also observed at subtelomeric regions.

This is a good and an interesting study that completes and refines the conclusion of previous work on the mobility of HP1 proteins. Importantly, the specific use of a more "physiological" expression system, to avoid erroneous interpretation caused by overexpression of HP1 proteins, demonstrates that Swi6 exists only as one dynamic population of proteins when analyzed by fluorescent microscopy. This is in contrast with what was previously proposed. Importantly also, this study reports the quite unexpected finding that Swi6 HP1 protein is required for avoiding H3K9 methylation propagation over natural borders of heterochromatin.

Altogether, this study brings significant advances on the dynamics of a well-studied HP1 protein and on the requirement of this protein in constraining the propagation of H3K9 methylation, a key epigenetic mark. The findings will be of interest to a broad readership in the field of chromatin biology. I have few concerns listed below.

Major points:

1. A major strength of this work is the use of a fully functional Swi6-EGFP tagged protein expressed under Swi6 endogenous promoter. From reading the text, it is not completely clear whether the level of this protein was checked and whether it is indeed similar to the endogenous Swi6. Because, the cellular level of Swi6 protein is critical to estimate properly the dynamics of the protein, as the authors indicate, it is important to double check that Swi6-EGFP and endogenous Swi6 are expressed a similar levels within the cell. Anti-Swi6 antibodies exist and allow such control by western blot analysis. The blot should be presented in the manuscript.

2. In the line-scan FRAP experiment, the measurement done in clr4Δ cells does not appear to be very informative. As it is being presented (Figure 1H and main text), the analysis does not discriminate between euchromatin and heterochromatin regions. In this case, the measurement is pretty much the same as the euchromatin measurement. Moreover, it does not inform on the mobility of Swi6 in the vicinity of DNA regions undergoing heterochromatin formation in wild-type cells.
A more informative measure would be to localize such genomic regions by using specific fluorescent markers, such as CenpA for centeromeres and Taz1 for telomeres, and to examine the dynamics of Swi6 in the close environment of these regions. Beyond the fact that this would be a better control, such experiment might actually show that Swi6 dynamics in these regions is in fact slower since heterochromatic RNAs accumulate strongly in clr4Δ cells. The available NLS-Swi6 and NLS-Swi6-KR25A constructions could also be used to further explore this possibility.

Minor points:

1. There are two HP1-like proteins in S. pombe, Swi6 and Chp2. Is what is found with Swi6 also true for Chp2? What is the impact of deleting chp2 gene on H3K9 methylation propagation? Unless this is addressed, the authors should make it clear that they are referring to Swi6/HP1 both in the title and the abstract of the MS. Moreover, they should mention the existence of two HP1 proteins in S. pombe at least in the introduction and discussion sections of the paper.

2. The authors convincingly show that Swi6 is required for avoiding propagation of H3K9 methylation beyond natural borders of heterochromatin. However, this finding does not necessarily imply that Swi6 has a function per se in blocking such propagation. This requirement could in fact be an indirect consequence of the loss of Swi6 lead to changes in the dynamics of heterochromatin formation and maintenance, and not a direct function of the protein. This possibility should therefore be mentioned in the discussion section.

3. Swi6 deletion is having different effects on heterochromatin spreading over natural borders of heterochromatin and over a reporter gene inserted within heterochromatin. In the first case, absence of Swi6 causes a spreading of H3K9me2 whereas in the second case it leads to a loss of H3K9me over the gene. How to explain this difference and reconcile this apparent contradiction with the proposed model? Mentioning and discussing this in the discussion could be useful.

4. The model needs to be improved to make it more readable and less confusing. They are multiple aspects being presented in the scheme with out necessarily a good schematic representation of these aspects. For example, the stop of heterochromatin spreading by three different systems is not easy to catch from the current scheme. Swi6+ and swi6 delta situation are not represented in an equivalent manner along the green and red band. It gives the impression that in swi6Δ cells methylation of H3K9 does not spread over a barrier, the contrary of what is show in the manuscript.

5. Page 14, the second last sentence of the last paragraph of the result section is not clear [At certain subtelomeric regions, Swi6 appears partially redundant in ... spreading of heterochromatin]. Swi6 is redundant with what?

6. Title of Figure 4, the use of the word "heterochromatin" is an overstatement. The formulation " methylation of H3 K9" or "H3K9 me2" would be more accurate and suitable. Showing the spreading of H3K9 methylation is not sufficient to conclude that this is actually spreading of heterochromatin.

Referee #2:

In this manuscript, two parts can be distinguished. In the first part which represents the main of the paper, by FRAP analysis, the authors show that Swi6 is higly mobile and binds only transiently to constitutive heterochromatin throughout the cell cycle. Swi6 dynamics are slowed down in the presence of the histone methyltransferase Clr4 or when they expressed in the cells a Swi6 mutant unable to bind to RNA. In the second part, by ChIP-sequencing analysis of H3K9me2, they demonstrate that Swi6 is required to prevent H3K9me2 spreading at centromeres.

The manuscript mostly focuses on the in vivo dynamics of Swi6 (3 figures out of 5). They performed FRAP on endogenous tagged Swi6-EGFP and they could confirm what it is already known since more than 10 years that HP1 proteins are higly mobile in yeast and in mammals. It is also not surprising that RNA decelarated Swi6 dynamics as it is the case in the absence of Clr4. Indeed, it is expected that mobility decreases when the number of interactors (RNA or H3K9me) increases. Thus this part of the manuscript does not bring any novelty to the field. Most importantly, it is not related to the second part.
The interesting part of this maunuscript is the second one puting forward a role for Swi6 in the spreading of the H3K9me2 mark at centromeres. This certainly explains why they entitle their manuscript « H3K9 methylation extends across natural boundaries of heterochromatin in the absence of an HP1 protein », although this part corresponds only to the panels A and C of the figure 4. This observation is potentially interesting and could expand our understanding of heterochromatin spreading at centromeres. However, these data are at a preliminary stage of analysis and need mechanistic improvment before publication can be envisaged.
The manuscript in its present form is not recommended for EMBO J.

Referee #3:

Stunnenberg and colleagues have used a number of techniques, largely focussed on FRAP methodology, to investigate the dynamic kinetics of the heterochromatin protein Swi6 in S. pombe cells. They report that, in contrast to earlier reports, the vast majority of Swi6 exists as a single dynamic population capable of switching rapidly between different genomic locations. The main difference between these studies and the earlier ones is that here Swi6 is not over-expressed and is expressed from its endogenous locus. Interestingly, the authors also show that loss of Swi6 leads to spreading of H3K9me at specific centromeric sites. These findings are thought provoking and they will be of interest to a reasonably wide readership. The manuscript is clearly written and the experiments appear to have been performed with a high degree of technical competence. However, there are a number of issues that the authors need to address.

Much of this manuscript uses a Swi6-EGFP (or derivative) fusion protein. It is claimed on page 6 that the fusion protein is fully function and the authors cite both published work and data not shown. It is essential to substantiate this important claim with as much data as possible. Therefore, the 'data not shown' must be shown to provide full proof for the claim.

The authors have used of a hinge swap version of Swi6 that no longer binds RNA. It is a real shame that they did not also analyse other mutant versions of Swi6 in their analyses. For example, chromodomain (CD) point mutation(s) could have been included to investigate how binding of Swi6 to H3K9me affects its kinetics. I appreciate that they studied the kinetics in cells lacking Clr4 (the sole H3K9 methyltransferase in pombe) and found they increased Swi6 kinetics by approximately 50ms, however complete removal of K9me is a rather blunt assay as it disrupts other pathways and interactions. The Swi6 CD mutant would be a 'cleaner' approach in my opinion. In a similar way, Swi6 chromo-shadow domain (CSD) mutants that inhibit Swi6 dimerization could have been analysed. These may have been particularly informative with respect to the observed spreading of H3K9me at specific centromeric locations.

The increase in t1/2 values (535ms to 790ms) induced by inclusion of the NLS (Fig. 2A) is concerning as it obviously affects Swi6 kinetics via unknown and presumably non-physiological mechanisms. Therefore, data generated by this fusion protein need to be interpreted with caution.

The authors state on page 12 that their results indicate that "telomeric heterochromatin appears permissive for RNA synthesis". However, their results simply suggest that RNA may be there, but there are no data to indicate that it was transcribed locally.

1st Revision - authors' response 28 July 2015

We would like to thank all reviewers for their overall positive recommendations. We are particularly grateful to reviewer 1 and 3 for their constructive feedback, which helped us to further substantiate our findings.

Besides additional experiments proposed by the reviewers, we have performed several experiments that revealed insights into the H3K9me2 spreading mechanism that is negatively regulated by Swi6. Firstly, our new results further support a direct role of Swi6 in demarcating heterochromatin. Secondly, we show that methylation of H3K9 in the absence of Swi6 is strictly dependent on the polymerization property of Tas3, a subunit of the RNA-induced transcriptional silencing (RITS) complex. The new data added to the revised version of our manuscript reveal intriguing details about the roles of Swi6 and the RNAi pathway in maintaining centromeric heterochromatin, which will be of interest to a broad audience.

Below we will respond to the reviewers' questions/suggestions point-by-point.

Detailed response to reviewer's comments
(The referees' comments are in italics, grey. Our responses are in black.)

Referee #1:

Heterochromatin, one of the two major states of chromatin present in eukaryotic cells, was believed for decades to be static. However, live microscopy analyses together with studies on RNA-mediated heterochromatin formation have demonstrated recently that heterochromatin is a rather dynamic state. Heterochromatin Protein 1 (HP1) type proteins are chromodomain-containing proteins binding to methylated lysine 9 of histone H3 (H3K9) and are considered to be building blocks of heterochromatin. In this manuscript, entitled "H3K9 methylation extends across natural boundaries of heterochromatin in the absence of an HP1 protein", Stunnenberg and co-workers report that, in the yeast S. pombe, the HP1 protein Swi6 exists mostly as a single nuclear population rapidly moving on and out of heterochromatin, as well as from one site of heterochromatin to another. By using different mutant cells, it is shown that Swi6 mobility is slowed down by its binding to either methylated lysine 9 of histone
H3 or RNA. Moreover, Swi6 mobility at pericentromeric and subtelomeric heterochromatin stays the same in G1, S and G2 phases of the cell cycle. Surprisingly, using H3K9 methylation chromatin

immunoprecipitation (ChIP) combined to massive sequencing, it is shown that Swi6, which plays only a minor role in maintaining a high level of H3K9 methylation at pericentric heterochromatin region, is actually required to avoid propagation of this epigenetic mark above the natural borders of this region. The requirement for Swi6 in restricting the spreading of H3K9 methylation over natural barriers is also observed at subtelomeric regions.

This is a good and an interesting study that completes and refines the conclusion of previous work on the mobility of HP1 proteins. Importantly, the specific use of a more "physiological" expression system, to avoid erroneous interpretation caused by overexpression of HP1 proteins, demonstrates that Swi6 exists only as one dynamic population of proteins when analyzed by fluorescent microscopy. This is in contrast with what was previously proposed. Importantly also, this study reports the quite unexpected finding that Swi6 HP1 protein is required for avoiding H3K9 methylation propagation over natural borders of heterochromatin.

Altogether, this study brings significant advances on the dynamics of a well-studied HP1 protein and on the requirement of this protein in constraining the propagation of H3K9 methylation, a key epigenetic mark. The findings will be of interest to a broad readership in the field of chromatin biology. I have few concerns listed below.

Major points:
1. A major strength of this work is the use of a fully functional Swi6-EGFP tagged protein expressed under Swi6 endogenous promoter. From reading the text, it is not completely clear whether the level of this protein was checked and whether it is indeed similar to the endogenous Swi6. Because, the cellular level of Swi6 protein is critical to estimate properly the dynamics of the protein, as the authors indicate, it is important to double check that Swi6-EGFP and endogenous Swi6 are expressed a similar levels within the cell. Anti-Swi6 antibodies exist and allow such control by western blot analysis. The blot should be presented in the manuscript.

We have included a Western Blot in Figure EV1A, which shows that Swi6-EGFP levels are similar to Swi6. We have also included a quantitative real-time RT-PCR experiment (Fig EV1B), demonstrating full functionality of Swi6-EGFP (see also below).

2. In the line-scan FRAP experiment, the measurement done in clr4Δ cells does not appear to be very informative. As it is being presented (Figure 1H and main text), the analysis does not discriminate between euchromatin and heterochromatin regions. In this case, the measurement is pretty much the same as the euchromatin measurement. Moreover, it does not inform on the mobility of Swi6 in the vicinity of DNA regions undergoing heterochromatin formation in wild-type cells.
A more informative measure would be to localize such genomic regions by using specific fluorescent markers, such as CenpA for centeromeres and Taz1 for telomeres, and to examine the dynamics of Swi6 in the close environment of these regions. Beyond the fact that this would be a better control, such experiment might actually show that Swi6 dynamics in these regions is in fact slower since heterochromatic RNAs accumulate strongly in clr4Δ cells. The available NLS-Swi6 and NLS-Swi6-KR25A constructions could also be used to further explore this possibility.

In this experiment, *clr4*D cells serve as a control. As pointed out by this reviewer, Swi6 mobility in the nucleoplasm of *wild type* cells is very similar to Swi6 mobility in *clr4*D cells. Therefore we can conclude that Swi6 is highly mobile throughout the nucleus, exchanging between different heterochromatin regions.
The additional line-scan FRAP experiments in *clr4*D cells would be technically very challenging. Anyhow, such an experiment seems redundant with experiments shown in Figure 2, which already demonstrate that Swi6 dynamics is slower when heterochromatic RNAs accumulate in *cid14D* cells. We note that RNA accumulating in *clr4*D cells can no longer be considered “heterochromatic”, which is the case in *cid14D* cells. Therefore, we believe that the proposed experiments are dispensable.

Minor points:

1. There are two HP1-like proteins in S. pombe, Swi6 and Chp2. Is what is found with Swi6 also true for Chp2? What is the impact of deleting chp2 gene on H3K9 methylation propagation?
Unless this is addressed, the authors should make it clear that they are referring to Swi6/HP1 both

in the title and the abstract of the MS. Moreover, they should mention the existence of two HP1 proteins in S. pombe at least in the introduction and discussion sections of the paper.

We have amended the text to make clear that there are two HP1-like proteins in fission yeast. In addition, we have deleted *chp2+* and we have assessed H3K9me2 spreading by ChIP. In contrast to *swi6D* cells, we do not observe spreading of H3K9me2 in *chp2D* cells. This data is now shown in Figure EV5B.

2. The authors convincingly show that Swi6 is required for avoiding propagation of H3K9 methylation beyond natural borders of heterochromatin. However, this finding does not necessarily imply that Swi6 has a function per se in blocking such propagation. This requirement could in fact be an indirect consequence of the loss of Swi6 lead to changes in the dynamics of heterochromatin formation and maintenance, and not a direct function of the protein. This possibility should therefore be mentioned in the discussion section.

To address this point, we have assessed H3K9me2 spreading in Swi6 point mutants that either prevent dimerization of Swi6 (*swi6L315E)* or abolish binding to H3K9me2 (*swi6W104A*). As observed in the absence of the Swi6 proteins, also these mutants cause spreading of H3K9 methylation. These results strongly argue against indirect effects caused by the absence of the Swi6 protein. In contrast, they reveal that dimerization and H3K9me2 binding are properties of Swi6 that are crucial to avoid spreading of H3K9me2 beyond natural heterochromatin borders. The new results are shown in Figure 5.

3. Swi6 deletion is having different effects on heterochromatin spreading over natural borders of heterochromatin and over a reporter gene inserted within heterochromatin. In the first case, absence of Swi6 causes a spreading of H3K9me2 whereas in the second case it leads to a loss of H3K9me over the gene. How to explain this difference and reconcile this apparent contradiction with the proposed model? Mentioning and discussing this in the discussion could be useful.

This statement is incorrect. H3K9 methylation of a centromeric *otr::ura4+* reporter does also occur independently of Swi6 (Sadaie et al, 2004; Motamedi et al, 2008, Li et al, 2009).

4. The model needs to be improved to make it more readable and less confusing. They are multiple aspects being presented in the scheme with out necessarily a good schematic representation of these aspects. For example, the stop of heterochromatin spreading by three different systems is not easy to catch from the current scheme. Swi6+ and swi6 delta situation are not represented in an equivalent manner along the green and red band. It gives the impression that in swi6Δ cells methylation of H3K9 does not spread over a barrier, the contrary of what is show in the manuscript.

Thank you. We have changed the model figure accordingly.

5. Page 14, the second last sentence of the last paragraph of the result section is not clear [At certain subtelomeric regions, Swi6 appears partially redundant in ... spreading of heterochromatin]. Swi6 is redundant with what?

We meant to say “partially contributing to spreading” at certain subtelomeres and we have revised the text accordingly.

6. Title of Figure 4, the use of the word "heterochromatin" is an overstatement. The formulation " methylation of H3 K9" or "H3K9 me2" would be more accurate and suitable. Showing the spreading of H3K9 methylation is not sufficient to conclude that this is actually spreading of heterochromatin.

We changed the title of this figure to “Methylation of H3K9 spreads across natural boundaries and heterochromatin becomes derepressed in *swi6*Δ cells.“

Referee #2:

In this manuscript, two parts can be distinguished. In the first part which represents the main of the paper, by FRAP analysis, the authors show that Swi6 is higly mobile and binds only transiently to constitutive heterochromatin throughout the cell cycle. Swi6 dynamics are slowed down in the *presence of the histone methyltransferase Clr4 or when they expressed in the cells a Swi6 mutant unable to bind to RNA. In the second part, by ChIP-sequencing analysis of H3K9me2, they demonstrate that Swi6 is required to prevent H3K9me2 spreading at centromeres.*

The manuscript mostly focuses on the in vivo dynamics of Swi6 (3 figures out of 5). They performed FRAP on endogenous tagged Swi6-EGFP and they could confirm what it is already known since more than 10 years that HP1 proteins are higly mobile in yeast and in mammals. It is also not surprising that RNA decelarated Swi6 dynamics as it is the case in the absence of Clr4. Indeed, it is expected that mobility decreases when the number of interactors (RNA or H3K9me) increases. Thus this part of the manuscript does not bring any novelty to the field. Most importantly, it is not related to the second part.

The interesting part of this maunuscript is the second one puting forward a role for Swi6 in the spreading of the H3K9me2 mark at centromeres. This certainly explains why they entitle their manuscript « H3K9 methylation extends across natural boundaries of heterochromatin in the absence of an HP1 protein », although this part corresponds only to the panels A and C of the figure 4. This observation is potentially interesting and could expand our understanding of heterochromatin spreading at centromeres. However, these data are at a preliminary stage of analysis and need mechanistic improvment before publication can be envisaged.

The manuscript in its present form is not recommended for EMBO J.

We disagree that the first part of our paper does not bring any novelty to the field and we are grateful to reviewers 1 and 3 for highlighting the significance of our work. It is well linked to the second part, which does now include many additional experiments that we have performed for the revised manuscript (see responses to the other reviewers).

Referee #3:

Stunnenberg and colleagues have used a number of techniques, largely focussed on FRAP methodology, to investigate the dynamic kinetics of the heterochromatin protein Swi6 in S. pombe cells. They report that, in contrast to earlier reports, the vast majority of Swi6 exists as a single dynamic population capable of switching rapidly between different genomic locations. The main difference between these studies and the earlier ones is that here Swi6 is not over-expressed and is expressed from its endogenous locus. Interestingly, the authors also show that loss of Swi6 leads to spreading of H3K9me at specific centromeric sites. These findings are thought provoking and they will be of interest to a reasonably wide readership. The manuscript is clearly written and the experiments appear to have been performed with a high degree of technical competence. However, there are a number of issues that the authors need to address.

Much of this manuscript uses a Swi6-EGFP (or derivative) fusion protein. It is claimed on page 6 that the fusion protein is fully function and the authors cite both published work and data not shown. It is essential to substantiate this important claim with as much data as possible. Therefore, the 'data not shown' must be shown to provide full proof for the claim.

Full functionality of Swi6-EGFP is now shown in Figure EV1B. We have also included a Western Blot, which shows that Swi6-EGFP levels are similar to Swi6 (Figure EV1A).

The authors have used of a hinge swap version of Swi6 that no longer binds RNA. It is a real shame that they did not also analyse other mutant versions of Swi6 in their analyses. For example, chromodomain (CD) point mutation(s) could have been included to investigate how binding of Swi6 to H3K9me affects its kinetics. I appreciate that they studied the kinetics in cells lacking Clr4 (the sole H3K9 methyltransferase in pombe) and found they increased Swi6 kinetics by approximately 50ms, however complete removal of K9me is a rather blunt assay as it disrupts other pathways and interactions. The Swi6 CD mutant would be a 'cleaner' approach in my opinion. In a similar way, Swi6 chromo-shadow domain (CSD) mutants that inhibit Swi6 dimerization could have been analysed. These may have been particularly informative with respect to the observed spreading of H3K9me at specific centromeric locations.

It has been previously demonstrated that Swi6 requires both the CSD and the CD to display full binding activity in vivo (Cheutin et al, 2004). Therefore, we don't think that repeating such measurements for CD and CSD mutants by FRAP would add much to the paper. However, we highly appreciate the suggestion to assess the spreading of H3K9me2 in these Swi6 mutants, which provided further support for the model we are proposing. The new data is shown in Figure 5 of the revised manuscript (see also response to reviewer 1).

The increase in t1/2 values (535ms to 790ms) induced by inclusion of the NLS (Fig. 2A) is concerning as it obviously affects Swi6 kinetics via unknown and presumably non-physiological mechanisms. Therefore, data generated by this fusion protein need to be interpreted with caution.

The results obtained in conjunction with these constructs reveal that RNA production within heterochromatin is greatly fluctuating and stochastic throughout the cell cycle. Because the NLS constructs are not used to make claims about the exact binding kinetics of Swi6, we are not concerned.

The authors state on page 12 that their results indicate that "telomeric heterochromatin appears permissive for RNA synthesis". However, their results simply suggest that RNA may be there, but there are no data to indicate that it was transcribed locally.

RNA transcripts are being synthesized from telomeric heterochromatin. We have included the raw data of a quantitative RT-PCR experiment in the revised version of the manuscript that demonstrates this clearly (Figure EV1C).

Additional round of consultation with Referee 3 with regard to comments from Referee 2

' Referee 1: In general, I agree with the comments from this referee. I particularly agree with Major point 1 (a point also made myself) that it is essential to show that Swi6-EGFP is fully functional. I believe the western blot requested by referee 1 is essential for this.

Swi6-EGFP is fully functional and expressed to similar levels as Swi6. This additional data is shown in Figure EV1 of the revised manuscript. We note that we can only fit Swi6-EGFP kinetics to a two-component model if we express Swi6-EGFP from a plasmid using the same condition as in Cheutin et al. (0.4µg/ml thiamine). Even though EGFP might slightly stabilize Swi6, this has no consequence on spreading or silencing of heterochromatin and we are not able detect a static fraction by FRAP. We therefore conclude that this fusion protein is fully functional.

Referee 2: Argues that most of the paper has little to offer over that which is already known. However, I believe the observation that expression of Swi6 from its endogenous locus (ie. not over expressed) indicates a predominantly single kinetic population of Swi6 is important as over-expression studies indicated at least two populations with different kinetics. Notwithstanding this, I do have some sympathy with his/her belief that the K9me spreading at centromeric positions in the absence of Swi6 is rather preliminary. Perhaps, the authors could enhance this section with additional data, maybe by exploring the effect of Swi6 mutants as I suggested. '

As acknowledged by all three reviewers, our finding that H3K9me2 spreads across natural boundaries in the absence of Swi6 is highly unexpected and thought provoking. Therefore, we believe that publication of this result on its own would have been fully justified. However, we are able to relate to the request for more mechanistic insight and we have therefore added a substantial amount of new data to the revised manuscript.

As already alluded to above, we have performed additional experiments with various Swi6 point mutants. The new results that we show in Figure 5 of the revised manuscript further support a direct role of Swi6 in counteracting the spreading of H3K9 methylation and allow us to propose a model in which Swi6 dimers, when adopting a specific conformation (Canzio et al, 2013), prevent the spreading of H3K9 methylation. We find this possibility intriguing and it will be exciting to explore this further.

In addition, we have performed experiments to test the hypothesis that spreading in the absence of Swi6 is mediated by self-association of the RITS subunit Tas3. Our hypothesis is based on a paper by the Moazed and Patel labs (Li et al, Molecular Cell, 2009), which demonstrated that a C-terminal Tas3 alpha-helical motif (TAM) promotes Tas3 self-association and thereby cis-spreading of the RITS complex. Indeed, we found that the ability of Tas3 to interact with itself is absolutely required for the methylation of H3K9me2 if Swi6 is missing.

2nd Editorial Decision 23 August 2015

Thank you for submitting a revised version of your manuscript. It has now been seen by two of the original referees whose comments are shown below.

As you will see they both find that all criticisms have been sufficiently addressed and recommend the manuscript for publication. However, before we can proceed to officially accept your manuscript there are a few editorial issues concerning text and figures that I would ask you to address:

-> Please rephrase the legend and text describing fig 6 as suggested by ref #1

-> Please fill out and include an author checklist as listed in out online guidelines (http://emboj.embopress.org/authorguide)

Thank you again for giving us the chance to consider your manuscript for The EMBO Journal, I look forward to your final revision.

REFEREE COMMENTS

Referee #1:

In this revised MS, Stunnenberg and co-workers provide a series of controls and new findings that further support the main conclusions made in the original version. These findings also provide additional insights into the role of a HP1 protein in restricting the spreading of H3K9 methylation over natural barriers of heterochromatin.

More specifically, the authors convincingly addressed the following points and issues, which were raised in my comments of the original manuscript.
First, the level and functionality of Swi6-GFP (expressed from swi6 locus) was checked and compared to wild-type Swi6. Western blot and RT-qPCR results show no pronounced difference in the levels of Swi6-GFP protein and mRNA, compared to wild-type Swi6. A measure of the efficiency of silencing in cells expressing Swi6-GFP (in place of Swi6) also shows that these cells have a heterochromatin gene silencing similar to wild-type cells.
Second, the implication of Chp2, the second HP1-type protein present in S. pombe, in regulating the spreading of H3K9 methylation was tested. The results indicate that only Swi6 is required for limiting such spreading.
Third, the possibility that the observed propagation of H3K9 methylation is an indirect consequence of swi6 deletion was addressed. Analysis of cells expressing Swi6 point mutants, which are defective for either Swi6 homodimerization or binding to H3K9me2, shows that they have similar extended propagation of H3K9 methylation. These results further support the idea that Swi6 is directly implicated in limiting H3K9me propagation.
Following on experiments asked or suggested by the other reviewers, the authors also provide more findings on what protein is responsible for the propagation of H3K9 methylation in absence of Swi6. It is found that this propagation is mediated by the protein Tas3 and requires Tas3's capacity to homodimerize.

Altogether, the additional experiments conducted and the new findings added in the revised manuscript significantly improve the quality and significance of this study.

I have only a minor comment on the revised version. Analysis of Tas3 requirement in the spreading of H3K9 methylation is limited to a pericentromeric region and not addressed for other heterochromatin regions. This should be indicated in figure 6 legend and the main text.

Referee #3:

The authors have done a good job in answering my prior concerns. They have included additional data which strengthens the manuscript by providing further mechanistic insight.

Curriculum Vitae

PhD Rieka Stunnenberg

Contact: Lehenmattstrasse 55
CH - 4052 Basel
riekastunnenberg@yahoo.de
tel. +41 (0)78 942 23 15

Date of birth: 10.03.1986
Place of birth: Heidelberg, Germany
Nationality: Dutch

Languages: - Fluent /Professional- **English, German and Dutch**
- Basic - Spanish and French

"I am an ambitious and enthusiastic molecular biologist who is passionate about science communication and wants to contribute to a healthy world. Working with complexity and dealing with setbacks is part of the game. International environments stimulate me, as I love to interact and communicate with different people. Determined to bring my knowledge, experience and great interpersonal skills with me to fuel innovation and transfer knowledge."

EDUCATION

2010 - 2014	**PhD**	**Biochemistry**, *cum laude* Friedrich Miescher Institute for Biomedical Research, Basel, Switzerland
2007 - 2009	**M.Sc.**	**Molecular mechanisms of disease**, *cum laude* Radboud University of Nijmegen, Nijmegen, The Netherlands
2004 - 2007	**B.Sc.**	**Molecular Life Science**, *bene meritum* Radboud University of Nijmegen, Nijmegen, The Netherlands

WORK EXPERIENCE

Current	**Media Monitoring & Business Relations Associate**	**CheckOrphan, Basel, Switzerland** Non-profit organization
		- Mission: Create awareness of rare diseases, treatments and Access programs. Tasks: Managing, monitoring and editing news. Networking, give workshops, present at conferences and representing the organization. Event management.
2010 - 2015	**PhD**	**FMI, Basel, Switzerland** M Bühler, Department of Epigenetics
		- Paper revisions: negotiating plan of action and replying to reviewers' requests, execution final experiments, finalizing and editing manuscript for resubmission to EMBO journal. - Independently investigated and managed scientific projects on cutting edge science of epigenetics and RNA biology. Therefore, I acquired and translated complex scientific knowledge, established a new methodology and provided help to colleagues. Given comprehensible external and internal presentations. Result: multiple co-authorships. - Given traineeship to students, organized meetings between interdisciplinary experts to advance in my projects. External collaboration and internal teamwork to investigate a mathematical and theoretical angle in my research. Multitasking, time-management and problem-analysis on daily basis for the completion of project experiments.
Jan – Aug 2009	**Research internship**	**UCSD, San Diego, CA, USA** MG Rosenfeld, Department of Medicine
		- Research on molecular function of a transcription factor in mammalian cells. Independently planning and executing experiments. Acquiring knowledge (literature research) and skills on microscopy, protein and chromatin biology. Given internal progress presentations and work within a highly international environment. Co-authorship on an article.

Feb – Oct 2008	**Research internship**	**RIMLS, Nijmegen, The Netherlands** HG Stunnenberg, Department of Molecular Biology Cancer associated molecular research in mammalian cells. Multiple Co-authorships.
Jun – Aug 2007	**Research internship**	**RIMLS, Nijmegen, The Netherlands** C Logie, Department of Molecular Biology Cell cycle research in yeast. Protein biology, genetics and microscopy. Written report.
2002 – 2005	**Side Job - Cashier**	**Albert Heijn, Nijmegen, The Netherlands**

MEETINGS

2015	Workshop, Presentation	**Early Access Programmes 2015**, London, UK
2013	Presentation	**Tiny European RNA meeting**, St. Feliu de Gruixols, Spain
2011	Presentation & Poster	**7th course on Epigenetics**, Institute Curie, Paris, France

CERTIFICATIONS

May 2015	Initiating and Planning Projects (Coursera), University of California, Irvine
June 2015	Budgeting and Scheduling Projects (Coursera), University of California, Irvine
July 2015	Introduction to Communication Science (Coursera), University of Amsterdam

PUBLICATIONS

1. Stunnenberg, R., Kulasegaran-Shylini, R., Kirschmann, M.A., Keller, C., Gelman, L. and Bühler, M. **(2015)**. H3K9 methylation extends across the natural boundaries of heterochromatin in the absence of an HP1 protein. ***EMBO Journal***
2. Stunnenberg, R., and Bühler, M. **(2012)**. A Detour to Mature. ***Mol. Cell*** 46, 719–721
3. Woolcock, K.J., Stunnenberg, R., Gaidatzis, D., Hotz, H.R., Emmerth, S., Barraud, P., and Bühler, M. **(2012)**. RNAi keeps Atf1-bound stress response genes in check at nuclear pores. ***Genes Dev.*** 26, 683–692.
4. Keller, C., Adaixo, R., Stunnenberg, R., Woolcock, K.J., Hiller, S., and Bühler, M. **(2012)**. HP1(Swi6) mediates the recognition and destruction of heterochromatic RNA transcripts. ***Mol. Cell*** 47, 215–227.

Additional co-authorships:	Oberti et al. **(2015)** *Cell Reports*	Benner et al. **(2013)** *PLoS Genetics*
	Costessi et al. **(2012)** *PLoS One*	Costessi et al. **(2011)** *EMBO Journal*

ACQUIRED SOFT SKILLS

- Public speaking
- Scientific writing (preview, articles and PhD thesis)
- Team work, dealing with conflicts, task delegation within the lab
- Problem analysis and problem-solving
- Work across disciplinary
- Time planning, managing deadlines
- Teaching: supervision of a master student

ACQUIRED HARD SKILLS

Communication:
Writing and editing (Word), presenting (PowerPoint), poster presentations (Adobe Illustrator), movies (iMovie, Fiji Imaging Software)

Data gathering and analysis:
Microsoft Excel, Pubmed, NCBI, ProteinDataBase, R studio, Yasara (Molecular-graphics software)

INTERESTS

Inline skating, classical massage, volleyball, snowboarding, bouldering, travelling, nature and playing piano.

REFERENCES

Prof. Dr. Marc Bühler
FMI, Basel, CH
marc.bühler@fmi.ch, +41 61 69 60438

Robert Derham
President and Owner of CheckOrphan
robert.derham@checkorphan.org